On the organization of non-nucleosidic pyrene- and fluorene-derivatives in a DNA scaffold

Inauguraldissertation

der Philosophisch-naturwissenschaftlichen Fakultät

der Universität Bern

vorgelegt von

Daniel Wenger

von Längenbühl BE

Leiter der Arbeit:

Prof. Dr. R. Häner

Departement für Chemie und Biochemie der Universität Bern

.

On the organization of non-nucleosidic pyrene- and fluorene derivatives in a DNA scaffold

Inauguraldissertation

der Philosophisch-naturwissenschaftlichen Fakultät

der Universität Bern

vorgelegt von

Daniel Wenger

von Längenbühl BE

Leiter der Arbeit:

Prof. Dr. R. Häner

Departement für Chemie und Biochemie der Universität Bern

Von der Philosophisch-naturwissenschaftlichen Fakultät angenommen.

Bern, (Prüfungsdatum)

Der Dekan:
Prof. Dr. S. Decurtins

Table of Contents

Chapter 1: Introduction 1

1.1 The discovery of DNA
1.2 History of the synthesis of DNA
1.3 The structure of DNA
1.4 Thermodynamic factors associated with helix formation
1.5 Nucleic acid guided assembly of aromatic chromophores
1.6 Nucleic acid based molecular switches
1.7 Aim of the work

Chapter 2: Influence of a B-Z transition on chromophore organization in bisegmental chimeric constructs 40

2.1 Abstract
2.2 Introduction
2.3 Results and discussion
2.4 Conclusion and outlook
2.5 Experimental section

Chapter 3: Influence of a B-Z transition on chromophore organization in trisegmental chimeric constructs 68

3.1 Abstract
3.2 Introduction
3.3 Results and discussion
3.4 Conclusion and outlook
3.5 Experimental section

Chapter 4: Trisegmental selfcomplementary chimeras 99

4.1 Abstract
4.2 Introduction
4.3 Results and discussion
4.4 Conclusion and outlook
4.5 Experimental section

Chapter 5: Bisalkynyl-fluorene derivatives as non-nucleosidic building blocks 126

5.1 Abstract
5.2 Introduction

5.3 Results and discussion
5.4 Conclusion and outlook
5.5 Experimental section

Chapter 6: Bisphenylfluorene: A differently linked fluorene derivative 162

6.1 Abstract
6.2 Introduction
6.3 Results and discussion
6.4 Conclusion and outlook
6.5 Experimental section

Chapter 7: Interactions between structurally different pyrene derivatives 176

7.1 Abstract
7.2 Introduction
7.3 Results and discussion
7.4 Conclusion and outlook
7.5 Experimental section

References 189

Acknowledgements 194

List of Publications 195

Curriculum Vitae 196

Chapter 1: Introduction

1.1 The Discovery of DNA

In 1869 the swiss physician and biologist **Friedrich Miescher** was the first to isolate DNA from white blood cells, the major component of the pus which he collected from bandages in a hospital, by treatment with weak alkaline solution [1]. Since he isolated the phosphorus containing chemical substance from the cell nuclei he deduced the term nuclein. The impact this molecule would have in the future, he was absolutely not aware of and ironically in his point of view the molecule of heredity was the protein. The isolation of DNA by Miescher was the beginning of a new era of research. The following decades the focus of research was on the function of DNA. **Phoebus Levene** determined then the components of DNA by discovering first the ribose (1909) and then the deoxyribose (1929) [2, 3]. He then came up with the incorrect tetranucleotide structure and the implication that it could not bear the information of heredity.

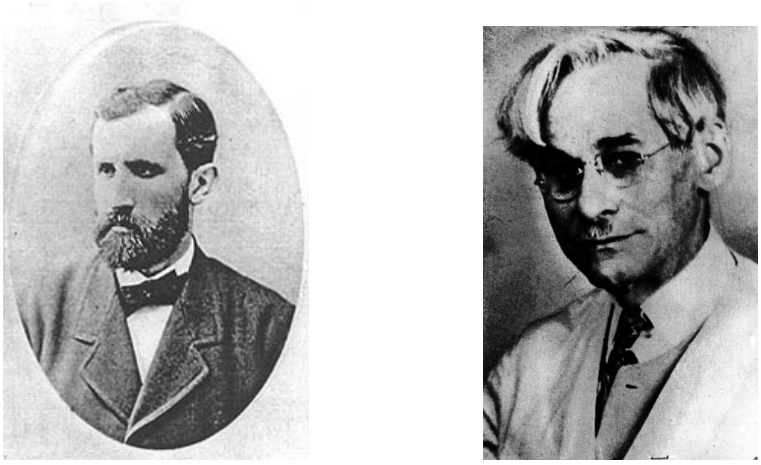

Figure 1.1 Friedrich Miescher (left); Phoebus Levene (right). (Illustration adapted from www.uni-tuebingen.de and www.mun.ca)

The **Avery–MacLeod–McCarty** experiment in 1944 suggested that DNA was indeed the heredity material [4]. For **Erwin Chargaff** the simple tetranucleotide structure proposed by Levene was unsatisfying and so in 1949 he isolated DNA from different organism and measured the proportion of each of the four nitrogenous bases. In contrast to the tetranucleotide hypothesis the bases showed only equal amount of adenine and thymine

and equal amount for guanine and cytosine [5]. Although he laid the basis for the elucidation of the double helical structure he was not able to deduce it by himself.

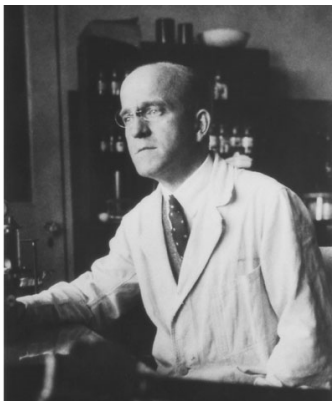

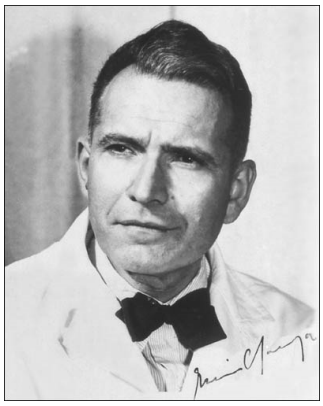

Figure 1.2 Oswald Avery (left); Erwin Chargaff (right). (Illustration adapted from www.history.nih.gov and www.de.academic.ru)

In 1952 **Rosalind Franklin** obtained X-ray diffraction patterns of DNA fibers of remarkable quality and deduced the basic dimensions of DNA as well as the conclusion that the phosphate groups were on the outside of the structure. **Maurice Wilkins** who was also working on the diffraction patterns showed the data obtained by Franklin to **Francis Crick** and **James Watson.** Her data supported and confirmed the model they have built and in 1953 Wilkins as well as Watson and Crick published their model based on the X-ray diffraction pattern obtained by Rosalind Franklin [6, 7].

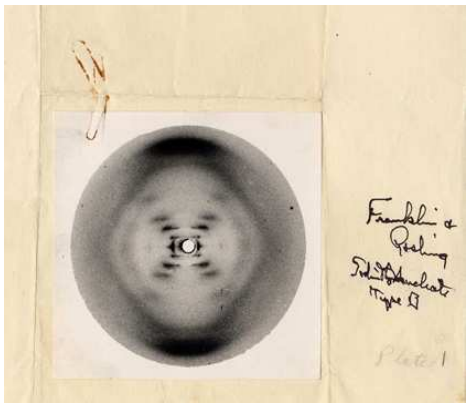

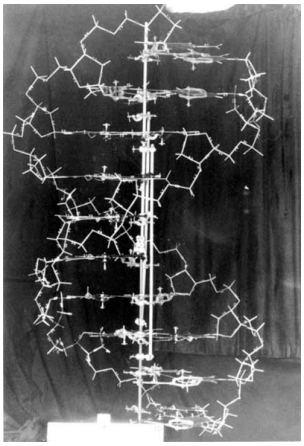

Figure 1.3 X-ray diffraction pattern recorded by Rosalind Franklin (left); DNA model build by James Watson and Francis Crick (right) (Illustration adapted from www.rockclimbing.com and www.cafemom.com)

The Nobel Prize in medicine was awarded to Wilkins, Crick and Watson (Roslind Franklin already died) for their work on the structure of DNA in the year 1962.

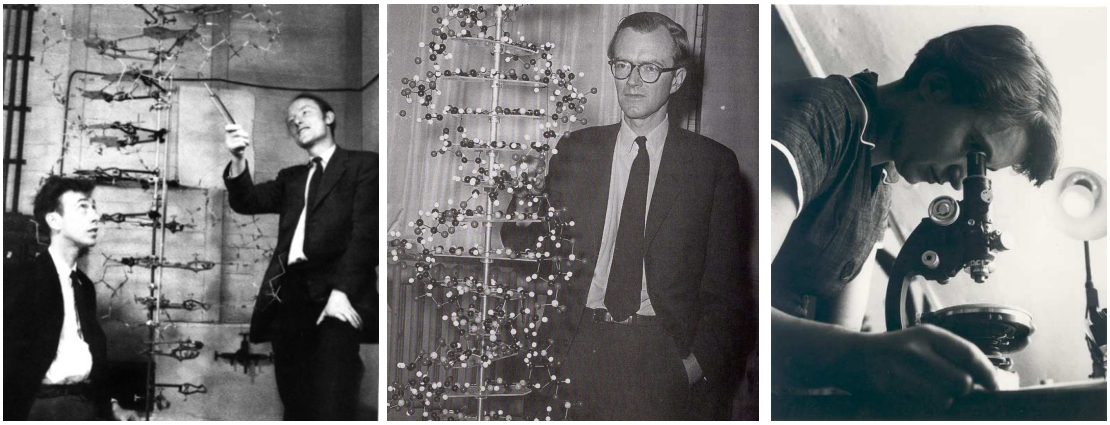

Figure 1.4 James Watson and Francis Crick (left); Maurice Wilkins (middle); Rosalind Franklin (right).

1.2 History of the synthesis of DNA

The elucidation of the structure of DNA initiated great interest in the research of nucleic acids not only in biochemistry and biology but also in chemistry. The synthesis of nucleic acids was a very important goal to achieve. The Indian American Biochemist **H. Gobind Khorana** achieved this goal by the first synthesis of a thymine dimer in 1956 by synthetic methods based on the already well developed solid phase synthesis of peptides [8]. The procedure developed by Khorana was very laborious, time consuming and inefficient and in the following two decades the synthesis of oligonucleotides was improved slowly and the approach was aiming at the automated synthesis. The development of automated solid phase synthesis of oligonucleotides by **Marvin**

Caruthers and **Hubert Koester** in the 1980`s based on phosphoramidite chemistry [9, 10, 11] revolutionized the chemical synthesis of short DNA sequences by being a very fast, easy to handle and efficient process. In the following years the solid support, the reagents and the apparature were improved and the efficiency was optimized [12]. These developments were the initiator for the investigation of fundamental properties of oligonucleotides by giving easy access to short sequences. Further more the possibility to introduce chemically modified nucleotides or even full artificial building blocks opened a whole new era of research based on the synthesis of DNA.

Figure 1.5. H. G. Khorana (left); Marvin Caruthers (middle); Hubert Koester (right).

1.3 The Structure of DNA

DNA is a linear polymer composed of four distinct monomers. Each monomeric unit, called nucleotide, is composed of three parts: a pentose sugar, a heterocyclic base and a phosphate residue, whereas the pentose sugar and the phosphate residue is the common component and the heterocyclic base is making the difference between the monomers.

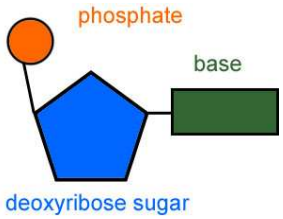

Figure 1.6 Basic components of nucleotide: A sugar moiety (blue), the nitrogenous base (green) and a phosphate residue (orange). (Illustration adopted from http://www.scienceaid.co.uk)

The nitrogen containing bases are namely the two pyrimidine bases thymine and cytosine, and the two purine bases adenine and guanine.

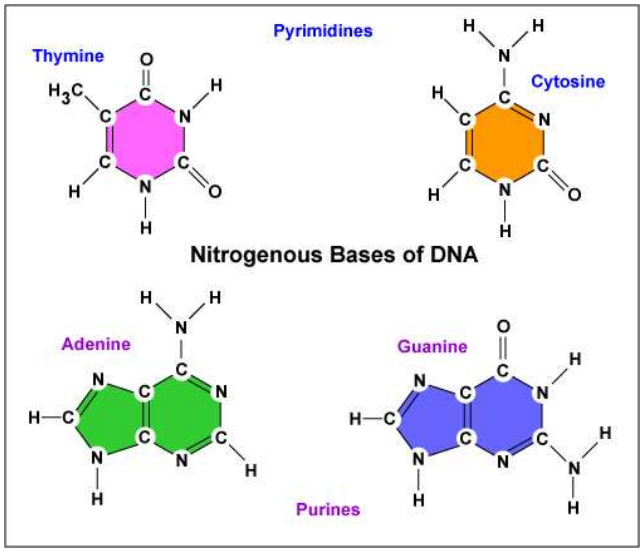

Figure 1.7 The four nitrogenous bases of DNA: Pyrimidines Thymine and Cytosine (top), and Puines Adenine and Guanine (bottom). (Illustiration adapted from http://www.student.ccbcmd.edu)

The connection between the base and the sugar moiety (C1`to N1 for the pyrimidines and C1`to N9 for the purines) is called the N-glycosidic bond and results in the nucleosides thymidine, cytidine, adenosine and guanosine.

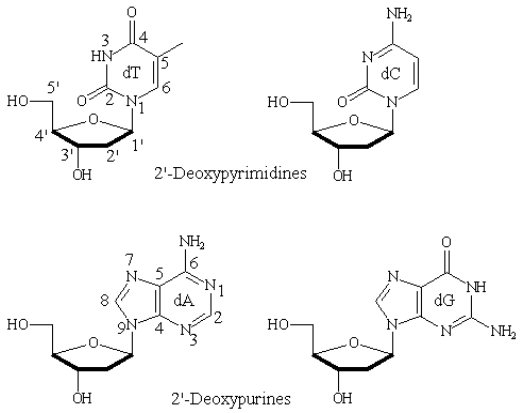

Figure 1.8 The four nucleosides: 2`-deoxypyrimidine (top), 2`-deoxypurine (bottom). (Illustration adapted from http://www.homepages.strath.ac.uk)

The nucleotides are then formed by the 5`- phosphate ester of the corresponding compounds.

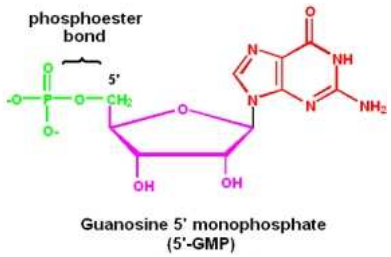

Figure 1.9 A representative example for a nucleotide: guanosine 5`-monophosphate. (Illustration adapted from www.mikeblaber.org)

The linkage between the monomers in the polymer is constituted by a phosphodiester bond. The phosphodiester bond connects the 5` and the 3` position of the neighboring nucleotides, thereby creating the polarity of the polymer.

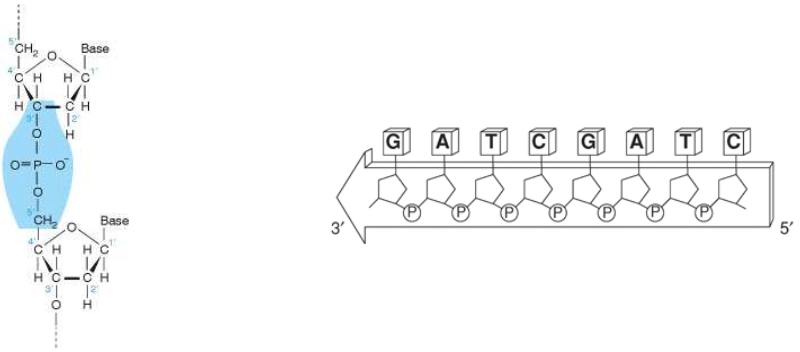

Figure 1.10 Linkage of the nucleotides by phosphodiester bonds (left) creating polarity (right). (Illustrations adapted from www.ncbi.nlm.nih.gov and www.media.wiley.com)

The linear polymer is called a **single strand** and the properties of the attached bases enable the polymer to form a dimeric structure by means of H-bonding with distinct pairing of A with T and C with G. Those pairs are called the canonical Watson Crick base pairs. The A-T base pair consists of 2 hydrogen bonds whereas the G-C base pair forms 3 hydrogen bonds. Building of the base pairs results in the formation of a **duplex** with distinct geometry. In a duplex the two strands interacting with each other pair in an anti-parallel arrangement. The polarity of the two single strands is in opposite direction.

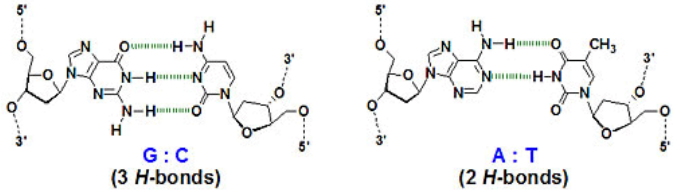

Figure 1.11 The canonical Watson-Crick base pairs: The G:C base pair (left) and the A:T base pair (right). (Illustration adapted from http://www.unit.aist.go.jp)

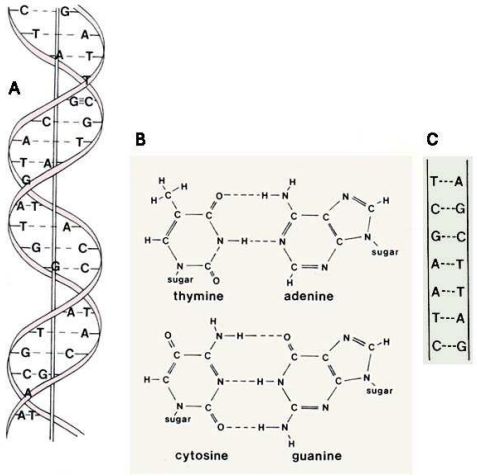

Figure 1.12 Formation of the duplex.

The formation of the duplex results in the formation of a helix, characterized by different parameters. There are two main conformations of the pentose sugar moiety, called the **sugar pucker s**ince the five-membered ring does not adopt a planar geometry but a puckered form. There exist mainly two different forms called the C2`-endo or south conformation (S) where the C2` of the sugar moiety is above the plane formed by the sugar and the alternative conformation is called the C3`-endo or north conformation (N), having the C3` of the sugar placed above the plane build by the sugar.

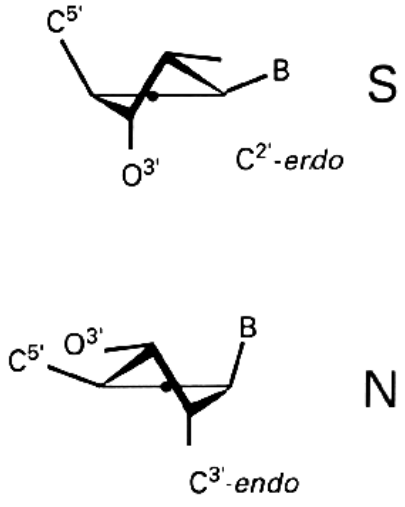

Figure 1.13 The sugar pucker: C2`endo/ S conformation (top), C3`endo/ N conformation (bottom). (Illustration adapted from www.online-media.uni-marburg.de)

The relative orientation of the base around the N-glycosidic bond is another conformational freedom and there are two different main conformations. Rotation about the N- glycosidic bond can interconvert these two conformations. The syn- form stands for the heterocyclic base placed above the sugar moiety whereas the anti-form places the base on the opposite side, away from the sugar.

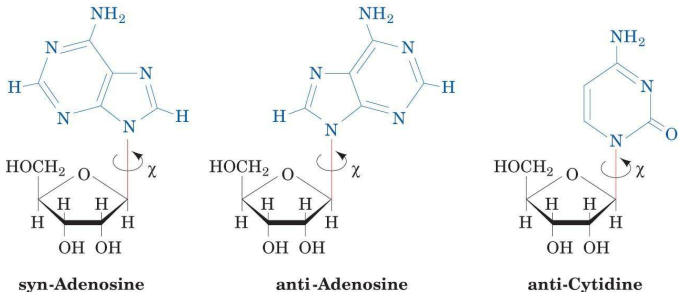

Figure 1.14 Conformation of the N-glycosidic bond: syn-Adenosine (left), anti-Adenosine (middle), anti-Cytidine (right). (Illustration adapted from www.siumed.edu)

The duplex formed by two single strands results in a double helix which in turn results in the formation of two grooves of different depth and width, formed by the two sugar phosphate backbones of each strand. These grooves are called minor and major groove and are an important characteristic of the overall geometry of the helix.

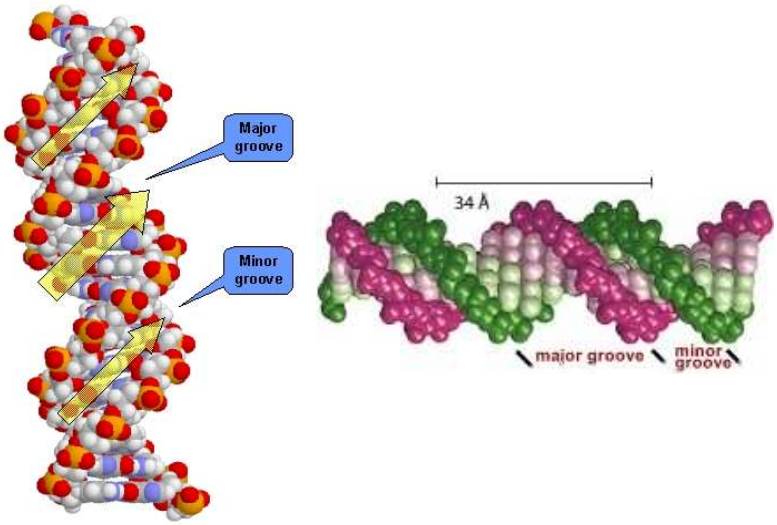

Figure 1.15 The two different grooves formed by B-DNA. (Illustration adapted from http://www.virtuallaboratory.colorado.edu)

The relative orientation of the bases constituting a base pair is also described in different parameters, such as the propeller twist. Besides the relative orientation of the bases in the base pair, even more important is the orientation of the base pairs relative to each other. An important example constitutes the twist describing the angle formed between two adjacent base pairs.

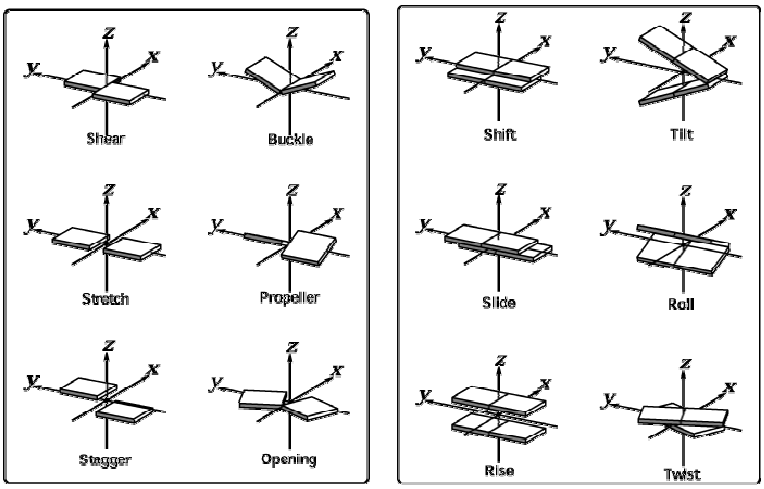

Figure 1.16 Relative orientations of the base to each other (left), relative orientation of the base pairs to each other (right). (Illustration adapted from www.3dna.rutgers.edu)

DNA exists as three major conformers described by the different parameters described above. These conformers are named A-DNA, B-DNA and Z-DNA.
B-DNA is the prototype and is commonly adopted by a DNA/DNA duplex in the fully hydrated form. A-DNA in contrast is observed when B-DNA is dehydrated in vitro. The unusual Z-DNA is found under increased ionic strength and is favoured in alternating purine/ pyrimidine sequences.

A-DNA and B-DNA both adopt right-handed helices whereas the Z-DNA adopts an unusual left-handed helix.

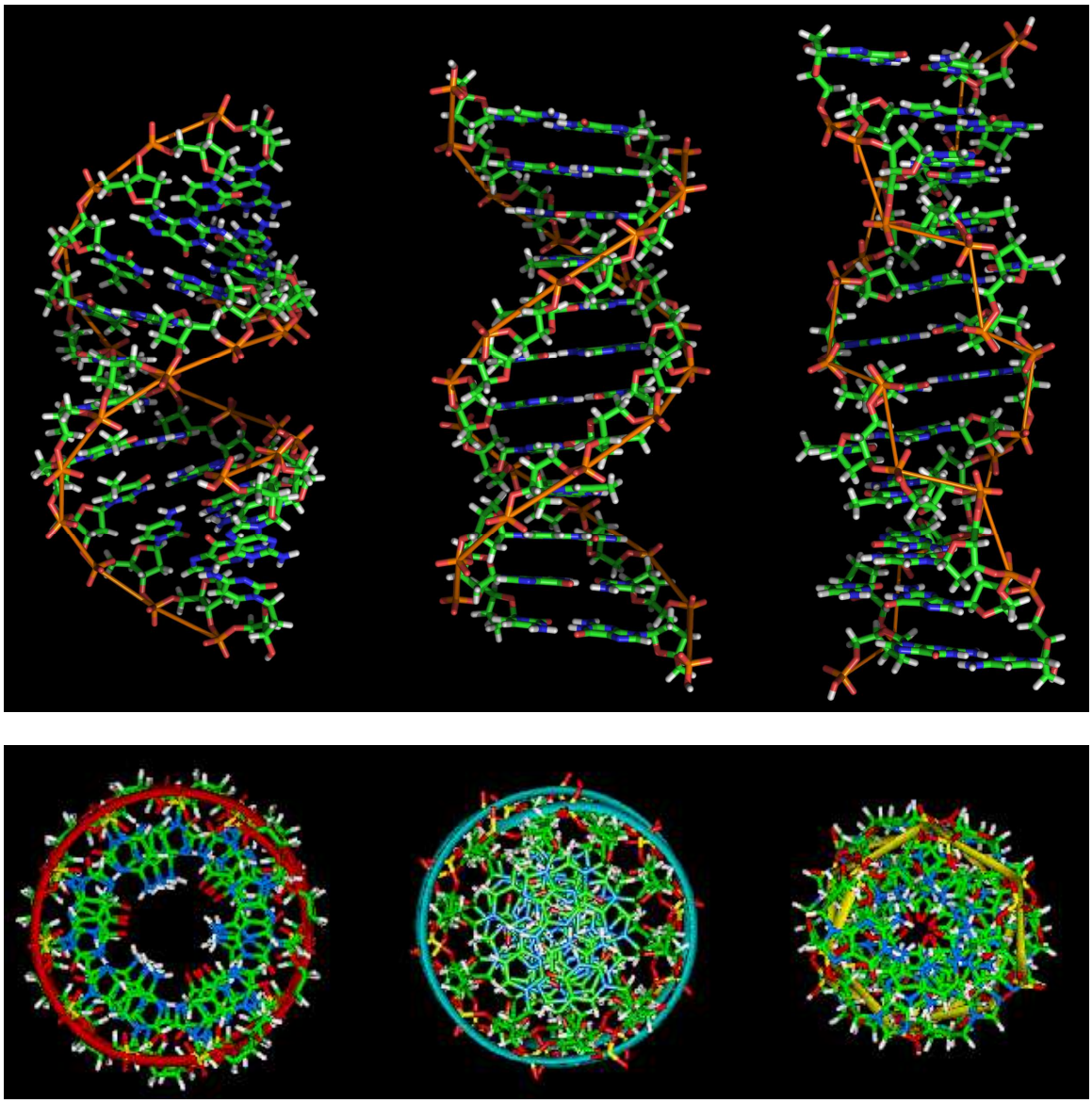

Figure 1.17 The three main conformers (front- and topview) of DNA: A-DNA (left), B-DNA (middle), Z-DNA (right).

Besides the most obvious difference of the helical sense the more subtile differences are found in the difference in sugar puckering and the glycosyl angle conformation. In the A-form the sugar pucker mode is C3`- endo in contrast to the C2`- endo conformation of the B-DNA form. In the Z-form the sugar pucker is alternating between neighbouring bases, namely the C2`- endo conformation is found for the pyrimidine bases and C3`- endo for the purine bases. Another difference is found in the conformation of the glycosidic bond.

A-DNA and B-DNA both have the anti conformation in all of their nucleotides whereas the Z-DNA has the pyrimidine bases *anti* and the purine bases *syn*.

Helix sense	Right-handed	Right-handed	Left-handed
Repeating helix unit	One base pair	One base pair	Two base pairs
Rotation per base pair	33.6°	t_t = 38.0° (4.4°)*	−60°/2
		t_g = 35.9° (4.2°)*	
Mean base pairs per turn	10.7	10.0 (1.2)*	12
Inclination of base normals to helix axis	+19°	−1.2° (4.1°)	−9°
Rise per base pair along helix axis	2.3 Å	3.32 Å (0.19 Å)*	3.8 Å
Pitch per turn of helix	24.6 Å	33.2 Å	45.6 Å
Mean propeller twist	+18°	+16° (7°)*	~ 0°
Glycosyl angle conformation	*anti*	*anti*	*anti* at C, *syn* at G
Sugar pucker conformation (Figs. 5 to 7)	C3′-*endo*	O1′-*endo* to C2′-*endo*	C2′-*endo* at C, C2′-*exo* to C1′-*exo* at G

Figure 1.18 The parameters of the three main conformers: B-DNA (left), A-DNA (middle), Z-DNA (right).

These differences are then manifested in the overall geometry of the helix besides the handedness. The repeating unit in the A- and B-form is one base pair and the rotation per basepair is a little smaller in the A-form than in the B-form resulting in 11 bases per turn in the case of A-DNA and 10 bases per turn in B-DNA. The Z-DNA in contrast has two base pairs as the repeating unit and 12 base pairs (6 dimers) per turn.

The grooves also differ in the three different conformers. In the case of the B-form the major groove is wide and the minor groove is narrow, in A-DNA the major groove is narrow and deep and the minor groove is broad and shallow. Z-DNA has a deep minor groove and a flattened out major groove.

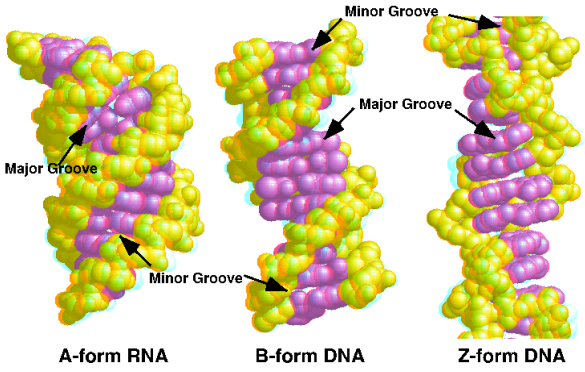

Figure 1.19 Comparison of the grooves of the different conformers: A-DNA (left), B-DNA (middle), Z-DNA (right). (Illustration adapted from http://www.profcupido.hpg.ig.com.br)

1.3.1 A closer look at Z-DNA

1.3.1.1 A brief history

In 1953, Watson and Crick propose the model for the right-handed double helical structure of DNA (based on fibre x-ray diffraction). The development of DNA synthesis resulted in the possibility of single-crystal x-ray diffraction. Pohl and Jovin showed in 1972 that the ultraviolet circular dichroism of poly(dG-dC) was nearly inverted in 4M sodium chloride solution (Figure 1.20.), thereby indicating the relationship between two "enantiomers" of the poly(dG-dC) sequence being R and L [13].

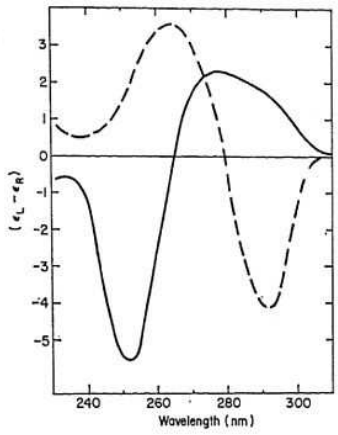

Figure 1.20 Circular dichroism spectra of poly (G-C). Salt induced change of the circular dichroism of poly d(GC), figure adapted from [13]. Solid line: 0.2 M NaCl, pH 7.2 at 25°C, dashed line: same solution after increasing the NaCl content to 20% (w/w).

In 1979 Alexander Rich et al. solved the first atomic resolution view of the double helix of the self-complementary $d(CG)_3$ hexamer. To their surprise the crystallized duplex showed in contrast what they would have expected a left-handed helix. This left-handed form was then named by the authors Z-DNA due to the "zig-zag like" nature of the phosphate backbone [14]. That the salt dependent nearly inverted circular dichroism spectrum of the poly d(G-C) motif found in 1972 corresponds to the left-handed Z-DNA, was confirmed in 1981 by comparing raman spectra of the $d(CG)_3$ crystals obtained by Rich et al. and solutions of DNA at 4M sodium chloride concentration [15].

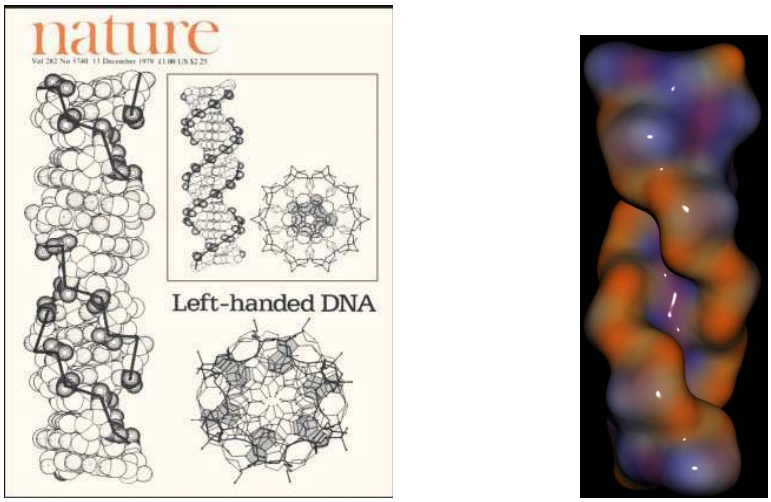

Figure 1.21 Cover page from Nature (left) adapted from [14], spacefilling model illustrating the zig-zag shape of the backbone (right), adapted from http://www.haveland.com

1.3.1.2 Structural features

The most obvious difference of Z-DNA is its helicity being left handed compared to the common B-DNA form. The original sequence which was found in the left-handed form was the alternating cytosine-guanine polymer, where this d(C-G) unit is the repeating unit (thus two base pairs) and the sugar pucker alternates between 2`- endo for the cytosine and 3`- endo for the guanosine. At the same time the guanosine adopts a *syn* conformation of the glycosidic bond and the cytosine adopts an *anti* conformation since the purine bases can have the *syn* conformation without paying any energy penalty as there is no steric block [16]. The sugar pucker being in the 3`- endo conformation results in bringing the negatively charged phosphate groups in closer proximity and therefore a repulsion under physiological ionic conditions happens. Although there might be a small fraction of the duplex in the Z-DNA conformation at physiological conditions, the repulsion puts the equilibrium far to the all 2`- endo conformation and hence to the B-form.

1.3.1.3 Conditions stabilizing Z-DNA

The most important requirement for the formation of left-handed Z-DNA is the sequence being an alternation of *purine-pyrimidine*. Not only the original found alternation of guanine and cytosine is suitable for the conversion to the left-handed form but also other purine-pyrimidine motifs are suitable although with different ease of formation. The order is the following: $d(GC)_n > d(AC)_n \cdot d(GT)_n >> d(AT)_n$. Not only the sequence plays an important role but also chemical modifications of the nucleobases can modify the formation of the left-handed helix. There exists the possibility of bromination of the C8 position of the guanine residue which facilitates the formation of Z-DNA at physiological salt concentrations. The bulky bromine atom put at the C8 of the guanine heterocycle shifts the *anti/ syn* equilibrium from the predominant *anti* conformation (having the proton on C8 in van der Waals contact with the sugar- phosphate backbone) to the *syn* conformation (with the bulky bromine atom pointing outwards of the helix with no constraints of size) thereby adapting the preferred alteration of *syn* and *anti* in the Z-DNA form [17]. Another possibility is the C5 position of cytosine, which can methylated and thereby facilitating the formation of the left-handed helix. In contrast to the bromination of C8 of the guanosine residue which simply shifts the *syn/anti* equilibrium and thereby supports the formation of Z-DNA, the reasons for the stabilizing effect of Z-DNA by methylation of cytosine residues is much more delicate. One possible reason is the methyl group leading to a destabilizing effect of B-DNA by interacting with water molecules in the major groove and a second reason could be the stabilization of Z-DNA through formation of a hydrophobic patch on the surface of the molecule [18, 19] Another important condition leading to the left-handed Z-form comes with high concentrations of mono- and bivalent salts, for example sodium chloride and magnesium chloride. It is also possible to induce the transition with low concentrations of multiple charged cations, for example the organic tetramine spermine or the inorganic cobalt (III) hexamine. For all cases the modification of a nucleobase can drastically lower the effective concentration of the salt needed for the transition to occur [18]. In Table 1 the different cations and the corresponding concentrations for the mid point of titration are shown for the unmodified poly d(GC) and the methylated of the 5 position of the cytosine residue poly d(Gm5C).

Ion	poly (dG-dC)	poly (dG-m5dC)
Na^{+}	2500	700
Mg^{2+}	700	0.6
Ca^{2+}	100 (strange CD)	0.6
Ba^{2+}	40 (strange CD)	0.6
$NH_3(CH_2)_2NH_3^{2+}$	no change up to 100 mM	1.0
$NH_3(CH_2)_3NH_3^{2+}$	no change up to 100 mM	1.0
$NH_3(CH_2)_4NH_3^{2+}$	no change up to 100 mM	2.0
$NH_3(CH_2)_5NH_3^{2+}$	no change up to 100 mM	30 (strange CD spectrum)
$Co(NH_3)_6^{3+}$	0.02	0.005
Spermidine $^{3+}$	B-form till 1 mM and then precipitation	0.05
Spermine $^{4+}$	B-form till 0.05 mM and then precipitation	0.002

Table 1.1 Concentrations of different cations at the midpoint of the B-Z transition for the poly (dG-dC) and poly (dG-m5dC). Ion concentrations in mM and all ions were added in the chloride form. All solutions contain 50 mM NaCl, 5 mM Tris, pH 8.0. The table is adapted from [17]

The observation that the chemically modified polymer poly (dG-5mdC) by means of methylation needed much lower concentrations of cations in order to change to the left-handed Z-DNA form hinted for a possible biological role of Z- DNA since the dinucleotide sequence m^5dC-dG occurs frequently in eukaryotic DNA and correlates with transcriptional activity of the corresponding gene [20]. Furthermore the presence of certain cations present at physiological conditions additionally pointed to a biological role of the left-handed helix of Z- DNA.

1.3.1.5 The B-Z junction

The possibility of segments of the alternating pyrimidine/ purine motif embedded in totally mixed sequences raised the question what happens in the region connecting the two segments? The formation of a junction between a right handed B-DNA and a left-handed Z-DNA was for a long time a field of speculation first on the mechanism and more pronounced on the exact structure of the junction [21, 22, 23]. Few years ago Rich et al. finally solved a crystal structure (at 2.6 Å resolution) of such a B to Z junction. [24] The crystal structure showed the breaking of one base-pair at the junction and that these

two bases were extruded and thereby making the transition from the right handed to the left handed helix possible.

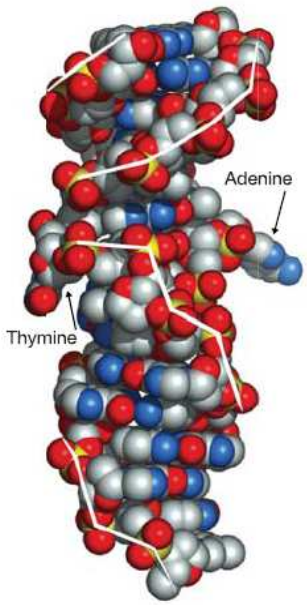

Figure 1.22 A van der Waals view of the 15-base-pair DNA structure containing a junction between left handed Z-DNA and right handed B-DNA (Illustration adapted from [24])

1.3.1.6 The Z-Z junction

Since the alternating pyrimidine/ purine motif is a requisite for the formation of the left-handed Z-DNA one can think of the emergence of a Z-Z junction by interrupting this alternating motif by addition or deletion of a base. Recently Rich and coworkers solved the crystal structure of such a Z-Z junction [25]. They show that the junction constists of a single base pair and that it leads to partial or full disruption of the helical stacking. In contrast to the B-Z junction the bases are not fully extruded and a contiuous stacking between the two left-handed helices is not possible.

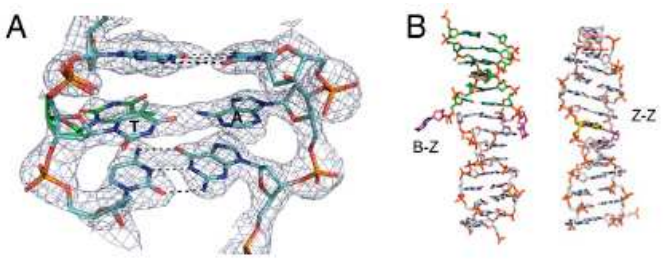

Figure 1.23 Electron density of the Z-Z junction (left) and comparison of the B-Z junction and Z-Z junction (right) (Illustration adapted from [25])

1.4 Thermodynamic factors associated with helix formation with DNA

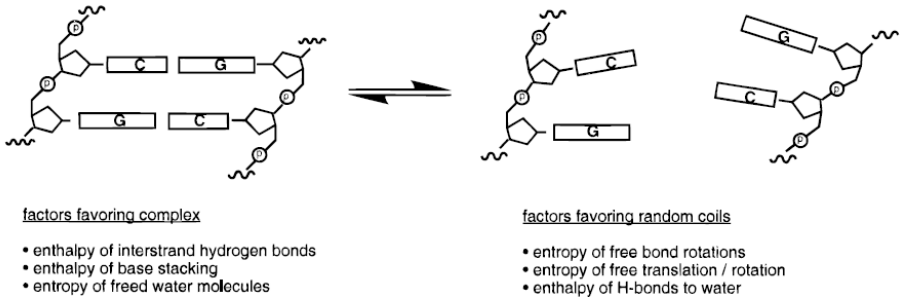

Figure 1.24 Illustration of the equilibrium between duplex and singlestrand and the factors favouring the two states

Looking at the thermodynamic factors associated with helix formation, the striking feature is the entropy term mainly favoring the random coil/single strand since upon hybridization the translational and rotational freedom of the single strand is lost as well the rotational freedom of the internal bonds. Another disfavoring factor is found in the hydrogen bonding of the nucleobases to water which must be broken and disturbed for the duplex formation, resulting in enthalpy reduction. In order to be a spontaneous reaction there is a major contribution of enthalpy. The enthalpy term results from the two major forces stabilizing the double helix: The force in the plane of the bases (horizontal) is the *hydrogen bonding* (base pairing) and the force perpendicular to the planes of the bases are the *π-π interactions* (base stacking).

1.4.1 Hydrogenbonding

Generally a hydrogen bond is formed if a hydrogen atom connects two atoms of higher electronegativity. These kinds of bonds can be either formed intramoleculary in a single

molecule or intermolecularly between different molecules like in DNA between the nucleobases. The strength of a hydrogen bond is weaker compared to an ionic bond or a covalent bond. In the context of DNA the Watson-Crick hydrogen bonds are responsible for the A-T and the G-C base pairing in the duplex. The role of the hydrogen bonds and their contribution in DNA have been the topic of several experimental and theoretical studies.

1.4.2 π-π interactions/ aromatic interactions

Aromatic or π-π interactions play an important role in a lot of biological systems such as peptides and DNA. But in contrast to hydrogen bonds which can be understood as electrostatic point-to-point interactions aromatic interactions are far more complex and are composed of several contributions of interactions which are shortly described.

Van der Waals interactions

This highly attractive interaction is the sum of the dispersion and repulsion energies and varies with r^{-6} and constrains the aromatic residues in Van der Waals contact (where r stands for the internuclear distance).

Electrostatic interactions between partial atomic charges

Electronegative atoms like nitrogen and oxygen polarize the electron density and so these and the neighboring atoms are associated with partial atomic charges. These interactions vary with r^{-1} and are therefore relatively long range effects. In DNA nucleobases which represent highly polarized aromatics the charges are relatively large. Therefore these are usually the largest single electrostatic interactions.

Electrostatic interactions between the charge distribution associated with the out of plane π-electron density

The charge distribution of aromatics is very characteristic. The nuclei form a positively charge sigma-framework which is sandwiched between two regions of negatively charged π-density. Electrostatic interactions between these charge distributions is not

favorable in a face to face stacked geometry however in a face to face offset stacked or t-shape geometry these interactions can be favorable.

Electrostatic interactions between the charge distributions associated with the out of plane electron density and the partial atomic charges

This term varies roughly with r^{-4} and is therefore quiet sensitive to geometry. It is also relatively large due to the large partial atomic charges.

Interaction of aromatic residues and solvent

This interaction has different names in literature such as solvation effect, desolvation, solvophobic force, solvation-driven force or hydrophobic effect. Suggesting by the number of different expressions used by different authors these interactions are debated controversially in literature.

1.5 Nucleic Acid guided Assembly of aromatic chromophores (based on [26])

1.5.1 Synthesis of oligonucleotide-chromophore conjugates

Offering a very sequence specific pairing as well as a defined geometry DNA emerged as a perfect candidate for the organization of aromatic chromophores for different purposes. There exist two different strategies for the attachment of the chromophores to the

oligonucleotides. The first possibility is the *post-synthetic approach* which means the conjugation of the desired chromophore to the preassembled oligonucleotide which bears functional groups which are then used to attach the chromophores via these groups. Suitable points of attachment are either reactive groups on the sugar moiety or the nucleobases as well as the 3`- or 5`- termini.

The second route used to attach chromophores is the *direct incorporation during oligonucleotide synthesis*. This approach offers the possibility of high flexibility in the number, type and placement of the chromophores. The prerequisite is the suitable functionalization of the chromophore prior to incorporation. By convenience these modifications follow the protection and reactivity scheme of phosphoramidite chemistry.

The approach of direct incorporation during oligonucleotide synthesis can be divided into two classes of modifications: one compromises the chromophores directly attached to either the sugar moiety or to the nucleobase. These *nucleoside-based* building blocks have the possibility to engage in Watson-Crick base pairing interactions and therefore may support high target specificity. There are many sites of attachment possible although the 5`-position of the pyrimidine bases takes an important role as the modification at this site does not interfere with base-pairing. There is either the possibility to attach a chromophore at a certain position of the nucleobase, replacing the nucleobase by alternative chromophore or even the extension of the aromatic system of the nucleobase itself.

The second class of modifications is the class of the *non-nucleosidic* chromophores. These chromophores are neither linked to a nucleobase nor to a sugar moiety. Although not capable of Watson-Crick base pairing these derivatives represent suitable and versatile building blocks which can be incorporated into DNA. There exist a large variety of different molecules with versatile characteristics which can be incorporated and used for various purposes; not only for basic research but also for diagnostic tools as well as novel materials with different and also tunable properties.

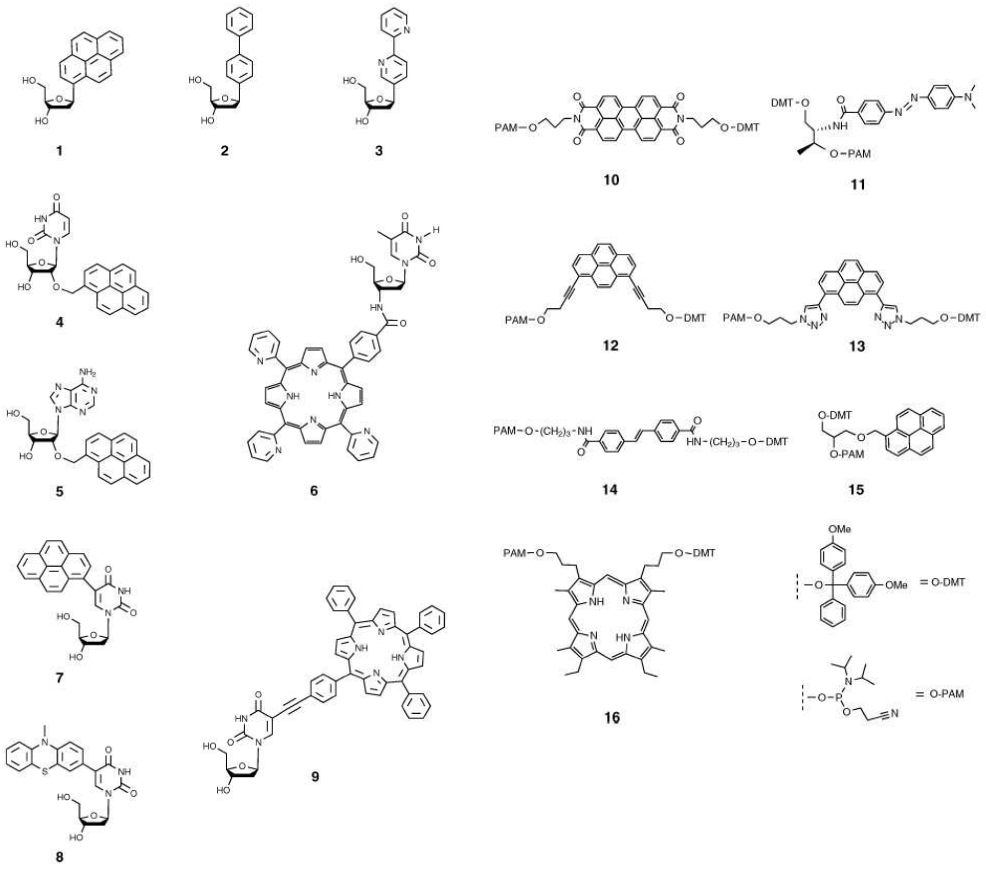

Figure 1.24 Selected examples of chromophore-containing nucleoside analogues (1-9) and non-nucleosidic ananlogues (10-16) (illustration adapted from [26])

1.5.2 Assembly of chromophores in a DNA framework

The conformation of a chromophore which is attached to DNA strongly depends on several factors as the site of attachment, the type and length of the connecting linker as well as the nature of the chromophore itself. Chromophores which posses an extended aromatic system are often involved in pi-pi interactions either with the neighboring nucleobases or among themselves if multiple incorporations are present. These interactions are possible by an intercalative mode if the site of attachment and the nature of the linker permit this binding mode geometrically. Another possibility is the binding of the chromophore either to the major or minor groove. This is mainly the case if the chromophore is attached to the 5`-position of the pyrimidine nucleoside or the 2`position of the sugar moiety. If multiple incorporations are present in close proximity these can

interact among themselves and form aggregates. In these systems DNA can be regarded as the framework for the precise arrangement of chromophore which can then interact with each other and from aggregates. These interactions among the chromophores as well as between the chromophores and the nucleic acids part depend on a number of different properties such as hydrophobicity, size, charge, polarity, hydrogen bonding ability and aromaticity. The possible influence and effect of these chromophore aggregate on duplex integrity and stability can be of various nature and is often almost impossible to predict. A further group of conjugates are hybrids between segments of DNA and segments of chromophores. In these chimeras the non-DNA sections can be organized in a specific way depending on the nature of the chromophores and the DNA part.

1.5.2.1 Intercalative Binding

As intercalation is one of the most important binding modes of chromophores in the context of DNA-chromophore-interaction it was realized that placing a suitable aromatic intercalator can greatly enhance the affinity for the complementary strand and thus increasing the duplex stability. The change in the spectroscopic properties of the chromophores upon binding and thus intercalation lead to the development of detection of base deletion for example by Asanuma and Coworkers [27] by introducing two threoninol-derived pyrene building blocks which show only monomer emission in the wildtype by intercalation where as an excimer signal is detected if the opposite base is deleted (Figure 1.25).

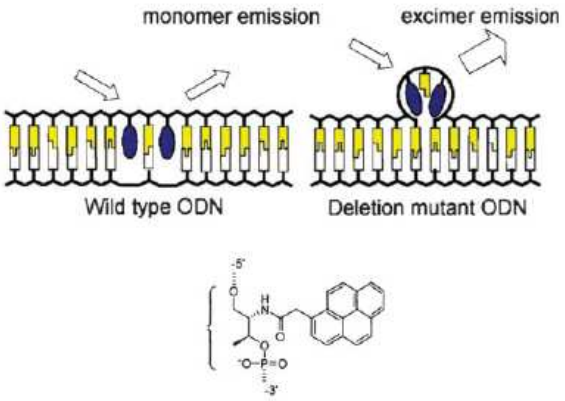

Figure 1.25 Threoninol-derived pyrene building blocks give rise to excimer fluorescence upon hybridization to a deletion mutant (Illustration adapted from [26])

Placing an intercalator opposite an abasic site normally leads to a significant increase in hybrid stability compared to the case when the natural nucleobase is placed opposite the abasic site. Furthermore the intercalation of an appropriate chromophore may bring a significant spectroscopical change of the chromophore. Shimidzu and coworkers [28] showed that placing the non-nucleosidic acridine derivative opposite an abasic site is accompanied by a considerable increase in the fluorescence signal (Figure 1.26 A). The increase of thermal stability by placing aryl-substituted nucleosides opposite an abasic site could be shown by several groups and Kool and coworkers [29] could show by NMR that a pyrene derived nucleoside can stack between the neighboring bases (Figure 1.26 B) and Leumann and coworkers [30] investigated hybrids with biphenyl and bipyridyl derivatives (Figure 1.26 C). The non-nucleosidic pyrene and phenanthroline derivatives [31] also showed a stabilizing effect on the hybrid stability when placed opposite an abasic site (Figure 1.26 D). The group of Wengel [32] investigated constructs with up to four pyrene-abasic site pairs separated by canonical base pairs with a pyrene-modified α-L-LNA and found a pronounced increase in fluorescence signal intensity upon hybridization (Figure 1.26 E).

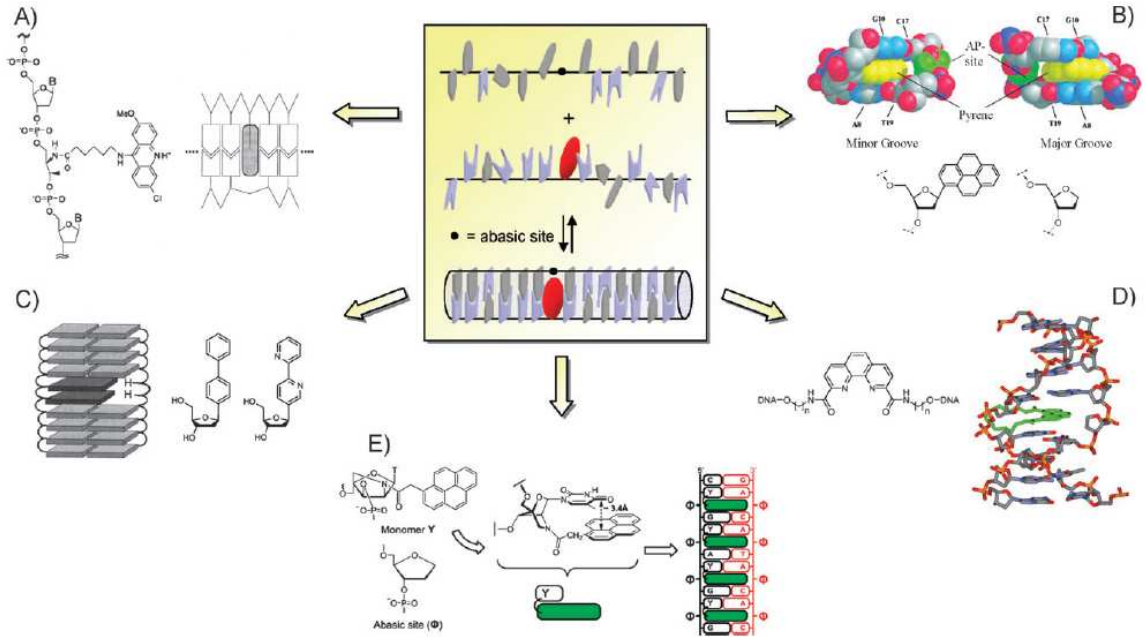

Figure 1.26 Arrangement of chromophores at abasic sites: (A) use of a threoninol-derived acridine derivative. (B) structure of a pyrene C-nucleoside stacked between nucleobases at an abasic site. (C) stacked arrangement of biphenyl and bipyridyl C-nucleosides. (D) stabilization of an abasic site by a non-nucleosidic phenanthroline building block. (E) double helical constructs containing multiple pyrene-modified α-L-LNA building blocks at separately located abasic sites (Illustration adapted from [26])

1.5.2.2 Interstrand stacking of aromatic chromophores

If the chromphores are situated in opposite positions in the DNA duplex they can interact and communicate with each other by an *interstrand stacking mode.* The interstrand interactions can be of hydrogen-bonding nature but in the context of aromatic building blocks the main contribution is found in π-π interaction between the chromophores. Pedersen and Christensen [33] showed double helical hybrids containing a trihydroxypropyl derived pyrene building block which when put in opposite position could interact by interstrand stacking which was confirmed by NMR analysis (Figure 1.27 A). The same strategy was used for the non-nucleosidic derivatives of phenantrene, phenanthroline and pyrene [34] which all from stable hybrids. Furthermore the fluorescent properties of the pyrene chromophore could be used to monitor the hybridization process by changing from the monomer emission in the single strand to the excimer emission upon hybridization when two pyrene moieties come into close proximity (Figure 1.27 B). Leumann and coworkers [35] proposed an interstrand stacking motif of sugar-based biphenyl derivatives with different substituents (Figure 1.27 C). For a pair of nitro- and methoxy-substituted biphenyls the interstrand stacking mode was confirmed by NMR analysis.

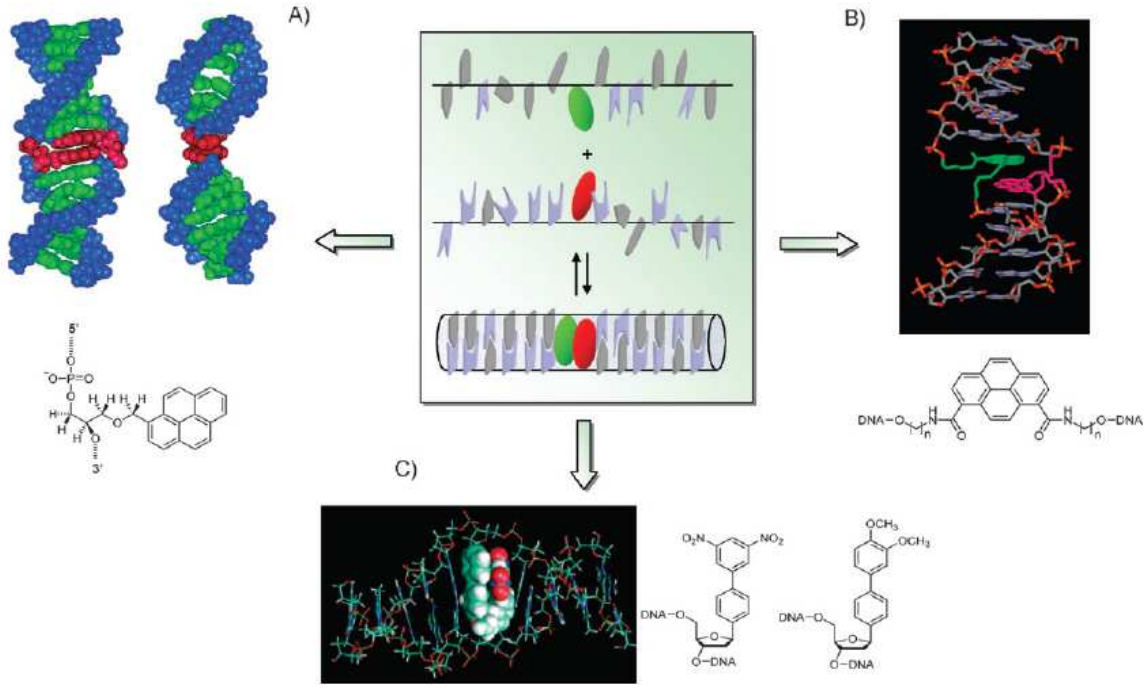

Figure 1.27 Interstrand stacked chromophores: (A) pyrene building block connected via a trihydroxypropyl linker. (B) non-nucleosidic pyrene dicarboxamides. (C) bisphenylic C-nucleosides. (Illustration adapted from [26])

1.5.2.3 The double helix as a scaffold for chromophore assembly: formation of arrays in the major and minor groove

As the double helix represents a rigid and well defined framework the attachment of multiple chromophores to it can result in well defined arrays of chromophores. The attachment via short and rigid linkers to either the nucleobase or the sugar moiety leads to the formation of π-stacked aggregates. The location of attachment can have an influence weather the chromophore array is located in the minor or major groove of the double helix. There exist several reports on the interaction of two chromophores which are attached in this way and the chromophore of choice in most of these reports is pyrene due to its fluorescence properties. Korshun and coworkers [36] described the formation of excimers in the major groove of 2`-arabino-linked pyrene derivatives if the pyrene containing building block were placed 3` to each other and separated by one base pair. Kim and coworkers [37] could also show excimer formation in the major groove by attaching the pyrene moiety in the 8-position of uracil and the 5-position of adenine. The

formation of excimers in the minor groove of DNA could be shown by the group of Wengel [38] with 2`-amino-LNA building blocks. Placing pyrene at the 2-position of adenine in RNA leads as well to excimer formation in the minor groove as could be shown by Engels and coworkers [39].

The arrangement of more than two incorporations of chromophores can lead to π-stacked arrays. Yamana and coworkers [40, 41] investigated such a system in which the hybridization process of RNA leads to the formation of a pyrene array along the minor groove which could be shown by a distinct CD signal of the pyrene units. An array of four pyrene units could be formed by attaching the pyrene units to the 2`-position of the ribose of one of the hybridizing singlestrand. They could extend the number of aligned pyrene units up to 10 when both strands were modified (Figure 1.29 A). Stulz and coworkers [42, 43] described a system where they could arrange terphenylporphyrine molecules along the major groove in DNA by attachment at the 5-position of pyrimidine. Hybrids containing up to eleven aligned porphyrine moieties could be shown later on by the same group (Figure 1.29 B). The group of Wagenknecht [44] investigated a double helix with five adjacent chromophores. Pyrene and phenothiazine were linked to the 5`-position of uracil and they form regular arrays when hybridized to the complementary non-modified singlestrand. The optical properties were depending on the composition of the modified singlestrand and the spatial arrangement of the two chromophores (Figure 1.29 C).

1.5.2.4 DNA-assisted self-organization of chromophore segments

Besides the organization of nucleosidic chromophores which can arrange either in the major or minor groove of DNA or RNA there exists also the possibility of putting multiple non-nucleosidic building blocks in the context of DNA. Asanuma and coworkers reported the multiple incorporations of the chromophore methyl-red via the chiral threoninol linkers into DNA [45]. The interstrand interactions were proofed by NMR analysis and they could show that the helical sense of the dye aggregate was depending on the absolute configuration to the chiral linker. (Figure 1.29 D) Baumstark and Wagenknecht recently showed the assembly of up to six perylenediimide moieties in an

alternating interstrand stacking mode [46]. The chromophores were incorporated using a (S)-aminopropan-2,3,-diol-linker in the middle of a DNA duplex forming alternating sequences of perylenediimides with thymines or an abasic analogue (Figure 1.29 E). In our group it was shown that extended stretches of an achiral non-nucleosidic pyrene building block [47] can form well defined double helical structure depending on the number of pyrenyl units (Figure 1.29 F).

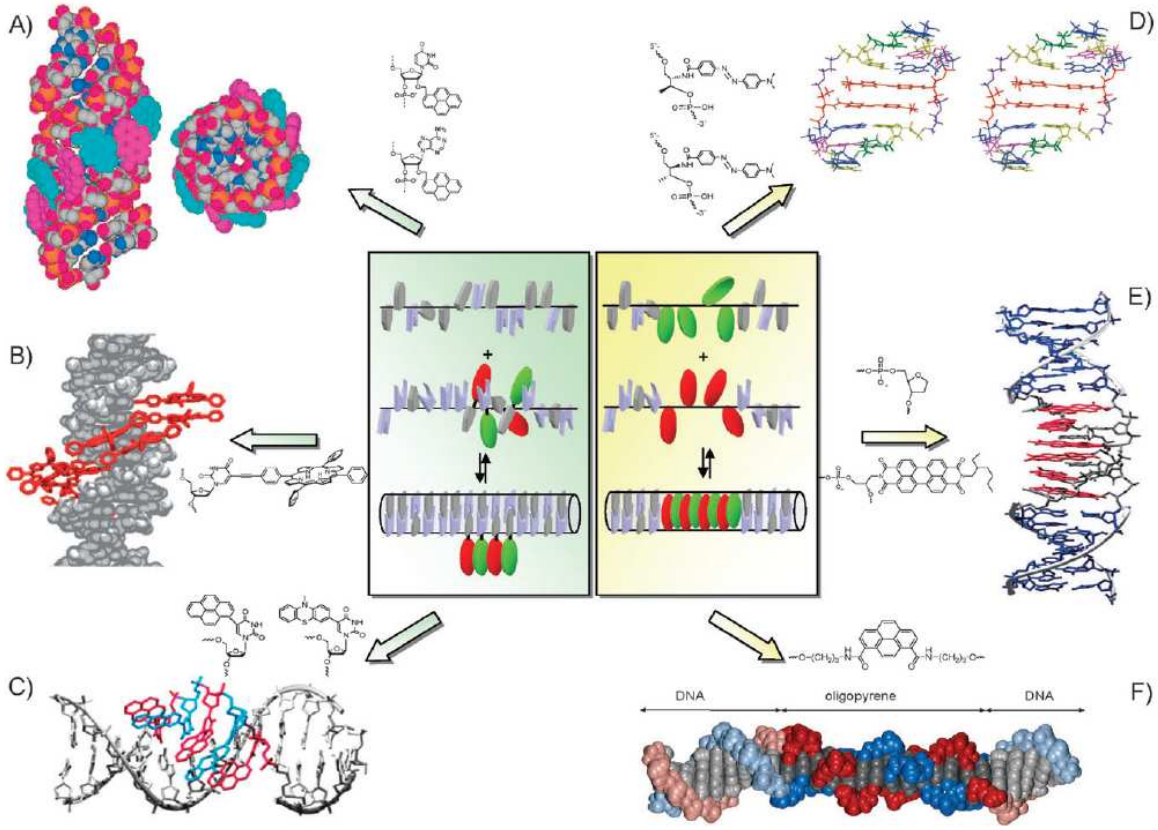

Figure 1.28 Oligonucleotide-assisted self-organization of chromophores: (A) formation of pyrene arrays in the major groove of an RNA duplex. (B) assembly of porphyrines in the DNA major groove. (C) alternating pyrene and phenothiazines assembled in the major groove of DNA. (D) methyl-red dyes froming an ordered structure within a DNA duplex. (E) interstrand stacked perylenediimides in a DNA duplex. (F) helical organization of oligopyrene segments in a DNA framework (Illustration adapted from [26])

1.5.2.5 Chromophore-guided assembly of nucleic acids

In all the examples above the guiding or dictating role was always taken by the nucleic acid part and not by the chromophores. But there exist a few examples where the leading

role or an equal important role is taken by the assembly of chromophores. In our group the assembly of a hybrid containing seven non-nucleosidic chromophores and five base pairs of DNA were shown to form a well ordered and stable duplex [48]. The formation of the five base pairs would not be possible without the stabilizing forces exerted by the formation of the interstrand stacked chromophores on one side and on the other side the base pairs are important for the unidirectional arrangement of the pyrene units (Figure 1.29 A). Li and coworkers designed a singlestrand of oligonucleotide with several incorporated perylenediimide derivatives which form loose structures at room temperature but upon heating form increasingly ordered aggregates of perylenediimde moieties [49]. Addition of the complementary oligonucleotide strand promotes hybridization induced unfolding of the ordered aggregates (Figure 1.29 B). Lewis and coworkers [50] found that using a non-nucleosidic perlyenediimde building block the synthesized conjugated can adopt either a duplex or a hairpin dimer structure depending on the sequence used (Figure 1.29 C). Iwaura and Shimidzu and coworkers describe the formation of J-aggregates of phenylenevinylen- or anthracene-connected thymidylic acid dimers [51, 52]. The assembly on an oligoadenylic strand of the thymines leads to a helical supramolecular structure of the chromophores (Figure 1.29 D).

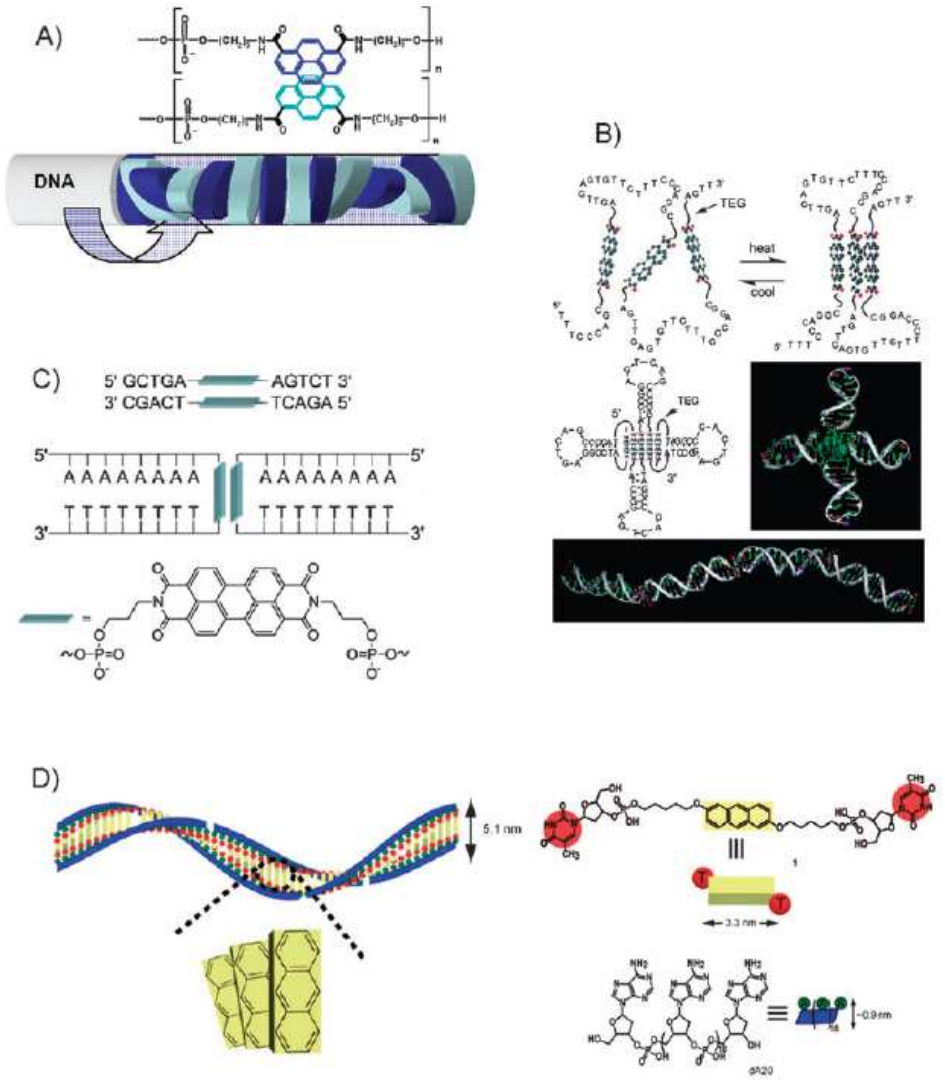

Figure 1.29 Organized structures of DNA-chromophore conjugates: (A) Formation of a bisegmental DNA-oligopyrene duplex. (B) Thermophilic foldable polymers composed of DNA and perylenediimde units. (C) PDI-linked oligonucleotides assemble into a duplex of form dimeric hairpin structure depending on the DNA sequence. (D) Formation of helical J-aggregates of anthracene-connected thymidylic acid dimers assembling on oligo-A strands (Illustration adapted from [26])

1.6 DNA based molecular switches

As DNA can change its helicity from the right-handed B form to the left-handed Z-form there were investigated different conjugates of a DNA part able to change its helicity with a variety of chromophores. The offered polymorphism of DNA was first used by Seeman and coworkers [53] as a mechanical switch. By the introduction of an alternating CG segment between two rigid DNA double crossover segments where one domain only of

the rigid structure is connected to the switching element where to the other domain two different fluorophores are attached they could show the FRET taking place only in the B-form. After switching to the Z-DNA form the fluorophores are changing their relative orientation and no FRET is detected (Figure 1.30).

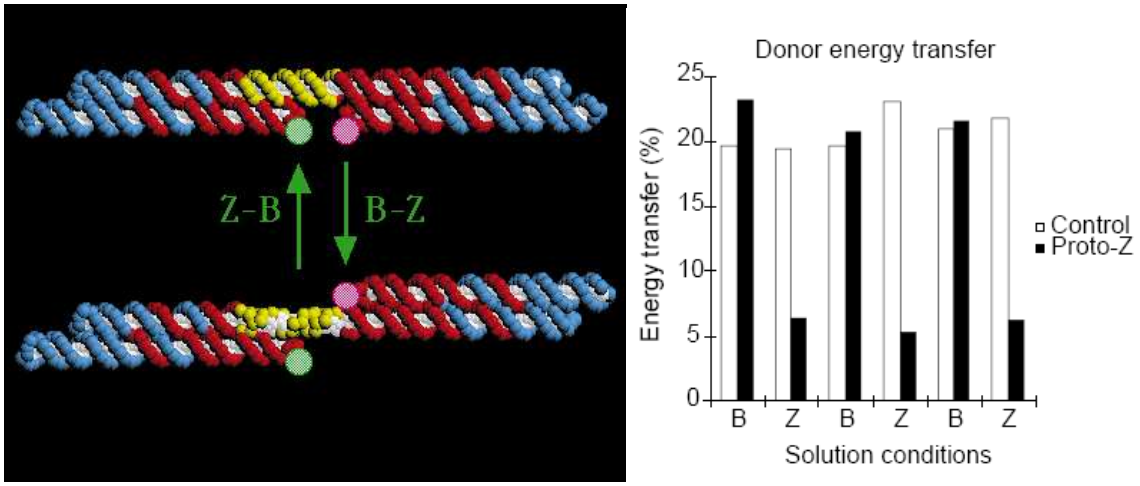

Figure 1.30 A nanomechanical device based on the B-Z transition of DNA. Schematic representation of the device (left) and the donor energy transfer depending on the nature of the connecting DNA (right) (Illustration adapted from [53])

The group of Saito [54] developed a fluorescent sensor which is able to follow the transition of the B to Z DNA form by change in the emission wavelength. They attach two pyrene derivative to the 5-postion of a cytosine and to the 8-position of a guanine residue. In the B-form the two pyrene moieties are exhibiting monomer emission only whereas in the Z-form they are getting in close proximity resulting in an excimer type of emission (Figure 1.31).

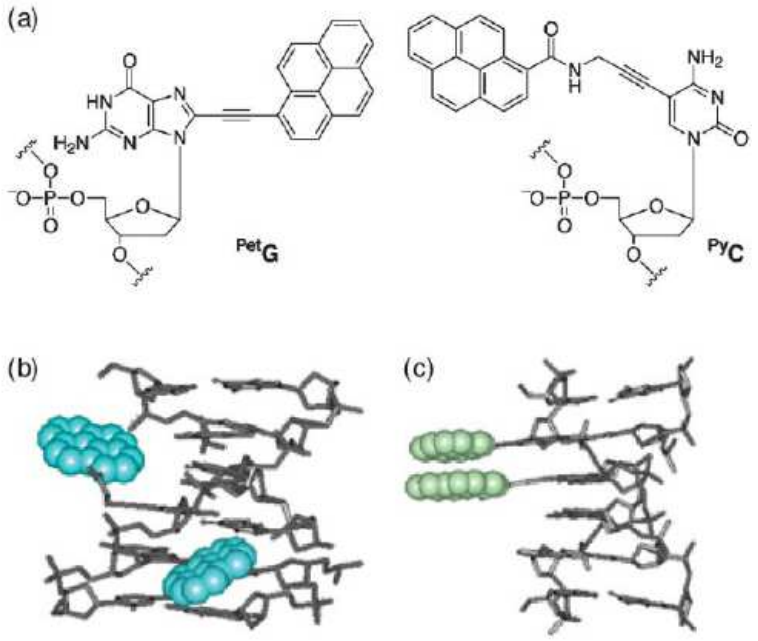

Figure 1.31 Structure of the pyrene modified nucleosides (a), molecular modeling of B-DNA containing the two modifications (b), molecular modeling of Z-DNA containing the two modifications (Illustration adapted from [54])

Also Berova and coworkers [55] established a conjugate between a CG sequence and a 5`-labeled non-nucleosidic porphyrine derivative which is able to monitor the change in helicity of the oligonucleotide part. They used the change in exciton coupled CD of the two porphyrine molecules communicating with each other differently based on the angular orientation of the dipole moments depending on the helicity of the oligonucleotide (Figure 1.32). The group

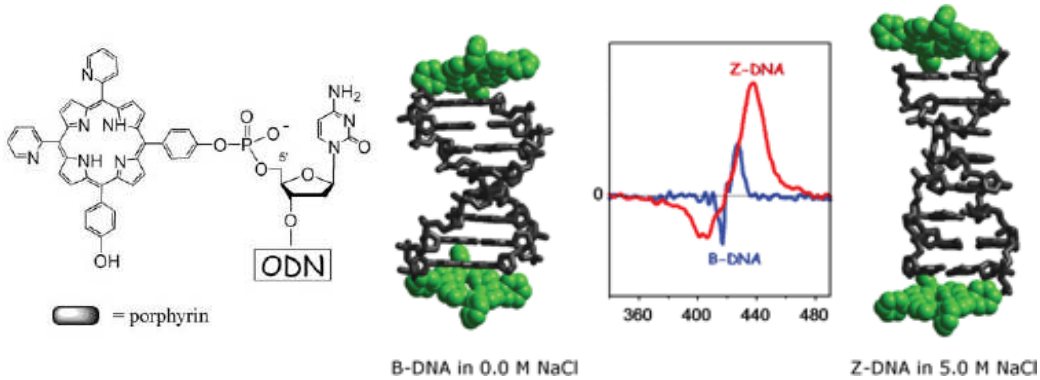

Figure 1.32 Structure of the pyrene modified nucleosides (a), molecular modeling of B-DNA (left) and Z-DNA (right) containing the two modifications with the corresponding CD signals inbetween (b) (Illustration adapted from [54])

The group of Sugiyama demonstrated a molecular switch based on the B to Z transition of DNA as well as the A to Z transition of RNA [55]. The fluorescent signal of the aminopurine used changed upon heating in both cases on a reversible basis. As the Z form of DNA is more stable at lower temperatures and the Z form of RNA is more stable at higher temperatures they could use these two switches comlementary (Figure 1.33).

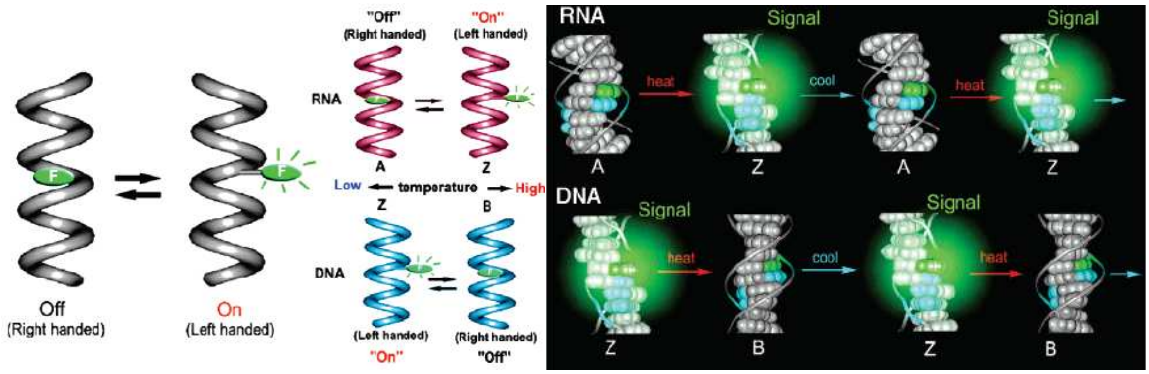

Figure 1.33 Concept of the on and off state based on the helicity (left), concept of the reversible thermal switching with the fluorescent signal as the output (right) (Illustration adapted from [55])

Inuye and coworkers recently developed an induced circular dichroism probe with a chromophore-linked alkynyldeoxyribose skeleton [56]. They could show that the chromophore attached to the 5`-end gives only an induced signal under conditions used for the left handed Z-form of DNA. Furhtermore they concluded that the modification applied does indeed facilitate the B to Z transition. (Figure 1.34)

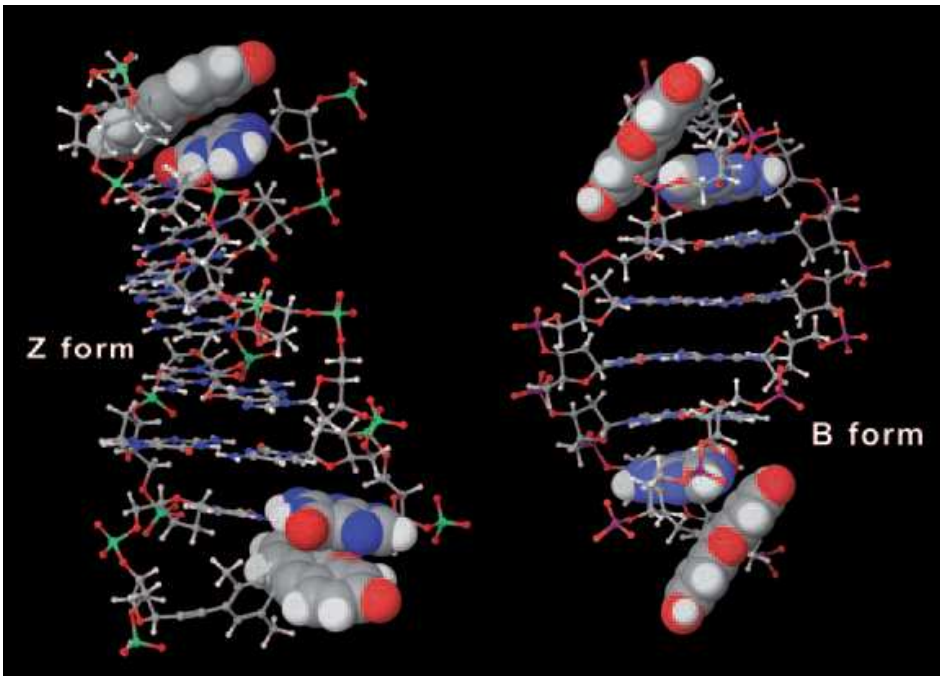

Figure 1.33 Molecular models for the B- and Z- form with the attached chromophore and the guanine bases at 5`- and 3`-end highlighted (Illustration adapted from [56])

1.7 Aim of the work

The assembly of nucleosidic as well as non-nucleosidic modified chromophores in the context of DNA or RNA has been shown to be of great use as DNA offers a scaffold with well known geometric features, variable sequence which can be designed for the used purpose and a rigid structure. The chromophores mostly adapt to the geometrical environment of the DNA structure as shown in chapter 1.5 for various examples and by changing the site of attachment or changing the nature of the linking unit the arrangement of the chromophores can be altered or modified. In our group the helical organization of the non-nucleosidic pyrene carboxamide has been extensively studied and the influence of the number of incorporated units has been shown to play a crucial role. The positive chirality of the pyrene units has been mainly ascribe to the helical nature of the DNA part namely the right handed form of B-DNA. To get deeper insight into this information transfer from the DNA part to the artificial pyrenyl part the question was arising weather a revearsal of chirality in the DNA part could eventually result in a change in chirality of the pyrene part. As the artificial non-nucleosidic chromophore the pyrene carboxamide with the C3 linker is used in all the studies. For the DNA part the well known alternating

cytosine/ guanine motif was chosen as being able to change from the right-handed B-DNA to the desired left-handed Z-DNA.

As a further aim the design and characterization of a new aromatic building block is formulated which can be incorporated into DNA and the influence on duplex stability and integrity can be studied. Furthermore interesting fluorescent properties can be investigated as well as interstrand interactions.

Chapter 2: Influence of a B-Z transition on chromophore organization in bisegmental chimeric constructs

2.1 Abstract

In this chapter the two segmental chimeras between a DNA and a pyrenyl part are studied with varying the number of pyrene units. It is shown that the pyrene units show a distinct dependence on the number incorporated and the behavior is first dictated by the oligonucleotide part when only one or two pyrene units are incorporated in the single strand, an intermediate position with no dominating part for three and four units in the singlestrand and an independent organization of they pyrene units for 5, 6 and 7 units.

2.2 Introduction

Previously it could be shown that a stack of non-nucleosidic pyrene building blocks can arrange in a helical fashion following the right-handed helicity of the canonical B-DNA [47, 48]. It was shown that the number of non-nucleosidic modifications play a crucial role in the ability to form a distinct helical arrangement. The amount of pyrene units was found to be at least six modifications in the singlestrand and twelve units in the duplex respectively. It was concluded that the arrangement of the pyrenyl units is not sequence dependent, so weather an AT base pair or an GC base pair is directly attached does not play an important rule. Furthermore the pyrenyl units showed also a similar behavior when not placed between two DNA sequences but only attached from one side of the stretch to an oligonucleotide part [48]. These studies so far included only seven pyrene units in the DNA end-attached arrangement or a bisegmental nature of the chimera. The idea was to investigate also a bisegmental chimera but with a DNA segment which should be able to change its helicity based on elevated ionic strength and study the possible influence it could have on the oligopyrenyl stretch. The study was also carried

out by varying the number of non-nucleosidic pyrenyl building blocks from one to seven in the singlestrand and two to fourteen in the duplex respectively.

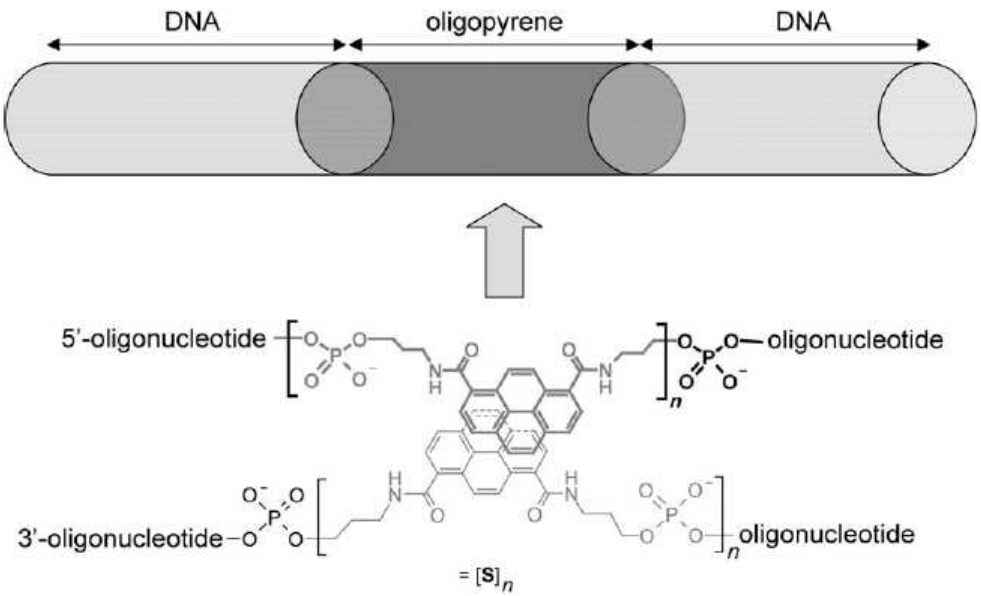

Figure 2.1 Sandwich-type arrangement of a non-nucleosidic oligopyrene stretch (Illustration adapted from [47]).

2.3 Results and discussion

The sequences in this study all contain the same natural oligonucleotide part which is the alternating d(CG) sequence which should be basically able to change its helicity from the right handed canonical B-DNA to the left-handed Z-DNA under appropriate conditions. To this common sequence which could act as a switchable element in the chimera the non-nucleosidic building block carboxamide pyrene with a C3 linker was attached from one building block up to seven building blocks per strand. Because of the polarity of the singlestrands containing d(CG)sequence (5` to 3`) and the bisegemental nature of the chimeras there had to be synthesized always two strands in order to get the desired duplex formed (**D1-II** to **D7-II**). Duplex **D8-II** was already available and represents a control sequences which does not contain the alternating CG motif and thus is not supposed to form the left-handed helix (Table 2.1).

Entry	Oligo #	Duplex
D1-II	**ON1-II** **ON2-II**	(5') CGCGCGCG **S** (3') GCGCGCGC **S**
D2-II	**ON3-II** **ON4-II**	(5') CGCGCGCG **SS** (3') GCGCGCGC **SS**
D3-II	**ON5-II** **ON6-II**	(5') CGCGCGCG **SSS** (3') GCGCGCGC **SSS**
D4-II	**ON7-II** **ON8-II**	(5') CGCGCGCG **SSSS** (3') GCGCGCGC **SSSS**
D5-II	**ON9-II** **ON10-II**	(5') CGCGCGCG **SSSSS** (3') GCGCGCGC **SSSSS**
D6-II	**ON11-II** **ON12-II**	(5') CGCGCGCG **SSSSSS** (3') GCGCGCGC **SSSSSS**
D7-II	**ON13-II** **ON14-II**	(5') CGCGCGCG **SSSSSSS** (3') GCGCGCGC **SSSSSSS**
D8-II	**ON15-II** **ON16-II**	(5') GCTAG **SSSSSSS** (3') CGATC **SSSSSSS**
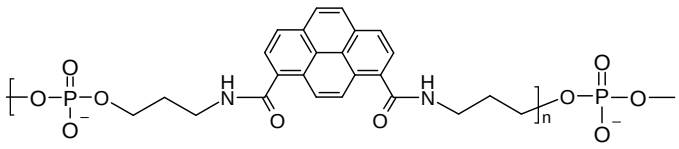 **S**		

Table 2.1 The sequences **ON1-II** to **ON16-II** and the non-nucleosidic pyrene building block (**S**) used in this study.

Temperature dependent UV-Vis

Using the absorption at different temperatures and at low and high ionic strength the hybrids could be studied on different levels. The absorption spectra offer different regions which can be attributed to either absorption of the natural bases only, the pyrenyl moieties only and the superposition of the two absorption regions. Especially the

absorption region of the pyrenyl moieties only was of main interest since it enables to give a statement on the organization of the units in the context of the formed hybrid. Another parameter of interest is the observed hyperchromicity upon heating the solution, comparing the absorption at room temperature and at 90°C. Last but not least the difference in the spectra comparing the low ionic strength case with the high ionic strength case can lead to some preconclusion about the influence of the natural on the artificial part.

The temperature dependent UV-Vis spectra of **D1-II** show a hyperchromic effect upon heating in the different areas of absorption. Furthermore the isosbestic point at 364 nm can be used as a hint for a two state model (Figure 2.1). A melting temperature of the hybrid was determined to be 71.5°C in the case of 100 mM NaCl and 68°C at 4 M NaCl (Figure 2.2).

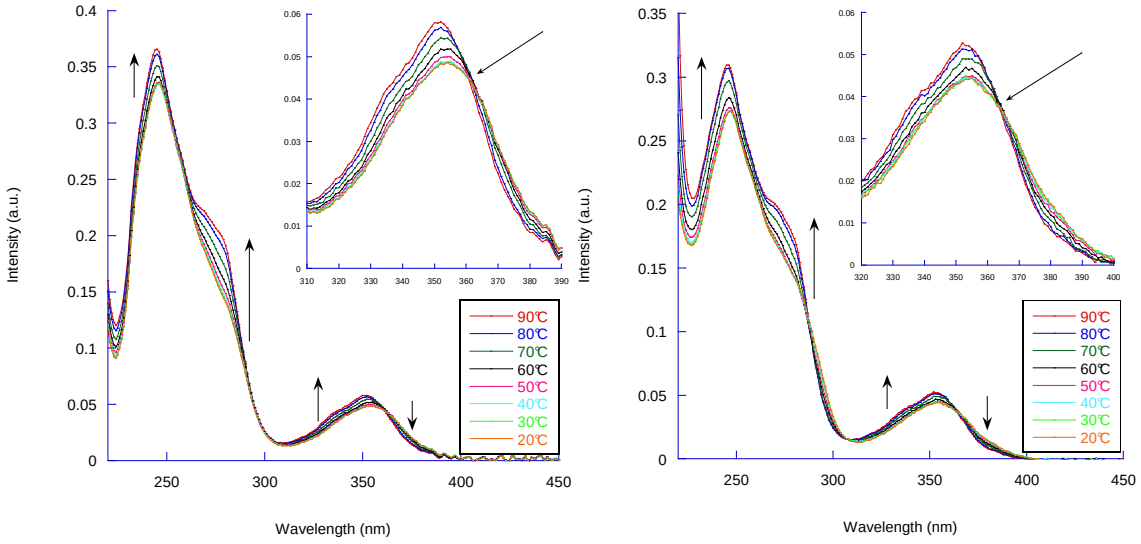

Figure 2.1 Temperature dependent (arrows indicate increase in temperature) UV-Vis spectra of hybrid **D1-II** at (*left*) low ionic strength (100 mM NaCl) and (*right*) at high ionic strength (4 M NaCl) with insets showing the isosbestic points indicated by an arrow; conditions: 1 µM singlestrand concentration, 10 mM phosphate buffer (pH 7.4).

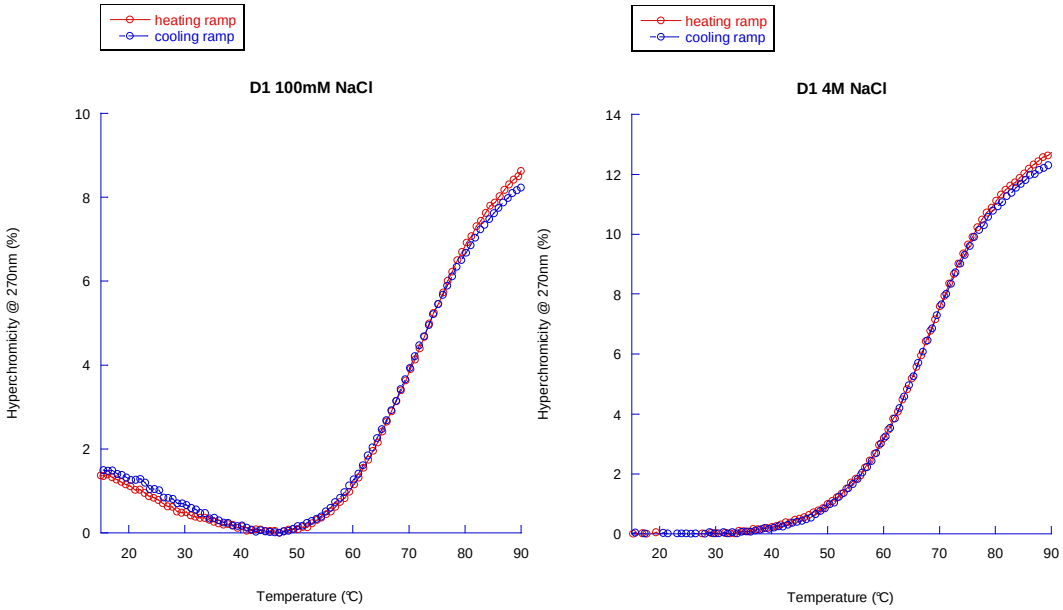

Figure 2.2 Melting profile of hybrid **D1-II** monitored at 270 nm at (*left*) low ionic strength (100 mM NaCl) and (*right*) at high ionic strength (4 M NaCl); conditions: 1 µM singlestrand concentration, 10 mM phosphate buffer (pH 7.4).

Temperature dependent UV-Vis spectra for all the other hybrids were recorded and there is a hyperchromic effect upon heating visible in all hybrids although to different extend. For hybrids **D1-II** to **D4-II** there is always an isosbestic point observable in the low energy absorption band of the pyrenyl units supporting a two state model. The melting profiles recorded show a larger hyperchromic effect in the case of 4 M NaCl and additionally the transitons in the high ionic case are sharper.

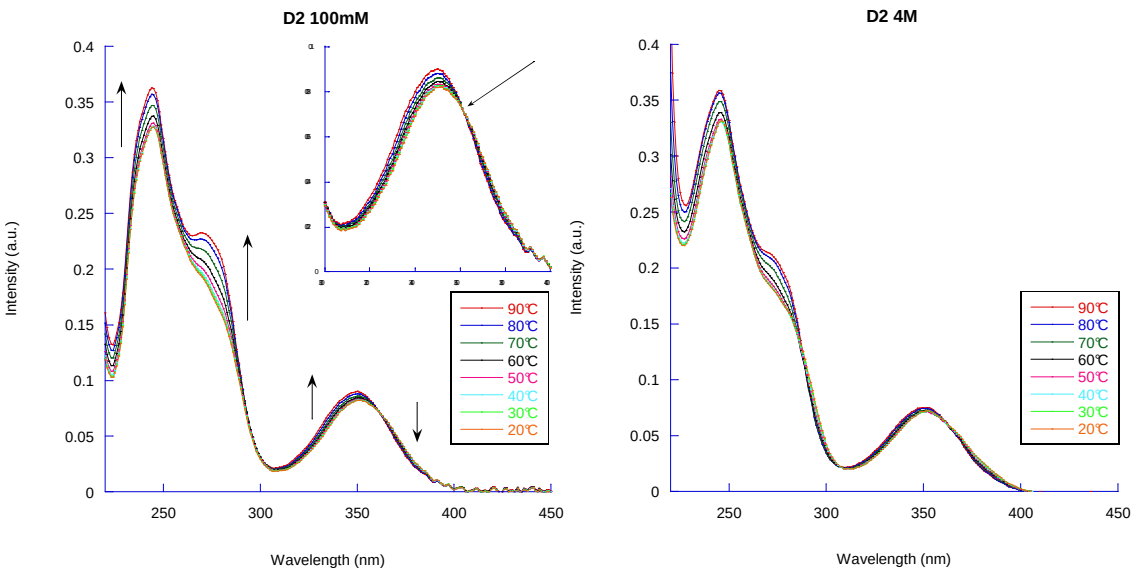

Figure 2.3 Temperature dependent UV-Vis spectra of hybrid **D2-II** at (*left*) low ionic strength (100 mM NaCl) and (*right*) at high ionic strength (4 M NaCl); conditions: 1 µM singlestrand concentration, 10 mM phosphate buffer (pH 7.4).

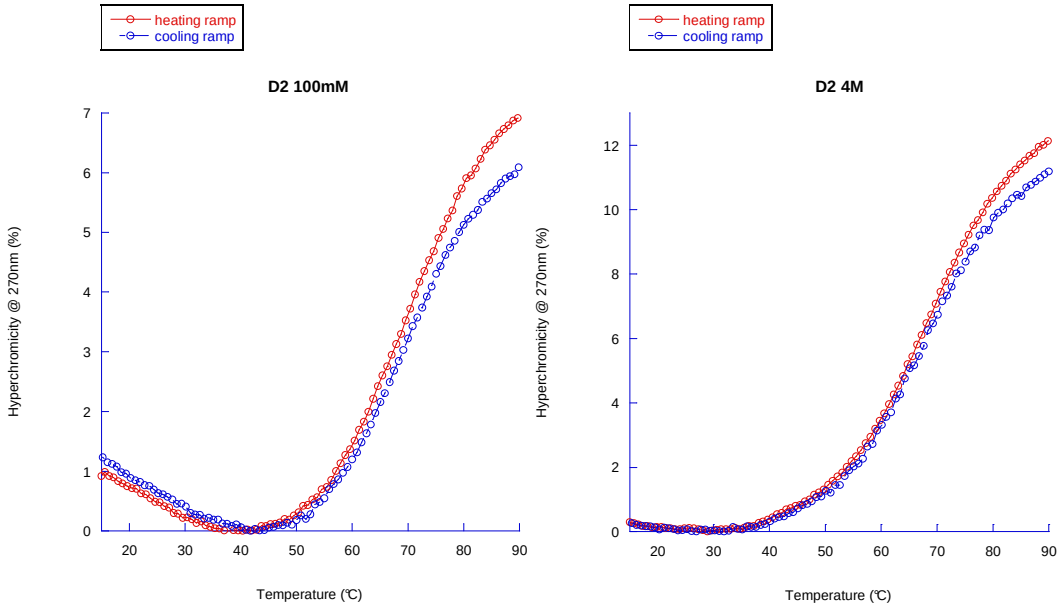

Figure 2.4 Melting profile of hybrid **D2-II** monitored at 270 nm at (*left*) low ionic strength (100 mM NaCl) and (*right*) at high ionic strength (4 M NaCl); conditions: 1 µM singlestrand concentration, 10 mM phosphate buffer (pH 7.4).

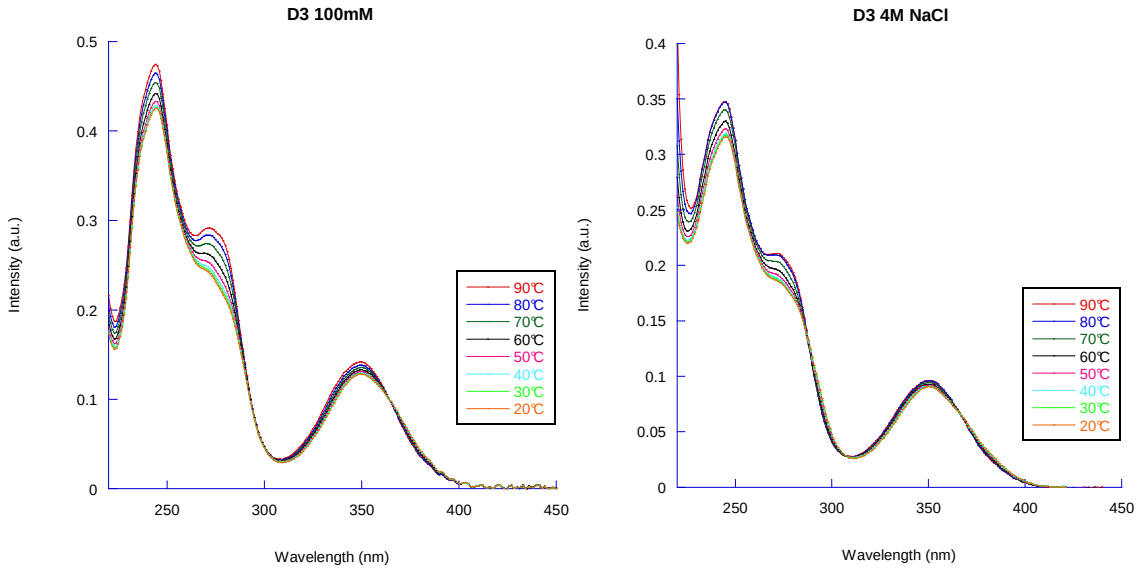

Figure 2.5 Temperature dependent UV-Vis spectra of hybrid **D3-II** at (*left*) low ionic strength (100 mM NaCl) and (*right*) at high ionic strength (4 M NaCl); conditions: 1 µM singlestrand concentration, 10 mM phosphate buffer (pH 7.4).

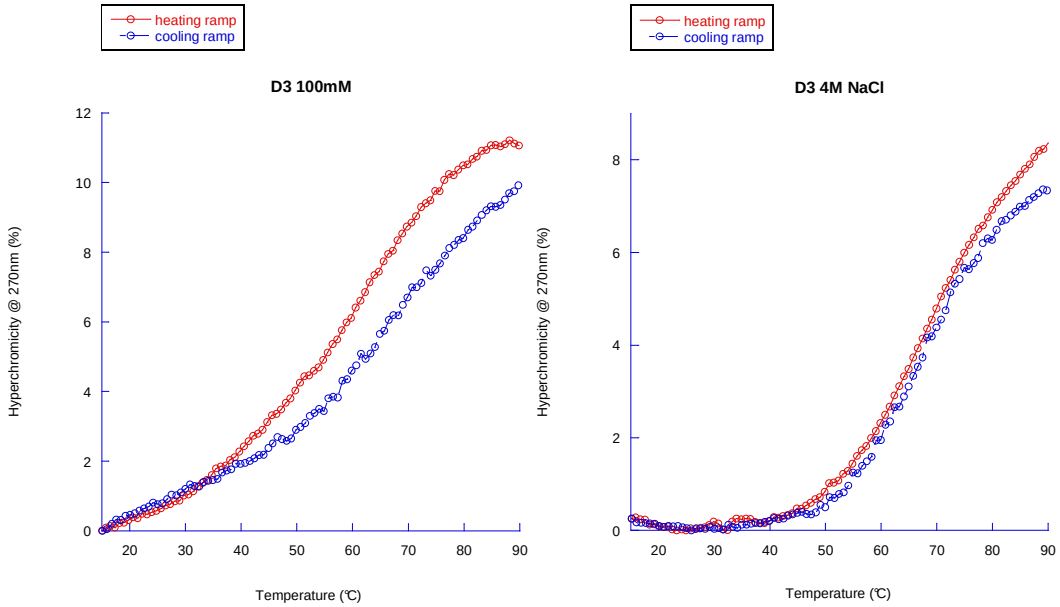

Figure 2.6 Melting profile of hybrid **D3-II** monitored at 270 nm at (*left*) low ionic strength (100 mM NaCl) and (*right*) at high ionic strength (4 M NaCl); conditions: 1 µM singlestrand concentration, 10 mM phosphate buffer (pH 7.4).

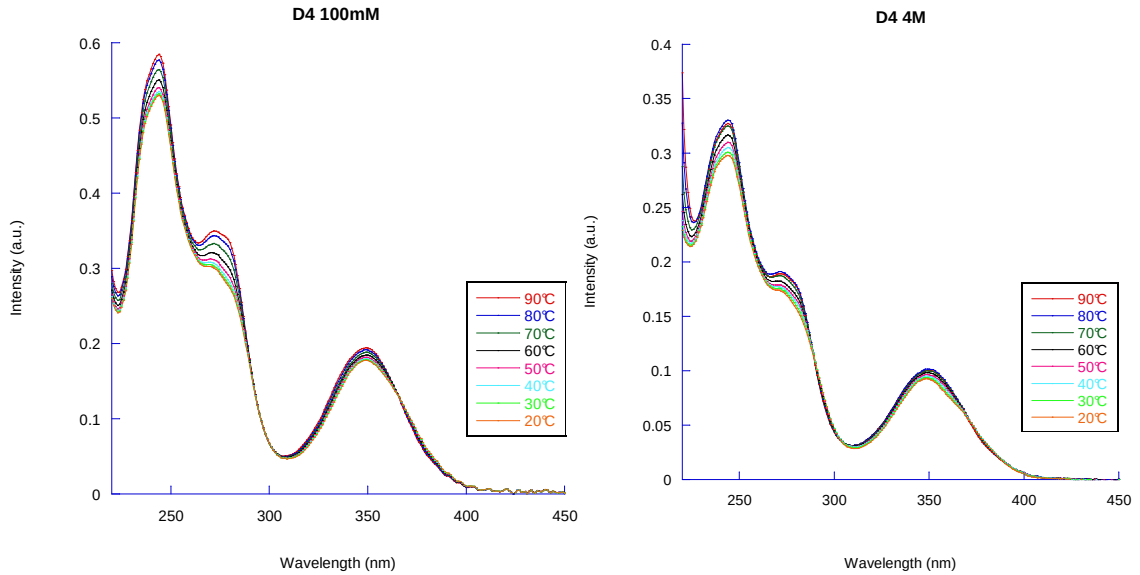

Figure 2.7 Temperature dependent UV-Vis spectra of hybrid **D4-II** at (*left*) low ionic strength (100 mM NaCl) and (*right*) at high ionic strength (4 M NaCl); conditions: 1 µM singlestrand concentration, 10 mM phosphate buffer (pH 7.4).

Starting with hybrid **D5-II** the difference between 100 mM NaCl and 4 M NaCl becomes obvious. Changing the units in the hybrid from eight to ten suddenly results in the resolution of vibronic structures in the absorption bands of the pyrene units hinting for a distinct organization resulting in a reduction of rotational freedom. This effect is then also observed for hybrids **D6-II** and **D7-II** with twelve and fourteen units in the hybridized duplex. The well resolved vibronic bands vanish upon heating in agreement with the melting of the formed duplex and disruption of the interstrand interactions.

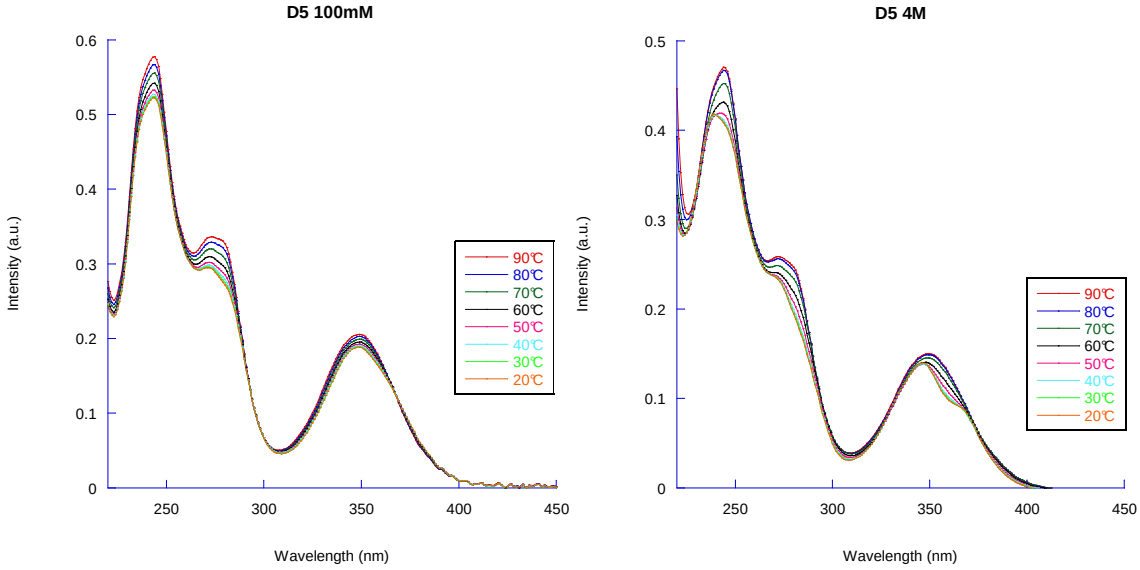

Figure 2.8 Temperature dependent UV-Vis spectra of hybrid **D5-II** at (*left*) low ionic strength (100 mM NaCl) and (*right*) at high ionic strength (4 M NaCl); conditions: 1 µM singlestrand concentration, 10 mM phosphate buffer (pH 7.4).

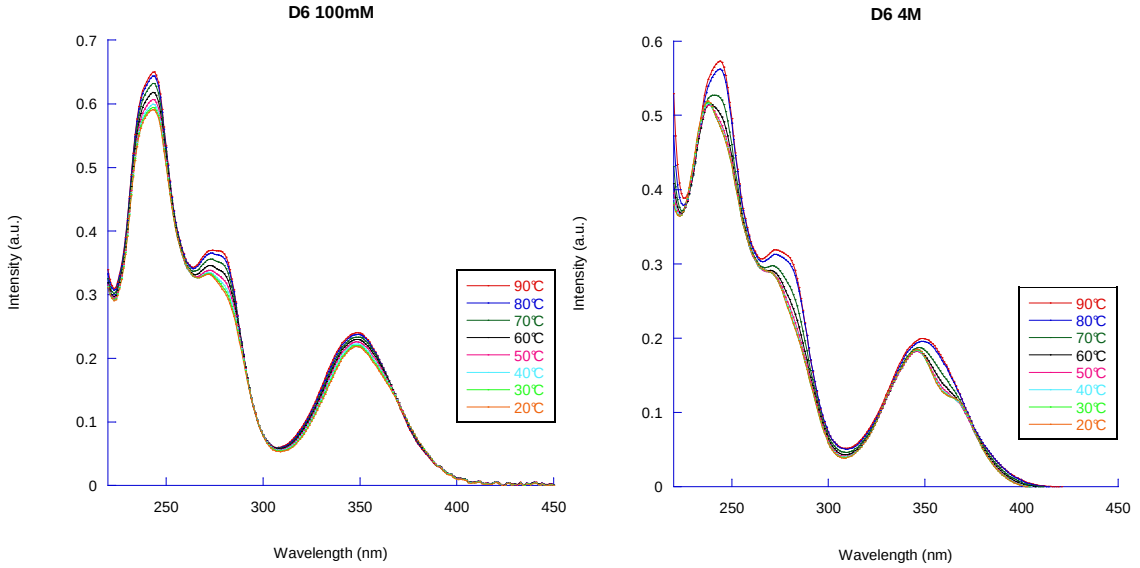

Figure 2.9 Temperature dependent UV-Vis spectra of hybrid **D6-II** at (*left*) low ionic strength (100 mM NaCl) and (*right*) at high ionic strength (4 M NaCl); conditions: 1 µM singlestrand concentration, 10 mM phosphate buffer (pH 7.4).

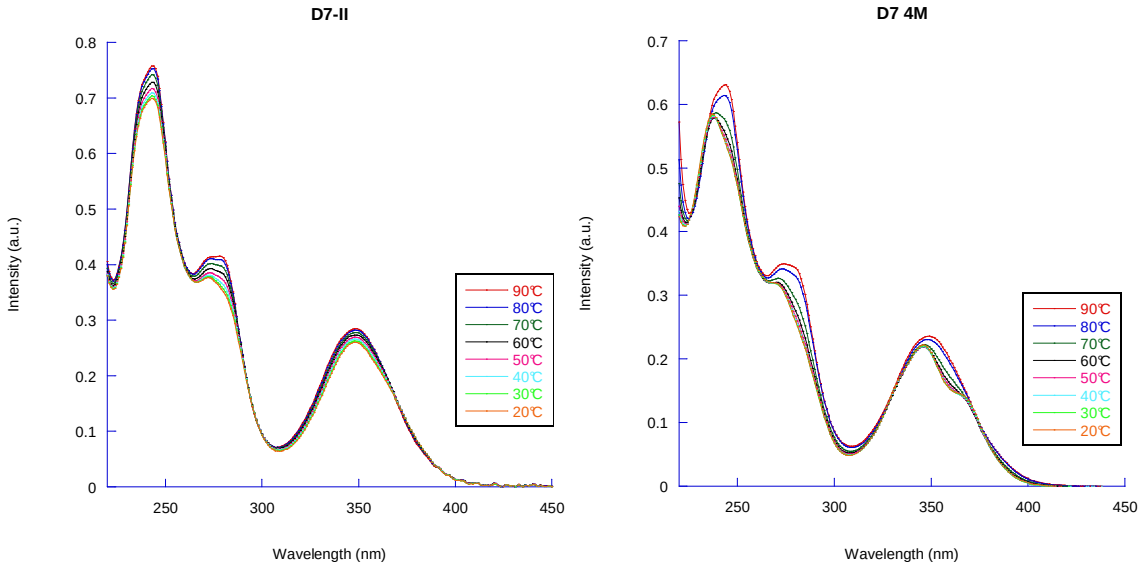

Figure 2.10 Temperature dependent UV-Vis spectra of hybrid **D7-II** at (*left*) low ionic strength (100 mM NaCl) and (*right*) at high ionic strength (4 M NaCl); conditions: 1 µM singlestrand concentration, 10 mM phosphate buffer (pH 7.4).

When looking at the control hybrid **D8-II** also there the resolution of vibronic bands is comparable to hybrids **D5-II**, **D6-II** and **D7-II** (Figure 2.11).

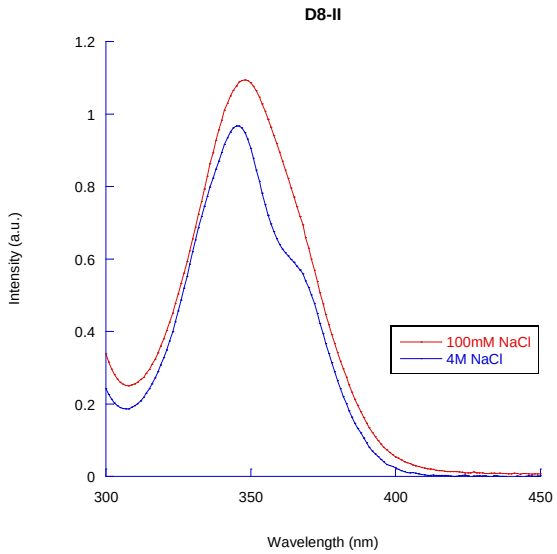

Figure 2.11 UV-Vis spectra of hybrid **D8-II** at low ionic strength (100 mM NaCl) and at high ionic strength (4 M NaCl) at 20°C; conditions: 5 µM singlestrand concentration, 10 mM phosphate buffer (pH 7.4).

Fluorescence spectroscopy

Fluorescence spectroscopy can give valuable information on the organization of the pyrene units. The case of duplex **D1-II** is a special case in the whole series of hybrids as this hybrid contains only one pyrene unit in the single strand and therefore is supposed to emit only monomer emission upon melting and should exhibit interstrand excimer formation upon hybridization. In all the other hybrids the formation of intramolecular excimer formation is expected and for these hybrids the exact emission wavelength of the excimer emission band depending on the temperature can give valuable information on the level of organization.

The temperature dependent fluorescence spectra of **D1-II** shows the expected change in emission from the typical structured monomeric emission around 400 nm at 90°C to the broad and structureless band around 500 nm which is attributed to excimer emission. This behavior confirms the desired arrangement of the two pyrene moieties being in close proximity. Comparing the excimer to monomer ratio for the low and the high ionic case one can see that in the prescence of 4 M NaCl this ratio is much larger. It seems that the proportion of the excimer emission is increased by increasing the salt concentration. A

possible explanation can be found by looking at the emission wavelength. For the physiological conditions the emission wavelength is 502 nm for the excimer band and for the high ionic strength the emission wavelength is 506 nm. The increase in ionic strength and the thereby increased polarity of the solvent can have an influence on the hydrophobic interactions between the pyrene moieties on one hand side and thereby modulating there interactions. Furthermore the possible change in helicity of the DNA part can also change the exact placement of the two pyrene moieties and thereby changing the energy of the excimer emission.

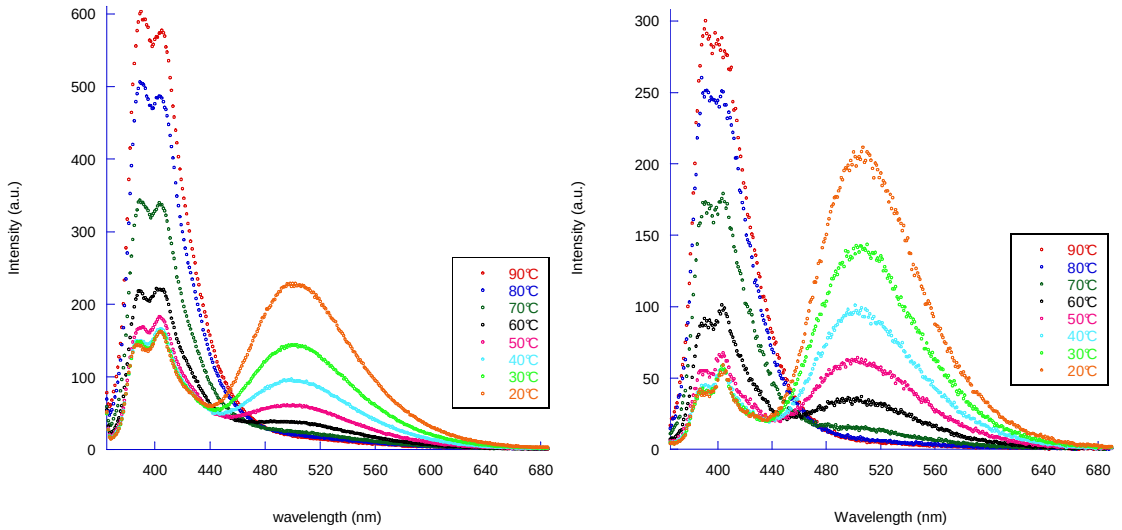

Figure 2.12 Temperature dependent fluorescence spectra of hybrid **D1-II** at (*left*) low ionic strength (100 mM NaCl) and (*right*) at high ionic strength (4 M NaCl); conditions: 1 µM singlestrand concentration, 10 mM phosphate buffer (pH 7.4), excitation wavelength 350 nm.

For the hybrids with at least two incorporated pyrenes per singlestrand namely **D2-II** to **D7-II** the picture of the temperature dependent fluorescence spectra looks different. In all those hybrids there is not only the possibility of interstrand excimer formation but also intramolecular excimer emission is observed. The portion of monomer emission is almost neclectable for all those hybrids.

The hybrid with two pyrene incorporations per singlestrand **D2-II** shows fluorescence spectra which are dominated by the excimer emission although the maximum of emission as well as the intensity is changing depending on the temperature. The emission at 20°C (507 nm for 100 mM NaCl and 510 nm for 4 M NaCl) is attributed to an overlap of inter- and intrastrand excimer formation. An increase in temperature leads first to a decrease in intensity and further heating is accompanied by a blueshift in excimer emission (499 nm for 100 mM NaCl and 500 nm for 4 M NaCl) which is attributed to intrastrand-only excimer formation as the hybrid melts and interstrand excimer formation is no longer possible. Also for this hybrid there is a slight difference of 3 nm in excimer emission wavelength between the low and the high ionic case which could be attributed to the change in helicity of the DNA part. As the duplex is melted the emission wavelength seems to be the same in the singlestrand at physiological conditions as well as in high ionic strength supporting the influence of the helicity of the formed duplex on the excimer emission wavelength in the hybridized state.

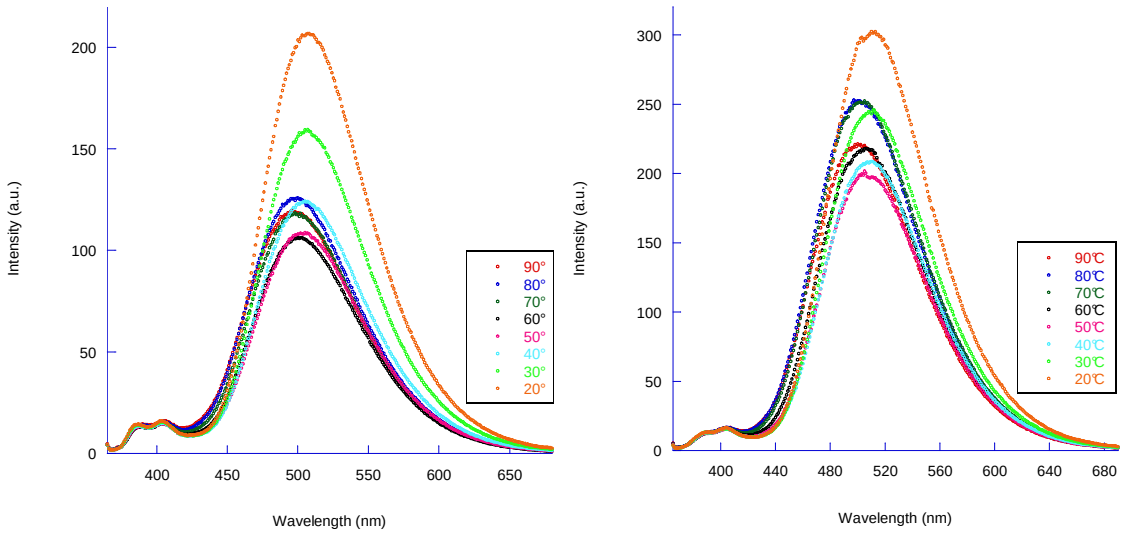

Figure 2.13 Temperature dependent fluorescence spectra of hybrid **D2-II** at (*left*) low ionic strength (100 mM NaCl) and (*right*) at high ionic strength (4 M NaCl); conditions: 1 µM singlestrand concentration, 10 mM phosphate buffer (pH 7.4), excitation wavelength 350 nm.

Further increase in the number of pyrenyl units leads to the observation of the same behavior as for hybrid **D2-II** until **D4-II** namely a red shift of excimer emission wavelength upon hybridization. When looking at the maxima of the emission

wavelength, hybrid **D5-II** somehow marks a turning point in the manner the emission wavelength evolved with changing of temperature. As the number of pyrene units reaches the number of five per singlestrand the excimer emission wavelength is no longer redshifted upon hybridization but first for **D5-II** in the case of low ionic strength stays the same at 20°C and at 90°C and then is blueshifted upon hybridization for **D6-II** and **D7-II** and in the case of high ionic strength **D5-II**, **D6-II** and **D7-II** show the same blueshift in excimer emission upon hybridization. This change depending on the number of incorporated pyrene moieties is in agreement with the previous study which has shown that the pyrenyl units arrange themselves in a helical fashion starting with six units [48]. The blueshift in excimer emission upon hybridization was assigned to the helical twisting of the pyrene units. In this study the high ionic strength leads to this blueshift in excimer emission already with five pyrene units.

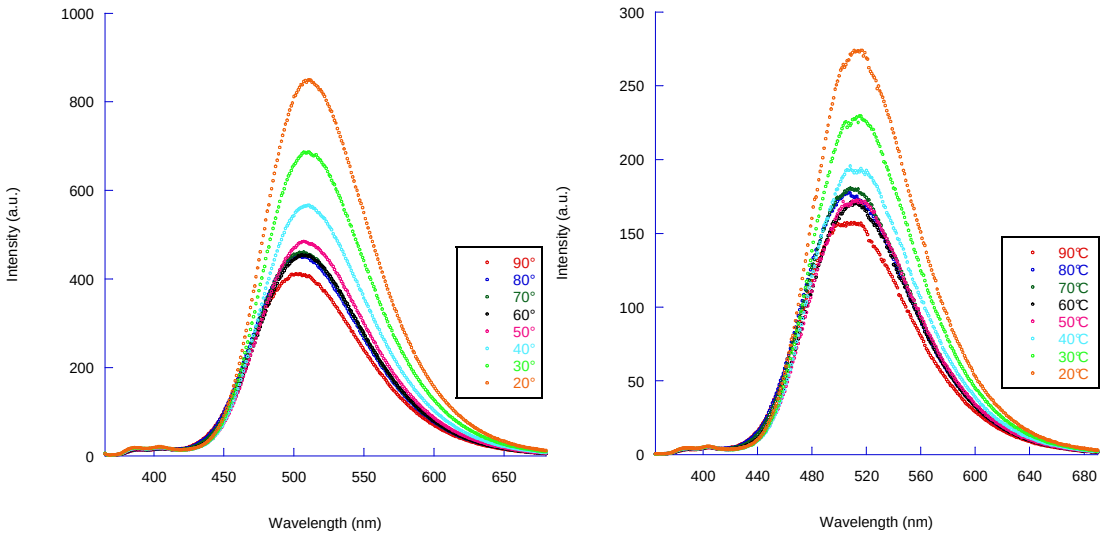

Figure 2.14 Temperature dependent fluorescence spectra of hybrid **D3-II** at (*left*) low ionic strength (100 mM NaCl) and (*right*) at high ionic strength (4 M NaCl); conditions: 1 µM singlestrand concentration, 10 mM phosphate buffer (pH 7.4), excitation wavelength 350 nm.

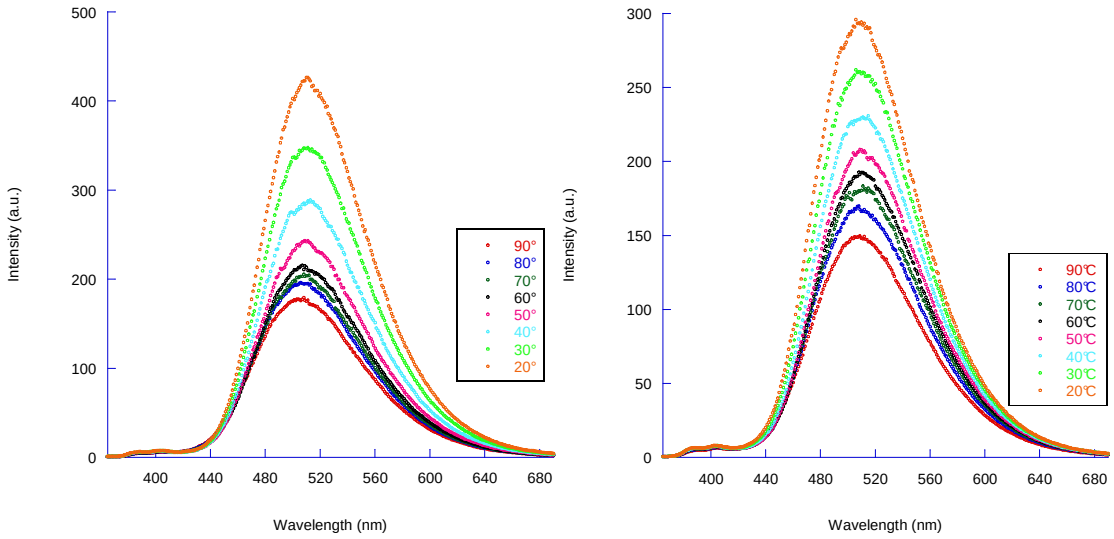

Figure 2.15 Temperature dependent fluorescence spectra of hybrid **D4-II** at (*left*) low ionic strength (100 mM NaCl) and (*right*) at high ionic strength (4 M NaCl); conditions: 1 µM singlestrand concentration, 10 mM phosphate buffer (pH 7.4), excitation wavelength 350 nm.

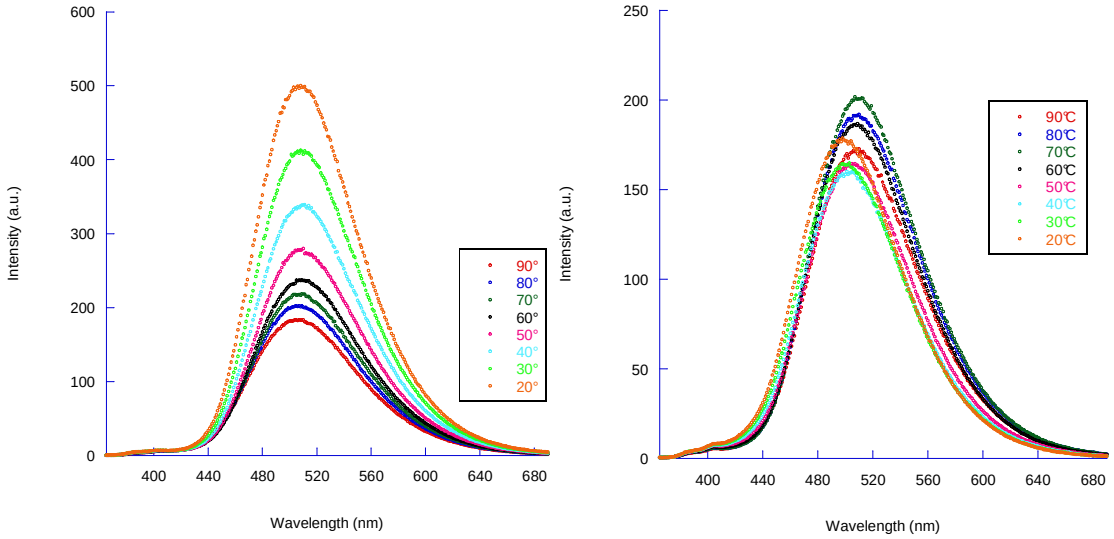

Figure 2.16 Temperature dependent fluorescence spectra of hybrid **D5-II** at (*left*) low ionic strength (100 mM NaCl) and (*right*) at high ionic strength (4 M NaCl); conditions: 1 µM singlestrand concentration, 10 mM phosphate buffer (pH 7.4), excitation wavelength 350 nm.

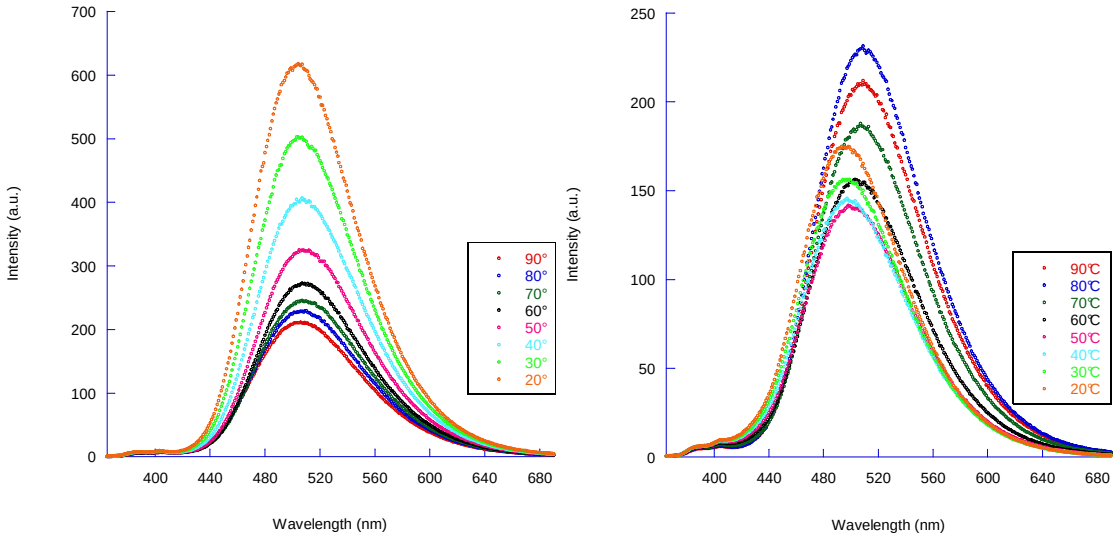

Figure 2.17 Temperature dependent fluorescence spectra of hybrid **D6-II** at (*left*) low ionic strength (100 mM NaCl) and (*right*) at high ionic strength (4 M NaCl); conditions: 1 µM singlestrand concentration, 10 mM phosphate buffer (pH 7.4), excitation wavelength 350 nm.

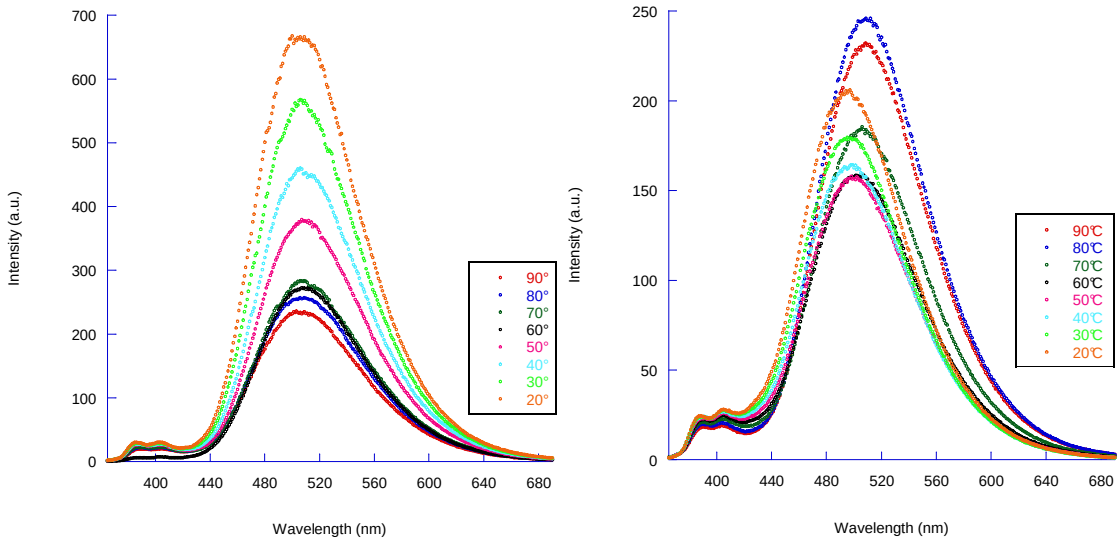

Figure 2.18 Temperature dependent fluorescence spectra of hybrid **D7-II** at (*left*) low ionic strength (100 mM NaCl) and (*right*) at high ionic strength (4 M NaCl); conditions: 1 µM singlestrand concentration, 10 mM phosphate buffer (pH 7.4), excitation wavelength 350 nm.

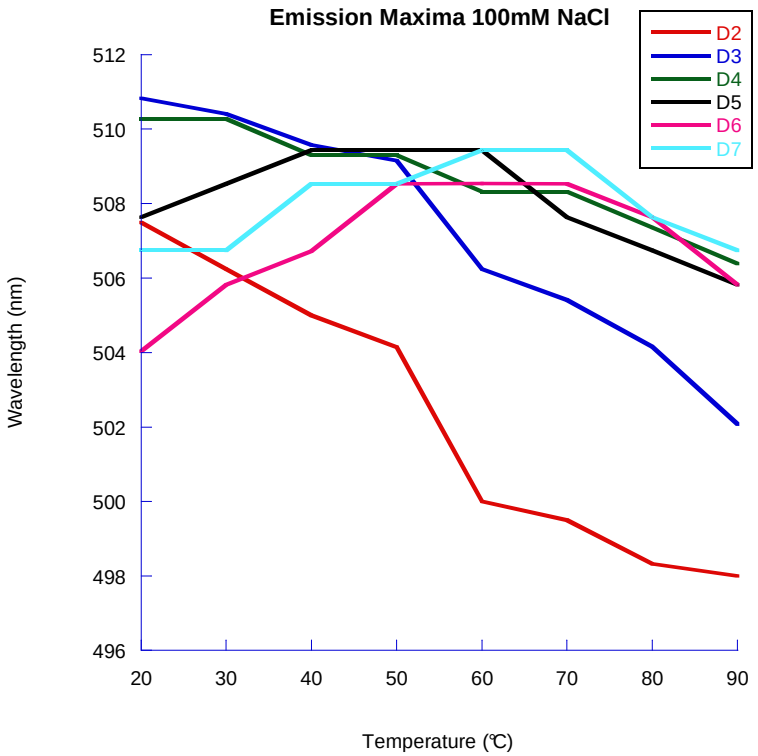

Figure 2.19 Wavelength of the emission maxima of the excimer fluorescence for the hybrids **D2-II** to **D7-II** in function of the temperature at 100 mM NaCl concentration.

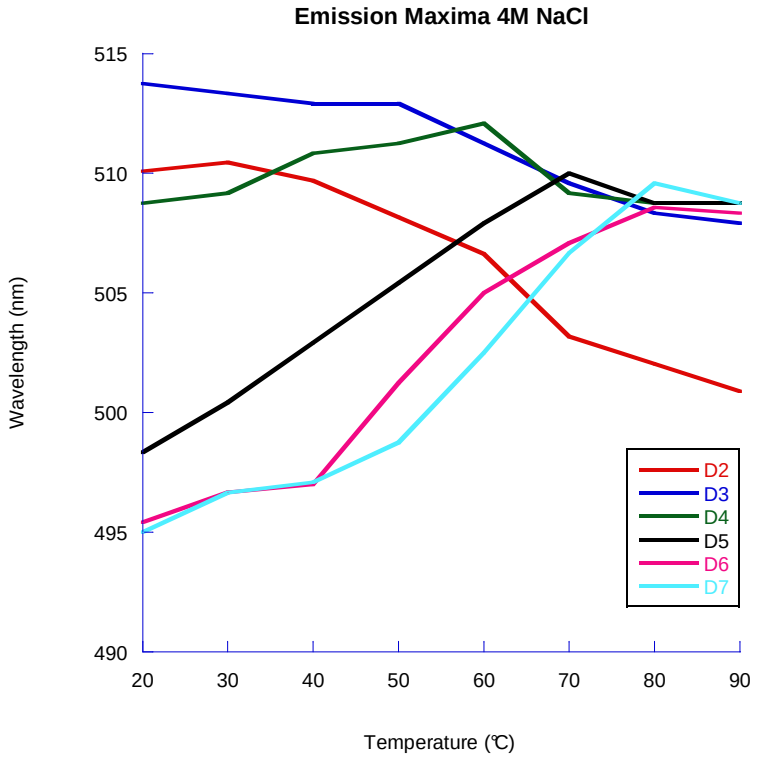

Figure 2.20 Wavelength of the emission maxima of the excimer fluorescence for the hybrids **D2-II** to **D7-II** in function of the temperature at 4 M NaCl concentration.

Circular dichroism experiments

By circular dichroism spectroscopy the main focus was on the investigation of the conformation first of the DNA weather it changes its helicity and secondly on the influence it would have on the arrangement of the pyrenyl units.

For hybrid **D1-II** the dominating part of the CD spectrum is the DNA part and it can be nicely shown that at physiological conditions the right-handed B-DNA is found characterized by a maximum at 276 nm and a through at 252 nm. The absorption region of the pyrene only does not show a significant signal. Changing to 4 M NaCl the spectrum show the characteristic near inversion of the signal with a negative signal at 293 nm and a positive signal at 270 nm. These signals are clearly assigned to the left handed Z-DNA. Furthermore there is a positive although weak induced type of CD signal with a maximum at 349 nm which corresponds to the pyrene only absorption (Figure 2.20).

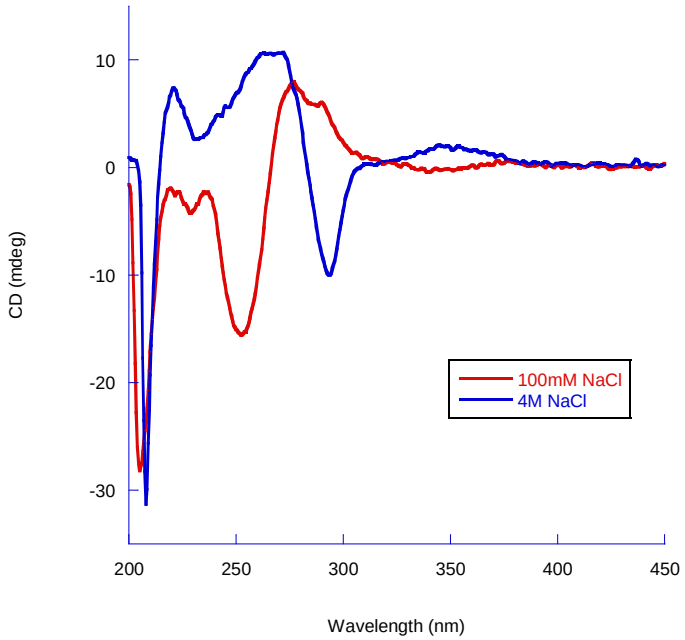

Figure 2.21 Circular dichroism spectra of hybrid **D1-II** at 100 mM NaCl (red) and at 4 M NaCl (blue); conditions: Singlestrand concentration 5 µM, 20°C, 10 mM phosphatebuffer.

For hybrid **D2-II** the signature of the natural part does not change and sticks to the same behavior namely being right-handed B-DNA at 100 mM NaCl with no CD signal around 350 nm and showing the characteristic left-handed Z-DNA signature at elevated ionic

strength. The big difference arises then with the spectrum at 4 M NaCl showing an exciton coupled type of CD with a negative cotton effect at 374 nm and a positive cotton effect at 346 nm (Figure 2.21).

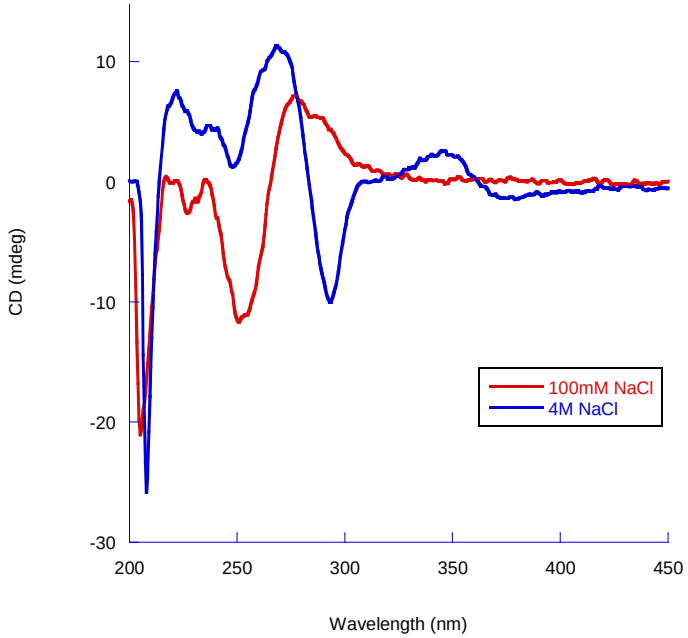

Figure 2.22 Circular dichroism spectra of hybrid **D2-II** at 100 mM NaCl (red) and at 4 M NaCl (blue); conditions: Singlestrand concentration 5 µM, 20°C, 10 mM phosphatebuffer.

As the signals are weak in intensity for the hybrids with only single and double incorporation in the singlestrand especially in the case of **D2-I** the hybrids were also measured at a higher concentration (Figure 2.23).

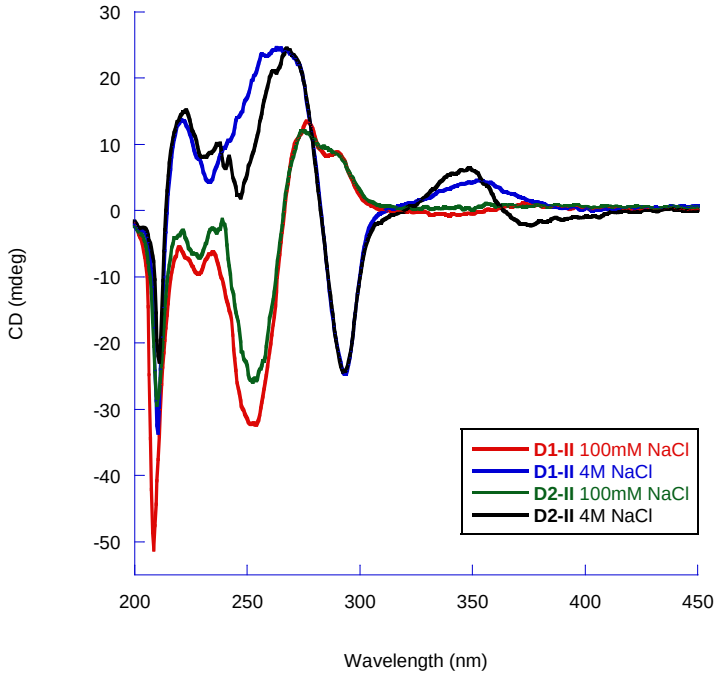

Figure 2.23 Circular dichroism spectra of hybrid **D1-II** and **D2-II** at 100 mM NaCl (red) and at 4 M NaCl (blue); conditions: Singlestrand concentration 10 µM, 20°C, 10 mM phosphatebuffer.

Hybids **D3-II** and **D4-II** show also the B-form at physiological conditions and the Z-form under high ionic strength but for those two cases there is no CD signal detectable at lower energy than 300 nm in contrast to **D1-II** and **D2-II** (Figure 2.24 and 2.25).

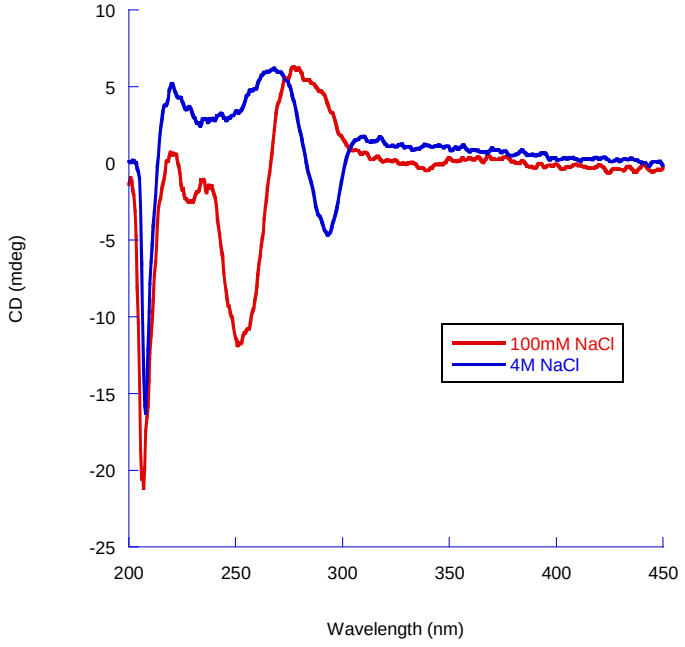

Figure 2.24 Circular dichroism spectra of hybrid **D3-II** at 100 mM NaCl (red) and at 4 M NaCl (blue); conditions: Singlestrand concentration 5 µM, 20°C, 10 mM phosphatebuffer.

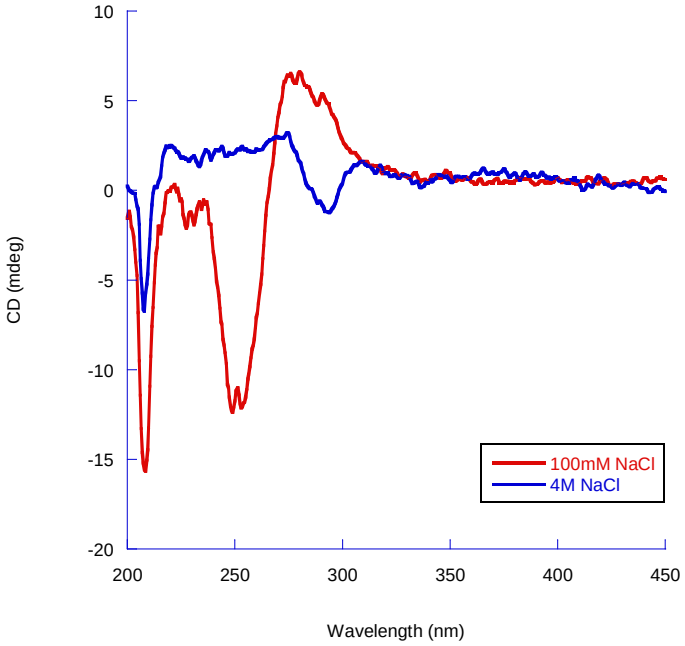

Figure 2.25 Circular dichroism spectra of hybrid **D4-II** at 100 mM NaCl (red) and at 4 M NaCl (blue); conditions: Singlestrand concentration 5 µM, 20°C, 10 mM phosphatebuffer.

Hybrid **D5-II** shows also the change in helicity in the DNA part with the change in NaCl concentration but for this chimera there is an exciton coupled type of signal visible with a positive cotton effect at 365 nm and a negative cotton effect at 335 nm. In contrast to **D2-II** this coupling effect is of inverse nature (Figure 2.26).

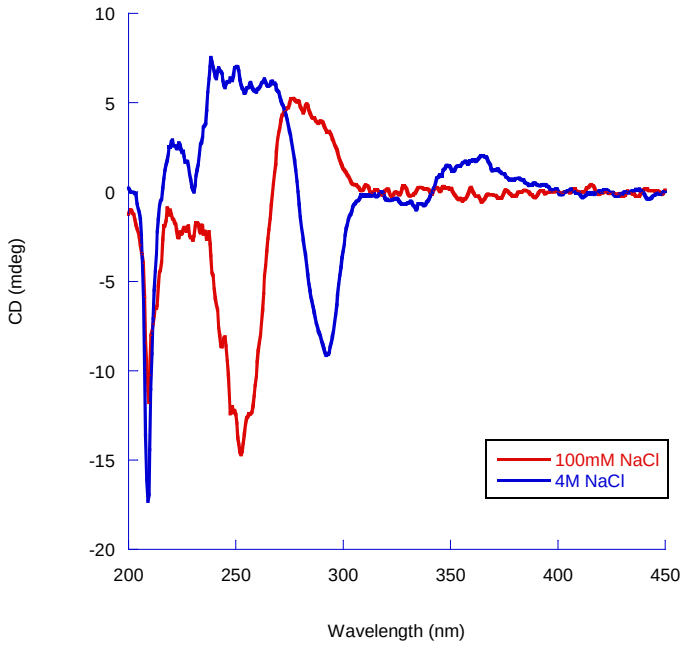

Figure 2.26 Circular dichroism spectra of hybrid **D5-II** at 100 mM NaCl (red) and at 4 M NaCl (blue); conditions: Singlestrand concentration 5 µM, 20°C, 10 mM phosphatebuffer.

The CD spectra of hybrid **D6-II** shows similar to **D5-II** the B to Z change of the DNA part. For this hybrid the exciton coupled CD signal at 4 M NaCl is of the same overall signature (+/-) as in **D5-II** but the cotton effects are more intense and a closer look reveals that this is not a simple exciton coupled CD but there seems to be an overlap of multiple cotton effects (-/+/+/-) (Figure 2.27).

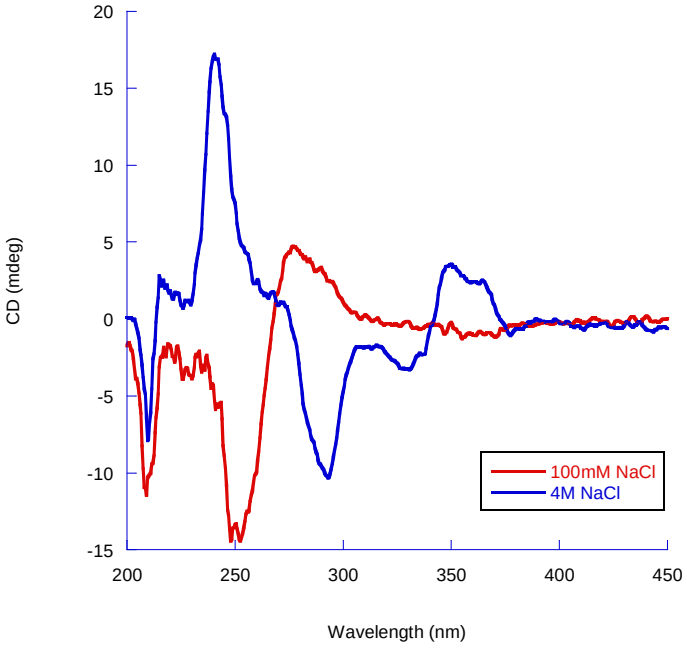

Figure 2.27 Circular dichroism spectra of hybrid **D6-II** at 100 mM NaCl (red) and at 4 M NaCl (blue); conditions: Singlestrand concentration 5 µM, 20°C, 10 mM phosphatebuffer.

This multiple cotton effects at elevated ionic strength are much better visible for the hybrid **D7-II** (Figure 2.28). There is first a negative cotton effect at 378 nm followed by a positive cotton effect at 363 nm which could be assigned as the first exciton couplet. This pair is followed by a positive cotton effect at 349 nm and a negative effect at 330 nm building the second coupling pair. At physiological conditions there is no distinct CD signal in the region at lower energies visible.

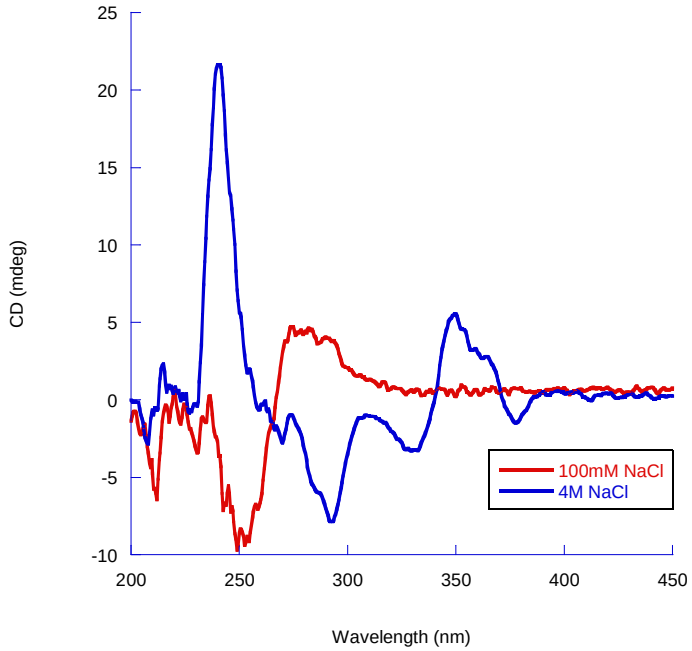

Figure 2.28 Circular dichroism spectra of hybrid **D7-II** at 100 mM NaCl (red) and at 4 M NaCl (blue); conditions: Singlestrand concentration 5 µM, 20°C, 10 mM phosphatebuffer.

The comparison to the hybrid **D8-II** shows that these multiple cotton effects are also present in chimeras without the possibility to change their helicity. The pattern at 4M NaCl is the same (-/+/+/-). The maxima of all the effects match exactly the wavelength of hybrid **D7-II**. The difference lies in the intensities of the signals. In the case of **D8-II** one encounters much more pronounced signals and the ratio between the exciton couplets at higher energy and at lower energy is larger. Another striking difference can be seen under physiological conditions. Whereas there seems no distinct organization of the pyrene units in the case of **D7-II** showing no CD signal there is an exciton type of CD signal visible in the case of **D8-II** with a positive cotton effect at 357 nm and a negative cotton effect at 335 nm although with weak intensities.

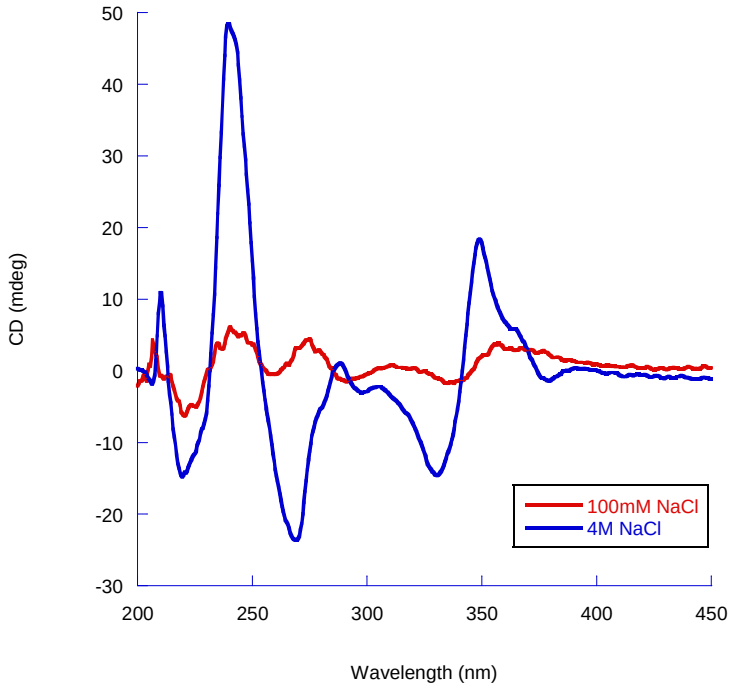

Figure 2.29 Circular dichroism spectra of hybrid **D8-II** at 100 mM NaCl (red) and at 4 M NaCl (blue); conditions: Singelstrand concentration 5 µM, 20°C, 10 mM phosphatebuffer.

The self-complemetary nature of the oligonucleotide part was addressed by looking at the CD spectra of the corresponding singlestrands **ON13-II** and **ON14-II** at low and high NaCl concentration and compared to the hybrid **D7-II** under these conditions (Figure 2.30). At physiological conditions the singlestrands show a typical B-DNA shape comparable to the hybrid **D7-II**. Also the singlestrands do not show any signals in the pyrene only absorption area. When increasing the ionic strength also the singlestrands show an organization in the pyrene part although of different nature than the hybrid. **ON14-II** shows also an exciton coupled CD whereas the couplet is almost superimposible with the exciton couplet of the higher energy in the case of **D7-II**. **ON13-II** also shows some cotton effects but of much smaller intensity. The negative band at 292 nm typical for Z-DNA though is only observed in the case of **D7-II** and not for the singlestrands.

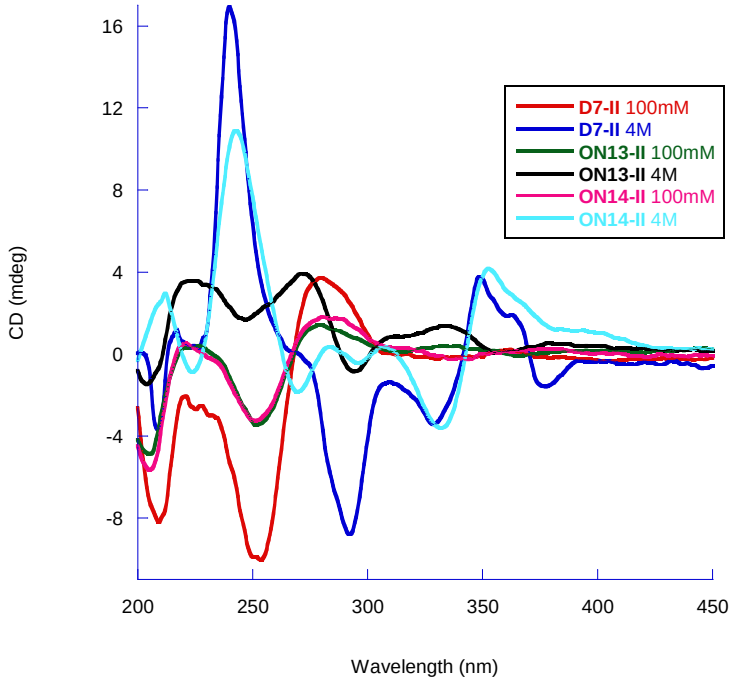

Figure 2.30 Circular dichroism spectra of hybrid **D7-II** in comparison with the corresponding singlestrands **ON13-II** and **ON14-II** at 100 mM NaCl (red) and at 4 M NaCl (blue); conditions: Singlestrand concentration 5 µM, 20°C, 10 mM phosphatebuffer.

2.4 Conclusion and outlook

It has been shown that the number of attached pyrene units is crucial for their degree of organization. The organization of the pyrenyl part at *physiological conditions* seems not to be defined for the hybrids **D1-II** to **D7-II**. Only hybrid **D8-II** shows a preferred organization already at physiological conditions. The reason for this fact can be maybe found in the self-complementary nature of the alternating cytosine/ guanine motif of hybrids **D1-II** to **D7-II**. There is not only the desired hybridization between the two singlestrands possible but also a self-pairing can be imagined. Furthermore there is also the possibility to hybridize in a slipped fashion by shifting the pairing oligonucleotides by two basepairs. Another point to consider is the proportion of pyrene to nucleotides which differs in hybrid **D8-II** in that the pyrene portion is dominating by shear number. For **D8-II** the base-pairing pattern is unambiguous and may therefore lead to a distinct arrangement of the pyrene units already at 100 mM NaCl.

At elevated ionic strength (4 M NaCl) the hybrids show different behavior in the pyrenyl region but they have all in common that the desired B to Z transition of the oligonucleotide is actually taking place. The hybrid **D1-II** shows an induced type of CD without any coupling which could also be originating from self-pairing of the singlestrands. Hybrid **D2-II** then shows an exciton coupled CD with a negative chirality which can indeed be interpreted as the pyrenyl units arrange in a way by following the left-handed helicity of the oligonucleotide part. Hybrids **D3-II** and **D4-II** both represent chimeras without a distinct organization of the pyrenyl units. These two hybrids take an intermediate position in the whole series. It could be argued that the number of pyrene units and the number of nucleotides are both in charge of the formation of the duplex and that none of them is truly taking the leader role thereby forming a variety of different hybrids. Hybrid **D5-II** containing five pyrene units in each singlestrand shows then the exciton coupled CD with positive chirality as already observed for the sandwichtype arrangement [48]. In this hybrid the interstrand forces excerted by the pyrenyl units seem to become dictating and behave independently of the helicity of the oligonucleotide part which is clearly in a left-handed form. **D6-II** and **D7-II** both show an even higher degree of organization in the pyreyl part as manifested by the multiple cotton effects. The signature observed is similar to the control duplex **D8-II** and shows that the pyrenyl part organizes independently of the helicty of the oligonucleotid part.

The elevated ionic strength used in this study showed that it does not only effect the oligonucleotide part thereby promoting the desired B to Z transition but it significantly influences the arrangement of the pyrene units as well. It has been shown that there exsists a delicate balance between the forces excerted by the nucleobases and the pyrene units. With only two and four pyrene units in the hybrid the oligonucleotide part dictates their arrangement. Increasing the number to six and eight respectively the two parts are on the same level of dictating power. Starting with ten units in the duplex the pyrene units start to organize independently and with twelve and fourteen units this independent organization is even increased and more pronounced.

The study in this chapter has the major drawback of involving a self-complementary oligonucleotide sequence which increases the possible structures formed and making the analysis harder. One possible way around that problem could be to choose an alternating pyrimidine/ purine motif but without just using cytosine/ guanine only but also incorporation of adenine and thymine residues thereby preventing the formation of self-paring and having only one possible hybrid structure. Another possibility it the attachment of a guiding mixed sequence before the alternating d(CG) sequence thereby making the self-pairing almost impossible (Chapter 3).

2.5 Experimental Section

The synthesis of the required non-nucleosidic pyrene building block with the corresponding C3 linker was done according to the published procedure [34]. Nucleoside phosphoramidites were purchased from SAFC (Proligo Reagents) with dG (dmf), dC (ac) and dA (bz). Oligonucleotides **ON1-II** to **ON14-II** were prepared via automated oligonucleotide synthesis using standard phosphoramidite chemistry (Activator: Ethylthiotetrazole) on a 394-DNA/RNA synthesizer (*Applied Biosystems*). The oligonucleotides with the non-nucleosidic pyrene moiety at the 3`- end were prepared on an already prepared CPG (controlled pore glass) support with a first pyrene moiety already attached to it. For the unnatural building block, which was coupled using 0.1 M solutions in 1,2 -dichloroethane, coupling times were increased to 120 seconds instead of 25 seconds used for the natural nucleosides. Cleavage from the solid support and final deprotection was performed manually by treatment with 30% NH_4OH solution at 55°C overnight. All oligonucleotides were purified by reverse phase HPLC (Instrument: LC-10 AT from *Shimadzu* with a UV detector, column: LiChrospher 100 RP-18, 5µm, *Merck*); eluent A= $(Et_3NH)OAc$ (0.1 M, pH 7.4); eluent B= 80% MeCN + 20% Eluent A; gradient 5-50% B over 38 min.

For the determination of oligonucleotide stock solution concentrations, small samples were diluted to 10% and the absorbance at 260 nm was measured on a Nanodrop ND-1000 Spectrophotometer from *Thermo Scientific*. Epsilon values were calculated using 15300, 11700, 7400 and 9000 for A, G, C and T, respectively, and 8600 for the pyrene building block.

Molecular mass determination of the oligonucleotides was performed with a Sciex QSTAR pulsar (hybrid qudrupole time-of-flight mass spectrometer, *Applied Biosystems*). ESI-MS (negative mode, CH_3CN/H_2O/TEA) data of the compounds **ON1-ON14** are presented in Table 2.2

Entry	Oligo #	**Duplex**	**Bruttoformula**	**Calc. aver. mass**	**Found mass**
D1-II	**ON1-II** **ON2-II**	(5') CGCGCGCG **S** (3') GCGCGCGC **S**	$C_{100}H_{120}N_{34}O_{52}P_8$ $C_{100}H_{120}N_{34}O_{52}P_8$	2878.0 2878.0	2878.1 2879.0
D2-II	**ON3-II** **ON4-II**	(5') CGCGCGCG **SS** (3') GCGCGCGC **SS**	$C_{124}H_{143}N_{36}O_{58}P_9$ $C_{124}H_{143}N_{36}O_{58}P_9$	3344.5 3344.5	3343.9 3344.0
D3-II	**ON5-II** **ON6-II**	(5') CGCGCGCG **SSS** (3') GCGCGCGC **SSS**	$C_{148}H_{166}N_{38}O_{64}P_{10}$ $C_{148}H_{166}N_{38}O_{64}P_{10}$	3810.9 3810.9	3809.9 3811.0
D4-II	**ON7-II** **ON8-II**	(5') CGCGCGCG **SSSS** (3') GCGCGCGC **SSSS**	$C_{172}H_{189}N_{40}O_{70}P_{11}$ $C_{172}H_{189}N_{40}O_{70}P_{11}$	4277.3 4277.3	4277.0 4277.0
D5-II	**ON9-II** **ON10-II**	(5') CGCGCGCG **SSSSS** (3') GCGCGCGC **SSSSS**	$C_{196}H_{212}N_{42}O_{76}P_{12}$ $C_{196}H_{212}N_{42}O_{76}P_{12}$	4743.8 4743.8	4744.0 4744.0
D6-II	**ON11-II** **ON12-II**	(5') CGCGCGCG **SSSSSS** (3') GCGCGCGC **SSSSSS**	$C_{220}H_{235}N_{44}O_{82}P_{13}$ $C_{220}H_{235}N_{44}O_{82}P_{13}$	5210.2 5210.2	5210.2 5209.0
D7-II	**ON13-II** **ON14-II**	(5') CGCGCGCG **SSSSSSS** (3') GCGCGCGC **SSSSSSS**	$C_{244}H_{285}N_{46}O_{88}P_{14}$ $C_{244}H_{285}N_{46}O_{88}P_{14}$	5676.6 5676.6	5676.0 5676.0

Table 2.2 Mass spectrometry data (brutto formula, calculated average mass, found mass).

Thermal denaturation experiments (1 µM singlestrand oligonucleotide concentration, 10 mM phosphate buffer pH 7.4, with varying NaCl concentration as indicated in each case) were carried out on Varian Cary 100 Bio UV-Visible spectrophotometer equipped with a Varian Cary temperature controller and data were collected with Varian WinUV software at various wavelengths as indicated in each case. Cooling- heating- cooling cycles in the temperature range of 90°C to 15°C and a heating/ cooling rate of 0.5°C/ min were used and data points every 0.5°C were recorded. Data were analyzed with KaleidaGraph 4 software from *Synergy Software*. Temperature melting values (T_m) were determined as the maximum of the first derivative of the melting curves. If necessary the curves were smoothed with a window of 5 in order to get a reasonable maximum of the first derivative.

Temperature dependent UV-Vis spectra were collected from 90°C to 20°C on a Varian Cary 100 Bio UV-Visible spectrophotometer equipped with a Varian Cary temperature controller. All experiments were carried out at a 1 µM singlestrand oligonucleotide concentration in 10 mM phosphatebuffer (pH 7.4) and the indicated concentration of NaCl.

Temperature dependent fluorescence spectra were recorded from 90°C to 20°C on a Varian Cary Eclipse fluorescence spectrophotometer equipped with a Varian Cary temperature controller (excitation wavelength at 350 nm, excitation and emission slitwidth as well as the detector voltage were varied according to the experiment as indicated). All experiments were carried out with a singlestrand concentration of 1 µM. Data were analyzed with KaleidGagraph 4 software from *Synergy Software*.

Circular dichroism spectra were recorded on a *JASCO* J-715 spectrophotometer equipped with a PFD-350S temperature controller. All experiments were carried out with a singlestrand concentration of 5 µM (if not indicated) in 10 mM phosphatebuffer (pH 7.4) and the indicated NaCl concentration.

Chapter 3: Influence of a B-Z transition on chromophore organization in trisegmental chimeric constructs

3.1. Abstract

In this chapter the influence of the DNA part on the organization of a pyrenyl stretch in function of the ionic strength is shown. The non-nucleosidic pyrenyl stretches are behaving differently weather attached to one side of a DNA duplex or if they are embedded in between two DNA segments. Putting the DNA already at physiological condition to the left-handed form seems to influence the arrangement of the pyrenyl stretch considerably in comparison to the case where the DNA part is converted to the left-handed form.

3.2. Introduction

Based on the results of the bisegmental study of the chimeras of a natural oligonucleotide part and an artificial oligopyrenyl part (see chapter 2), a system was developed, consisting of three different segments in the chimera (Table 3.1). The segment common to all of the designed chimeras is the oligopyrenyl part, having 7 non-nucleosidic pyrene moieties which have proofed to be necessary in order to form a helical arrangement. The attached natural oligonucleotide segments are the variable element and may result in different arrangements of the pyrenyl part under different conditions.

3.3. Results and Discussion

D1-III and **D2-III** were designed also accordingly to chapter 2, with the potentially Z-DNA segment directly attached to the oligopyrenyl part from one side and additionally the GC part was elongated with a third segment of natural oligonucleotide part which

adopts canonical B-DNA. This part was attached in order to prevent self association of the single strand and increasing the stability of the desired duplex. The difference between **D1-III** and **D2-III** lies in the guanosine nucleoside in the CG forming sequence. In the case of **D2-III** the guanine was replaced by the 8-bromo-guanine which facilitated the B-Z transition by adopting the *syn* conformation and enables the study of the transition already at physiological conditions e.g. low ionic strength. This construct was designed in order to distinguish between the indirect influence of the increased ionic strength by changing the helicity of the natural oligonucleotide part from right to left handedness and the direct influence the increased salt concentration might have on the oligopyrenyl stretch.

D3-III represents a sandwich type arrangement of the three parts having on one side of the oligopyrenyl strand the potential Z-forming element and on the other side a sequence which should be predominantly in the B-form. This is exactly the same mixed sequence as has been used for the **D1-III** and **D2-III** in order to stabilize the desired arrangement. This chimera could show the influence of different handedness exerted on the oligopyrenyl part from two sides.

Finally the duplex **D4-III** represents the natural part of **D1-III** only and is used to attribute the contribution to thermal stability of the pyrenyl stretch of duplex **D1-III**.

Entry	Oligo #	**Sequence**	**Tm (°C)**
D1-III	**ON1-III** **ON2-III**	(5`) ACG TGA CGC GCG CG SSSSSSS(3`) (3`) TGC ACT GCG CGC GC SSSSSSS(5`)	78.1
D2-III	**ON3-III** **ON4-III**	(5`) ACG TGA CG*C G*CG* CG* SSSSSSS(3`) (3`) TGC ACT G*CG* CG*C G*C SSSSSSS(5`)	69.3
D3-III	**ON5-III** **ON6-III**	(5`) ACG TGA SSSSSSS CGC GCG CG (3`) (3`) TGC ACT SSSSSSS GCG CGC GC (5`)	57.2
D4-III	**ON7-III** **ON8-III**	(5`) ACG TGA CGC GCG CG (3`) (3`) TGC ACT GCG CGC GC (5`)	69.1
S =	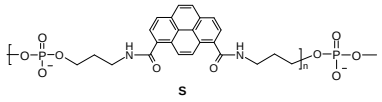		
G* =	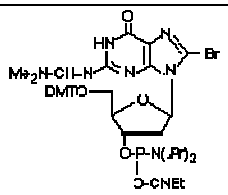		

Table 3.1 Hybridization data (Tm, °C) of different oligonucleotides duplexes containing a stretch of pyrene based building blocks with a three carbon linker (S) and with a 8-Bromo-guanine (G*). All measurements were carried out at pH 7.4 in phosphatebuffer and 100 mM NaCl.

Melting experiments (monitored at 260 nm)

To get an idea about the thermal stability of the desired hybrids, melting experiments were carried out at physiological conditions. The two “end-attached” oligopyrenyl hybrids **D1-III** and **D2-III** were compared to the natural reference duplex **D4-III** in order to get some idea about the contribution of the pyrenyl units to the overall stability of the hybrids. Furthermore the direct comparison was possible between the end-attached variant and the sandwich type incorporated pyrene units.

For all the hybrids the melting profile did not show any hysteresis and the cooling-heating-cooling cycle was superimposable for all hybrids. The sharpness of the transitions was different for the different arrangements. The oligopyrenyl part end-

attached (**D1-III** and **D2-III)** results in sharper transitions in comparison to the sandwich-type architecture. The modified oligopyrenyl part brings about 9°C stability to **D1-III** (78.1°C) in comparison to the fully natural reference hybrid **D4-III** (69.1°C). Furthermore the hybrid shows a very sharp transition but reduced hyperchromicity at 260nm (8%) for **D1-III** compared to the natural hybrid **D4-III** (14%). This difference can be attributed to the overlap of absorption of the natural nucleobases and of the pyrenyl absorption bands and their intrinsic hyperchromic effect.

D2-III (69.3°C) shows the same melting temperature as the reference duplex **D4-III** (69.1°C) which can be explained by attributing a negative effect of the 8-Bromo-dG (which lies in the *syn* conformation) on the thermal stability of the duplex while having an opposing positive (stabilizing) effect of the pyrene moieties as seen in the case of **D1-III**. So it is by chance that the two hybrids **D2-III** and **D4-III** show the same thermal stability. In addition also the transition of **D2-III** is sharp in nature and hints for a high level of cooperativity.

The profile for **D3-III** is not that sharp in nature as the other hybrids and the thermal stability is decreased by almost 12°C in comparison to **D4-III** (57.2°C for hybrid **D3-III** and 69.1°C for hybrid **D4-III)**. The main difference is that the modified non-nucleosidic part is embedded in a sandwichtype manner in between the natural oligonucleotide part thus disrupting the continuous stack present in all the other hybrids. The disruption of the natural oligonucleotide part not only results in a lower level of cooperativity seen by the less sharp transition but it also leads to a lower thermal stability.

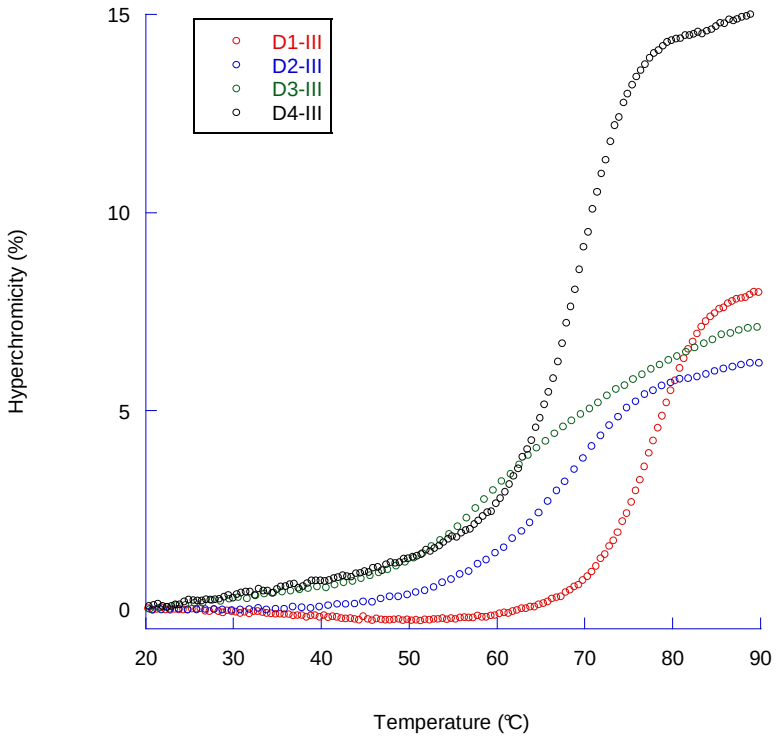

Figure 3.1 Thermal melting profile of **D1-III** to **D4-III** at 100 mM NaCl, 10 mM phosphatebuffer, monitored at 260 nm.

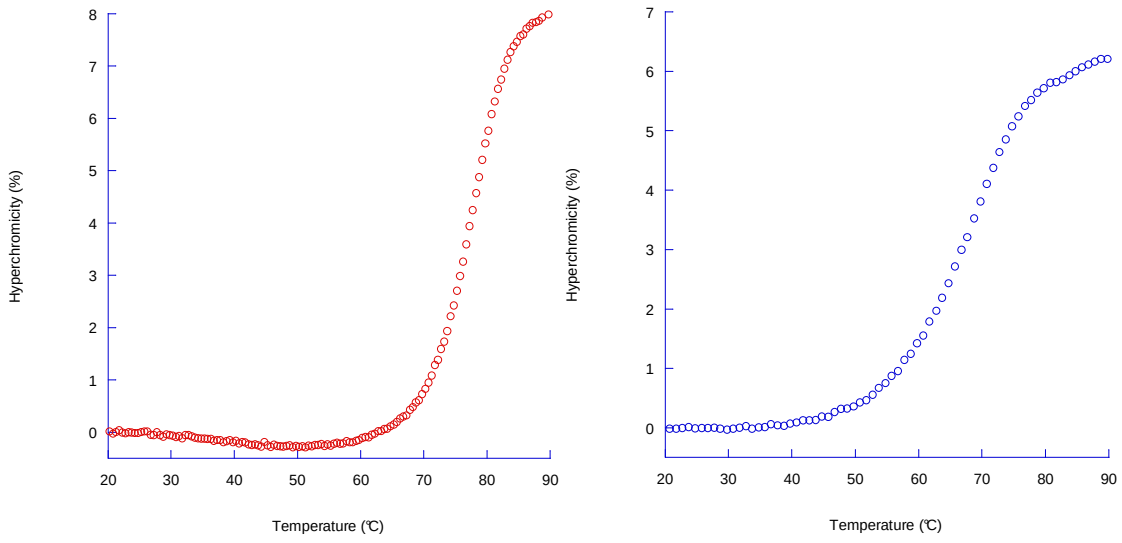

Figure 3.2 Melting profile of **D1-III** (left) and **D2-III** (right) at 100 mM NaCl, 10 mM phosphatebuffer, monitored at 260 nm.

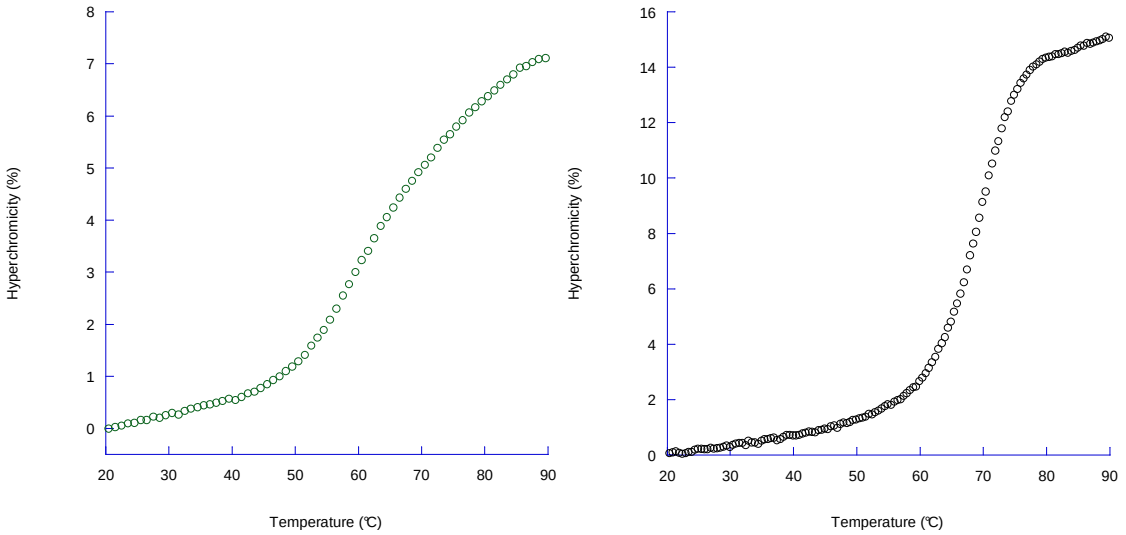

Figure 3.3 Melting profile of **D3-III** (left) and **D4-III** (right) at 100 mM NaCl, 10 mM phosphatebuffer, monitored at 260 nm

UV-Vis absorption of **D1-III** at low and high NaCl concentration

The temperature dependent absorption spectrum of hybrid **D1-III** at 100 mM NaCl shows three main absorption bands which mainly correspond to the absorption bands of the pyrenyl moiety, with maxima at 349 nm, 272 nm and 245 nm (Figure 3.4). The absorption band of the oligonucleotide part around 260 nm is only weakly visible and overlapped by the pyrene absorption. The hyperchromic effect upon heating can be nicely seen in all of the three main absorption bands although the band at 349 nm only shows the weakest hyperchromic effect since this band is not overlapped by the absorption of the natural part. The increasing absorptivity between 70°C and 80°C is in good agreement with the determined melting temperature (78.1°C) and a result of interstrand pyrene aggregation.

Another feature of the spectrum is the observable isosbestic point at 372 nm which hints for a two-state model for the melting behavior of the hybrid. Additionally all three absorption bands show a vibronic fine structure hinting for reduced rotational freedom of the pyrene moieties in the hybrid. This reduced freedom is lost again going from the low to high temperature by the melting process and thus disappearance of the vibronic structure.

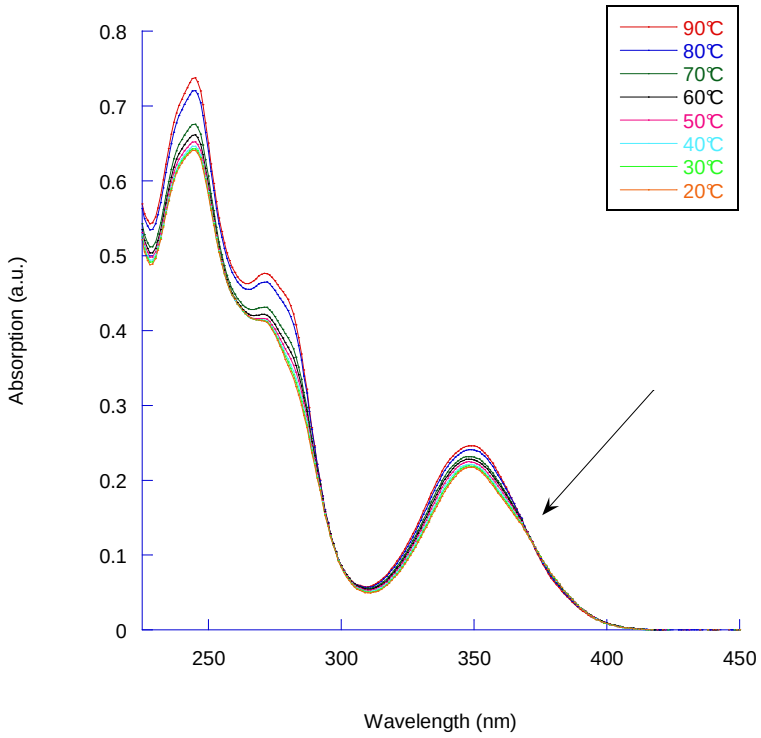

Figure 3.4 Temperature dependent UV-Vis absorption spectra of hybrid **D1-III** (arrow indicates isosbestic point). Oligonucleotide concentration: 1 µM, 100 mM NaCl, 10 mM phosphatebuffer pH 7.4.

The temperature dependent UV-Vis absorption spectra of hybrid **D1-III** at high ionic strength (4 M NaCl) shows several features which are different from the case at low ionic strength. Again the three bands arising form the pyrene moieties are again nicely visible. The overall absorptivity of these bands though is reduced in all three cases hinting for a closer packing of the pyrene molecules and thus a hypochromic effect in comparison to the low ionic strength. As in analogy to the low ionic strength also at 4 M NaCl concentration the hyperchromic effect upon increasing the temperature is nicely visible for all three bands although more pronounced for the two high energetic bands.

The most striking difference is the much more pronounced occurrence of the vibronic structure. Especially in the case of the 350 nm band the vibronic structure is very well defined hinting for the further reduced rotational freedom of the pyrene moieties in the hybrid. The absence of isosbestic point hints for a more complex model in comparison to the case at low ionic strength.

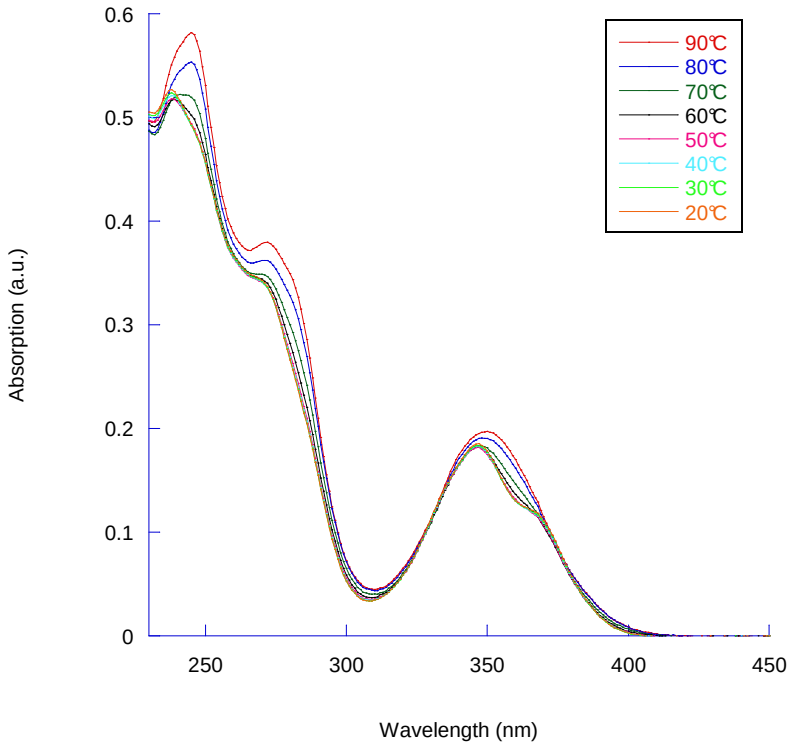

Figure 3.5 Temperature dependent UV-Vis absorption spectra of hybrid **D1-III**. Oligonucleotide concentration: 1 µM, 4 M NaCl, 10 mM phosphatebuffer pH 7.4.

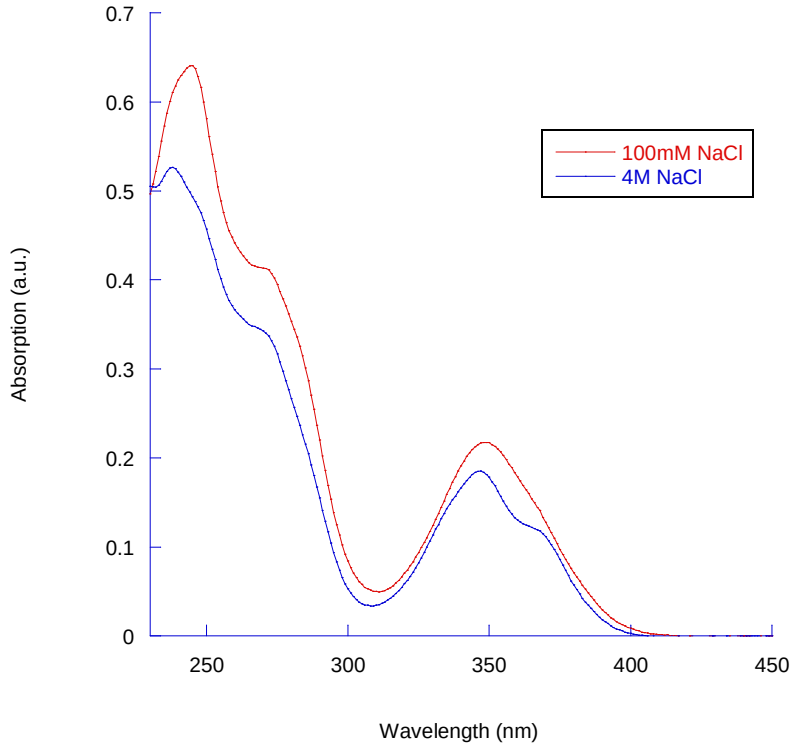

Figure 3.6 Comparison of the UV-Vis absorption spectra of hybrid **D1-III** at 100 mM and 4 M NaCl at 20°C. Oligonucleotide concentration: 1 µM, 10 mM phosphatebuffer pH 7.4.

UV-Vis absorption of **D2-III** at low and high NaCl concentration

Comparable to the hybrid **D1-III** at low ionic strength the temperature dependent absorption spectra of hybrid **D2-III** show the same three absorption bands (349 nm, 272 nm, 245 nm). The intensities are reduced though and the hyperchromic effect is reduced as well compared to **D1-III**. Looking especially at the 350 nm absorption band one can see the weak vibronic structure of the band which is then vanishing once going to elevated temperatures. The indicated isosbestic point at 369 nm is exactly at the same wavelength as in **D1-III**. Additionally, there are two more isosbestic points visible at 307 nm and at 290 nm (Figure 3.7).

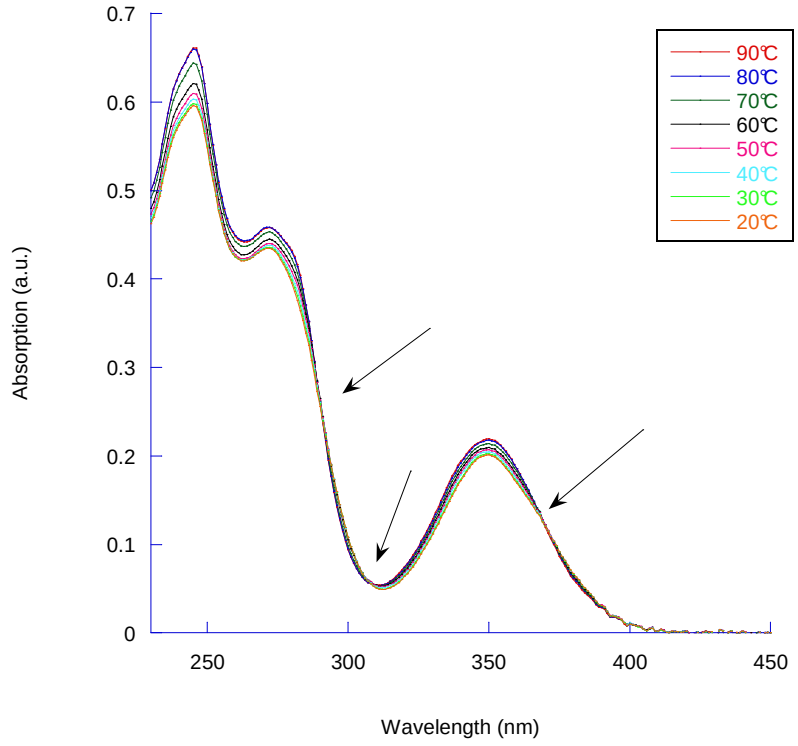

Figure 3.7 Temperature dependent UV-Vis absorption spectra of hybrid **D2-III**. Oligonucleotide concentration: 1 µM, 100 mM NaCl, 10 mM phosphatebuffer pH 7.4.

The temperature dependent spectra of hybrid **D2-III** at elevated ionic strength shows also a reduced absorptivity compared to the low ionic strength. The reduction of the hyperchromic effect upon heating the system is as well visible. The appearance of well resolved vibronic bands upon cooling is in analogy to the hybrid **D1-III**.

The vibronic bands are most pronounced for the absorption band at 245 nm and 350 nm. The band at the energy between those bands shows only weak vibronic bands probably due to the overlap of the absorption bands of the natural bases and the pyrene absorption band around 270 nm. The lacking of isosbestic points hints for a more complex model than just two states.

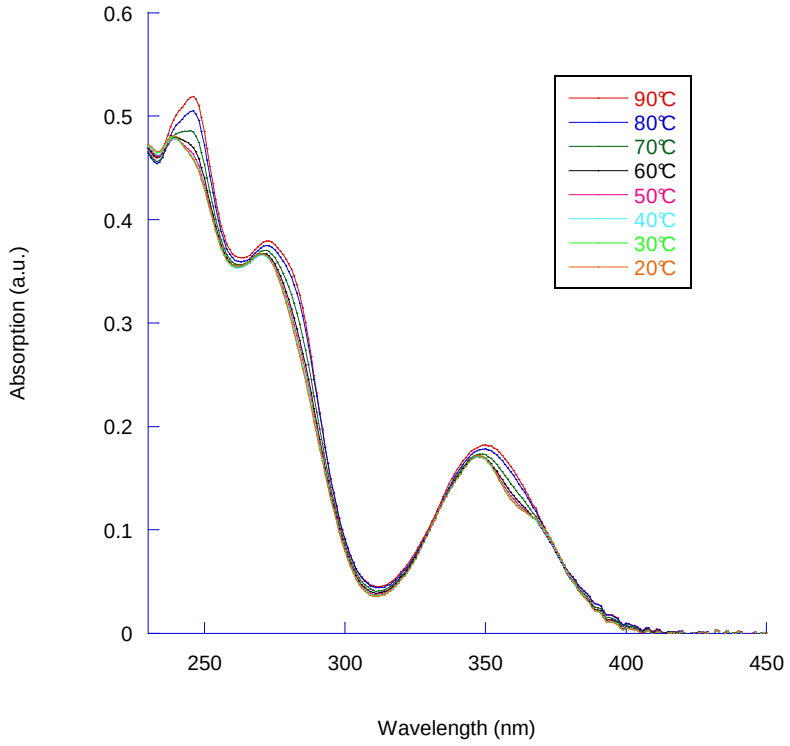

Figure 3.8 Temperature dependent UV-Vis absorption spectra of hybrid **D2-III**. Oligonucleotide concentration: 1 µM, 4 M NaCl, 10 mM phosphatebuffer pH 7.4.

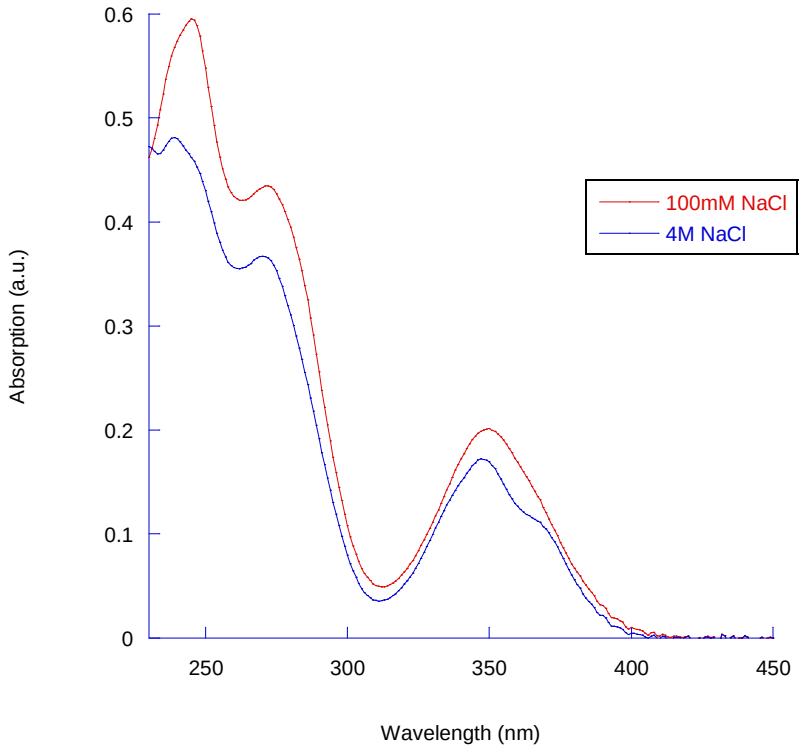

Figure 3.9 Comparison of the UV-Vis absorption spectra of hybrid **D2-III** at 100 mM and 4 M NaCl at 20°C. Oligonucleotide concentration: 1 µM, 10 mM phosphatebuffer pH 7.4.

UV-Vis absorption of **D3-III** at low and high NaCl concentration

The main three absorption bands typical for the pyrene building block incorporated into the hybrid are again seen also in hybrid **D3-III** which has the sandwich type arrangement of the pyrenyl stretch in contrast to the end type arrangement of **D1-III** and **D2-III**. The hyperchromic effect upon heating is well visible for all three bands, indicating the interstrand stacking of the pyrene molecules. The hyperchromic effect seems to be more pronounced in this sandwich-type of trisegmental arrangement. Fixation of both ends of the oligopyrenyl stretch seems to be in favor of stacking interactions. Looking at the low energy absorption band of pyrene again a vibronic structure although weak is visible. In addition an isobestic point at 372 nm is visible, so slightly redshifted compared to the hybrids **D1-III** and **D2-III**.

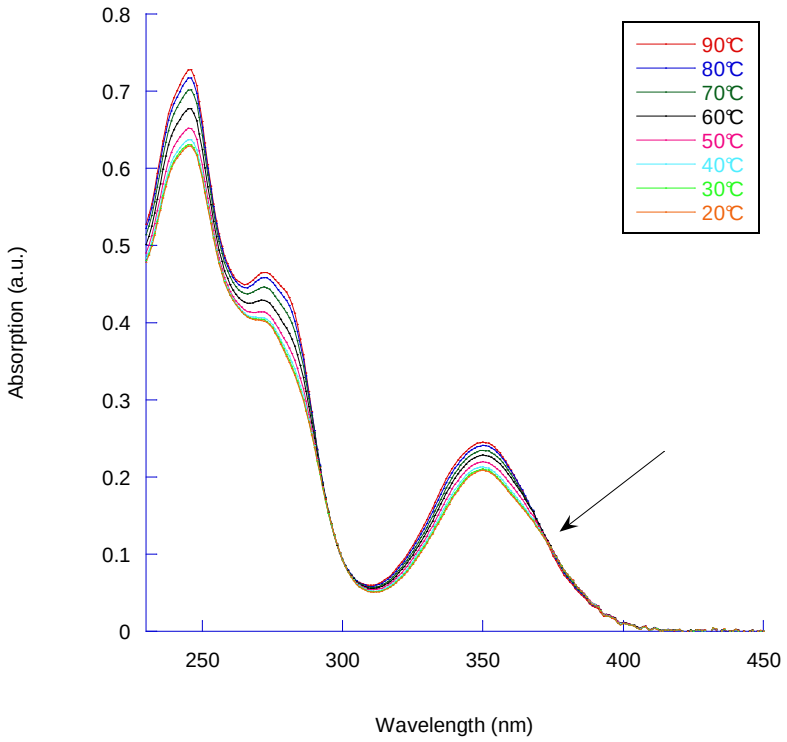

Figure 3.10 Temperature dependent UV-Vis absorption spectra of hybrid **D3-III**. Oligonucleotide concentration: 1 µM, 100 mM NaCl, 10 mM phosphatebuffer pH 7.4.

Increasing the ionic strength to 4 M NaCl, results again in a decrease of the overall absorptivity as in the other two hybrids although the effect is not that drastic. The main difference is found in the vibronic structure of the absorption bands. Whereas in **D1-III** and **D2-III** the vibronic structure was much better resolved upon increasing the ionic strength, **D3-III** shows not at all that dramatic changes in the vibronic band structure. The overall signature remains unchanged. In contrast to **D1-III** and **D2-III** where the isobestic points were lost in high ionic strength, **D3-III** shows the appearance of two new isobestic points at 292 nm and 303 nm.

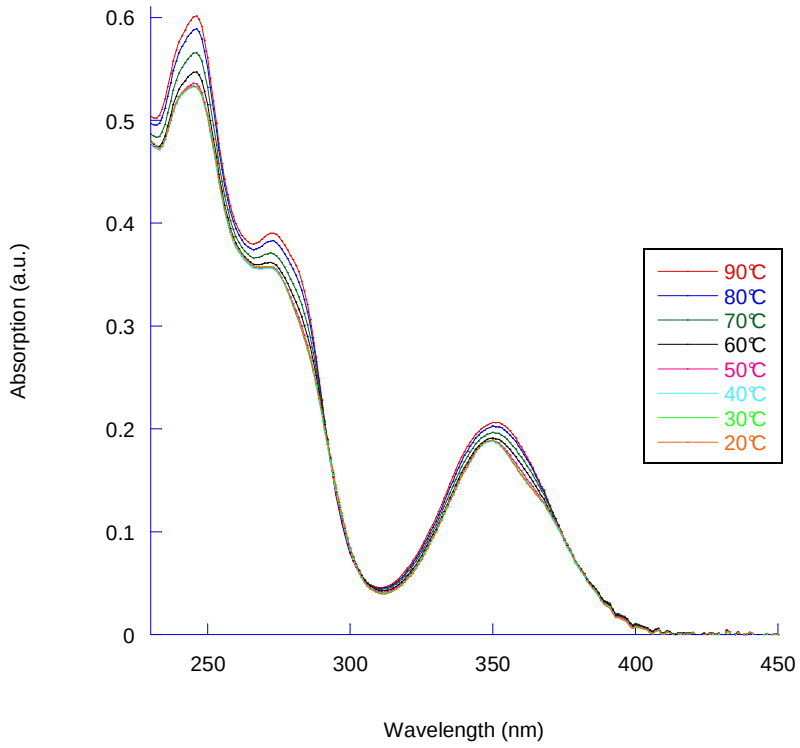

Figure 3.11 Temperature dependent UV-Vis absorption spectra of hybrid **D3-III**. Oligonucleotide concentration: 1 µM, 4 M NaCl, 10 mM phosphatebuffer pH 7.4.

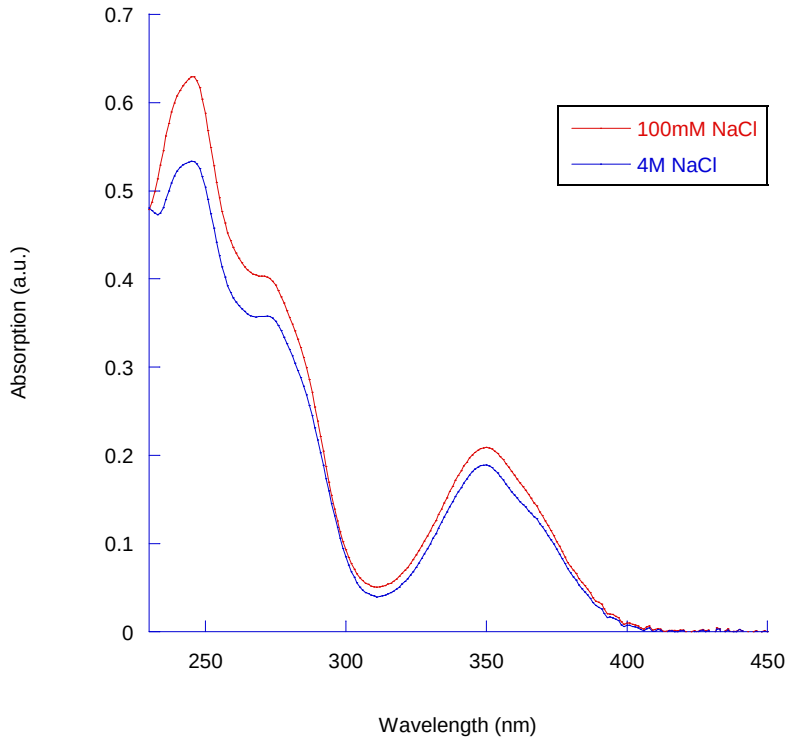

Figure 3.12 Comparison of the UV-Vis absorption spectra of hybrid **D3-III** at 100 mM and 4 M NaCl at 20°C. Oligonucleotide concentration: 1 µM, 10 mM phosphatebuffer pH 7.4.

Fluorescence of **D1-III** at low and high ionic strength

The fluorescence properties of the hybrids were measured depending on temperature and ionic strength. In the case of **D1-III** the spectra is dominated by the intra- and intermolecular excimer emission. Whereas the emission intensity steadily decreases in the case of 100 mM NaCl by increasing the temperature in the case of the high ionic strength (4 M NaCl) the behavior of the intensity by changing the temperature is somewhat different: First the intensity decreases by increasing the temperature as in the case of the physiological conditions. Increasing the temperature beyond 60°C the intensity is going to higher values again and reaches the same intensity at 90°C as it shows for 20°C. The most interesting feature though is the change in emission wavelength which stays in the case of low ionic strength more or less constant (for 20°C it is 503 nm and for 90°C it is 505 nm) while in the case of the high ionic strength shows a considerable shift of about 12 nm (for 20°C it is 495 nm and for 90°C it is 507 nm). So the main difference lies in the hybridized form at 20°C with a difference in emission wavelength of about 8 nm.

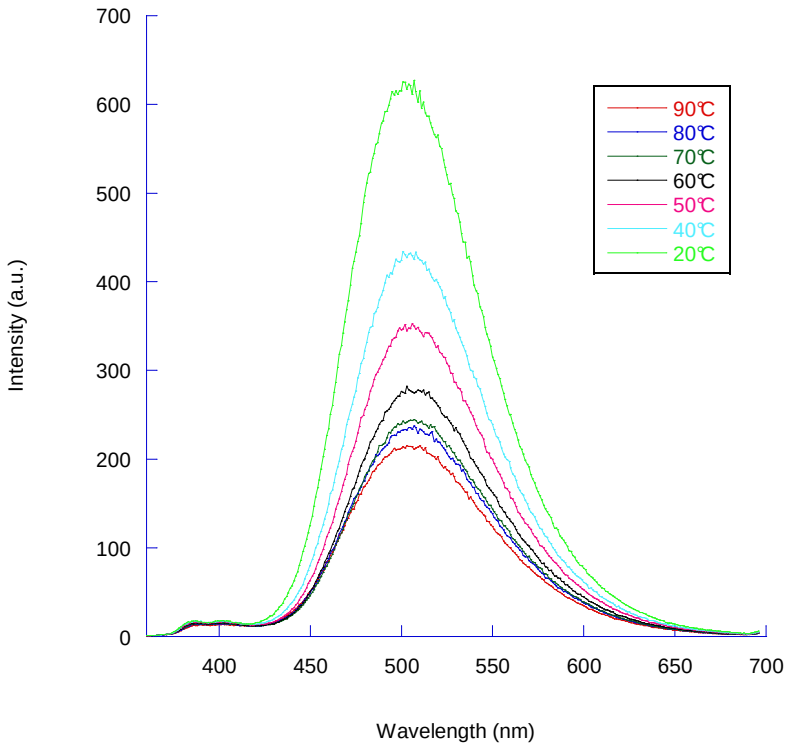

Figure 3.13 Temperature dependent fluorescence spectra of hybrid **D1-III**. Oligonucleotide concentration: 1 µM, 100 mM NaCl, 10 mM phosphatebuffer pH 7.4. Excitation wavelength: 350 nm, detector: 800 V, slit width: 5 nm/5 nm.

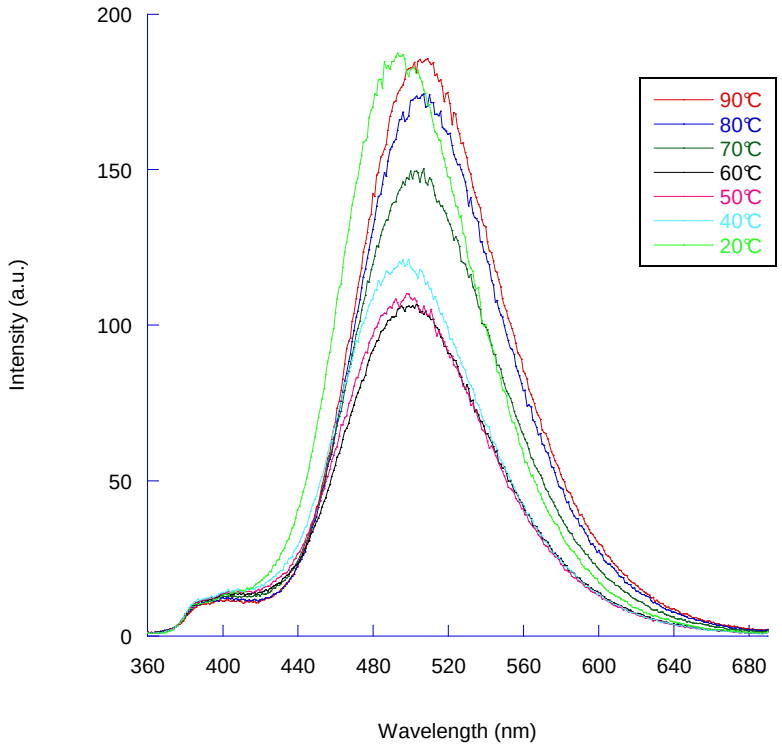

Figure 3.14 Temperature dependent fluorescence spectra of hybrid **D1-III**. Oligonucleotide concentration: 1 µM, 4 M NaCl, 10 mM phosphatebuffer pH 7.4. Excitation wavelength: 350 nm, detector: 800 V, slit width: 5 nm/5 nm.

Fluorescence of **D2-III** at low and high ionic strength

The main difference of **D2-III** in comparison with **D1-III** is certainly the much higher portion of monomer intensity (430 nm to 360 nm) especially in the high ionic strength case. The behavior of the emission wavelength depending on temperature is the same for **D2-III** as for **D1-III** by showing almost no change at physiological conditions (505 nm at 90°C to 504 nm at 20°C). In the case of the high ionic strength the blueshift upon hybridization of about 7nm is comparable as well (505 nm at 90°C to 498 nm at 20°C).

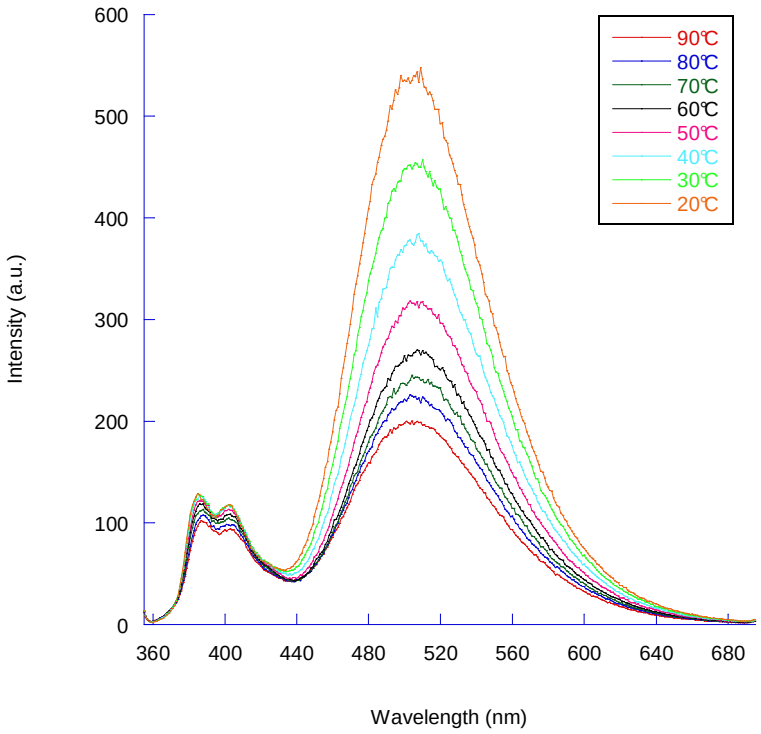

Figure 3.15 Temperature dependent fluorescence spectra of hybrid **D2-III**. Oligonucleotide concentration: 1 µM, 100 mM NaCl, 10 mM phosphatebuffer pH 7.4. Excitation wavelength: 350 nm, detector: 800 V, slit width: 5 nm/5 nm.

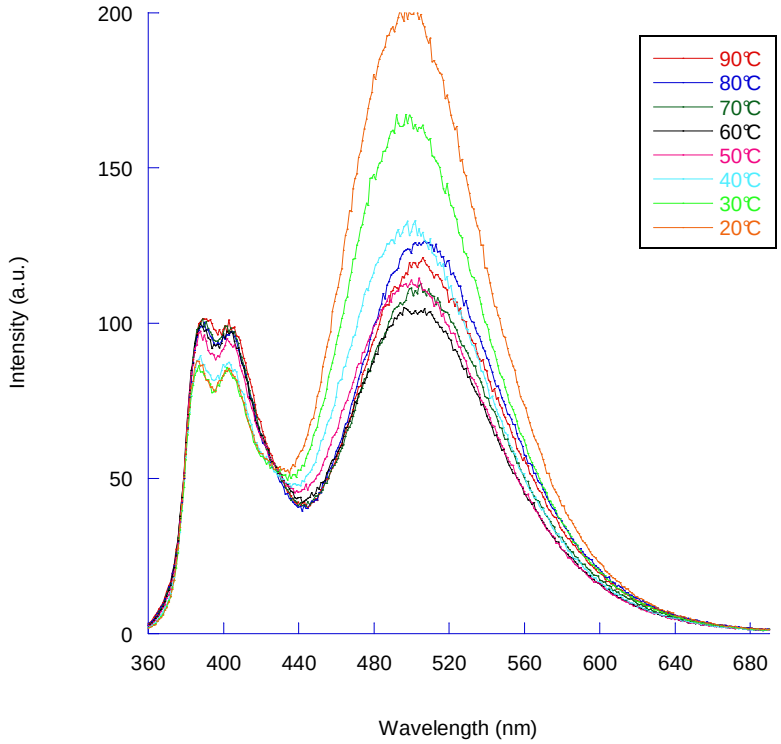

Figure 3.16 Temperature dependent fluorescence spectra of hybrid **D2-III**. Oligonucleotide concentration: 1 µM, 4 M NaCl, 10 mM phosphatebuffer pH 7.4. Excitation wavelength: 350 nm, detector: 800 V, slit width: 5 nm/5 nm.

Fluorescence of **D3-III** at low and high ionic strength

Although the pyrene units are attached differently in the case of **D3-III** the temperature dependent emission wavelength changes in the same manner as for the **D1-III** and **D2-III.**

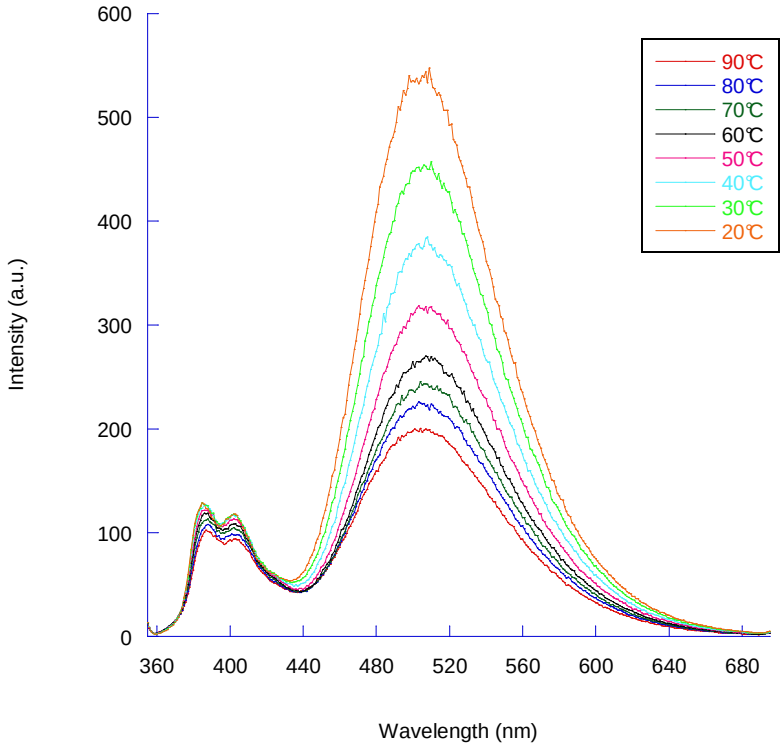

Figure 3.17 Temperature dependent fluorescence spectra of hybrid **D3-III**. Oligonucleotide concentration: 1 µM, 100 mM NaCl, 10 mM phosphatebuffer pH 7.4. Excitation wavelength: 350 nm, detector: 800 V, slit width: 5 nm/5 nm.

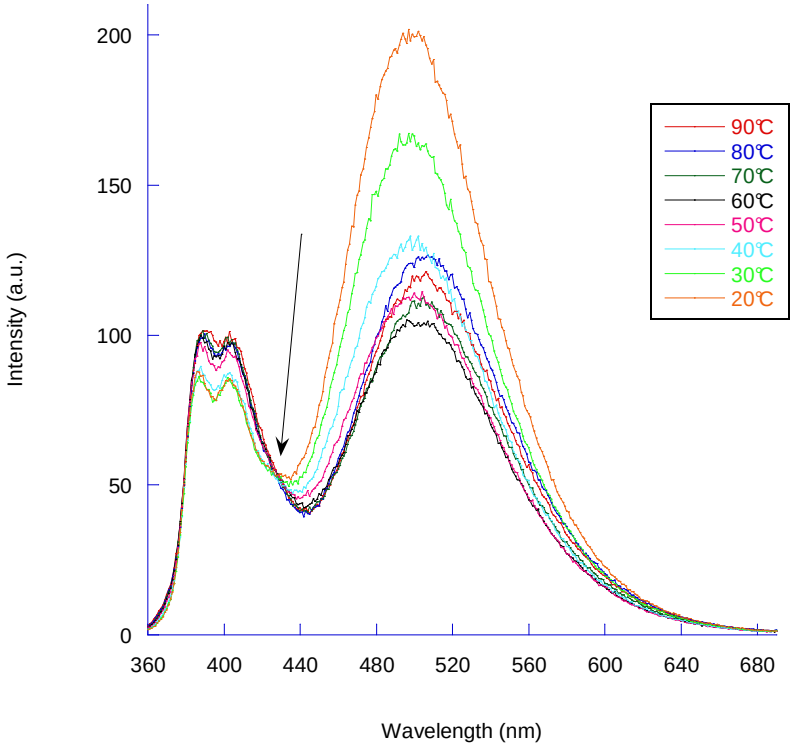

Figure 3.18 Temperature dependent fluorescence spectra of hybrid **D3-III**. Oligonucleotide concentration: 1 µM, 4 M NaCl, 10 mM phosphatebuffer pH 7.4. Excitation wavelength:350 nm, detector: 800 V, slit width: 5 nm/5 nm.

Circular dichroism of **D4-III**

As the natural sequence used for **D1-III** and **D2-III** can lead to a B-Z junction and therefore may hinder the transition of the alternating d(CG) sequence the circular dichroism spectra was measured at 2 mM $MgCl_2$ and at 700mM $MgCl_2$. As the spectra indicate there seems to be a certain transition visible as can be seen by the reduction of the positive band at 277 nm characteristic for B-DNA. As the CD spectra are the sum of the B-form and the Z-form it can be concluded that there is a certain portion of the alternating d(CG) sequence in a left-handed form but the transition is hindered by the formation of the B to Z junction.

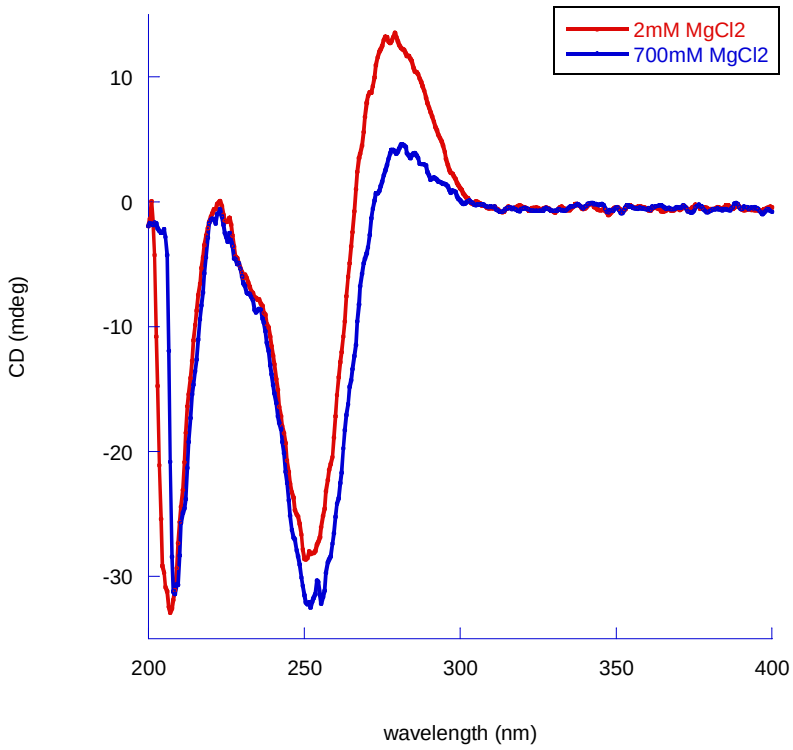

Figure 3.19 Circular dichroism of **D4-III** at 20°C. Oligonucleotide concentration: 5 µM, 2 mM $MgCl_2$ and 700 mM $MgCl_2$, 10 mM phosphatebuffer pH 7.4.

Circular dichroism of **D1-III**

Looking at the spectrum of **D1-III** at physiological conditions the CD reveals that it is clearly B-DNA type and that the pyrene units do not show any CD activity.

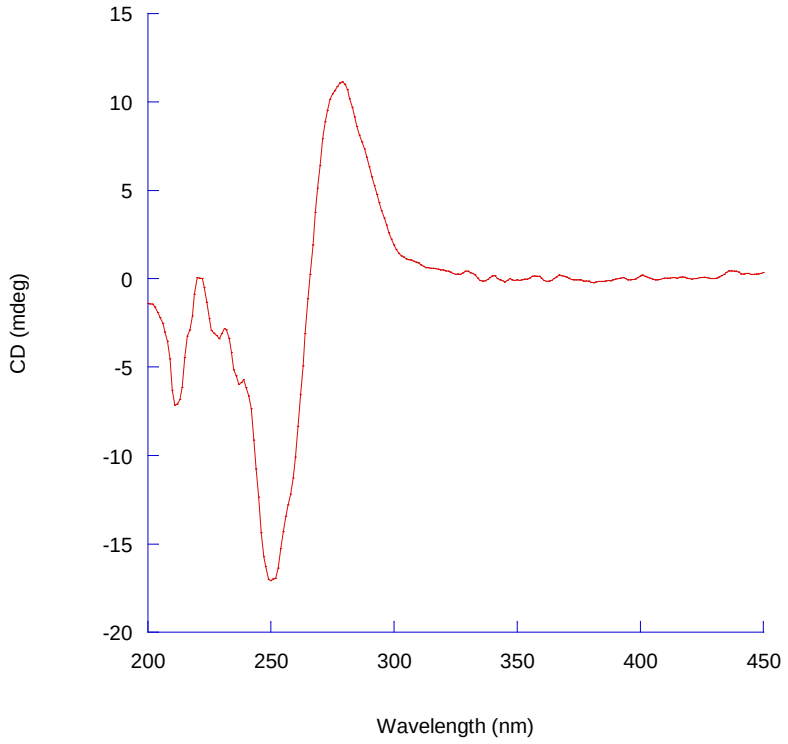

Figure 3.20 Circular dichroism of **D1-III** at 20°C. Oligonucleotide concentration: 5 µM, 100 mM NaCl, 10 mM phosphatebuffer pH 7.4.

When increasing the concentration to 4 M NaCl the signals originating from the pyrene moieties are the dominating part in the CD spectrum. At lower energy there is a multiple cotton effect pattern visible with a negative cotton effect at 374 nm followed by a positive effect at 361 nm. This couplet is followed by a positive cotton effect at 348 nm and a negative effect at 328 nm which can also be attributed as a second exciton couple. As the intensity of the CD signals from the pyrene units is much higher than from the natural oligonucleotide part it is very hard to judge about the conformation of the DNA part. There is actually a negative band visible at 293 nm which can hint for a certain amount of the DNA part adopting a left-handed helix. When heating the hybrid to 90°C the CD signal of the DNA part only remains showing typical signature of singlestrands and the signals from the pyrenyl stretch vanish. A titration with $MgCl_2$ shows that the multiple cotton effects are developing with increasing level of ionic strength and that there is certain amount of left-handed DNA present.

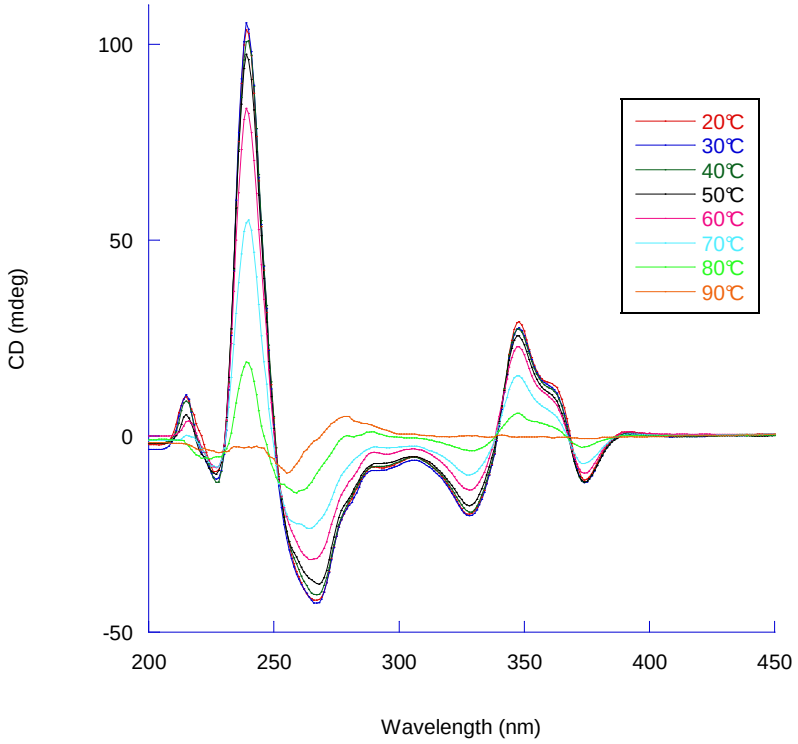

Figure 3.21 Temperature dependent circular dichroism of **D1-III**. Oligonucleotide concentration: 5 µM, 4 M NaCl, 10 mM phosphatebuffer pH 7.4.

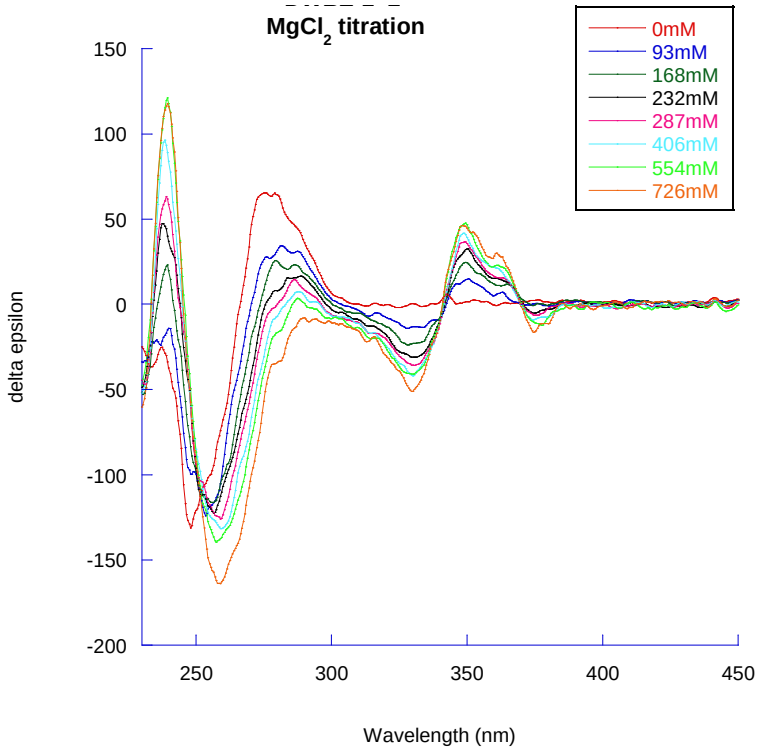

Figure 3.22 $MgCl_2$ dependent circular dichroism of **D1-III**. Oligonucleotide concentration: 5 µM, 10 mM phosphatebuffer pH 7.4, 20°C

Circular dichroism of **D2-III**

The CD at physiological conditions for hybrid **D2-III** first of all shows that the desired left-handed Z-DNA is already formed manifested by the negative band at 294 nm and the positive band at 270 nm. Interestingly there seems to be an exciton coupled CD visible with positive chirality in the pyrene only absorption region although of very weak nature. Upon heating the hybrid, the left-handed duplex is destroyed and the typical CD spectrum of a singlestrand becomes visible accompanied by the disappearance of the exciton coupled CD of the pyrene units.

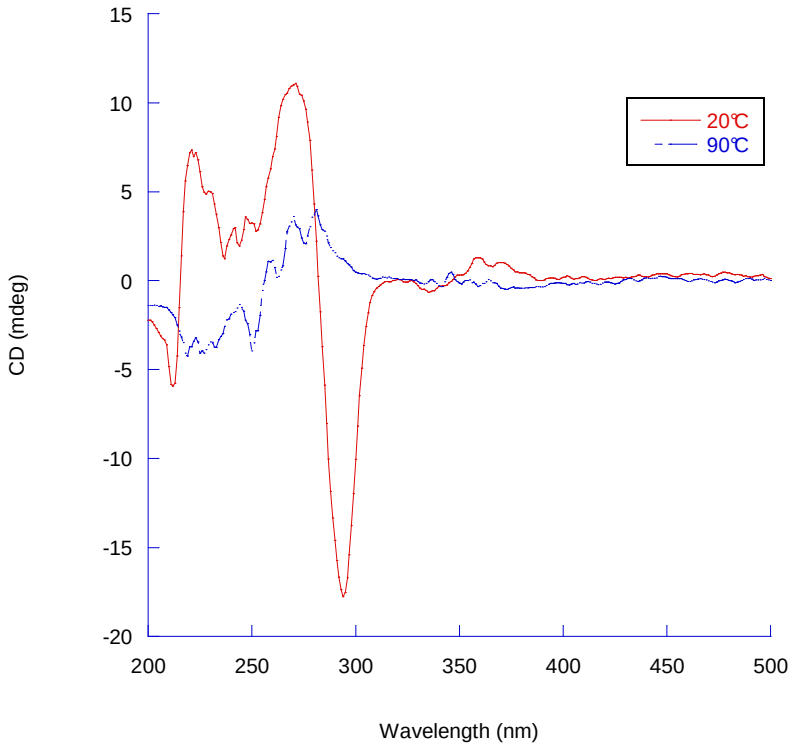

Figure 3.23 Temperature dependent circular dichroism of **D2-III**. Oligonucleotide concentration: 5 µM, 100 mM NaCl, 10 mM phosphatebuffer pH 7.4.

At 4 M NaCl the left-handed hybrid is still nicely visible as seen by the negative band at 294 nm. The signature of the pyrene units though change dramatically in comparison to hybrid **D1-III**. There is also a multiple cotton effect visible composed of a negative effect at 375 nm followed by a positive effect at 361 nm. Then a positive cotton effect is visible at 346 nm and a negative effect at 322 nm although of very weak nature. The pattern observed here for **D2-III** is exactly the same as the one observed for **D1-III** concerning

the signs (-/+/+/-). The obvious difference can be found in the relative intensities and the shifts of the bands. The CD signals of **D2-III** are much less intense when compared to the case of **D1-III**. Looking at the relative intensities of the cotton effects there lays the big difference. The negative cotton effect at 375 nm is the most intense in this pattern whereas in the case of **D1-III** this effect is much less pronounced compared to the other cotton effects present. Furthermore the two effects at 346 nm and 322 nm are blueshifted compared to **D1-III** and the effect at 328 nm showing high intensity for **D1-III** in the case of **D2-III** this effect at 322 nm is almost not visible.

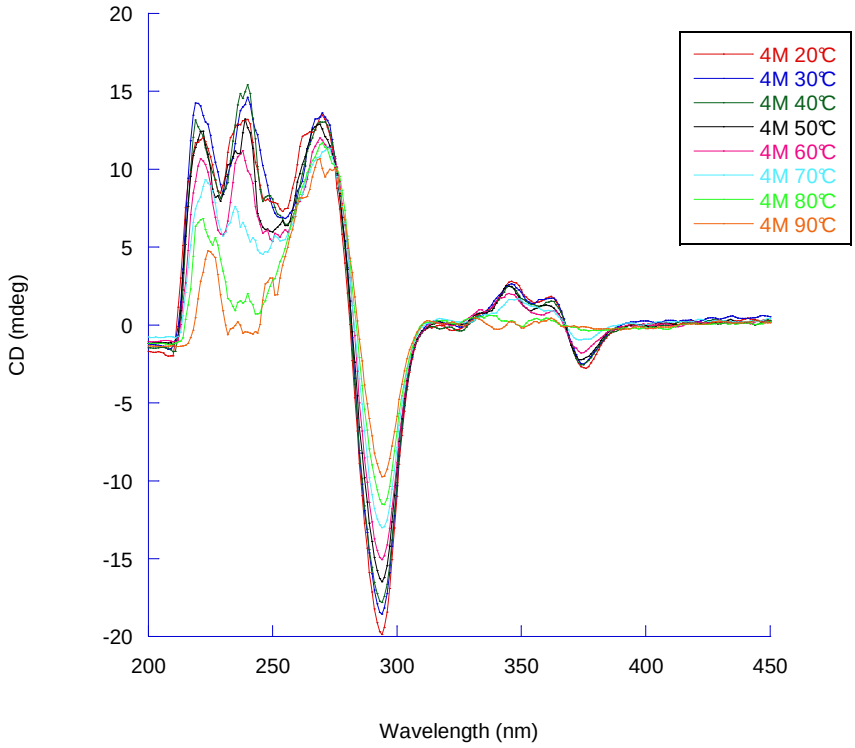

Figure 3.24 Temperature dependent circular dichroism of **D2-III**. Oligonucleotide concentration: 5 µM, 4 M NaCl, 10 mM phosphatebuffer pH 7.4.

The titration experiment with $MgCl_2$ shows the development of the multiple cotton effects with increasing concentration of the salt by simultaneously keeping the left-handed form (seen by the negative band at 294 nm) of the DNA part.

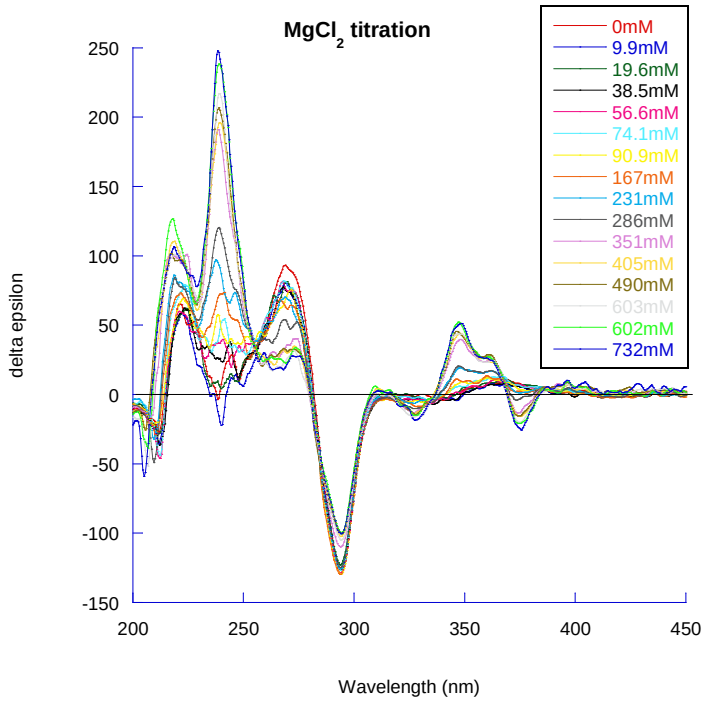

Figure 3.25 $MgCl_2$ dependent circular dichroism of **D2-III**. Oligonucleotide concentration: 5 µM, 10 mM phosphatebuffer pH 7.4, 20°C.

Circular dichroism of **D3-III**

Hybrid **D3-III** shows a somewhat different picture compare to the first two hybrids. At physiological conditions the exciton coupled CD with a positive cotton effect at 354 nm and a negative at 334 nm is clearly visible. Heating of this hybrid results in disappearance of the CD signal of the pyrene only absorption band. At elevated ionic strength the exciton coupled CD remains the same with a positive cotton effect at 353 nm and a negative at 333 nm although with a much larger intensity.

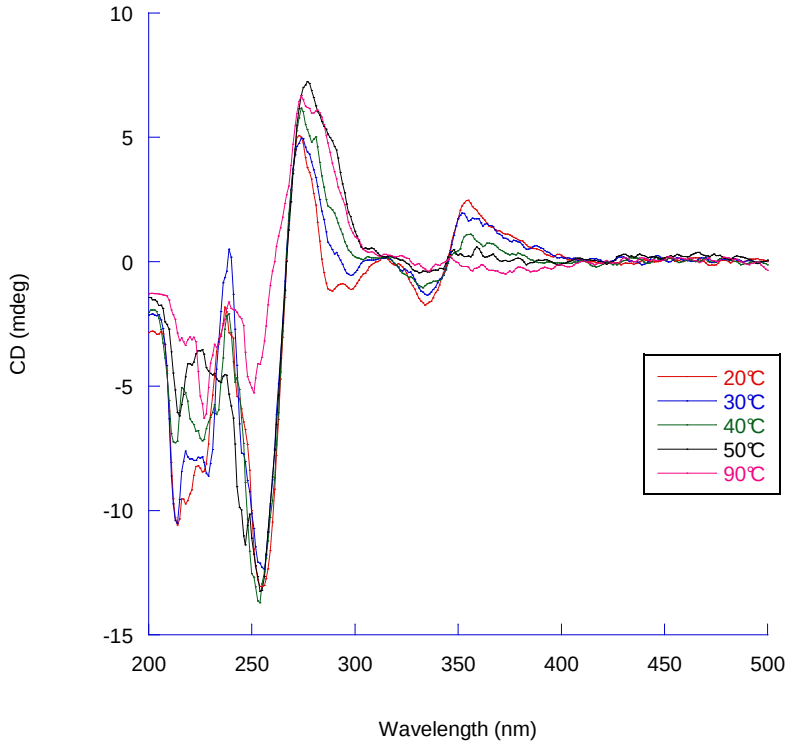

Figure 3.26 Temperature dependent circular dichroism of **D3-III**. Oligonucleotide concentration: 5 µM, 100 mM NaCl, 10 mM phosphatebuffer pH 7.4.

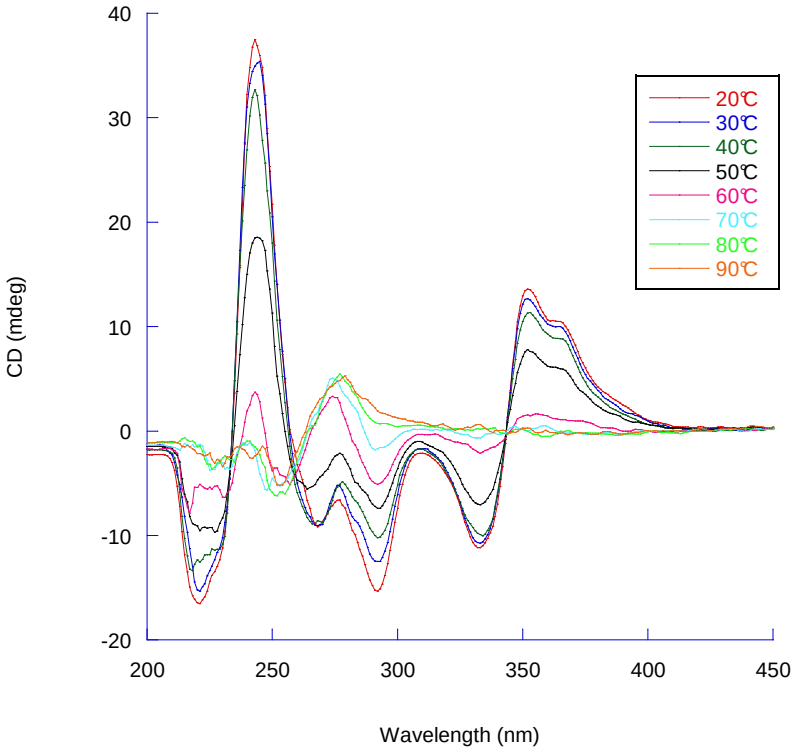

Figure 3.27 Temperature dependent circular dichroism of **D3-III**. Oligonucleotide concentration: 5 µM, 4 M NaCl, 10 mM phosphatebuffer pH 7.4.

The titration experiment shows that the signature of the exciton coupled CD signal does not change although growing in intensity upon increasing the amount of salt. The embedded pyrenyl part is not much affected by the increase in salt for this chimera.

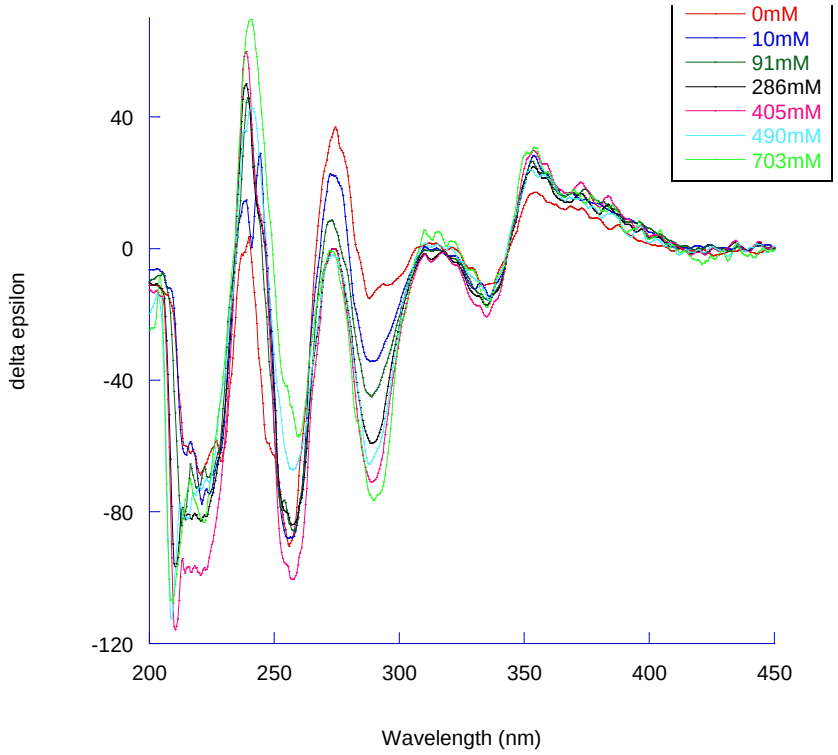

Figure 3.28 $MgCl_2$ dependent circular dichroism of **D3-III**. Oligonucleotide concentration: 5 µM, 10 mM phosphatebuffer pH 7.4, 20°C.

Quantum Yields

In order to look at another aspect which could be the result of different arrangements of the stretches of non-nucleosidic pyrene residues the quantum yields of the different hybrids was measured. The standard used was the quinine sulfate and the results are shown in Table 3.2.

Duplex	**Sequence**	Quantum Yield (%)
D1-III	(5`) ACG TGA CGC GCG CG SSSSSSS(3`) (3`) TGC ACT GCG CGC GC SSSSSSS(5`)	0.182
D2-III	(5`) ACG TGA CG*C G*CG* CG* SSSSSSS(3`) (3`) TGC ACT G*CG* CG*C G*C SSSSSSS(5`)	0.175
D3-III	(5`) ACG TGA SSSSSSS CGC GCG CG (3`) (3`) TGC ACT SSSSSSS GCG CGC GC (5`)	0.169

Table 3.2 Quantum Yields for the hybrids **D1-III** to **D3-III** at physiological conditions

As can be seen by the obtained values the quantum yield of the pyrene stacks is not affected by the neighboring DNA part. Weather the oligopyrenyl part is attached only on one side of the nucleic acid part like for **D1-III** and **D2-III** or if it is embedded in the DNA duplex **D3-III** the quantum yield does not change. (18.2% and 17.5% for the end-attachment versus 16.9% for the sandwich type arrangement). Furthermore also the conformation of the attached duplex seems also not to play a defined role. If the DNA directly attached to the pyrene strand is right- or left handed does not seem to influence the quantum yield as can be seen by the comparison of **D1-III** and **D2-III**.

3.4 Conclusion and outlook

In conclusion the three segmental hybrids synthesized in this study showed a distinct difference between the case where the non-nucleosidic pyrenyl stretch is attached only from one side (**D1-III** and **D2-III**) and the case when the pyrene part is flanked by two segements of DNA (**D3-III**). *Thermal stability* of the hybrids **D1-III** and **D2-III** is increased by the attachment of the pyrene stretch thereby not disturbing the contiunuous base stacking of the DNA part. When this DNA part is split into two parts by the non-nucleosidic pyrenes as is the case for **D3-III** the thermal stability decreases probably due to the distruption of the possible base stacking of the two segments. *Fluorescence spectroscopy* shows almost the same behavior of emission wavelength in function of the temperature and ionic strength for all three hybrids. There is no or only a slight red shift in excimer emission upon hybridization at low ionic strength. At high ionic strength the emission maxima shift to higher energy when the temperature is decreased. CD spectroscopy shows that the hybrids **D2-III** and **D3-III** already have some organization of the pyrene chromophores at physiological conditions although for **D2-III** this is of weak nature. In the case of **D3-III** this can be attributed to the sandwich-type nature of the non-nucleosidic pyrene building blocks between the two segments of DNA. Although the multiple cotton effects with different relative intensities of the hybrids **D1-III** and **D2-III** are hard to rationalize they are indeed a hint for the difference in arrangement of the pyrenyl stretch in the context of right- or left-handed DNA.

As could be shown the attachment of the pyrene stretch either to one side of the duplex only or between two helical DNA parts significantly influences the possible structural arrangements. In a next step the alternating motif d(CG) already seen in chapter 2 but with putting the pyrenyl stretch between the two flanking sequences could give more insight into the helical arrangement and the context dependence of the non-nucleosidic pyrene units.

3.5. Experimental Section

The synthesis of the required non-nucleosidic pyrene building block with the corresponding C3 linker was done according to the published procedure [34]. Nucleoside phosphoramidites were purchased from *SAFC* (Proligo Reagents) with dG (dmf), dC (ac) and dA (bz) and the 8-Bromo dG (dmf) was purchased from *Glen Research*. Oligonucleotides **ON1-III** to **ON6-III** were prepared via automated oligonucleotide synthesis using standard phosphoramidite chemistry (Activator: Ethylthiotetrazole) on a 394-DNA/RNA synthesizer (*Applied Biosystems*). Oligonucleotides **ON7-III** and **ON8-III** were ordered from *MicroSynth*, Switzerland. The unnatural building block was used as a 0.1 M solutions in 1,2-dichloroethane and the coupling time was increased to 120 seconds instead of 25 seconds used for the natural nucleosides. Cleavage from the solid support and final deprotection was performed manually by treatment with 30% NH_4OH solution at 55°C overnight. All oligonucleotides were purified by reverse phase HPLC (Instrument: LC-10 AT from *Shimadzu* with a UV detector, column: LiChrospher 100 RP-18, 5µm, *Merck*); eluent A= $(Et_3NH)OAc$ (0.1M, pH 7.4); eluent B= 80% MeCN + 20% Eluent A; gradient 5-50% B over 38 min.

For the determination of oligonucleotide stock solution concentrations, small samples were diluted to 10% and the absorbance at 260 nm was measured on a Nanodrop ND-1000 Spectrophotometer from *Thermo Scientific*. Epsilon values were calculated using 15300, 11700, 7400 and 9000 for A, G, C and T, respectively, and 8600 for the pyrene building block.

Molecular mass determination of the oligonucleotides was performed with a Sciex QSTAR pulsar (hybrid quadrupole time-of-flight mass spectrometer, *Applied Biosystems*). ESI-MS (negative mode, CH_3CN/H_2O/TEA) data of the compounds **ON1-III** to **ON6-III** are presented in Table 3.3.

	Oligo #	**Duplex**	**Bruttoformula**	**Calc. aver. mass**	**found mass**

D1-III	**ON2-III** **ON1-III**	(5`) ACG TGA CGC GCG CG SSSSSSS(3`) (3`) TGC ACT GCG CGC GC SSSSSSS(5`)	$C_{303}H_{331}N_{71}O_{123}P_{20}$ $C_{302}H_{332}N_{66}O_{125}P_{20}$	7554.8 7505.8	7555.1 7506.5
D2-III	**ON4-III** **ON3-III**	(5`) ACG TGA CG*C G*CG* CG* SSSSSSS(3`) (3`) TGC ACT G*CG* CG*C G*C SSSSSSS(5`)	$C_{303}H_{327}N_{71}O_{123}P_{20}Br_4$ $C_{302}H_{332}N_{66}O_{125}P_{20}Br_4$	7870.3 7821.3	7870.5 7822.5
D3-III	**ON5-III** **ON6-III**	(5`) ACG TGA SSSSSSS CGC GCG CG (3`) (3`) TGC ACT SSSSSSS GCG CGC GC (5`)	$C_{303}H_{331}N_{71}O_{123}P_{20}$ $C_{302}H_{332}N_{66}O_{125}P_{20}$	7554.8 7505.8	7555.3 7505.7

Table 3.3 Mass spectrometry data (brutto formula, calculated average mass, found mass)

Thermal denaturation experiments (1 µM singlestrand oligonucleotide concentration, 10 mM phosphatebuffer pH 7.4, with varying NaCl concentration as indicated in each case) were carried out on Varian Cary 100 Bio UV-Visible spectrophotometer equipped with a Varian Cary temperature controller and data were collected with Varian WinUV software at various wavelengths as indicated in each case. Cooling- heating- cooling cycles in the temperature range of 90°C to 15°C and a heating/ cooling rate of 0.5°C/ min were used and data points every 0.5°C were recorded. Data were analyzed with KaleidaGraph 4 software from *Synergy Software*. Melting temperature values (T_m) were determined as the maximum of the first derivative of the melting curves. If necessary the curves were smoothed (with a data window of 5) in order to get a reasonable maximum of the first derivative.

Temperature dependent UV-VIS spectra were collected from 90°C to 20°C on a Varian Cary 100 Bio UV-Visible spectrophotometer equipped with a Varian Cary temperature controller. All experiments were carried out at a 1 µM singlestrand oligonucleotide concentration in 10 mM phosphatebuffer (pH 7.4) and the indicated concentration of NaCl.

Temperature dependent fluorescence spectra were recorded from 90°C to 20°C on a Varian Cary Eclipse fluorescence spectrophotometer equipped with a Varian Cary temperature controller (excitation wavelength at 350 nm, excitation and emission slitwidth as well as the detector voltage were varied according to the experiment as indicated). All experiments were carried out with a singlestrand concentration of 1 µM. Data were analyzed with KaleidGagraph 4 software from *Synergy Software*.

Circular dichroism spectra were recorded on a *JASCO* J-715 spectrophotometer equipped with a PFD-350S temperature controller. All experiments were carried out with a singlestrand concentration of 5 µM (if not indicated) in 10 mM phosphatebuffer (pH 7.4) and the indicated NaCl concentration.

Chapter 4: Trisegmental selfcomplementary chimeras

4.1. Abstract

In this chapter the formation of a hairpin-like structure consisting of an oligopyrenyl loop which is able to change its helicity upon changing the helicity of the stem part from right-handed B- to left-handed Z-DNA is investigated. Furthermore the change in molecularity upon increasing the NaCl concentration when shortening the stem is presented.

4.2. Introduction

As it has been shown in the chapter 3 that the mode of incorporation is crucial (end attachment versus sandwich type attachment) in this chapter the flanking DNA sequences are changed to the all alternating d(CG) repeat in contrast to the hybrids in chapter 3 which were synthesized in order to get the desired duplex. In this study the sequences used are self-complementary and a possible self-association was expected.

4.3. Results and Discussion

The single strands **ON1-IV** and **ON2-IV** represent two chimeras which have on both sides of the oligopyrenyl part attached self complementary GC repeats sequences. These were designed in addition to the bisegmental chimeras of chapter 2 and the trisegmental chimeras of chapter 3, but here having the pyrenyl part in a sandwich type manner between the natural oligonucleotide parts in contrast to the single attachment of chapter 2. The variation in length of the potential left-handed forming element (for **ON1-IV** there are 3 GC dinucleotide repeats on each side of the pyrenylpart and for ON2-IV there are 2 GC repeats) was designed in order to get stable but not too stable hybrids in order to study their molecularity. The third oligonucleotide **ON3-IV** was synthesized with the aim

to compare the behavior of a mixed sequence not able to form a left-handed helix at elevated ionic strength with the behavior of **ON1-IV** and **ON2-IV**. For **ON1-IV** and **ON2-IV** there is also the possibility to compare to the reference sequences **ON4-IV** and **ON5-IV** which represent the same alternating GC sequence with different length but the oligopyrenyl part is replaced by 4 thymidine residues in order to simulate the loop region. Table 4.1 shows all the synthesized and characterized oligonucleotides.

ON1-IV	(5`) GCGCGC SSSSSSS GCGCGC (3`)	>90°C
ON2-IV	(5`) GCGC SSSSSSS GCGC (3`)	76.3°C
ON3-IV	(5`) ACG GAA SSSSSSS TTC CGT (3`)	70.5°C
ON4-IV	(5`) GCGC TTTT GCGC (3`)	69.3°C
ON5-IV	(5`) GCGCGC TTTT GCGCGC (3`)	85.1°C
	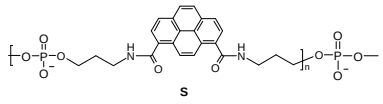 **S**	

Table 4.1 Sequences used in this study, with the determined melting temperature. Conditions: 10 mM phosphatebuffer, 100 mM NaCl, 1 µM oligonucleotide concentration.

Melting experiments

The thermal stability of the possible constructs formed by the single strands was measured by means of thermal denaturation experiments monitored at different wavelengths. The wavelength to monitor the melting profile of the structure formed was chosen in each case based on the temperature dependent UV-Vis absorption spectra comparing the absorption at 20°C and 90°C. Since the overlap of the pyrene absorption and the nucleobase absorption band vary from case to case the wavelength chosen was different in most cases. Since the possibility arises in all the cases to form either the monomolecular hairpin structure or the bimolecular duplex structure the investigation by

concentration dependent melting experiments could give a hint on the molecularity in these structures.

The melting profiles for all oligonucleotides show a cooperative melting process without any hysteresis. Therefore only one cooling ramp is presented. The melting temperature for **ON1-IV** could not be detected as it actually never reaches a plateau and the maximum of the first derivative lies at 90°C and the real melting point is probably beyond 90°C. Because of this high stability the concentration dependent melting experiments did not lead to a conclusion about the molecularity of this structure since already at 1 µM concentration the melting point is above 90°C and not determinable and by increasing the oligonucleotide concentration the melting point would either be the same for a monomolecular process or would even increase in the case of a bimolecular process. By means of concentration dependent melting experiments the molecularity of **ON1** can not be determined.

Comparing **ON1-IV** to **ON5-IV** one can see that also in the case of **ON5-IV** a determination of the thermal stability is almost impossible as the melting temperature is very high indeed and the determined melting point of about 85.1°C is not that meaningful as also in this case the maximum of the first derivative is near 90°C. Also in the case of **ON5-IV** a concentration dependent melting experiment is not really helpful since the melting point is very high and almost impossible to determine.

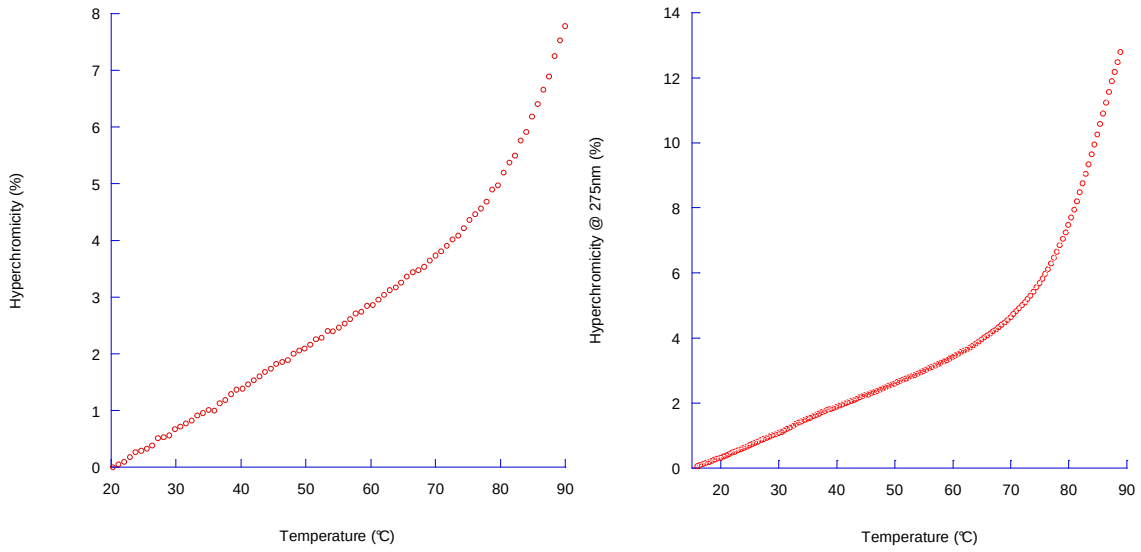

Figure 4.1 Melting profile at 278 nm for **ON1-IV** (left) and at 275 nm for **ON5-IV** (right), Conditions: 10 mM phosphatebuffer, 100 mM NaCl, 1 µM oligonucleotide concentration.

ON2-IV represents the shorter GC sequence and the determined melting point is 76.3°C. The transition though is not really sharp in nature but a melting point is still determinable. Furthermore the melting temperature is independent of the oligonucleotide concentration. This circumstance hints for a monomolecular process which in turn points to a hairpin like structure of this oligonucleotide **ON2-IV**. **ON5-IV** shows a slightly reduced thermal stability of 69.3°C and as well shows no dependence of the melting point on different oligonucleotide concentration at physiological conditions (100 mM NaCl) in agreement with the postulated hairpin structure.

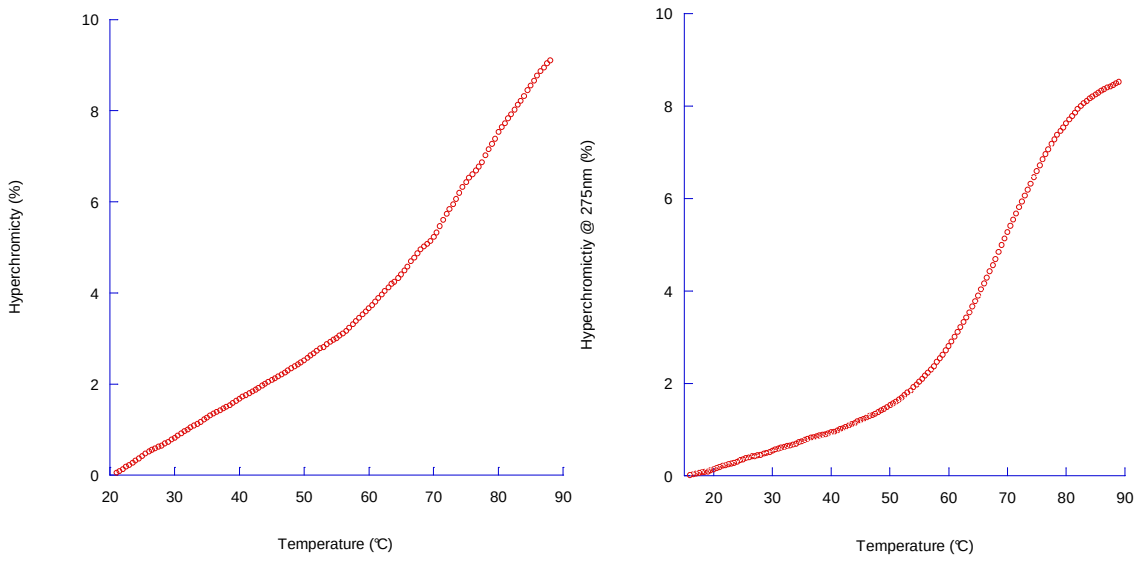

Figure 4.2 Melting at 280 nm for **ON2-IV** (left) and at 275 nm for **ON4-IV** (right), Conditions: 10 mM phosphatebuffer, 100 mM NaCl, 1 µM oligonucleotide concentration.

The melting profile for **ON3-IV** shows a reduced thermal stability in comparison to **ON1-IV** and **ON2-IV** which is mainly due to the nature of the sequence having less GC content. The melting point of 70.5°C is comparable to the one of **ON4-IV** and also the sharpness of the transition is comparable to the one of **ON4-IV**. In the case of **ON3-IV** the concentration dependent melting experiments yield the conclusion of a monomolecular structure. So also in this case a hairpin like structure is hypothesized.

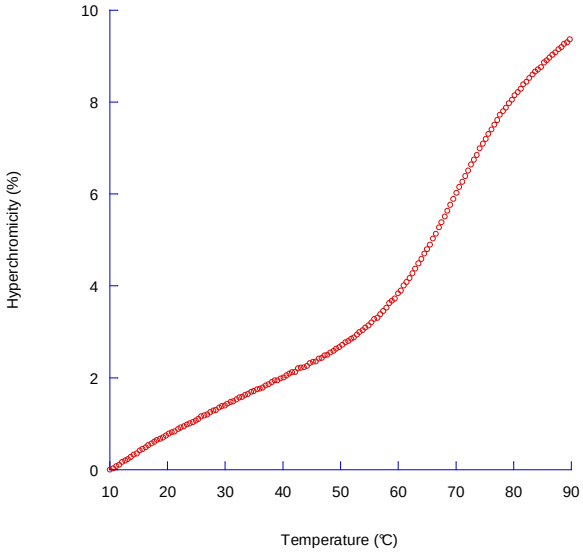

Figure 4.3 Melting profile **ON3-IV** at 245 nm, Conditions: 10 mM phosphatebuffer, 100 mM NaCl, 1 µM oligonucleotide concentration.

UV-Vis

Measuring the temperature dependent absorption spectra of the different hybrids can give different insight into the organization of the pyrene units in the context of the helical scaffold of the DNA. The information gained by the UV-VIS spectra at different temperatures is most valuable in the region where the pyrenyl units only absorb namely between 400 and 300 nm. At higher energies (300 to 200 nm) the absorption bands from the nucleobases as well as the two high energy absorptions from the pyrene units are overlayed and one observes the superposition.

In all the hybrids and under both NaCl concentrations there is the hyperchromic effect observable originating from the reduced absorption of the nucleobases and the pyrene units in the hybridized state compared to the absorption at elevated temperatures or in the singlestrands being not hybridized. There are mainly three bands visible which can be followed: the 350 nm which can be purely attributed to the pyrene absorption, the band between 280 nm and 260 nm which is composed of the second absorption of the the pyrene units (around 275 nm) and the main absorption of the nucleobases (260 nm) and the absorption band highest in energy around 245 nm which can be attributed mainly to the highest energy absorption of the pyrene units and with a certain amount of contribution of the nucleobases with the underlying absorption band around 260 nm.

Another common feature of all the hybrids **ON1-IV** to **ON3-IV** is the reduced absorptivity at elevated ionic strength probably due to increased hydrophobic interactions by increased polarity of the solvent.

Looking at the absorption band at 350 nm of **ON1-IV** one can see as described above the hyperchromic effect in 100 mM NaCl as well as in 4 M NaCl. In the case of **ON1-IV** at 4 M NaCl conditions at 20°C one can see a slight resolution of the vibronic bands of the absorption band at 350 nm.

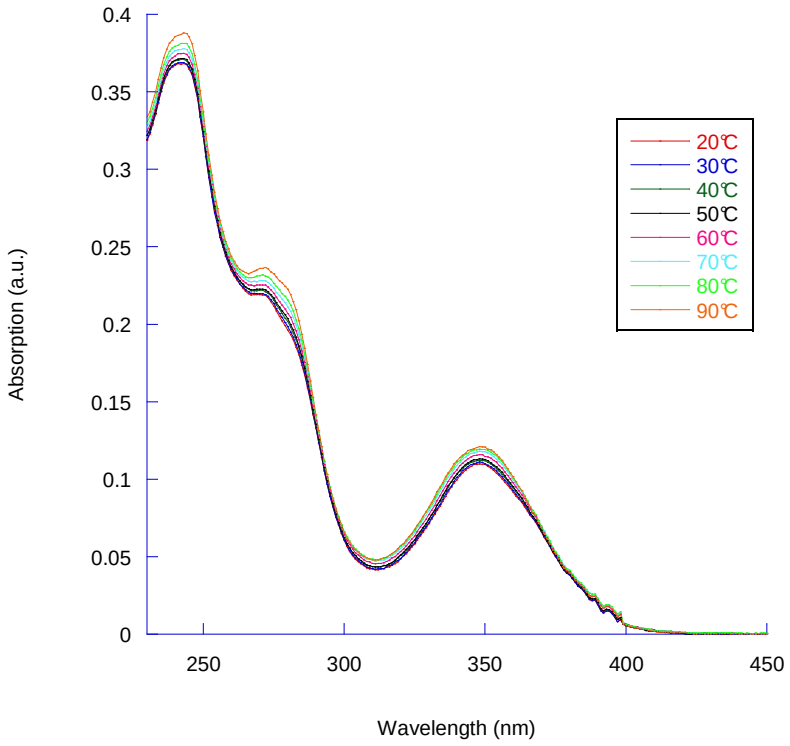

Figure 4.4 Temperature dependent UV-Vis absorption spectra of oligonucleotide **ON1-IV**. Oligonucleotide concentration: 1 µM, 100 mM NaCl, 10 mM phosphatebuffer pH 7.4.

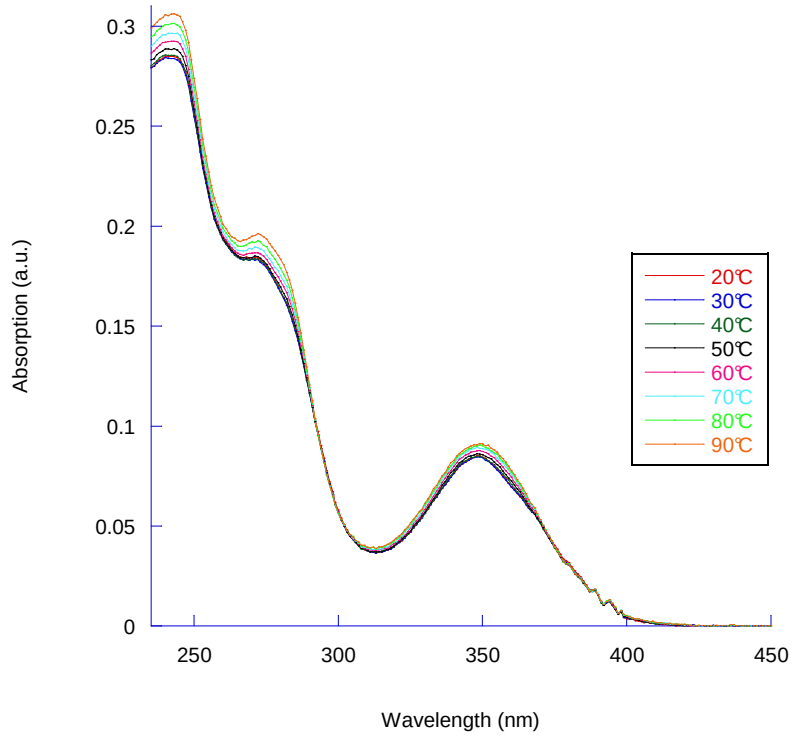

Figure 4.5 Temperature dependent UV-Vis absorption spectra of oligonucleotide **ON1-IV**. Oligonucleotide concentration: 1 µM, 4 M NaCl, 10 mM phosphatebuffer pH 7.4.

Also for the oligonucleotide **ON2-IV** the hyperchromic effect is visible for the absorption band around 350 nm. Again the overall absorption under high ionic strength is reduced as well. The striking difference to **ON1-IV** is the much better resolution of the vibronic bands under high ionic strength hinting for a different arrangement of the pyrenyl units that might originating for a change in molecularity.

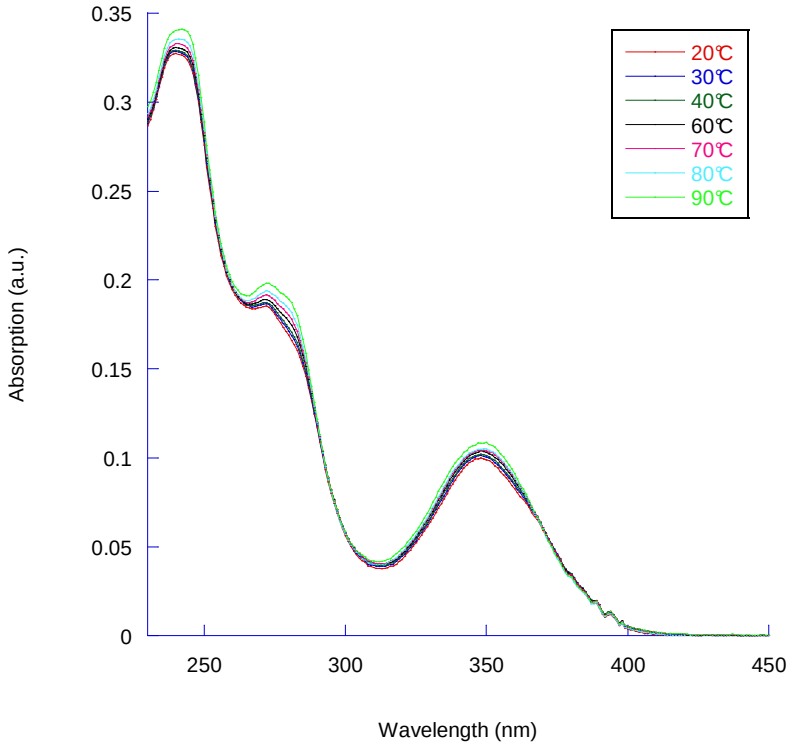

Figure 4.6 Temperature dependent UV-Vis absorption spectra of oligonucleotide **ON2-IV**. Oligonucleotide concentration: 1 µM, 100 mM NaCl, 10 mM phosphatebuffer pH 7.4.

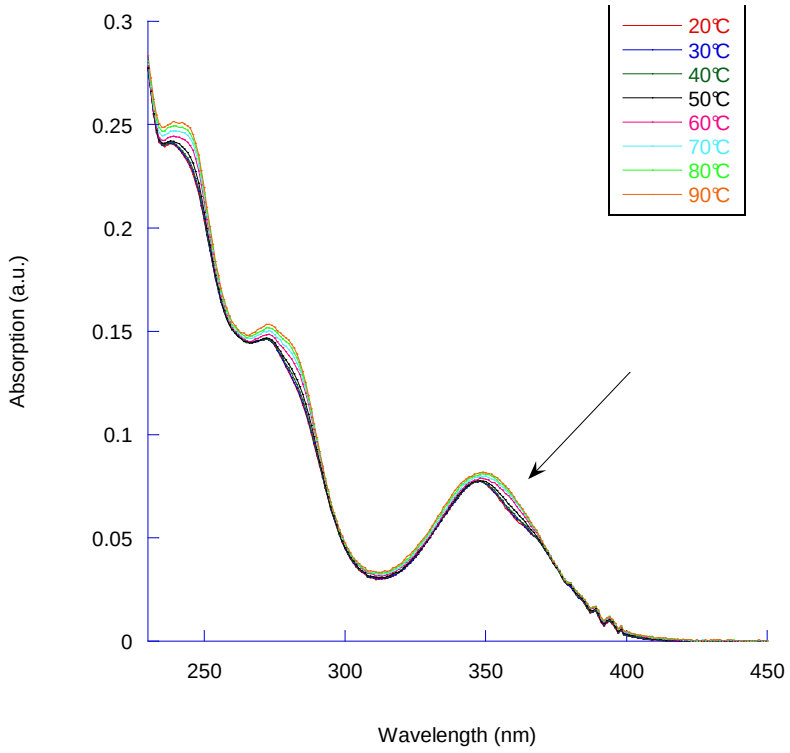

Figure 4.7 Temperature dependent UV-Vis absorption spectra of oligonucleotide **ON2-IV**. Oligonucleotide concentration: 1 µM, 4 M NaCl, 10 mM phosphatebuffer pH 7.4.

The case of **ON3-IV** is similar to **ON2-IV** in that the absorption band at 350nm also shows the resolution of vibronic bands at elevated ionic strength although not the pronounced as for the oligonucleotide **ON2-IV**. Also the hyperchromic effect is nicely visible as well as the reduced overall absorptivity of this oligonucleotide as 4M NaCl.

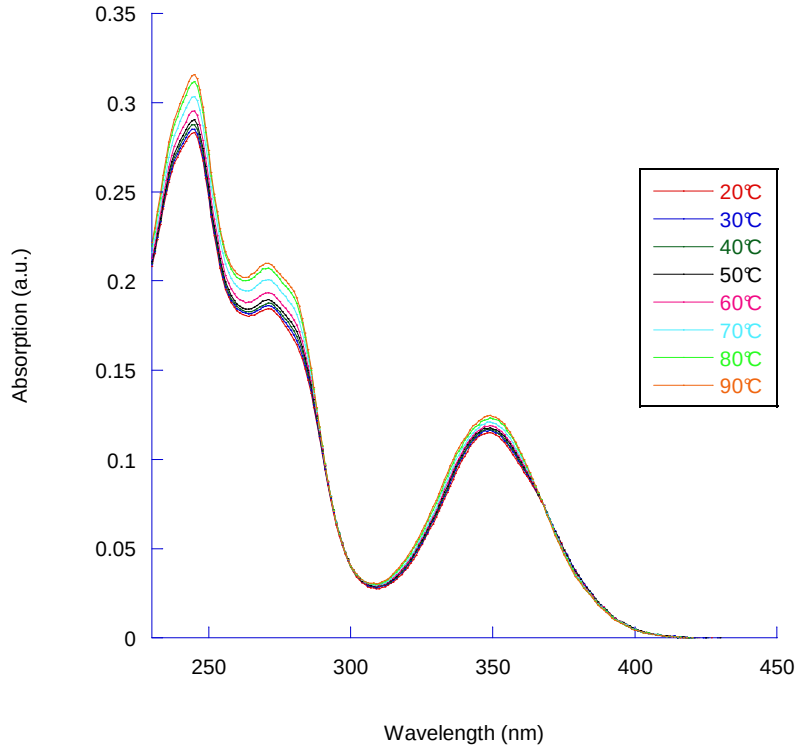

Figure 4.8 Temperature dependent UV-Vis absorption spectra of oligonucleotide **ON3-IV**. Oligonucleotide concentration: 1µM, 100mM NaCl, 10mM phosphatebuffer pH 7.4.

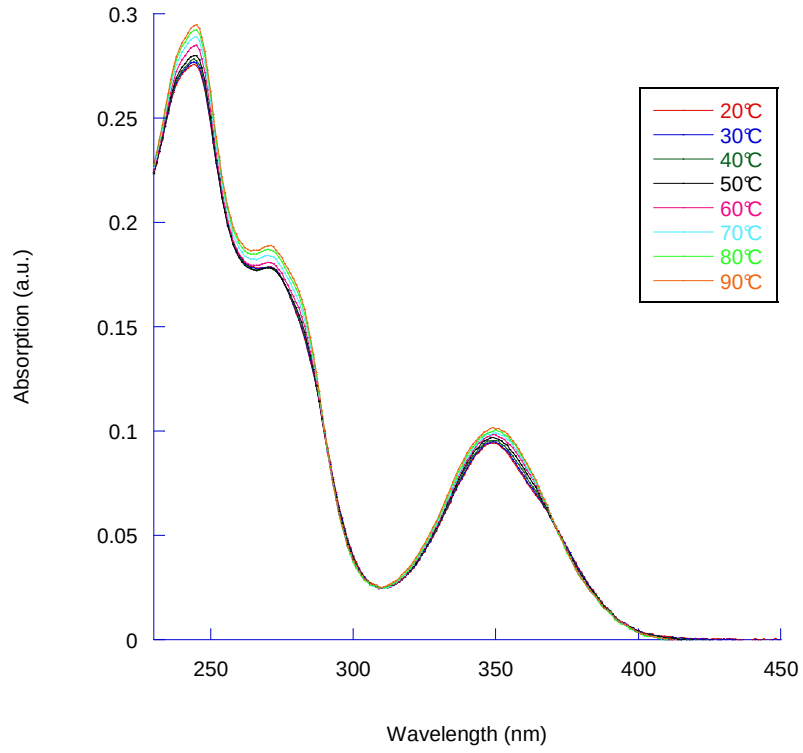

Figure 4.9 Temperature dependent UV-Vis absorption spectra of oligonucleotide **ON3-IV**. Oligonucleotide concentration: 1 µM, 4 M NaCl, 10 mM phosphatebuffer pH 7.4.

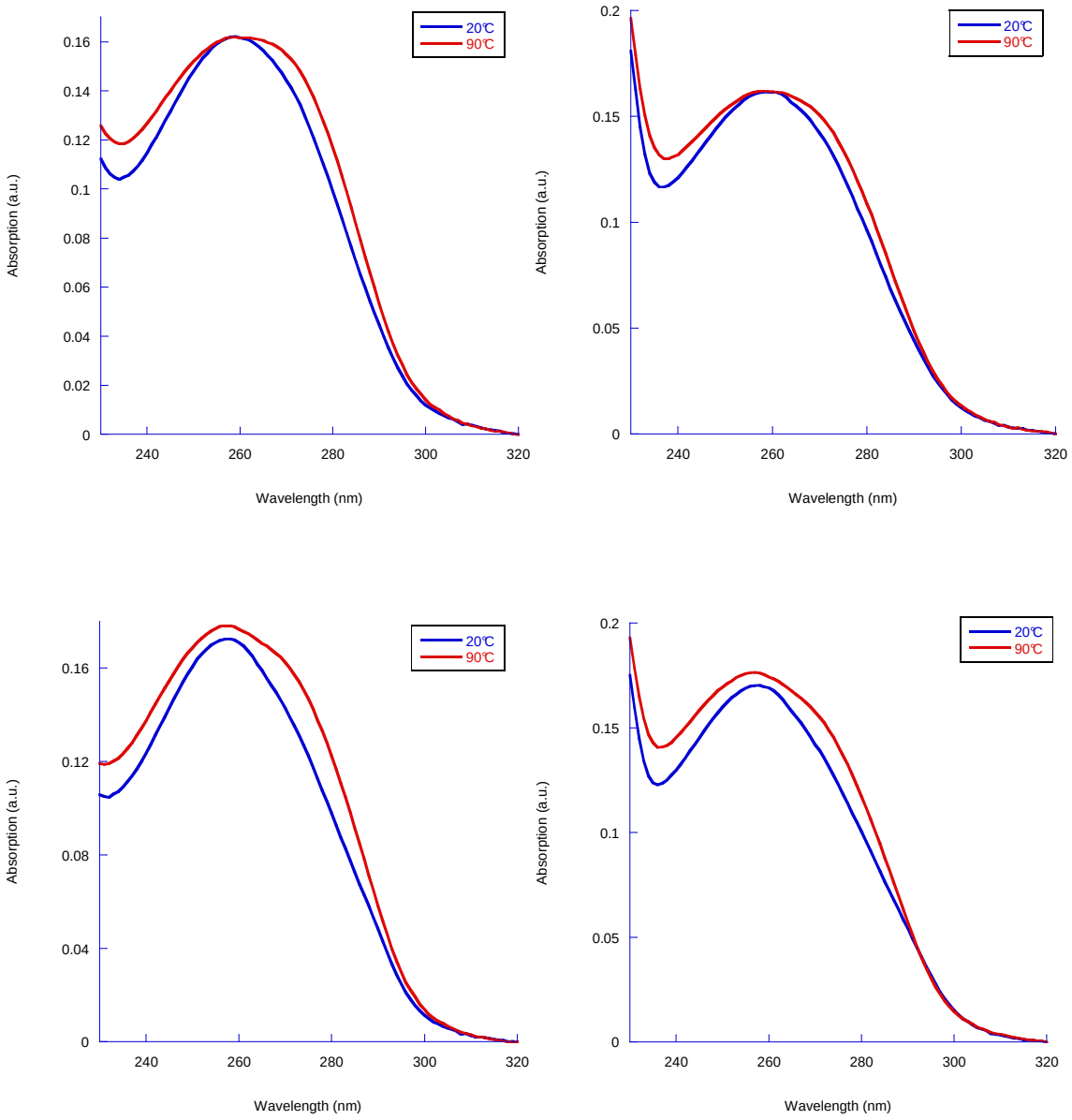

Figure 4.10 Temperature dependent UV-Vis absorption spectra at 20°C and 90°C of oligonucleotide **ON4-IV** at 100 mM NaCl (top left) 4 M NaCl (top right) and **ON-5-IV** at 100 mM NaCl (bottom left) and 4 M NaCl (bottom right). Oligonucleotide concentration: 1 µM, 10 mM phosphatebuffer pH 7.4.

Fluorescence

For all the fluorescent studies of the three hybrids the emission spectra is dominated by the excimer emission weather intra- or intermolecular excimer emission. The maximum of the excimer emission band varies with temperature and with ionic strength.

The emission spectrum of **ON1-IV** at physiological conditions shows a slight bathochromic shift upon hybridization from 504 nm to 508 nm. When going to high ionic strength the maximum of the emission wavelength does not alter with decreasing temperature or only a neglectable shift is observed (from 506 nm to 505 nm). At 20°C there is a blue shift of the emission when moving from the physiological to the high salt conditions of about 3 nm which can be attributed by the increased hydrophobic interactions forced by the increase in polarity of the solvent and thereby enabling a closer packing of the pyrene units. Having a look at the intensities one can see that the emission is gradually decreasing when heating the solution in both cases starting with the highest quantum yield at 20°C. Another interesting feature is the development of the monomer signal with increasing temperature. In the case of physiological conditions the intensity of the monomeric emission constant and of minor intensity. In contrast the monomeric emission in the case of 4 M NaCl gains in intensity when going to higher temperatures.

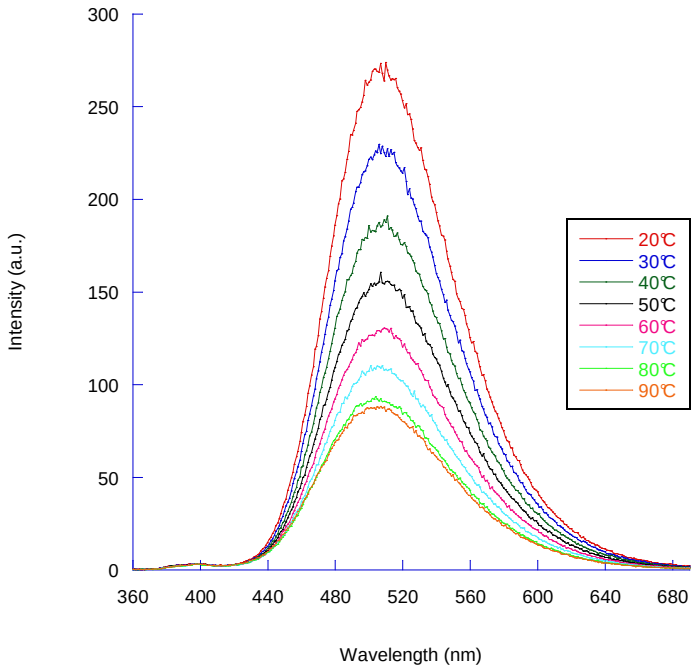

Figure 4.11 Temperature dependent fluorescence spectra of oligonucleotide **ON1-IV**. Oligonucleotide concentration: 1 µM, 100 mM NaCl, 10 mM phosphatebuffer pH 7.4, excitation wavelength: 350 nm.

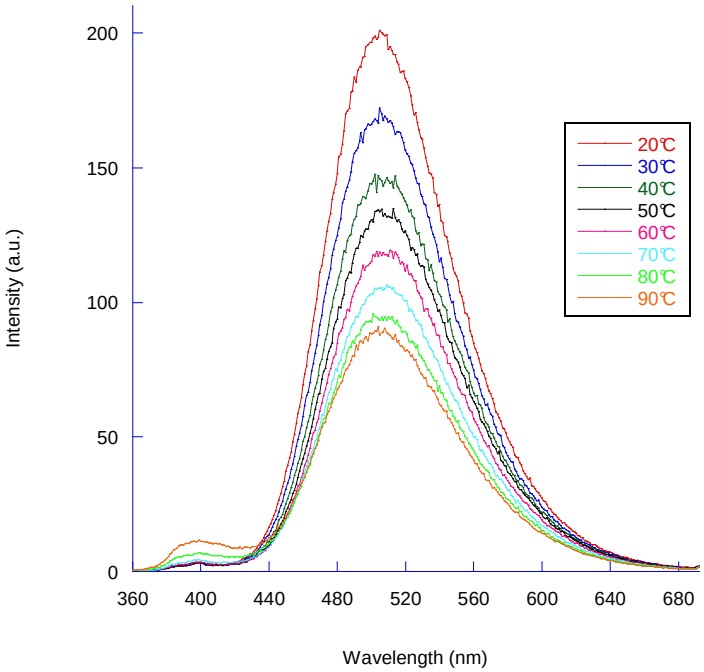

Figure 4.12 Temperature dependent fluorescence spectra of oligonucleotide **ON1-IV**. Oligonucleotide concentration: 1 µM, 4 M NaCl, 10 mM phosphatebuffer pH 7.4, excitation wavelength: 350 nm.

In the case of the version with the shortened oligonucleotide part **ON2-IV** the fluorescent spectra are again dominated by the excimer emission. At physiological conditions the behavior is comparable to the case of **ON1-IV**. The bathochromic shifted emission upon hybridization from 505 nm to 508 nm is observed as well as the gradual decrease in the emission intensity. When moving to high ionic strength there is a somewhat different picture visible. The striking difference is mainly the hypsochromic shift of the emission band upon hybridization from 506 nm in the case of 90°C to 500 nm at roomtemperature. This blueshift of about 6nm has already been observed in the case of the intermolecular sandwich type arrangement where the oligopyrenyl stretch is in the middle of two natural oligonucleotide parts. (angewandte). The change in intensity in function of the temperature is comparable to all the other cases as the intensity gradually decreases by increasing the temperature. The hypsochromic shift observed for **ON2-IV** at high ionic strength in contrast to **ON1-IV** at high ionic strength supports the possibility of a change in molecularity when moving to high ionic strength from a monomolecular hairpin structure to the bimolecular duplex structure.

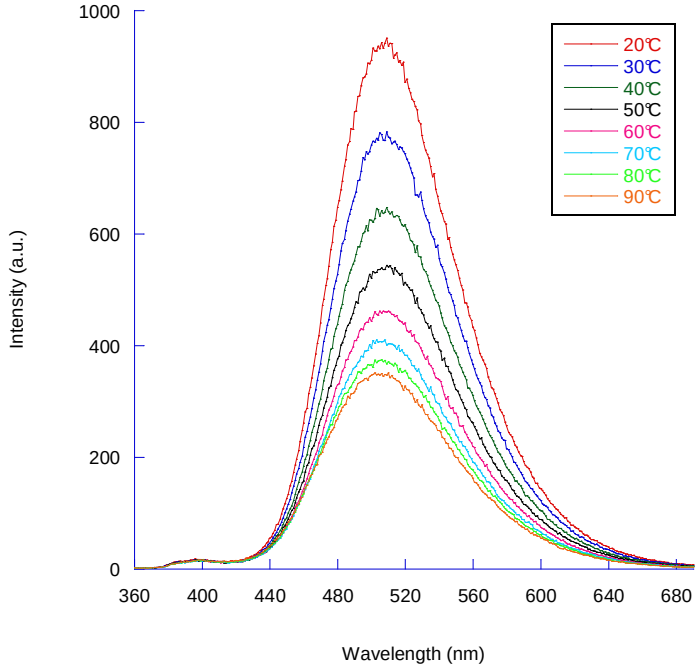

Figure **4.13** Temperature dependent fluorescence spectra of oligonucleotide **ON2-IV**. Oligonucleotide concentration: 1 µM, 100 mM NaCl, 10 mM phosphatebuffer pH 7.4, excitation wavelength: 350 nm.

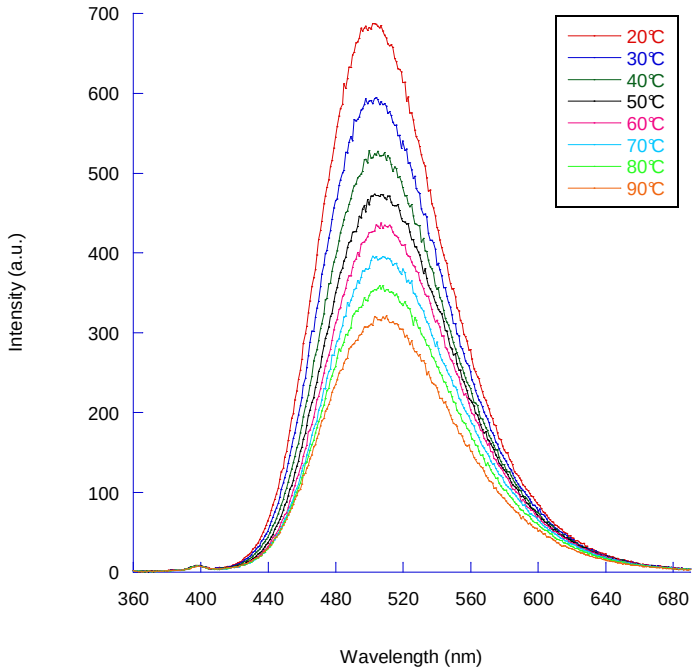

Figure 4.14 Temperature dependent fluorescence spectra of oligonucleotide **ON2-IV**. Oligonucleotide concentration: 1 µM, 4 M NaCl, 10 mM phosphatebuffer pH 7.4, excitation wavelength: 350 nm.

ON3-IV shows a bathochromic shift upon hybridization from 503 nm to 507 nm at physiological conditions. At high ionic strength the behavior is of opposite nature namely upon hybridization a hypsochromic shift is observed from 506 nm to 497 nm. This change in the shift observed at elevated ionic strength is similar to the behavior of **ON2-IV** and hints for the same or comparable arrangement of the pyrenyl units in these two constucts.

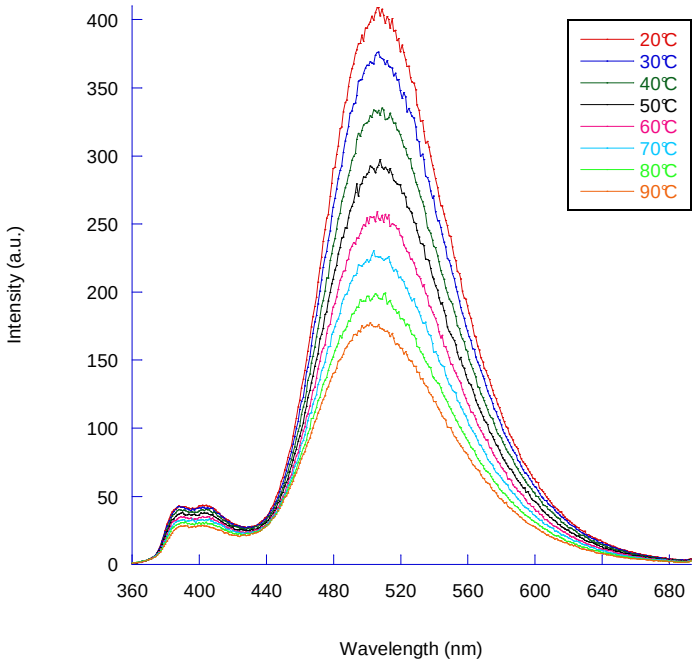

Figure 4.15 Temperature dependent fluorescence spectra of oligonucleotide **ON3-IV**. Oligonucleotide concentration: 1 µM, 100 mM NaCl, 10 mM phosphatebuffer pH 7.4, excitation wavelength: 350 nm.

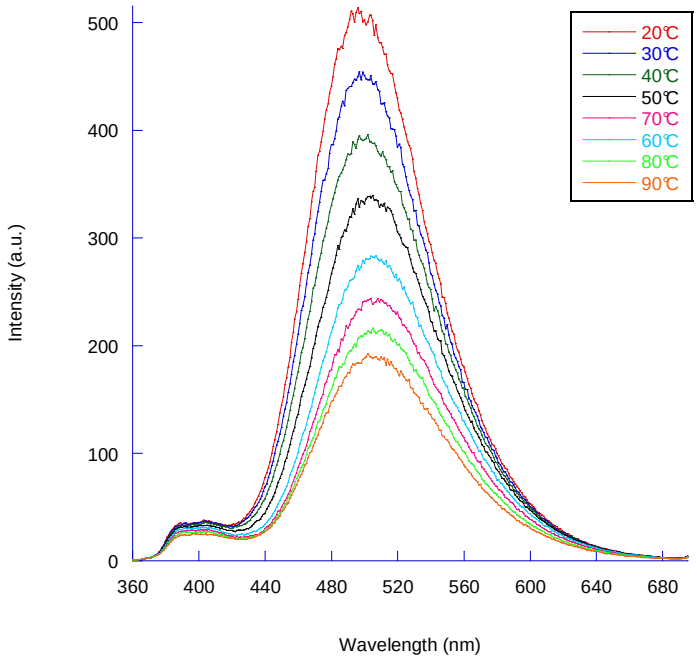

Figure 4.16 Temperature dependent fluorescence spectra of oligonucleotide **ON3-IV**. Oligonucleotide concentration: 1 µM, 4 M NaCl, 10 mM phosphatebuffer pH 7.4, excitation wavelength: 350 nm.

Circular dichroism

The study of the oligonucleotides by circular dichroism spectroscopy at low and high ionic strength was assumed to give the most valuable information about the possible change in helicity of the oligonucleotide part as well as the possible influence on the artificial pyrenyl part embedded. Furthermore the influence of the 4 M NaCl concentration on the pyrenyl part without the possible switching of chirality in the natural oligonucleotide part can be investigated with **ON3-IV**.

In the case of **ON1-IV** one can divide the spectra into two parts: below 300 nm the signature of the oligonucleotide part can be studied although with some overlap with the pyrenyl absorption and above 300 nm the pyrenyl units can be looked at since the absorption in this region solely originates from the absorption band of pyrene around 350 nm. At physiological conditions the DNA part shows the well known signature of the

right handed B-DNA with a positive maximum at 275 nm and a negative maximum at 250 nm. Looking at the region at lower energy (above 300 nm) the circular dichroism shows an exciton coupling with a negative cotton effect at 365 nm and a positive cotton effect at 338 nm hinting for the coupling of the pyrene units. In contrast to the before observed exciton coupled CD of the oligopyrenyl parts at physiological conditions the one observed for **ON1-IV** shows negative chirality. Increasing the sodium chloride concentration to 4M the change in the region of the natural oligonucleotide part changes dramatically and shows almost an inversion of the signal. This can be attributed to the change of helicity to the left-handed Z-DNA form. This signature is characteristic with the negative maximum at 293 nm and the positive maxima at 270 nm and 242 nm. Moving to lower energy the signature also changed dramatically. The exciton coupled CD signature is totally inverted and now the signal show positive chirality with a positive cotton effect at 365 nm and a negative cotton effect at 337 nm. The CD spectra obtained for **ON1-IV** at low and high sodium chloride concentrations show the not only the helicity of the DNA part changes from the right-handed B-DNA form to the left-handed Z-DNA form but also that the chirality in the modified oligopyrenyl part can be changed from the negative chirality in the case of the physiological conditions to positive chirality at elevated ionic strength.

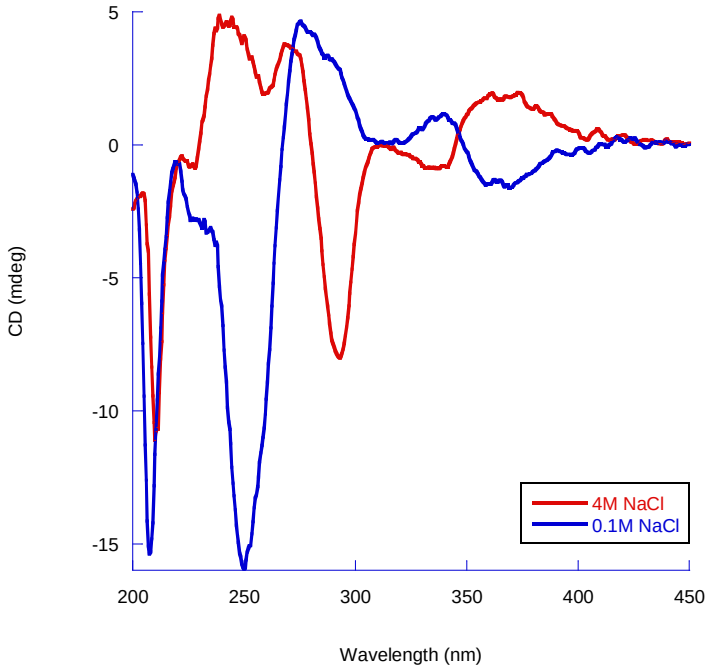

Figure 4.17 Circular dichroism spectra of oligonucleotide **ON1-IV** at low (100 mM) and high (4 M) NaCl concentration. Oligonucleotide concentration: 10 µM, 10 mM phosphatebuffer pH 7.4, 20°C.

The spectra of **ON2-IV** show a somewhat different picture. Looking at the situation at physiological conditions the signal observed is comparable to the case of **ON2-IV** and resembles the form of the right handed B-DNA, seen by the positive maximum at 275 nm and the negative maximum at 250 nm. Also the signature of the pyrenyl band above 300nm shows exactly the same shape: An exciton coupled circular dichroism with a negative cotton effect at 367 nm and a positive cotton effect at 340 nm. As in the case of **ON1-IV** the signal of the pyrene units shows a negative chirality. Increasing the ionic strength to 4 M NaCl has a dramatic effect on the intensity of the signals and their position. The only feature comparable to the spectrum of **ON1-IV** at elevated ionic strength is the inversion of the exciton coupled CD for the pyrene only absorption band which changes to positive chirality. But instead of being an almost perfect mirror image as observed for **ON1-IV** there is a huge increase in signal intensity of about 5-fold. But not only the absorption region above 300 nm is involved also the below 300 nm there is a tremendous change. The signal is mainly dominated be the absorption band of the pyrene units and it is difficult to assign the change of the natural part only. The signals are dominated by the absorption bands of the pyrene units at 270 nm and 240 nm. Additionally the CD signal observed for the sandwich type arrangement (angewandte) seems to correlate very well with the CD signal measured here, hinting for the formation of a duplex instead of the hairpin. The CD spectra at low and high sodium chloride concentration suggest that there is a possible change in molecularity involved.

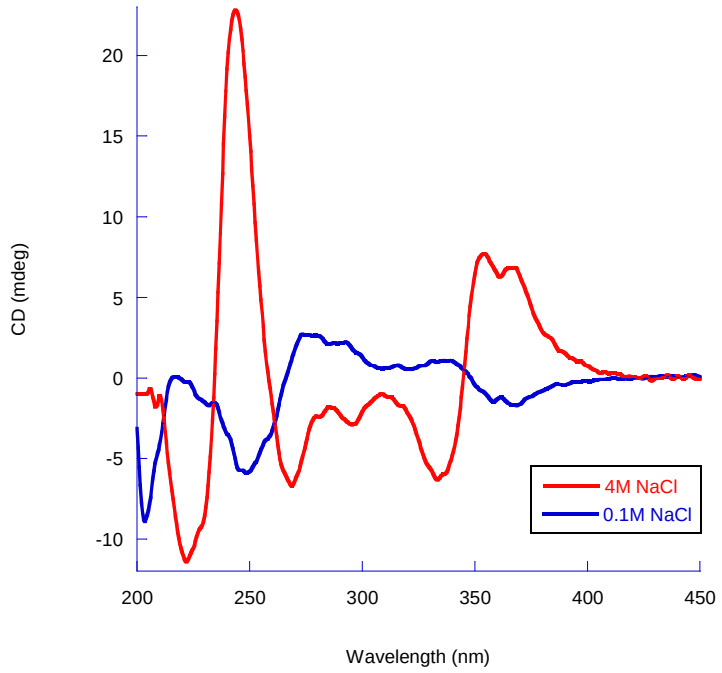

Figure 4.18 Circular dichroism spectra of oligonucleotide **ON2-IV** at low (100 mM) and high (4 M) NaCl concentration. Oligonucleotide concentration: 5 µM, 10 mM phosphatebuffer pH 7.4, 20°C.

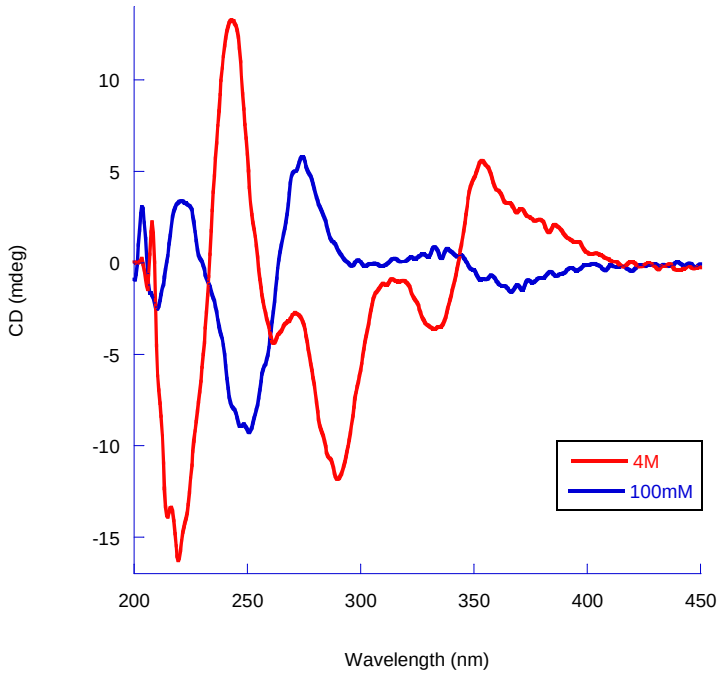

Figure 4.19 Circular dichroism spectra of oligonucleotide **ON3-IV** at low (100 mM) and high (4 M) NaCl concentration. Oligonucleotide concentration: 5 µM, 10 mM phosphatebuffer pH 7.4, 20°C.

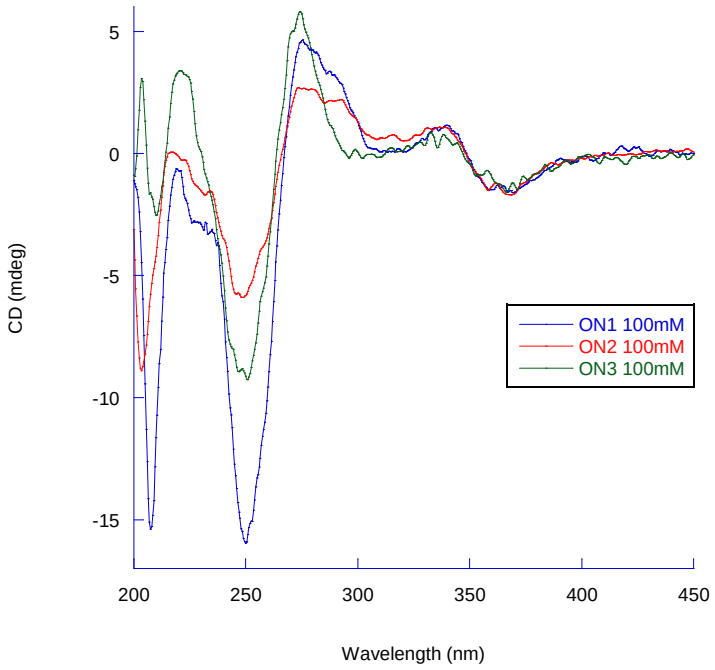

Figure 4.20 Circular dichroism spectra of oligonucleotide **ON1-IV, ON2-IV and ON3-IV** at low (100 mM) NaCl concentration. Oligonucleotide concentration: 5 µM, 10 mM phosphatebuffer pH 7.4, 20°C.

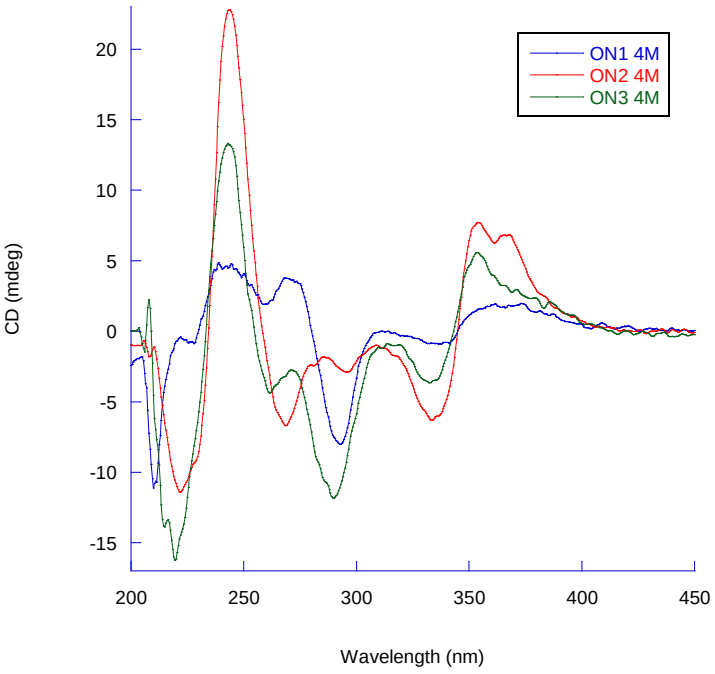

Figure 4.21 Circular dichroism spectra of oligonucleotide **ON1-IV, ON2-IV and ON3-IV** at high (4 M) NaCl concentration. Oligonucleotide concentration: 5 µM, 10 mM phosphatebuffer pH 7.4, 20°C.

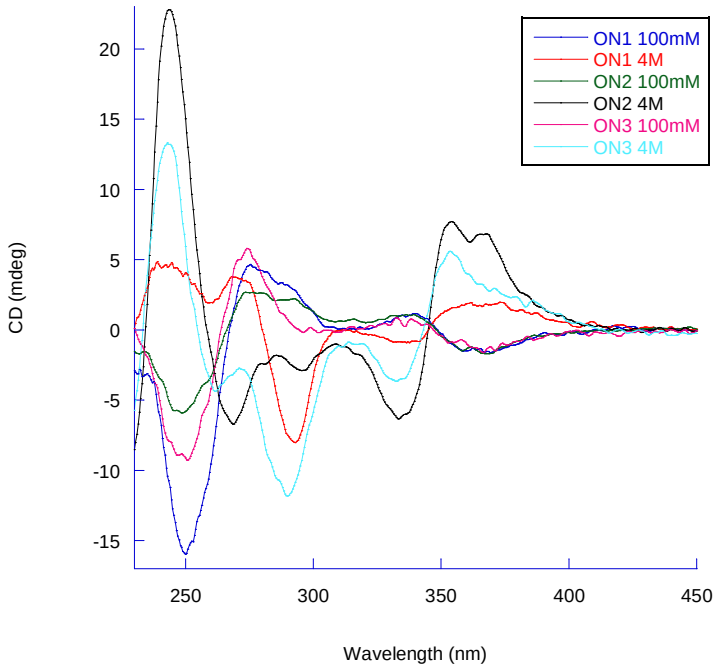

Figure 4.22 Circular dichroism spectra of oligonucleotide **ON1-IV, ON2-IV and ON3-IV** at low (100 mM) and high (4 M) NaCl concentration. Oligonucleotide concentration: 5 µM, 10 mM phosphatebuffer pH 7.4, 20°C.

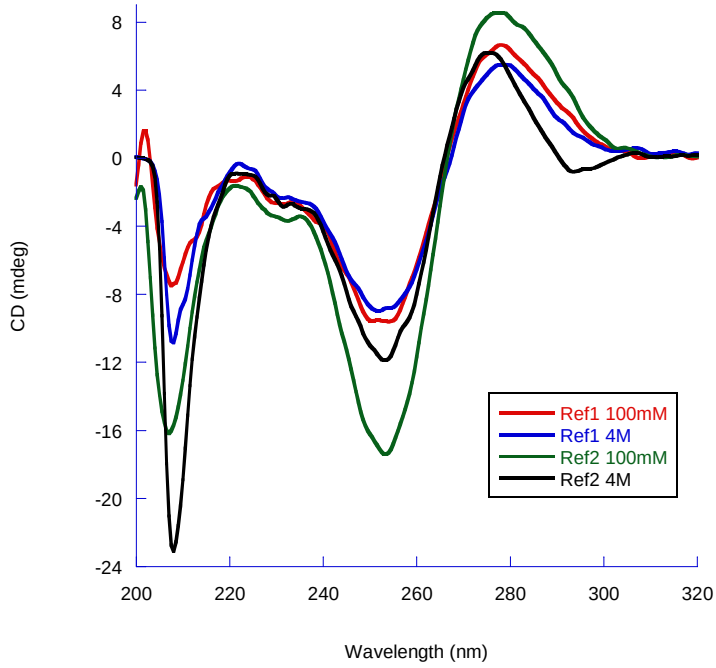

Figure 4.23 Circular dichroism spectra of oligonucleotide **ON4-IV** and **ON5-IV** at low (100 mM) and high (4 M) NaCl concentration. Oligonucleotide concentration: 5 µM, 10 mM phosphatebuffer pH 7.4, 20°C.

4.4. Conclusions and Outlook

There are mainly three observations which lead to the conclusion that **ON1-IV** is indeed forming a switchable pyrenyl hairpin structure and that **ON2-IV** and **ON3-IV** not change their helicity but instead change their molecularity.

1. Resolution/ No resolution of vibronic bands at high ionic strength

ON1-IV shows no or only to a minor extend resolved vibronic bands of the 350 nm absorption band neither at low nor at high ionic strength. The mode of interactions between the pyrenyl units seems to be of the same nature in these two cases supporting the model of the hairpin structure with different helicity of the natural oligonucleotide part as well as the pyrenyl part.

ON2-IV and **ON3-IV** show resolved vibronic bands of the 350 nm absorption band at elevated ionic strength. This hints for a different mode of interactions among the pyrenyl units and would fit the model of change molecularity.

2. Hypsochromic/ bathochromic change in eximer emission wavelength upon hybridization under high ionic strength

Upon hybridization **ON1-IV** shows at physiological conditions as well as in high ionic condtions the same behavior: In both cases as bathochromic shift of the maximum in eximer emission is observed again hinting for a similar mode of interaction at those two different conditions.

For **ON2-IV** and **ON3-IV** the situation is merely different: At 100 mM NaCl the bathochromic shift upon hybridization is also observed comparable to **ON1-IV**. Changing to 4 M NaCl the situation changes dramatically by showing a hypsochromic shift of the maximum in excimer emission which is comparable to the case of the sandwich type arrangement (angewandte, chemistry a European journal) again pointing to a change in molecularity.

3. Intensity of the exciton coupled CD

When looking at the intensities of the exciton coupled CD of **ON1-IV** one can see that on hand side that the signal is completely inversed when comparing 100 mM NaCl and 4 M NaCl concentration indication a change in helical arrangement. Also for **ON2-IV** and **ON3-IV** this signature changes from a negative chirality at physiological conditions to a positive chirality at elevated ionic strength. But the striking difference is the change in intensity of the signal. Whereas for **ON1-IV** the intensity stays the same for both cases and only the chirality changes which again hints for no change in molecularity and the same mode of interactions between the pyrene units, for **ON2-IV** and **ON3-IV** the situation is different: for those oligonucleotides the intensity increases drastically when moving from low to high ionic strength. This observation again supports the hypothesis of a change in molecularity when moving from physiological NaCl concentration to high ionic strength (4 M NaCl). Last but not least the overall intensity of the signal can be originating from the circumstance that only 7 units are communicating among each other in the case of a hairpin like structure whereas in the case of bimolecular structure there are 14 units coupling together.

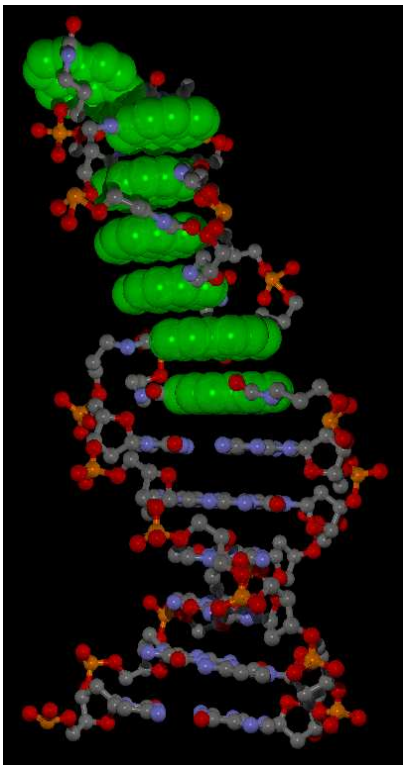

Figure 4.24 Molecular model illustrating the postulated hairpin like structure of the pyrenyl units (green).

At physiological conditions with the right handed B-DNA

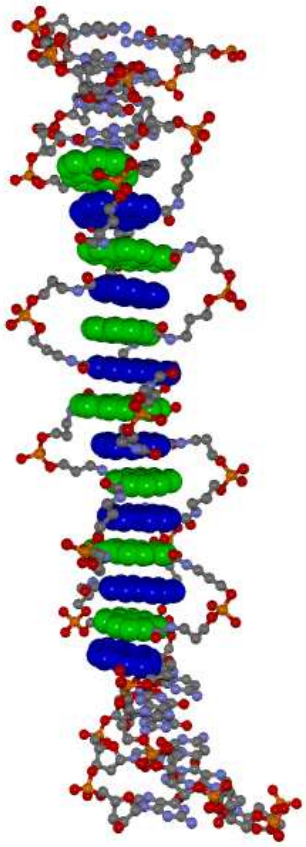

Figure 4.25 Molecular model illustrating the postulated bimolecular hybrid for **ON2-IV** with interstand stracked pyrenyl units (green and blue).

An additional idea and more insight into the nature of the artificial pyrene hairpin structure would certainly give the construct of **ON1-IV** but with the canonical guanosine nucleotide replaced by the modified 8-Bromo dG. This sequence would most probably be already present in the left-handed form since the 8-Bromo guanine adopts the *syn* conformation at physiological conditions which is the prerequisite for the formation of the left-handed Z-DNA. In this manner one would be enabled to study weather the assumed right handed hairpin formation of the pyrenyl units at elevated ionic strength is already present at low sodium chloride conditions.

4.5 Experimental Section

The synthesis of the required non-nucleosidic pyrene building block with the corresponding C3 linker was done according to the published procedure [34]. Nucleoside phosphoramidites were purchased from *SAFC* (Proligo Reagents) with dG (dmf), dC (ac) and dA (bz) and the 8-Bromo dG (dmf) was purchased from *Glen Research*. Oligonucleotides **ON1-IV** to **ON3-IV** were prepared via automated oligonucleotide synthesis using standard phosphoramidite (Activator: Ethylthiotetrazole) on a 394-DNA/RNA synthesizer (*Applied Biosystems*). Oligonucleotides **ON4-IV** and **ON5-IV** were ordered from *MicroSynth*, Switzerland. For the unnatural building block, which were coupled using 0.1 M solutions in 1,2-dichloroethane, coupling times were increased to 120 seconds instead of 25 seconds used for the natural nucleosides. Cleavage from the solid support and final deprotection was performed manually by treatment with 30% NH_4OH solution at 55°C overnight. All oligonucleotides were purified by reverse phase HPLC (Instrument: LC-10 AT from *Shimadzu* with a UV detector, column: LiChrospher 100 RP-18, 5µm, *Merck*); eluent A= $(Et_3NH)OAc$ (0.1M, pH 7.4); eluent B= 80% MeCN + 20% Eluent A; gradient 5-50% B over 38 min.

For the determination of oligonucleotide stock solution concentrations, small samples were diluted to 10% and the absorbance at 260 nm was measured on a Nanodrop ND-1000 Spectrophotometer from *Thermo Scientific*. Epsilon values were calculated using 15300, 11700, 7400 and 9000 for A, G, C and T, respectively, and 8600 for the pyrene building block.

Molecular mass determination of the oligonucleotides was performed with a Sciex QSTAR pulsar (hybrid qudrupole time-of-flight mass spectrometer, *Applied Biosystems*). ESI-MS (negative mode, CH_3CN/H2O/TEA) data of the compounds **ON1-IV** to **ON3-IV** are presented in Table 4.2.

Oligo #	**Sequence**	**Bruttoformula**	**Calc. aver. mass**	**Found mass**
ON1-IV	(5`) GCGCGC SSSSSSS GCGCGC (3`)	$C_{303}H_{331}N_{71}O_{123}P_{20}$	7554.8	7554.7

		$C_{302}H_{332}N_{66}O_{125}P_{20}$	7505.8	7506.2
ON2-IV	(5`) GCGC SSSSSSS GCGC (3`)	$C_{303}H_{327}N_{71}O_{123}P_{20}Br_4$ $C_{302}H_{332}N_{66}O_{125}P_{20}Br_4$	7870.3 7821.3	7870.5 7821.7
ON3-IV	(5`) ACG GAA SSSSSSS TTC CGT (3`)	$C_{303}H_{331}N_{71}O_{123}P_{20}$ $C_{302}H_{332}N_{66}O_{125}P_{20}$	7554.8 7505.8	7554.9 7505.7

Table 4.2 Mass spectrometry data (brutto formula, calculated average mass, found mass)

Thermal denaturation experiments (1 µM singlestrand oligonucleotide concentration, 10 mM phosphate buffer pH 7.4, with varying NaCl concentration as indicated in each case) were carried out on Varian Cary 100 Bio UV-Visible spectrophotometer equipped with a Varian Cary temperature controller and data were collected with Varian WinUV software at various wavelength as indicated in each case. Cooling- heating- cooling cycles in the temperature range of 90°C to 15°C and a heating/ cooling rate of 0.5°C/ min were used and data points every 0.5°C were recorded. Data were analyzed with KaleidaGraph 4 software from *Synergy Software*. Temperature melting values (T_m) were determined as the maximum of the first derivative of the melting curves. If necessary the curves were smoothed with a window of 5 in order to get a reasonable maximum of the first derivative.

Temperature dependent UV-VIS spectra were collected from 90°C to 20°C on a Varian Cary 100 Bio UV-Visible spectrophotometer equipped with a Varian Cary temperature controller. All experiments were carried out at a 1 µM singlestrand oligonucleotide concentration in 10 mM phosphatebuffer (pH 7.4) and the indicated concentration of NaCl.

Temperature dependent fluorescence spectra were recorded from 90°C to 20°C on a Varian Cary Eclipse fluorescence spectrophotometer equipped with a Varian Cary temperature controller (excitation wavelength at 350 nm, excitation and emission slitwidth as well as the detector voltage were varied according to the experiment as indicated). All experiments were carried out with a singlestrand concentration of 1 µM. Data were analyzed with KaleidGagraph 4 software from *Synergy Software*.

Circular dichroism spectra were recorded on a *JASCO* J-715 spectrophotometer equipped with a PFD-350S temperature controller. All experiments were carried out with a singlestrand concentration of 5 µM (if not indicated) in 10 mM phosphatebuffer (pH 7.4) and the indicated NaCl concentration.

Chapter 5: Fluorene derivatives as non-nucleosidic building blocks

5.1. Abstract

In this chapter a fluorene derivative is synthesized and incorporated into DNA. The hybrids show interesting optical properties such as the oberservation of a huge hyperchromic effect of the fluorene units upon melting the duplex, an increased thermal stability of the modified duplex and the formation of intra- and interstrand excimer emission. The chiroptical properties of the fluorene is further depending on the nature of the connecting linker which is manifested by a mirror image in the exciton coupled CD.

5.2. Introduction

As there has been a variety of non-nucleosidic building blocks incorporated into the DNA with different purpose and function there is the need to develop novel types of such building blocks in order to expand the functionality and applicability of DNA-based assemblies. The use of aromatic non-nucleosidic building blocks has been described as artificial substitutes of natural nucleosides. In search of additional aromatic building blocks for the incorporation into DNA the aromatic fluorene molecule takes an intermediate position between two already incorporated building blocks: On one side this is the biphenyl nucleoside which was studied with different substitution pattern and its influence on the thermal stability of the formed hybrids [57, 58] and on the other side phenanthrene was used as a non-nucleosidic building block and its influence on duplex integrity was studied [59]. Fluorene takes an intermediate position as the two phenyl rings are additionally connected through one methylene unit compared to the biphenyl whereas the phenanthrene has an additional ethene bridge (Figure 5.1).

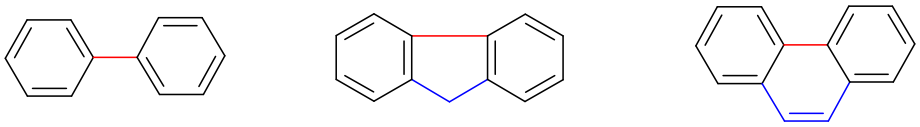

Figure 5.1 Chemical structure of biphenyl (left), fluorene (middle) and phenantrene (right) showing the common bond in red and the additional bonds in blue.

Fluorene derivatives are intensively investigated as monomeric units for polymerization in the development of organic light emitting diodes and have already found wide spread application therein [60-63]. As the protons on position C9 of the fluorene molecule exhibits relatively strong acidity the modification at this position became very important in the field of polymeric materials as an alkylation point in order to get better and tuneable solubility properties [64-67]. Furthermore the use of fluorene unit in the construction of oligomers in order to create model systems of π-stacked aggregates for the study of optical properties as well as for electrical conductivity has become important. [68-73]

Fluorene has also found a use in practical organic synthesis as a base labile amino protecting group [74], known as the Fmoc (9- Fluorenylmethoxycarbonyl, Figure 5.2) group which was developed in 1972 and revolutionized solid phase peptide synthesis (Fmoc strategy instead of the Boc strategy) since up to then, the amino protecting groups were mostly acid labile and thus they were lacking orthogonality. In addition to the very mild conditions needed for the deprotection of the N-terminal of the growing peptide chain, the fluorene proofed to be a very useful protecting group because of its chromophoric nature. Due to it UV-absorbance the deprotection could be easily monitored.

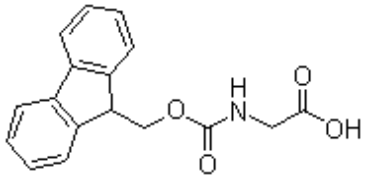

Figure 5.2 Fmoc protected glycine

The use as monomeric building block for polymerchemistry gave fluorene a new role as a chromophore in the context of material science. Synthetic polymers showed very high electrical conductivities which first of all was pioneered by polyacetylene with its delocalized electronic structure. Due to problems of stability and processibility of polyacetylene, the more stable aromatic synthetic polymers proofed to be suitable candidates for the intended purpose. First via electropolymersation and then with synthetic methods a lot of new and well defined aromatic polymers were developed. Among those were the very promising polyfluorene derivatives which showed very desirable characteristics: The rigid biphenyl unit results in a large band gap and the desired blue emission with high efficiency and the position C9 is easily accessible for modification for the purpose of better solubility and processability without disturbing the conducting part of the polymer.

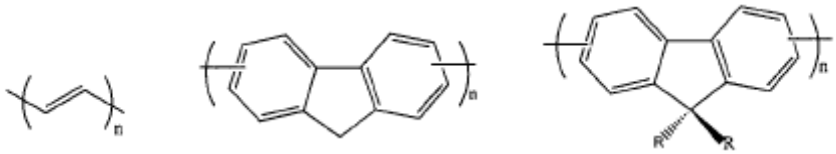

a) b) c)

Figure 5.3 a) Polyacetylene b) unsubstituted polyfluorene c) substituted polyfluorene

In molecular biology the chromophoric nature of fluorene led to the development of a molecular beacon involving fluorene as the fluorophore [75]. The fluorene moiety was attached to the natural base via a triple bond and led to the concept of the quencher free beacon. The fluorescent properties of these derivatives were then very sensitive for change in the environment without the need for a specific quencher. It was the target which would alter the fluorescence properties of the fluorophore dramatically thereby indicating whether there is a mismatch or not (Figure 5.4).

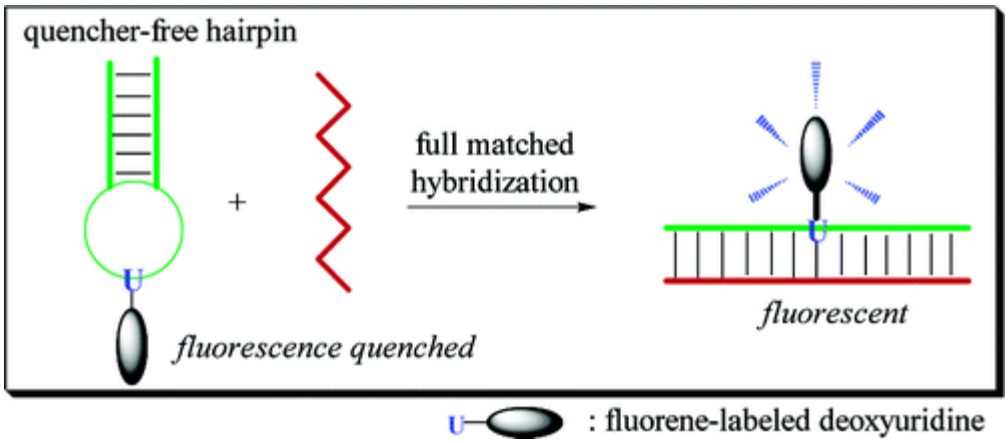

Figure 5.4 Working principle of the quencher-free molecular beacon based on the deoxyuridine labeled with a fluorene moiety (Illustration adapted from [75]).

5.3 Results and Discussion

Chemical synthesis of the fluorene phosphoramidite building block is shown in Scheme 5.1. The dibromoderivative **1** was commercially available. The addition of the triplebonds was achieved via sonogashira coupling of an alcohol functionalized alkyne with two different length, namely a butyinol and a hexyinol, resulting in the diol **2a** and **2b**. The thus obtained diol was then further treated with 4,4`-dimethoxy tritylchloride under controlled conditions (see experimental section) resulting in the mono-protected intermediates **3a** and **4b**. The unprotected alcohol was then used to transform the intermediate into the phosphoramidite derivatives **4a** and **4b**.

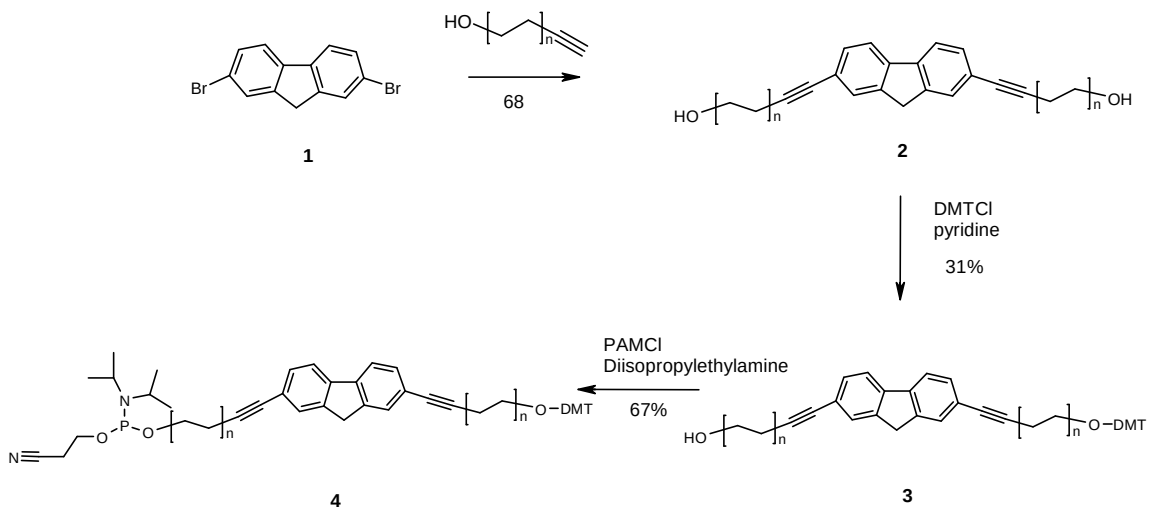

Scheme 5.1 Synthesis of the bisalkynyl fluorene derived phosphoramidite building blocks. n=1: 2a, 3a and 4a, n=2: 2b, 3b and 4b.

Building blocks **4a** and **4b** were then incorporated into oligonucleotides by standard phosphoramidite procedure. In order to increase the yield of the non-nucleosidic building block incorporation, the coupling time was increased (see experimental section). Cleavage from the support as well as deprotection of the resulting oligonucleotides was then achieved by treatment with concentrated ammonia at 55°C overnight. The purification of the cleaved and deprotected oligonucleotides was then done by reversed phase HPLC, yielding oligonucleotides **ON1-V to ON8-V**.

Hybrid #	Oligo #	**Duplex**	**Tm (°C)**	**ΔTm (°C)**	**ΔTm/mod (°C)**
D1-V	**REF2** **REF1**	(5`) TGC ACT CTC GAT GAC CGA GCT (3`) ACG TGA GAG CTA CTG GCT CGA	70.7	-	-
D2-V	**ON2-V** **ON1-V**	(5`) TGC ACT CTC G**Y**T GAC CGA GCT (3`) ACG TGA GAG C**Y**A CTG GCT CGA	72.0	+1.3	**+1.3**
D3-V	**ON4-V** **ON3-V**	(5`) TGC ACT CTC G**YY** GAC CGA GCT (3`) ACG TGA GAG C**YY** CTG GCT CGA	75.9	+5.2	**+2.6**
D4-V	**ON6-V** **ON5-V**	(5`) TGC ACT CTC G**Z**T GAC CGA GCT (3`) ACG TGA GAG C**Z**A CTG GCT CGA	72.0	+1.3	**+1.3**
D5-V	**ON8-V** **ON7-V**	(5`) TGC ACT CTC G**ZZ** GAC CGA GCT (3`) ACG TGA GAG C**ZZ** CTG GCT CGA	76.7	+6.0	**+3.0**
D6-V	**ON2-V** **ON5-V**	(5`) TGC ACT CTC G**Y**T GAC CGA GCT (3`) ACG TGA GAG C**Z**A CTG GCT CGA	71.3	+0.6	**+0.6**
D7-V	**ON6-V** **ON1-V**	(5`) TGC ACT CTC G**Z**T GAC CGA GCT (3`) ACG TGA GAG C**Y**A CTG GCT CGA	71.3	+0.6	**+0.6**
D8-V	**ON4-V** **ON7-V**	(5`) TGC ACT CTC G**YY** GAC CGA GCT (3`) ACG TGA GAG C**ZZ** CTG GCT CGA	76.1	+5.4	**+2.7**
D9-V	**ON8-V** **ON3-V**	(5`) TGC ACT CTC G**ZZ** GAC CGA GCT (3`) ACG TGA GAG C**YY** CTG GCT CGA	76.0	+5.3	**+2.7**
D10-V	**REF2** **ON3-V**	(5`) TGC ACT CTC GAT GAC CGA GCT (3`) ACG TGA GAG C**YY** CTG GCT CGA	63.8		

Y =	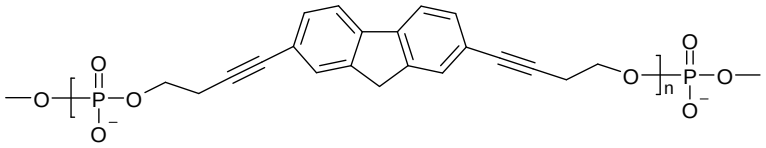
Z =	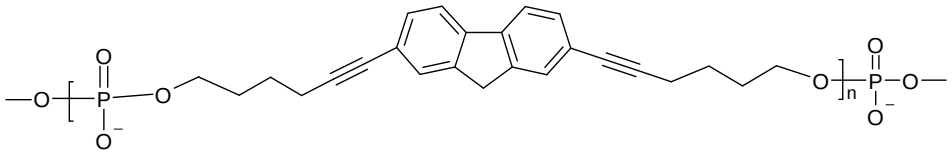

Table 5.1 Hybridization data (Tm, °C) of different oligonucleotides duplexes containing a fluorene based building block with a butyinol linker (Y) and with a hexyinol linker (Z). All measurements were carried out at pH 7.4 in phosphatebuffer and 100 mM NaCl.

UV-Vis absorption

The UV-Vis spectra of the hybrids **D2-V** and **D3-V** are composed of two main absorption bands: The more intense band with a maximum around 260 nm which is mainly assigned to the absorption of the natural bases and the less intense band around 330nm corresponding to the main absorption band from the fluorene derivative. Looking at the temperature dependent spectrum of hybrid **D2-V** (Figure 5.5) one can nicely see the hyperchromic effect of the two main absorption bands at increasing temperature. Furthermore the band arising from the fluorene derivative shows a redshift upon hybridization from 329 nm to 332 nm. Additionally an isosbestic point is visible at 335 nm, indicative for a two state model.

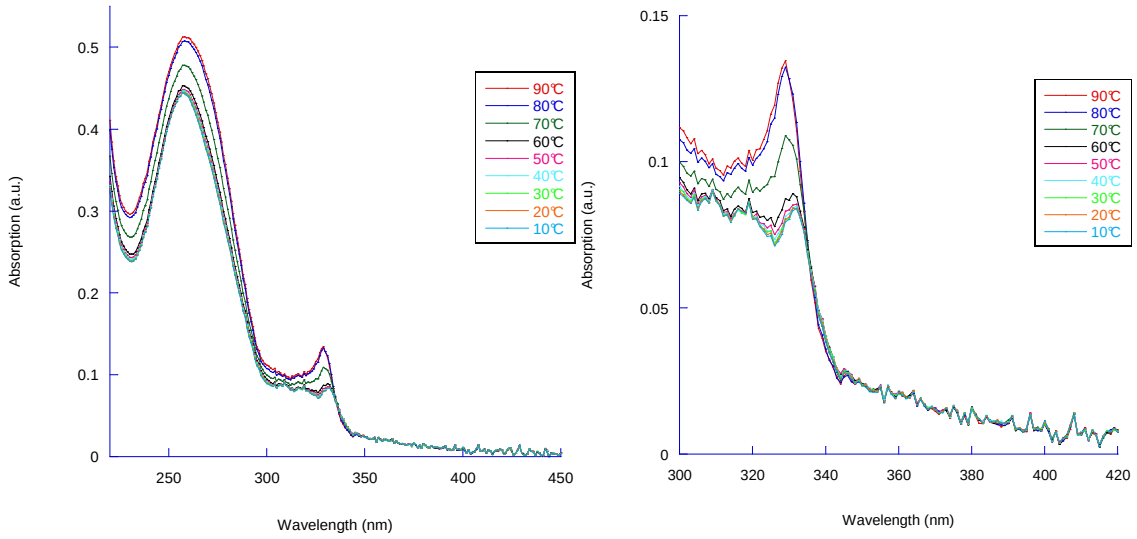

Figure 5.5 Temperature dependent UV-Vis absorption spectrum of hybrid **D2-V**. Singlestrand concentration: 1 µM, 100 mM NaCl, 10 mM phosphatebuffer pH 7.4.

In the case of hybrid **D3-V** (Figure 5.6) the hyperchromic effect is as well visible but in comparison to hybrid **D2-V** the maximum of the absorption band of the fluorene is not redshifted upon hybridization but remains constant at 329nm. Also an isosbestic point is lacking, hinting for a more complex model.

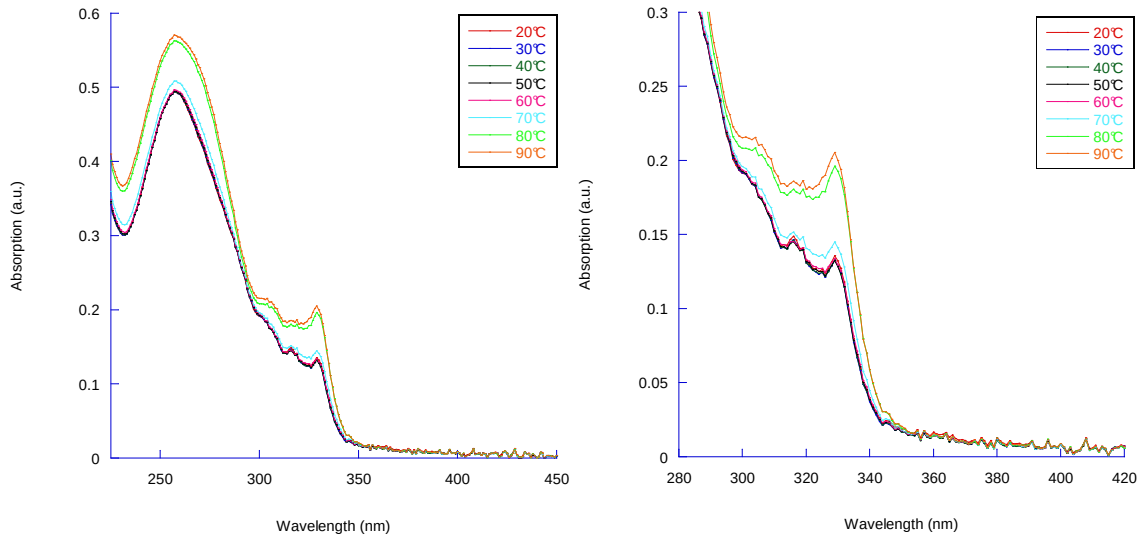

Figure 5.6 Temperature dependent UV-VIS absorption spectrum of hybrid **D3-V**. Singlestrand concentration: 1 µM, 100 mM NaCl, 10 mM phosphatebuffer pH 7.4.

Melting profiles of the hybrids

Although the linear nature of the non-nucleosidic building block would suggest that embedded in the DNA duplex it would lead to a delicate destabilization, the data obtained from melting experiments show the opposite effect (Table 1). If an A-T base is replaced by a "fluorene-fluorene" pair, the melting temperature is increased and therefore the hybrid is stabilized. Increasing the length of the linker by moving from the butynyl to the hexynyl linker, seems not to play a crucial role in the stabilizing effect. In both cases one observes an increase in melting temperature of about 1.3°C if the modifications opposite each other have the same linker length (hybrid **D2-V** and **D4-V**). If one mixes the linker length (hybrid **D6-V** and **D7-V**) there is still a slight increase in melting temperature of about 0.6°C but it appears that the different linker length has some disadvantages for the hybrid, although the contribution is still in the same range as a canonical A-T base pair.
Having two consecutive modification in the single strand and putting them in opposite position (hybrid **D3-V** and **D5-V**) resulting in two fluorene-fluorene "base pairs", gives rise to another drastic stabilization of the hybrids. In the case of hybrid **D3-V**, this increase of 5.2°C of the melting temperature compared to the fully natural reference hybrid **D1-V**, means there is 2.6°C of stabilization per modified base pair. On the other hand, hybrid **D5-V** has an even larger increase in melting temperature, namely 6.0°C for the overall hybrid, and therefore 3°C per modified base pair. If the two modifications with the short linker are placed opposite the modifications with the longer hexynyl linker (hybrid **D8-V** and **D9-V**) the increase in melting temperature is intermediate with 5.4°C respectively 5.3°C. The further increase in stabilization is not just an additive effect by going from one to two modifications in the single strand but the intrastrand interactions play an important role.

In all of the measured melting profiles there is no hysteresis observed and all of the modified hybrids melt in a cooperative way (Figure 5.7). Every melting profile exhibits a very sharp transition indicative for high cooperativity. The incorporation of the linear modification in the duplex seems not to disturb the overall hybrid, it even gives the

hybrid additional stability, only provided by aromatic interactions since H-bonding acceptors and donors are completely lacking.

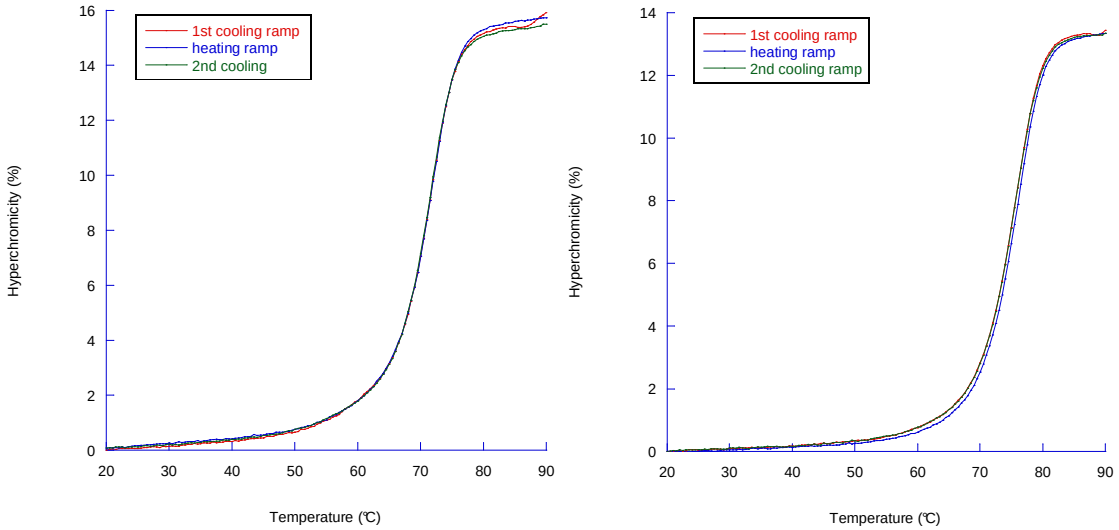

Figure 5.7 Melting ramps of hybrid **D2-V** (left) and **D3-V** (right) with two cooling ramps and one heating ramp monitored at 260 nm. Oligonucleotide concentration: 1 µM singlestrand, 100 mM NaCl, 10 mM phosphatebuffer pH 7.4.

Comparing the hyperchromicity of the different hybrids to the natural reference duplex (Figure 5.8 and Figure 5.9), the main observation is the decrease of hyperchromicty monitored at 260 nm moving from no modifications (hybrid **D1-V**) to four modifications (hybrid **D3-V**& **D5-V**). This overall decrease of hyperchromicity from 17 % for the reference duplex **D1-V**, to 15 % for the replacement of one base pair (hybrid **D2-V** and **D4-V**) and to 13 % for the replacement of two base pairs (hybrid **D3-V** and **D5-V**) indicates the loss of stacking interactions in the modified hybrids compared to the fully natural duplex. The removal of the natural base pair adjacent to the neighboring bases results in the loss of stacking interactions with the bases. The increased thermal stability of the modified hybrids can not be explained by increased π-π-interactions between the fluorene moieties and the adjacent base pairs.

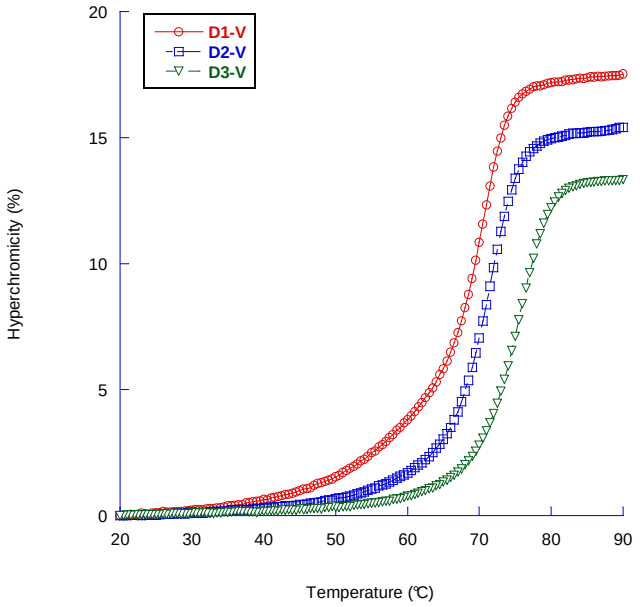

Figure 5.8 Comparison of the melting curves of hybrid **D1-V** (red), **D2-V** (blue) and **D3-V** (green) monitored at 260 nm. Oligonucleotide concentration: 1 µM singlestrand, 100 mM NaCl, 10 mM phosphatebuffer pH 7.4.

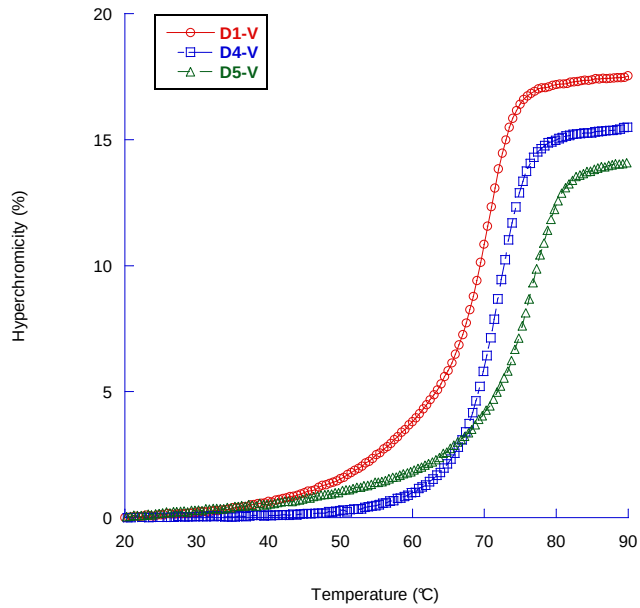

Figure 5.9 Comparison of the melting curves of hybrid **D1-V** (red), **D4-V** (blue) and **D5-V** (green) monitored at 260 nm. Oligonucleotide concentration: 1 µM singlestrand, 100 mM NaCl, 10 mM phosphatebuffer pH 7.4.

The melting profile was not only monitored by the absorption band of 260 nm but was also monitored by the main absorption band of the fluorene derivatives, namely the 330 nm band (Figure 5.10). First of all, also these melting curves show no hysteresis at all, indicative for cooperative melting. Secondly if one compares the melting temperature

derived from these melting curves, they fit exactly the temperatures received with the band monitored at 260 nm. Looking at the hyperchromicity, the effect is very drastic. The main absorption of the fluorene unit in the hybrid or in the single strand is very different yielding in a huge hyperchromicity. In the case of the hybrid **D2-V** the hyperchromicity is in the range of 70 % whereas in increasing the number of modifications (hybrid **D3-V**) results in a hyperchromic effect of about 50 %. The environment of the fluorophore in the single strand obviously differs dramatically from the hybrid structure. Favourable stacking effects among the fluorene residues seem dominate in the duplex leading to a stabilizing effect. From the decreasing hyperchromicity at 260 nm by substitution of a natural base pair and a parallel increasing hyperchromicity at 330 nm leads to the assumption that the fluorene units interact among themselves while being independent of the neighbouring natural bases.

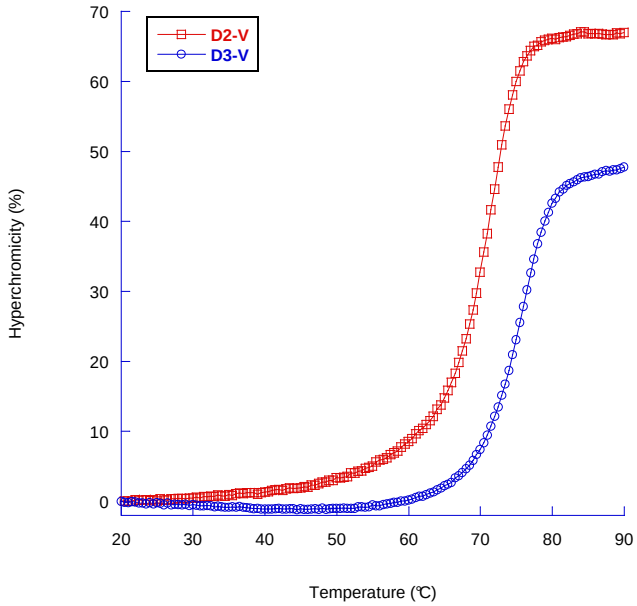

Figure 5.10 Comparison of the melting curves of hybrid **D2-V** and **D3-V** monitored at 330 nm. Oligonucleotide concentration: 1 µM singlestrand, 100 mM NaCl, 10 mM phosphatebuffer pH 7.4.

Fluorescence of the hybrids

By incorporation of the fluorene building block into oligonucleotides the study of the interstrand interactions by means of fluorescence may result in valuable information. The temperature dependent fluorescence spectra for hybrid **D2-V** and **D4-V** show the distinct difference when going from the single strand state (at 90°C) to the duplex (at 20°C). At 90°C the emission spectrum is more or less the sharp emission bands attributed to the monomeric unit at around 350 nm. By decreasing the temperature this emission bands decrease drastically and a new band appears around 400nm. (Figure 5.11) This band is in comparison to the single strand emission bands broad and structureless. The structure of this band is indicative for an excimer type of emission band. The opposite fluorene units may interact with each other giving rise to this redshifted emission band. The low intensity of the emission band may indicate that the interaction is not very strong although there is almost no monomer emission left in the duplex at 20°C. Another possibility might be that the quantum yield is drastically reduced in the duplex compared to the single strands.

Comparing the influence of the linker length now shows that the shorter C4 linker (hybrid **D2-V**) (Figure 5.11) seems to favor the formation of the excimer in comparison to the C6 linker (hybrid **D4-V**) (Figure 5.12). When mixing the two single strands with different linker length (hybrid **D7-V**) the excimer like emission band has an intermediate intensity between hybrid **D2-V** and **D4-V**. (Figure 5.13)

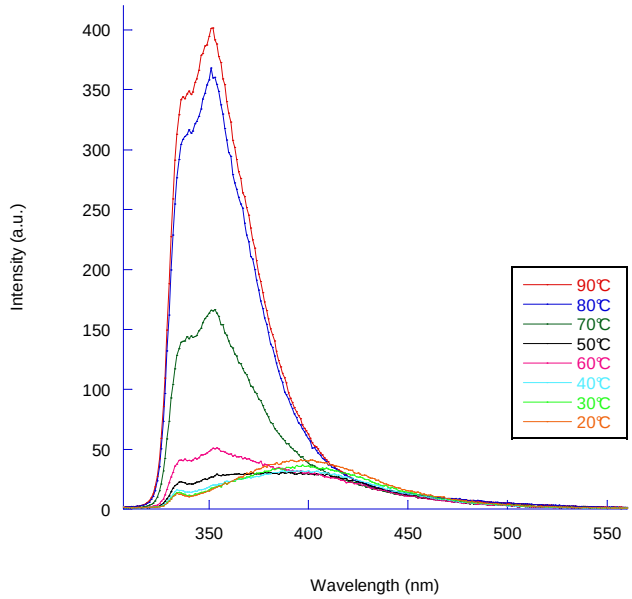

Figure 5.11 Temperature dependent fluorescence spectra of hybrid **D2-V**. Oligonucleotide concentration: 1 µM singlestrand, 100 mM NaCl, 10 mM phosphatebuffer pH 7.4. Excitation wavelength: 300 nm.

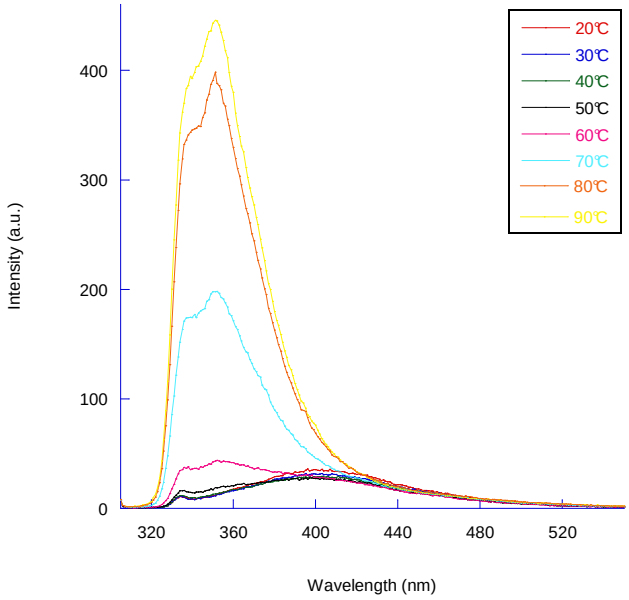

Figure 5.12 Temperature dependent fluorescence spectra of hybrid **D6-V**. Oligonucleotide concentration: 1 µM singlestrand, 100 mM NaCl, 10 mM phosphatebuffer pH 7.4. Excitation wavelength: 300 nm.

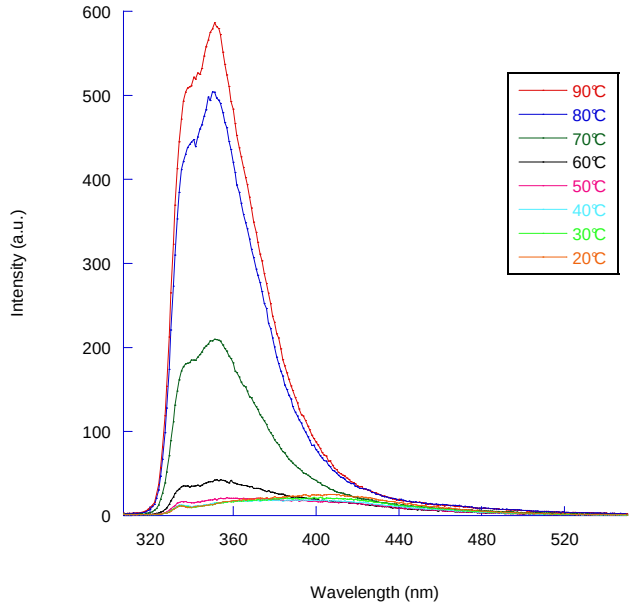

Figure 5.13 Temperature dependent fluorescence spectra of hybrid **D4-V**. Oligonucleotide concentration: 1 µM singlestrand, 100 mM NaCl, 10 mM phosphatebuffer pH 7.4. Excitation wavelength: 300 nm.

The proposed excimer model is supported by the spectra for the hybrids with two modifications in the single strand (Figure 5.14 and 5.15). In these hybrids not only the possibility of interstrand excimer formation exists but also intramolecular excimer formation is possible. When looking at the temperature dependent spectrum of hybrid **D3-V** one can see that also in the melted state at 90°C the main emission band is a structureless and broad band around 400 nm indicative for an intrastrand excimer emission. In addition the shoulder around 350 nm seems to be remaining monomer emission. Decreasing the temperature first results in a reduction of the intensity of the intrastrand excimer emission band and at the same time yields a reduction of the monomeric portion. Further reduction of the temperature leads to an increase of the excimeric emission band which can be attributed to interstrand excimer emission. Again this emission band is broad and structureless and in comparison to the intrastrand emission band is redshifted by about 10 nm.

Comparing the hybrids **D3-V** and **D5-V** the influence of the linker is quiet dramatic. As in analogy to hybrid **D3-V** also in hybrid **D5-V** the formation of intrastrand excimer emission is observed although slightly redshifted (398 nm for hybrid **D3-V**, 395 nm for

hybrid **D5-V**). The main difference seems so be in the portion of the monomer emission which is much larger in the case of the longer linker (hybrid **D5-V**) in comparison to the shorter linker (hybrid **D3-V**) which exhibit a much smaller portion of monomer emission. By decreasing the temperature, both monomer and excimer intensity decrease and analogues to the hybrid **D3-V** the excimer emission band increases again whereas the monomer emission band disappears. The excimer emission band which can again be attributed to interstrand interactions is also broad and structureless and even more redshifted than in the case of hybrid **D3-V** (20 nm for hybrid **D5-V** and 10 nm for hybrid **D3-V**).

The mixed hybrid **D8-V** exhibits the same characteristics as the hybrids **D3-V** and **D5-V** namely the intrastrand eximer emission band around 400 nm at elevated temperature and the redshifted (by about 10 nm) interstrand excimer emission band at the hybridized state. The portion of monomer emission at 90°C is almost as low as in the case of the hybrid **D3-V**.

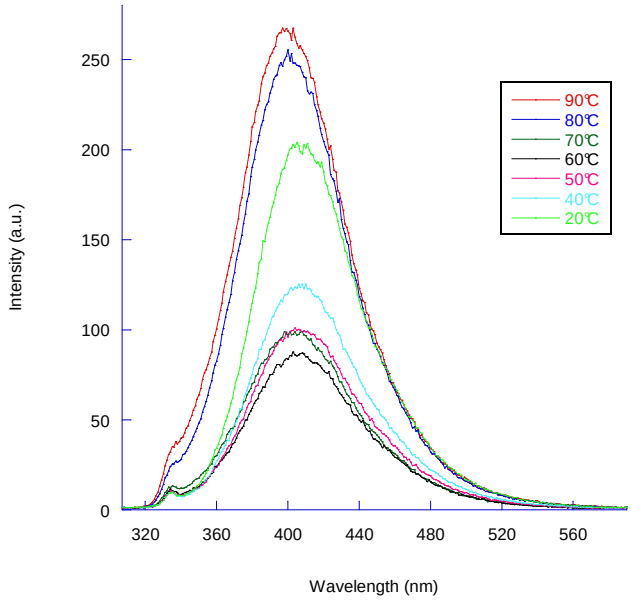

Figure 5.14 Temperature dependent fluorescence spectra of hybrid **D3-V**. Oligonucleotide concentration: 1 µM singlestrand, 100 mM NaCl, 10 mM phosphatebuffer pH 7.4. Excitation wavelength: 300 nm.

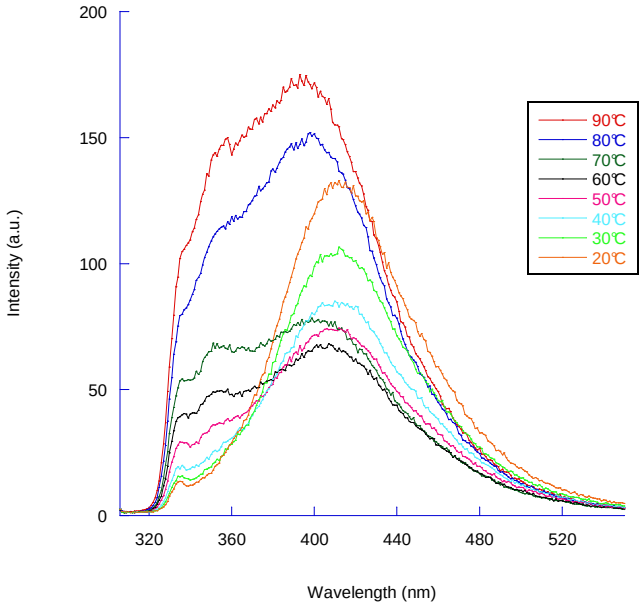

Figure 5.15 Temperature dependent fluorescence spectra of hybrid **D5-V**. Oligonucleotide concentration: 1 µM singlestrand, 100 mM NaCl, 10 mM phosphatebuffer pH 7.4. Excitation wavelength: 300 nm.

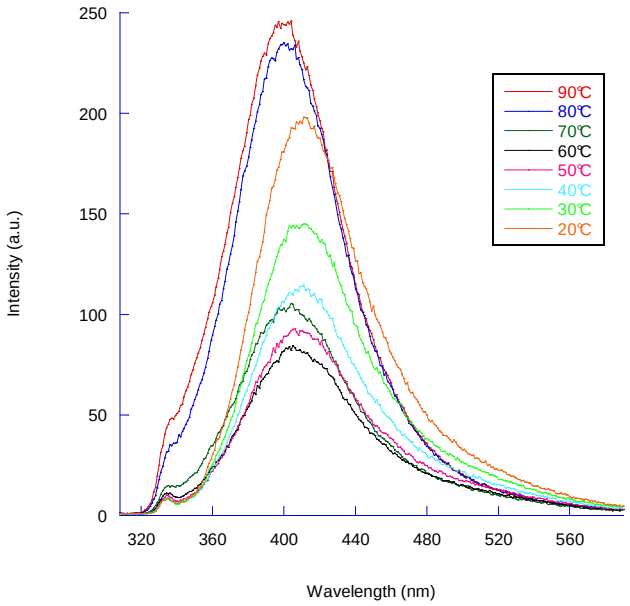

Figure 5.16 Temperature dependent fluorescence spectra of hybrid **D8-V**. Oligonucleotide concentration: 1 µM singlestrand, 100 mM NaCl, 10 mM phosphatebuffer pH 7.4. Excitation wavelength: 300 nm.

To test the hypothesis of excimer emission resulting from interstrand interactions, the hybrid **D10-V** which places two fluorene moieties opposite two natural bases was measured. The emission at 90°C is also attributed to mostly intrastrand excimer emission

with a certain amount of structured monomer emission. Decreasing the temperature resulted in a decrease in this broad and structureless emission band and at the same time of the monomeric emission band. The excimer emission band increases again in analogy to the hybrids **D3-V** and **D5-V** but to a much smaller extent. Additionally the redshift of the excimer emission band is almost neglectable. The redshift observed for the hybrids **D3-V**, **D5-V** and **D8-V** might originate therefore from interstrand interactions between the two modifications.

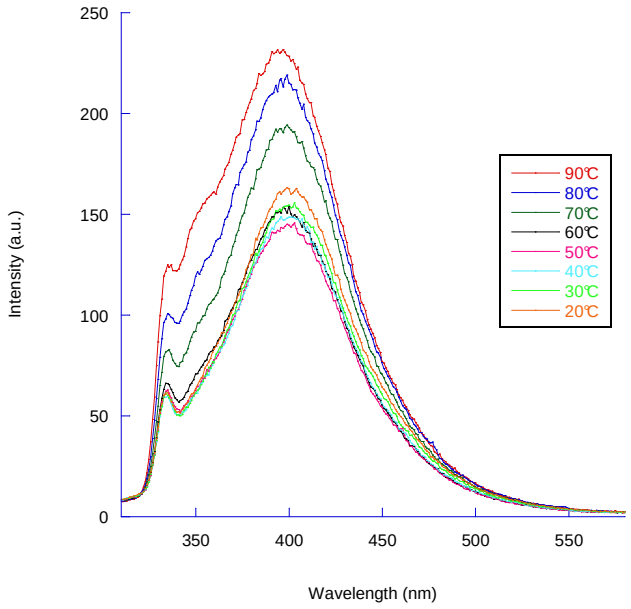

Figure 5.17 Temperature dependent fluorescence spectra of hybrid **D10-V**. Oligonucleotide concentration: 1 µM singlestrand, 100 mM NaCl, 10 mM phosphatebuffer pH 7.4. Excitation wavelength: 300 nm.

Circular Dichroism

Potential interactions of the fluorene units were monitored by CD spectroscopy. For all the hybrids the main signature for B-DNA is conserved indicated by the positive maximum at 283 nm and the negative minimum at 254 nm with only slight deviations. The modifications seem not to disturb the overall structure which is in agreement with the cooperative melting process and the very sharp transition. Also the melting of the hybrid is nicely monitored by CD spectroscopy with the decreasing peaks of the canonical B-DNA at 254 nm and 283 nm.

The main absorption region of the fluorene units is separated from the absorption region of the bases and is therefore well suited to study the interactions among the fluorene units.

For the hybrid **D2-V** the observed CD signal appears to be of exciton coupled type with a negative band at 336 nm which is followed by two positive signals at 315 nm and 305 nm indicative for the interaction of the two chromophores in agreement with the excimer formation seen by fluorescence. Furthermore, the signal at 336 nm is redshifted by 5 nm compared to the maximum observed in the UV-absorbance spectrum. These change in from negative to positive as well the shift of the observed signals compared to the absorption spectrum support the assumption of an exciton coupled CD with negative chirality for **D2-V**. By increasing the temperature the signal vanishes which is also in aggrement with the two interacting chromophores being separated in the singlestrands (Figure 5.18).

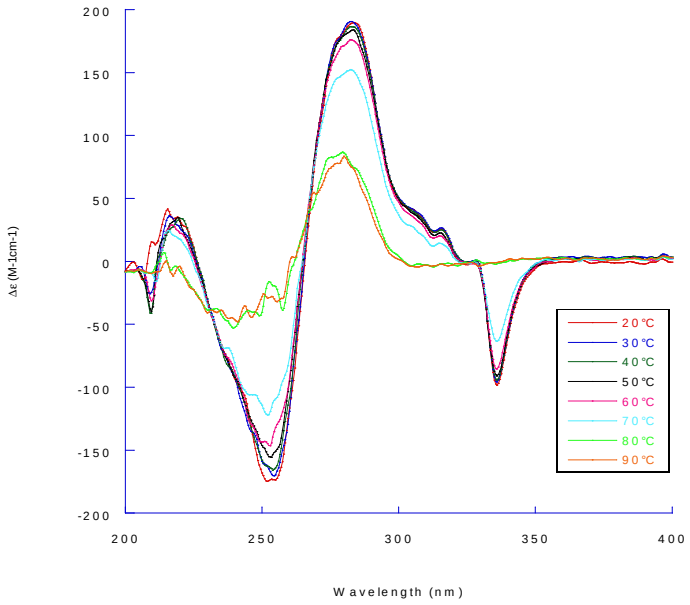

Figure 5.18 Temperature dependent circular dichroism of hybrid **D2-V**. Oligonucleotide concentration: 5 µM singlestrand, 100 mM NaCl, 10 mM phosphatebuffer pH 7.4.

Looking at hybrid **D4-V** and directly comparing it to **D2-V** at roomtemperature the observed signal is completely reversed in the absorption region of the fluorene moiety (Figure 5.19). For hybrid **D4-V** first a positive signal at 336 nm is followed by two negative signals at 315 nm and 305 nm forming the almost complete mirror image of the signal of **D2-V**. Also for **D4-V** the same arguments apply as for **D2-V** with the change in the sign of the signals as well the redshift of the signal band compared to the absorption spectra. Also in this case the CD spectrum hints for an exciton coupled CD although with a positive chirality.

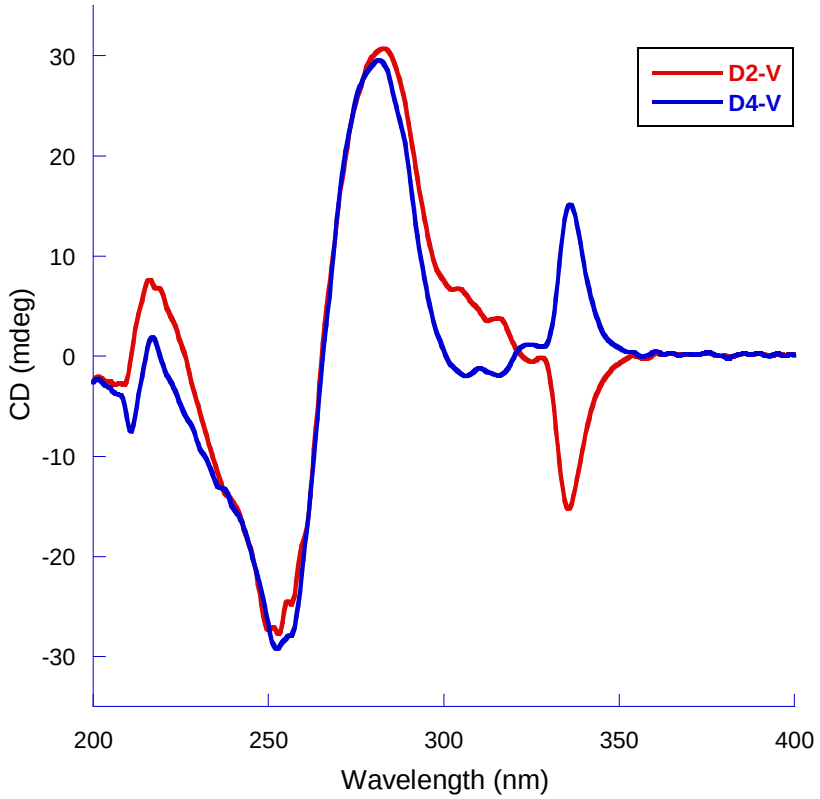

Figure 5.19 Circular dichroism of hybrid **D2-V** and **D4-V** at 20°C. Oligonucleotide concentration: 5 µM singlestrand, 100 mM NaCl, 10 mM phosphatebuffer pH 7.4.

For the hybrid **D3-V** and the CD signal in the main absorption region of the fluorene takes the signature of a positive induced CD signal. There is no obvious coupling visible by CD although the fluorescence spectra indicate a severe coupling.

Hybrid **D4-V** and **D5-V** both with the longer linker exhibit a positive induced CD with more or less the same maxima comparable hybrid **D3-V**.

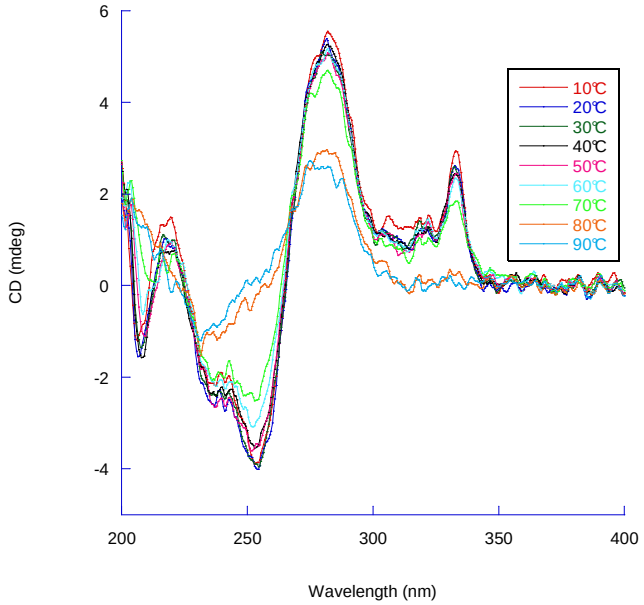

Figure 5.20 Temperature dependent circular dichroism of hybrid **D3-V**. Oligonucleotide concentration: 1 µM singlestrand, 100 mM NaCl, 10 mM phosphatebuffer pH 7.4.

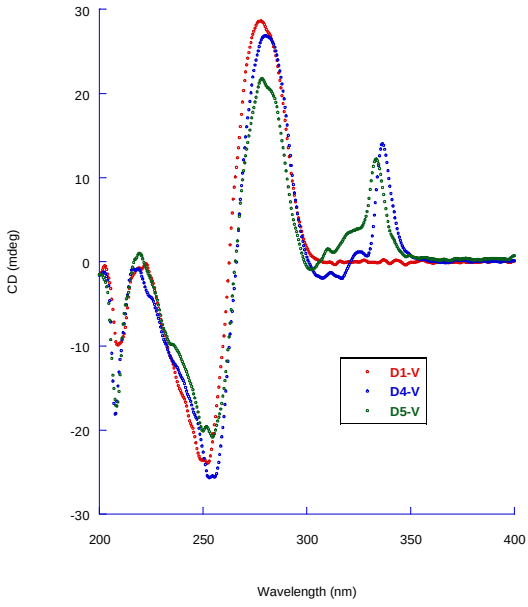

Figure 5.21 Comparison of the circular dichroism spectra of hybrid **D1-V**, **D4-V** and **D5-V**. Oligonucleotide concentration: 5 µM singlestrand, 100 mM NaCl, 10mM phosphatebuffer pH 7.4.

5.4. Conclusions and Outlook

It has been shown that the non-nucleosidic fluorene derivatives used in this study lead to a remarkable stabilization of the overall hybrid stability when used instead of a canonical A-T base pair. Furthermore the cooperativity is maintained and there is no hysteresis observed for all hybrids. Interstrand excimer although of weak nature is observed for the hybrids containing one fluorene moiety in the singlestrand. This excimer emission disappears upon heating and melting the hybrid and monomer emission only remains. When two fluorene units are incorporated next to each other in the singlestrand strong intrastrand excimer formation is observed which is supported also by the fact that upon heating this excimer emission band is still present. As revealed by CD spectroscopy the overall B-form of the DNA is no disrupted by the prescene of the fluorene modifications. The fluorene moieties themselves show strong CD activity. Putting two fluorene units in opposite positions in the hybrids results in an exciton coupled CD. This exciton coupled CD shows depending on the length of the linker either a positive chirality in the case of the longer linker and a negative chirality for the shorter linker. Having two fluorene moieties in the singlestrands and four in the hybridized state results in an induced type of CD with a positive cotton effect which can be attributed to the fluorene moieties forming aggregates in the chiral environment of DNA.

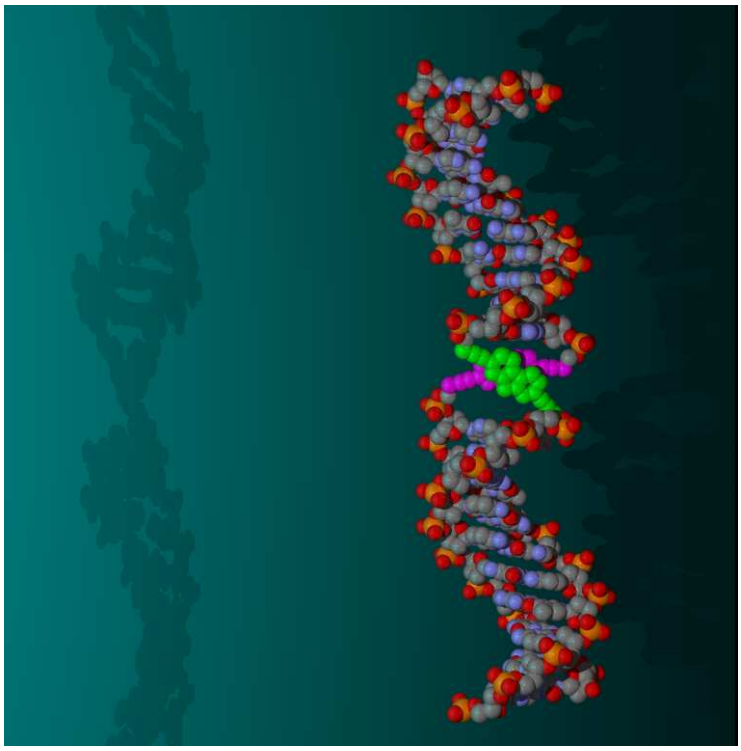

Figure 5.22 Molecular model of a possible arrangement two fluorene moieties in opposite position upon formation of the DNA duplex

As the length of the linker seems to play a crucial role in the relative orientation of the fluorene moieties, this issue can be addressed by synthesizing the intermediate linker length or even a longer linker. Additionally the incorporation of multiple fluorene units can be a possible idea to further explore the organizing nature of these fluorene building blocks. Since the position C9 of the fluorene unit is synthetically interesting the modification at this position could lead to a different behavior and arrangement of the fluorene units in the context of DNA which can be explored. As the phosphodiester bond separates two fluorene moieties also the idea of conjugated systems would lead to another set of materials embedded in DNA.

5.5. Experimental Section

Synthesis of the non-nucleosidic fluorene building blocks

(Experiements referring to scheme 5.1)

2,7-Bis(4-hydroxybut-1-yn-1-yl)fluorene **(1)**

1.00 g (3.085 mmol) 2,7-dibromofluorene was dissolved in 30 ml of THF. To this solution 7 mg (0.0375 mmol) of copper(I) iodide and 53 mg (0.075 mmol) of $(PPh_3)_2Cl_2Pd$(II) was added. The solution was heated under reflux, once reaching 70°C, 20 ml of freshly degassed triethylamine was added. Finally 1.19 ml (18.3 mmol) of 3-butyn-1-ol was added and the solution was stirred under reflux over night. After cooling to room temperature, THF and triethylamine was evaporated and the remaining solid was dissolved in 50 ml of THF. This suspension was filtered over celite and THF was evaporated again. The solid was taken up in EtOAc after which the precipitate was filtered of and the solution was washed with citric acid (10 %) and with $NaHCO_3$ (sat) and dried over $MgSO_4$. The volume of the organic phase was reduced until precipitation. The solution was then put in a cool ultrasonic bath and the resulting precipitate was filtered off and dried under reduced pressure resulting in 638 mg (68 %) of a light brownish solid.

^{1}H-NMR (300MHz, D_6-DMSO): 2.58 (4H, t, J= 7.0), 3.6 (4H, q, J= 6.6), 3.90 (2H, s), 4.91 (2H, t, J= 5.5), 7.41 (2H, d, J= 8.1), 7.60 (2H, s), 7.86 (2H, d, J= 7.9). ^{13}C-NMR (75MHz, D_6-DMSO): 23.4, 36.1, 59.8, 81.6, 88.7, 120.4, 121.7, 128.0, 130.2, 140.1, 143.5.

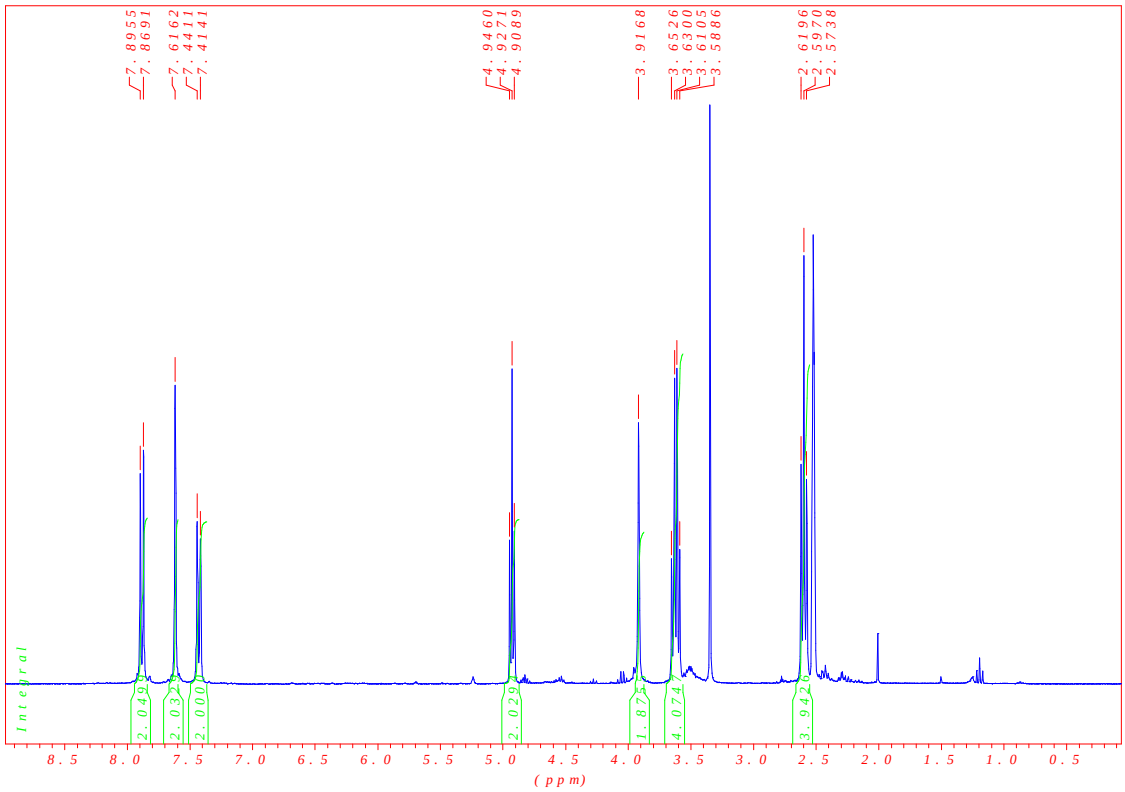

2,7-Bis(6-hydroxyhex-1-yn-1-yl)fluorene (**2**)

1.00 g (3.085 mmol) 2,7-dibromofluorene was dissolved in 30ml of THF. To this solution 30ml triethylamine filtered over aluminiumoxide was added. The solution was degassed for 30 minutes. Afterwards 110 mg (0.156 mmol) of $(PPh_3)_2Cl_2Pd(II)$ and 29 mg (0.156 mmol) copper (I) iodide was added. Finally 0.77 ml (6.9 mmol) of 5-hexyn-1-ol was added the reaction mixture was heated under reflux overnight. After cooling to room temperature the mixture was filtered over celite, THF and triethylamine was evaporated and solid was dissolved in EtOAc. The residue was purified by column chromatography over silica gel with pure EtOAC. The product fractions were combined, EtOAc evaporated and the resulting solid was dried under high vacuum yielding in 250 mg (28 %) of a white yellow solid.

^{1}H-NMR (300MHz, D_6-DMSO): 1.5-1.7 (8H, m), 2.4-2.5 (4H, m), 3.4-3.5 (4H, m), 3.90 (2H, s), 4.43 (2H, t, J= 5.1), 7.40 (2H, d, J= 7.9), 7.58 (2H, s), 7.86 (2H, d, J= 7.9). ^{13}C-NMR (75MHz, D_6-DMSO): 18.6, 24.9, 31.7, 36.0, 60.2, 81.2, 90.9, 120.3, 121.8, 127.9, 130.1, 140.1, 143.5.

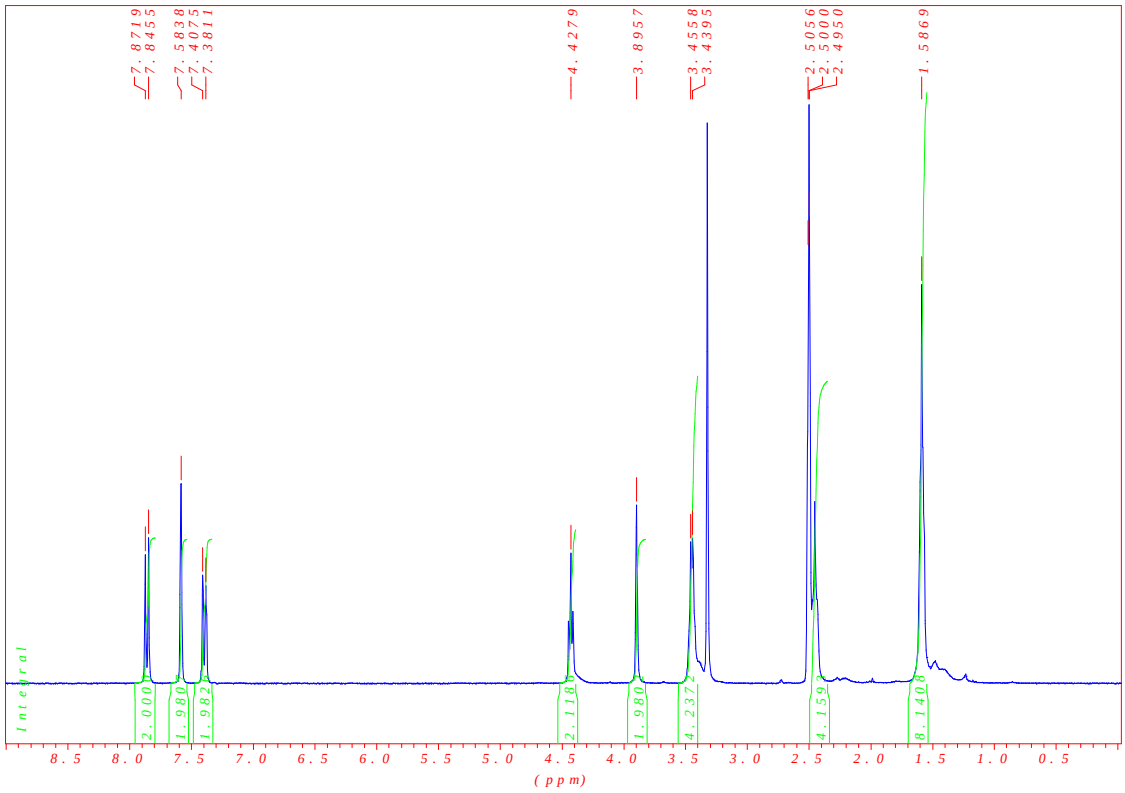

*2-**[**4-(4,4`-Dimethoxytriphenylmethyloxy)but-1-yn-1-yl**]**-7-(4-hydroxybut-1-yn-1-yl) fluorene* (**3**)

To a solution of 490 mg (1.62 mmol) of **1** in 13 ml THF and 7 ml pyridine, a solution of 553 mg (1.62 mmol) 4,4`-dimethoxytrityl chloride in 3.5 ml THF was added dropwise under argon over 2 hours at room temperature. THF and pyridine were then evaporated. The solid was then taken up in 150 ml EtOAc, filtrated and washed with citric acid (10%) and $NaHCO_3$ (sat) and dried over $MgSO_4$. EtOAc was removed under reduced pressure and the resulting residue was purified by column chromatography on silica gel (EtOAc/Hexane 1:1 + 2 % triethylamine to EtOAc/Hexane 1:1 + 2 % triethylamine + 4 %

methanol). The product fractions were combined, evaporated and dried under high vacuum to furnish 254 mg (26 %) of a yellow white foam.

^{1}H-NMR (300MHz, D_6-DMSO): 2.58 (2H, t, J=7.0), 2.73 (2H, t, J=6.2), 3.16 (2H, t, J=6.2), 3.60 (2H, q, J_1=5.8, J_2=6.6), 3.91 (2H, s), 3.73 (6H, s), 4.91 (1H, t, J= 5.7), 6.88 (4H, d, J=8.9), 7.18-7.27 (1H, m), 7.27-7.36 (6H, m), 7.4-7.5 (4H, m), 7.60 (2H, d, J=5.1), 7.88 (2H, m).

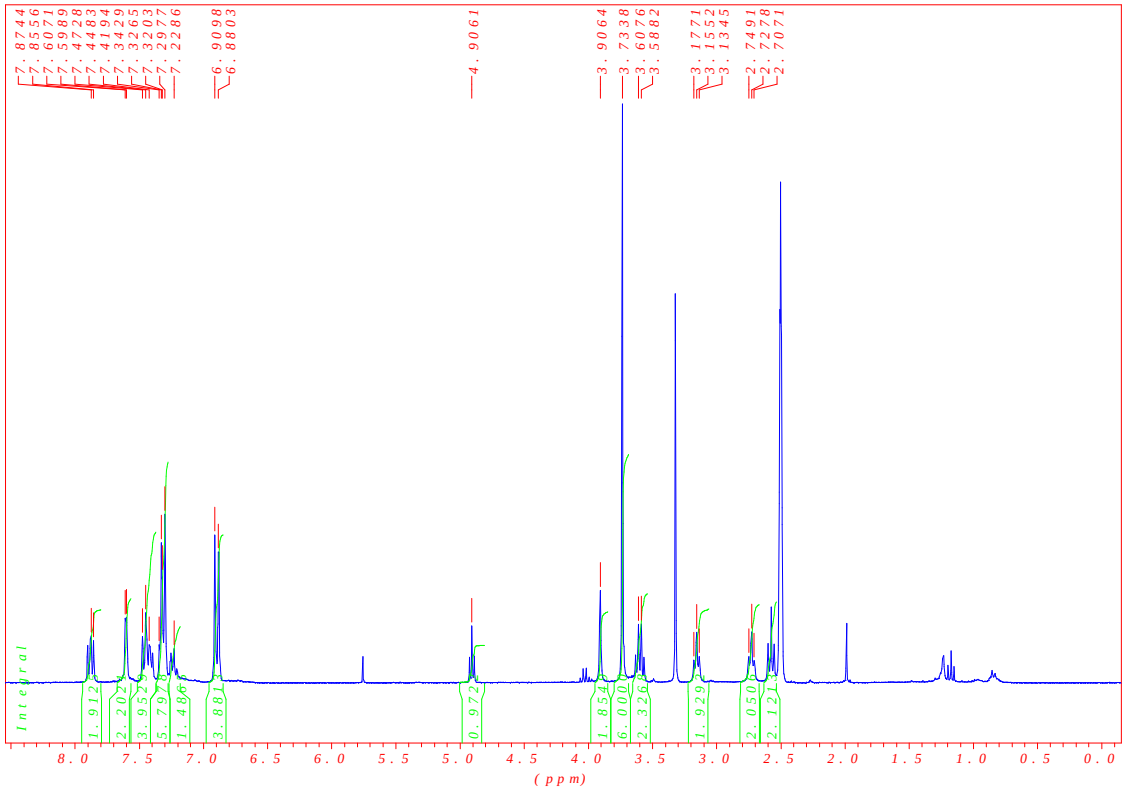

2-[6-(4,4`-Dimethoxytriphenylmethyloxy)hex-1-yn-1-yl]-7-(6-hydroxyhex-1-yn-1-yl) fluorene (**4**)

To a solution of 250 mg (0.697 mmol) of **2** in 15 ml THF and 6 ml pyridine, a solution of 238 mg (0.7 mmol) 4,4`-dimethoxytrityl chloride in 5 ml THF was added dropwise under argon over 2 hours at room temperature. THF and pyridine were then evaporated. The solid was then taken up in 80 ml EtOAc, filtrated and washed with citric acid (10 %) and $NaHCO_3$ (sat) and dried over $MgSO_4$. EtOAc was removed under reduced pressure and the resulting residue was purified by column chromatography on silica gel (EtOAc/Hexane 1:1 + 2 % triethylamine). The product fractions were combined, evaporated and dried under high vacuum to furnish 95 mg (22 %) of a yellow white foam.

^{1}H-NMR (300MHz, D_6-DMSO): 1.5-1.8 (8H, m), 2.35-2.47 (4H, m), 3.03 (2H, t, J=6.0), 3.4-3.5 (2H, m), 3.72 (6H, s), 3.89 (2H, s), 4.43 (1H, t, J= 5.3), 6.88 (4H, d, J=8.9), 7.2-7.35 (7H, m), 7.35-7.45 (4H, m), 7.60 (2H, d, J=5.1), 7.88 (2H, d, J=7.9).

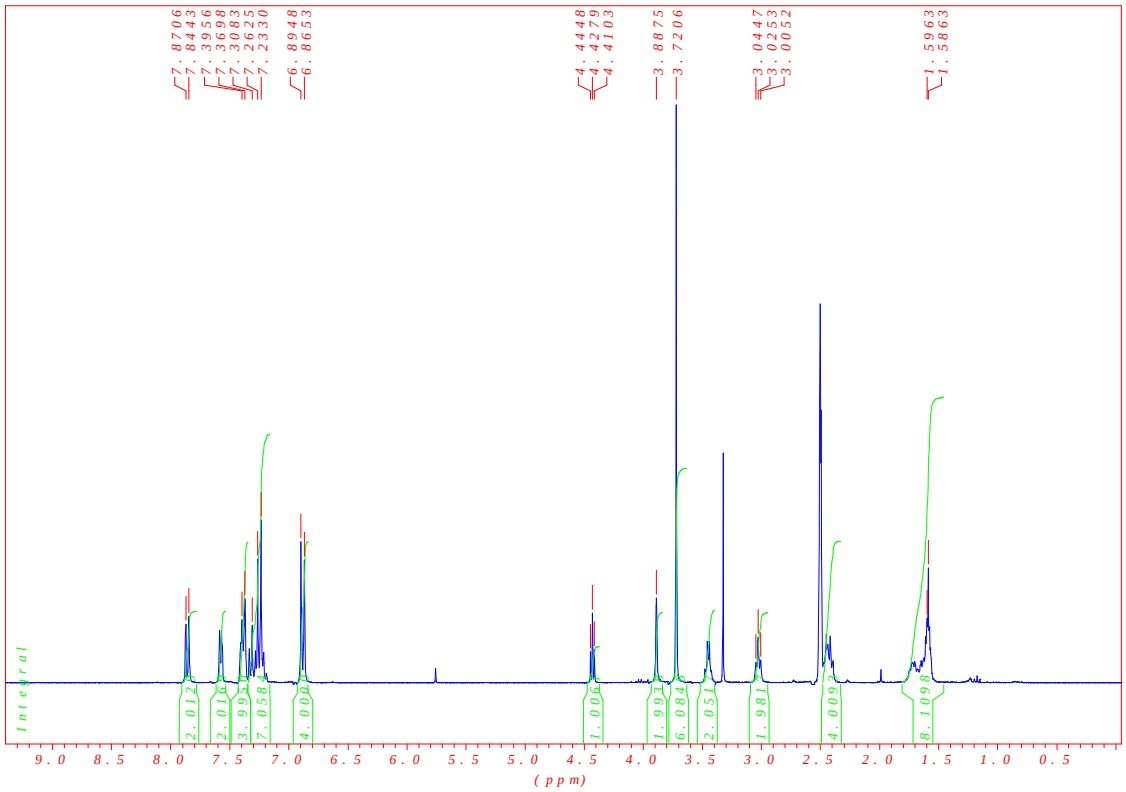

*O-2-Cyanoethyl-O`-{**[**4-(4,4`-Dimethoxytriphenylmethyloxy)but-1-yn-1-yl)fluorene-1-yl**]** - but-3-yn-1-yl) fluorene-N,N-diisopropyl phosphoramidite* (**5**)

450 mg (0.74 mmol) of **3** was dissolved in 15 ml CH_2Cl_2 and 383 µL (2.23 mmol) diiosopropylethylamine. 194 mg (0.81 mmol) of 2-cyanoethyl-N,N-diisopropyl-chlorophosphoramidite was then added dropwise at roomtemperature under argon. The reaction mixture was stirred for 1 hour. The volume of CH_2Cl2 was then reduced and a column chromatography over silica gel was directly performed with pure CH_2Cl_2 with 2 % triethylamine. After evaporation and drying under high vacuum, 401 mg (67 %) of a yellow white foam resulted.

^{1}H-NMR (300MHz, D_6-DMSO): 1.16 (12H, dd, J=4.5), 3.15 (2H, t, J=6.6), 3.73 (6H, s), 3.91 (2H, s), 6.90(4H, d, J=8.85), 7.2-7.5 (11H, m), 7.60 (2H, d, J=6.39), 7.9 (2H, dd, J=3.75).

^{31}P-NMR (121.5MHz, $CDCl_3$): 147.25

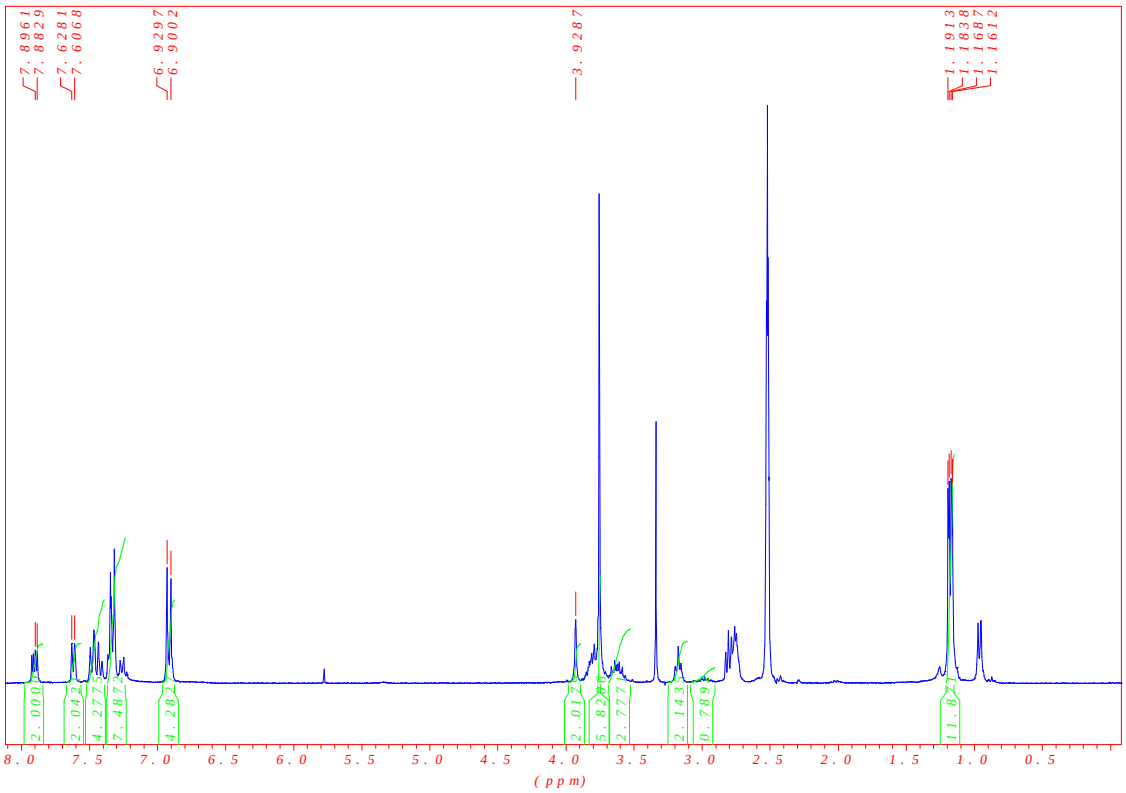

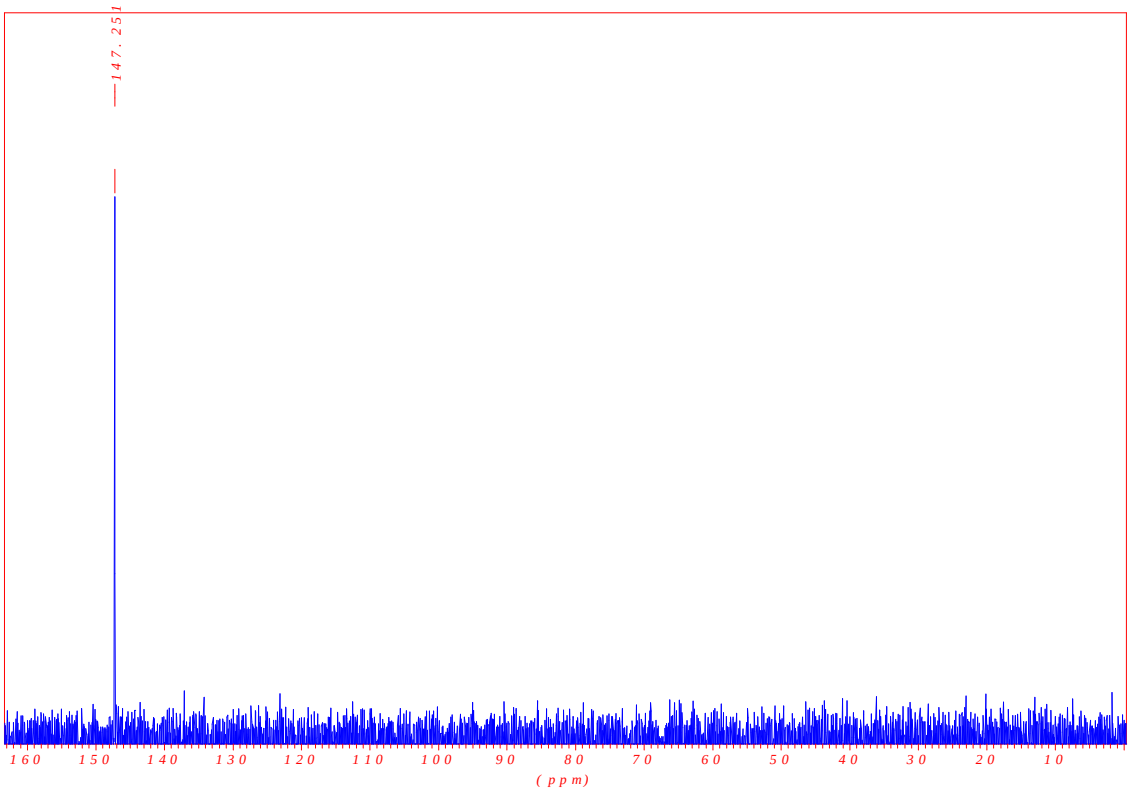
147.251
160
150
140
130
120
110
100
90
80
70
60
50
40
30
20
10
(ppm)

O-2-Cyanoethyl-O`-{[4-(4,4`-Dimethoxytriphenylmethyloxy)hex-1-yn-1-yl)fluorene-1-yl] - hex-5-yn-1-yl) fluorene-N,N-diisopropyl phosphoramidite (**6**)

272 mg (0.41 mmol) of **5** was dissolved in 15 ml CH_2Cl_2 and 211 µL (1.23 mmol) diiosopropylethylamine. 108 mg (0.45 mmol) of 2-cyanoethyl-N,N-diisopropyl-chlorophosphoramidite was then added dropwise at roomtemperature under argon. The reaction mixture was stirred for 1 hour. The volume of CH_2Cl_2 was then reduced and a column chromatography over silica gel was directly performed with pure CH_2Cl_2 with 2 % triethylamine. After evaporation and drying under high vacuum, 280 mg (79 %) of a yellow white foam resulted.

^{1}H-NMR (300MHz, D_6-DMSO): 1.1 (12H, d, J=6.8), 1.55-1.8 (8H, m), 2.45-2.5 (2H, m), 2.76 (2H, t, J=5.82), 3.03 (2H, t, J=6.03), 3.5-3.8 (12H, m), 3.89 (2H, s), 6.88 (4H, d, J=9.03), 7.15-7.45 (11H, m), 7.57 (2H, d, J=3.39), 7.86 (2H, d, J=7.92).
^{31}P-NMR (121.5MHz, $CDCl_3$): 146.59

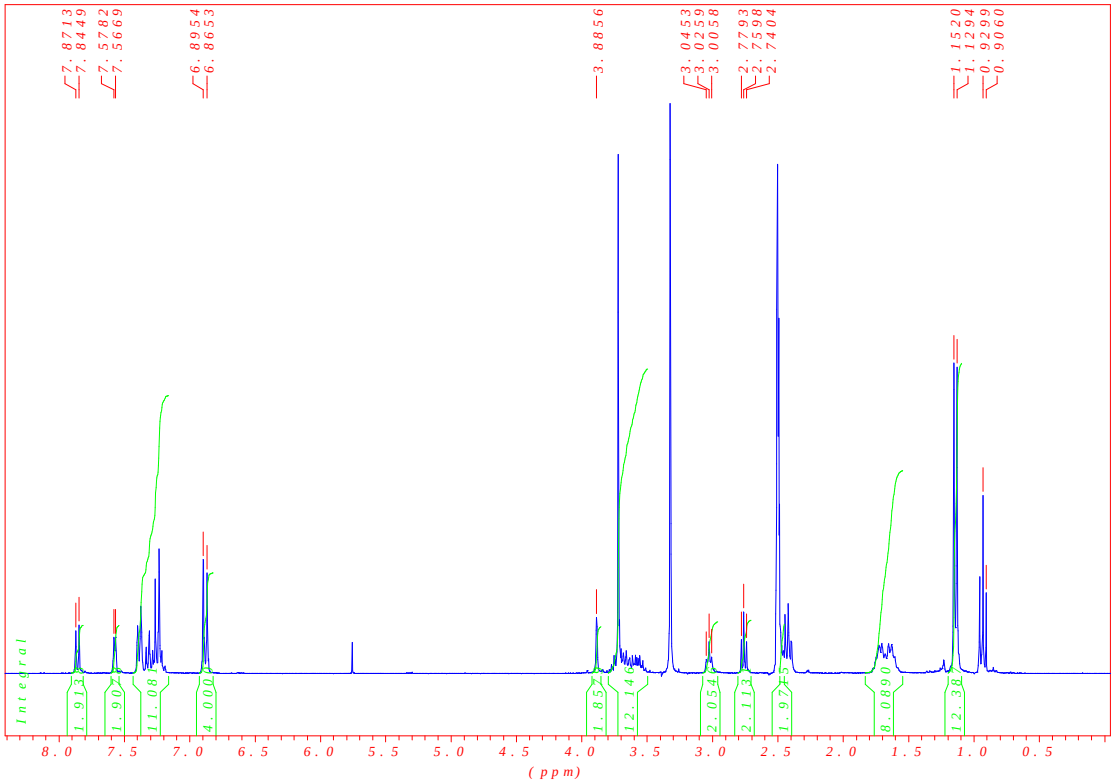
7.8713
7.8449
7.5782
7.5669
6.8954
6.8653
3.8856
3.0453
3.0259
3.0058
2.7793
2.7598
2.7404
1.1520
1.1294
0.9299
0.9060
Integral
1.91
1.90
11.08
4.00
1.85
12.14
2.05
2.11
1.97
8.08
12.38
8.0 7.5 7.0 6.5 6.0 5.5 5.0 4.5 4.0 3.5 3.0 2.5 2.0 1.5 1.0 0.5
(ppm)

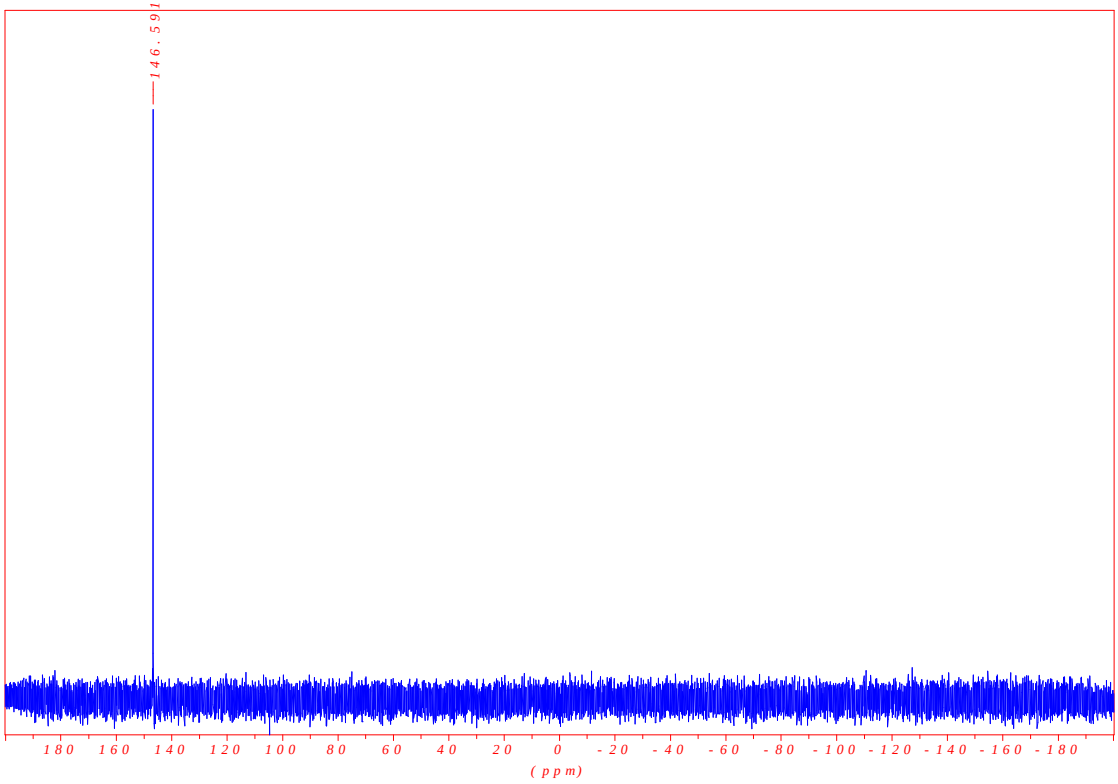
146.591
180 160 140 120 100 80 60 40 20 0 -20 -40 -60 -80 -100 -120 -140 -160 -180
(ppm)

Oligonucleotide synthesis

Nucleoside phosphoramidites were purchased from *SAFC* (Proligo Reagents) with dG (dmf), dC (ac) and dA (bz). Oligonucleotides **ON1-V** to **ON8-V** were prepared via automated oligonucleotide synthesis using standard phosphoramidite chemistry (Activator: Ethylthiotetrazole 0.3 M in Acetonitrile) on a 394-DNA/RNA synthesizer (*Applied Biosystems*). Oligonucleotides **ON9-V** and **ON10-V** were ordered from *MicroSynth*, Switzerland. For the unnatural building block, which were coupled using 0.1 M solutions in 1,2-dichloroethane, coupling times were increased to 120 seconds instead of 25 seconds used for the natural nucleosides. Cleavage from the solid support and final deprotection was performed manually by treatment with 30 % NH_4OH solution at 55°C overnight. All oligonucleotides were purified by reverse phase HPLC (Instrument: LC-10 AT from *Shimadzu* with a UV detector, column: LiChrospher 100 RP-18, 5 µm, *Merck*); eluent A= $(Et_3NH)OAc$ (0.1 M, pH 7.4); eluent B= 80 % MeCN + 20 % Eluent A; gradient 5-60 % B over 38 min.

For the determination of oligonucleotide stock solution concentrations, small samples were diluted to 10% and the absorbance at 260 nm was measured on a Nanodrop ND-1000 Spectrophotometer from *Thermo Scientific*. Epsilon values were calculated using 15300, 11700, 7400 and 9000 for A, G, C and T, respectively, and 4600 for the fluorene building block as determined from UV-VIS absorption spectra of the corresponding diol derivatives in THF.

Molecular mass determination of the oligonucleotides was performed with a Sciex QSTAR pulsar (hybrid qudrupole time-of-flight mass spectrometer, *Applied Biosystems*). ESI-MS (negative mode, CH_3CN/H_2O/TEA) data of the compounds **ON1-V** to **ON8-V** are presented in Table 5.3.

	Oligo #	Duplex	Bruttoformula	Calc. aver. mass	Found mass
D2-V	**ON2-V**	(5`) TGC ACT CTC G**Y**T GAC CGA GCT	$C_{214}H_{263}N_{71}O_{124}P_{20}$	6433.1	6433.7
	ON1-V	(3`) ACG TGA GAG C**Y**A CTG GCT CGA	$C_{216}H_{261}N_{81}O_{120}P_{20}$	6531.1	6532.4
D3-V	**ON4-V**	(5`) TGC ACT CTC G**YY** GAC CGA GCT	$C_{225}H_{267}N_{69}O_{121}P_{20}$	6493.0	6492.7
	ON3-V	(3`) ACG TGA GAG C**YY** CTG GCT CGA	$C_{227}H_{266}N_{76}O_{119}P_{20}$	6582.0	6582.5
D4-V	**ON6-V**	(5`) TGC ACT CTC G**Z**T GAC CGA GCT	$C_{218}H_{271}N_{71}O_{124}P_{20}$	6489.1	6490.0
	ON5-V	(3`) ACG TGA GAG C**Z**A CTG GCT CGA	$C_{220}H_{269}N_{81}O_{120}P_{20}$	6587.2	6587.9
D5-V	**ON8-V**	(5`) TGC ACT CTC G**ZZ** GAC CGA GCT	$C_{225}H_{267}N_{69}O_{121}P_{20}$	6605.1	6606.1
	ON7-V	(3`) ACG TGA GAG C**ZZ** CTG GCT CGA	$C_{235}H_{282}N_{76}O_{119}P_{20}$	6694.2	6695.3

Table 5.3 Mass spectrometry data (brutto formula, calculated average mass, found mass)

Thermal denaturation experiments (1 µM singlestrand oligonucleotide concentration, 10mM phosphate buffer pH 7.4, 100 mM NaCl) were carried out on Varian Cary 100 Bio UV-Visible spectrophotometer equipped with a Varian Cary temperature controller and data were collected with Varian WinUV software at various wavelength as indicated in each case. Cooling- heating- cooling cycles in the temperature range of 90°C to 20°C and a heating/ cooling rate of 0.5°C/ min were used and data points every 0.5°C were recorded. Data were analyzed with KaleidaGraph 4 software from *Synergy Software*. Temperature melting values (T_m) were determined as the maximum of the first derivative of the melting curves. If necessary the curves were smoothed with a window of 5 in order to get a reasonable maximum of the first derivative.

Temperature dependent UV-VIS spectra were collected from 90°C to 20°C on a Varian Cary 100 Bio UV-Visible spectrophotometer equipped with a Varian Cary temperature controller. All experiments were carried out at a 1 µM singlestrand oligonucleotide concentration in 10 mM phosphatebuffer (pH 7.4) and 100 mM NaCl.

Temperature dependent fluorescence spectra were recorded from 90°C to 20°C on a Varian Cary Eclipse fluorescence spectrophotometer equipped with a Varian Cary temperature controller (excitation wavelength at 300 nm, excitation and emission slitwidth as well as the detector voltage were varied according to the experiment as indicated). All experiments were carried out with a singlestrand concentration of 1µM. Data were analyzed with KaleidGagraph 4 software from *Synergy Software*.

Circular dichroism spectra were recorded on a *JASCO* J-715 spectrophotometer equipped with a PFD-350S temperature controller. All experments were carried out with a singlestrand concentration of 5 µM (if not indicated) in 10mM phosphatebuffer (pH 7.4) and 100 mM NaCl.

Quantum yields were calculated by using quinine sulphate in 0.1 M H_2SO_4 at 20°C as the standard. Excitation wavelength used for **ON1-V, ON2-V, ON5-V** and **ON6-V**: 320 nm, excitation wavelength used for **ON3-V, ON4-V, ON7-V** and **ON8-V**: 330 nm. The absorption at the excitation wavelength was in the range of 0.05 and 0.1 units.

Chapter 6: Bisphenylfluorene: A differently linked fluorene derivative

6.1 Abstract

The synthesis of a non-nucleosidic fluorene phosphoramidite derivative with the linkage at the carbon 9 is presented. The single incorporation into an oligonucleotide and the placement of two modifications opposite each other in the duplex is shown to destabilize the over hybrid stability although maintaining a cooperative melting behavior. The two chromophores seem not to interact with each other as shown by fluorescent monomer emission and the induced type of CD.

6.2 Introduction

The introduction of a close to linear fluorene derivative as a base substitution and possible attractive building block (Chapter 5) led to the idea of exploring the nature of interactions of fluorene in an interstrand interactive mode and with the neigbouring bases but with a completely different connection between them. The choice fell on a derivative which would connect the fluorene moiety to the backbone through the quarternary carbon 9. By having this as the anchor point connecting the two adjacent nucleotides a completely different arrangement could possibly be achieved.

6.3 Results and Discussion

Synthesis of the phosphoramidite building block

The synthesis of the bisphenylfluorene derivative starts out with the commercially available bisphenolfluorene **1.** After reaction with the 2`-chloro-ethanol the corresponding diol **2** is achieved and subsequently protected with DMTCl giving the compound **3** and finally the mono-protected alcohol is further reacted to the corresponding phosphoramidite **4** which in turn is needed in order to incorporate into oligonucleotide on the automated synthesizer.

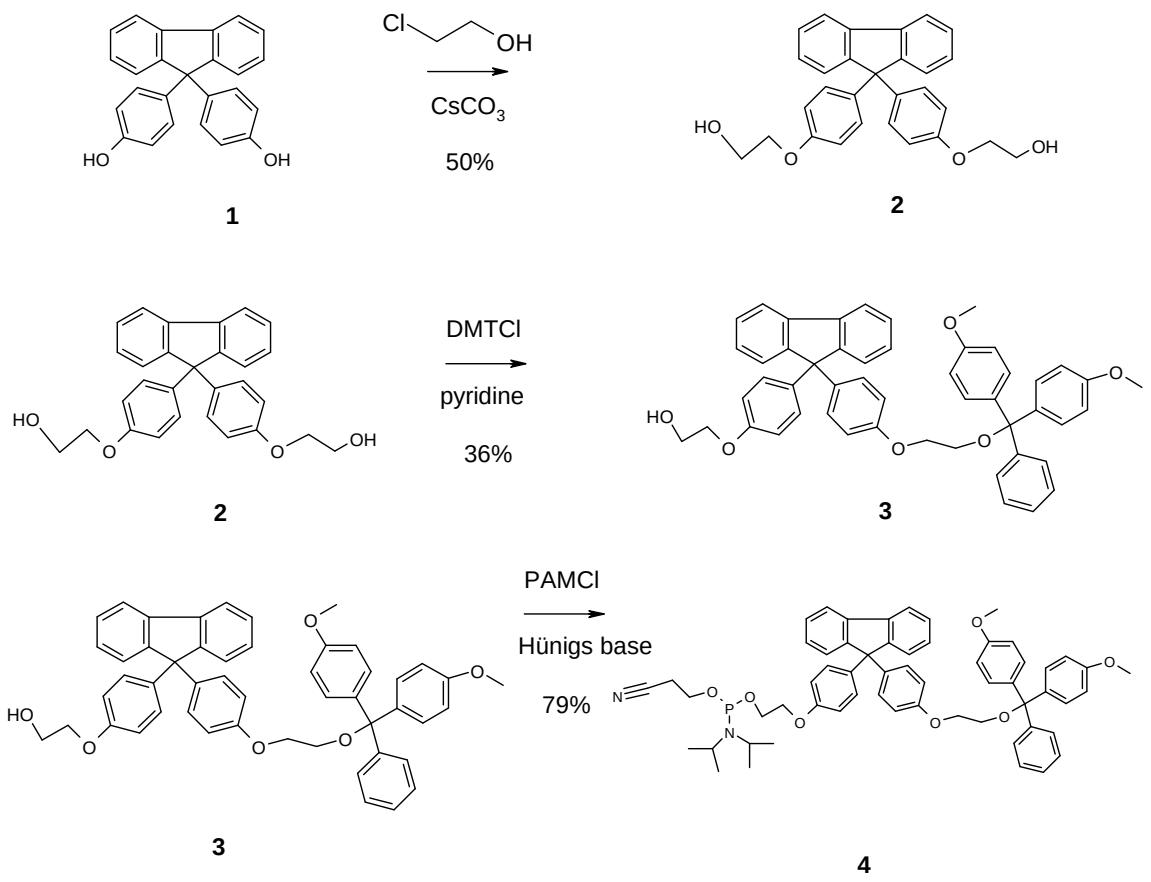

Scheme 6.1 Synthesis of the bisphenylfluorenephosphoramidite

Sequence and melting temperature

The incorporation into oligonucleotides was achieved in 1, 2-dichloroethane and the standard protocol for oligonucleotide synthesis was used except the coupling time was extended to 2 minutes instead of 25 seconds for the standard phosphoramidites. In order to study this fluorene derivative as a placeholder for a natural nucleotide, in the standard 21mer an A-T basepair was replaced by a diphenylfluorene “base-pair” so that the two modifications are placed opposite each other in the context of the double helical structure.

Hybrid	Oligo	Sequence	Tm
D1-VI	**Ref-1** **Ref-2**	(3`) ACG TGA GAG CTA CTG GCT CGA (5`) (5`) TGC ACT CTC GAT GAC CGA GCT (3`)	69.5°C
D2-VI	**ON1-VI** **ON2-VI**	(3`) ACG TGA GAG C**V**A CTG GCT CGA (5`) (5`) TGC ACT CTC G**V**T GAC CGA GCT (3`)	65.7°C
V= 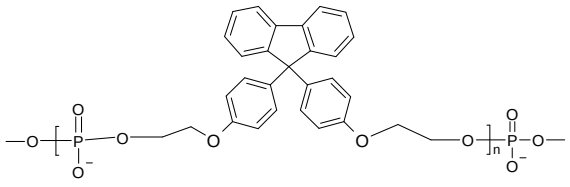			

Table 6.1 Sequences used in this study and melting temperature determined by monitoring 260 nm band

Melting profile of the hybrid

A melting profile was recorded for hybrid **D2-VI** and the melting temperature was compared to the fully natural reference hybrid **D1-VI**. The modified hybrid exhibits a destabilization of 3.8°C compared to the non-modified hybrid in contrast to the fluorene derivatives in the previous chapter (Chapter 5). The striking feature again is the extremely sharp transition and that there is absolutely no hysteresis observed. The modification does not disturb the overall cooperative melting process although bringing some destabilization probably due to the lacking of the hydrogen bonds and furthermore the lack of interstrand interactions. The intrastrand interaction with the adjacent bases seems to sustain the cooperativity.

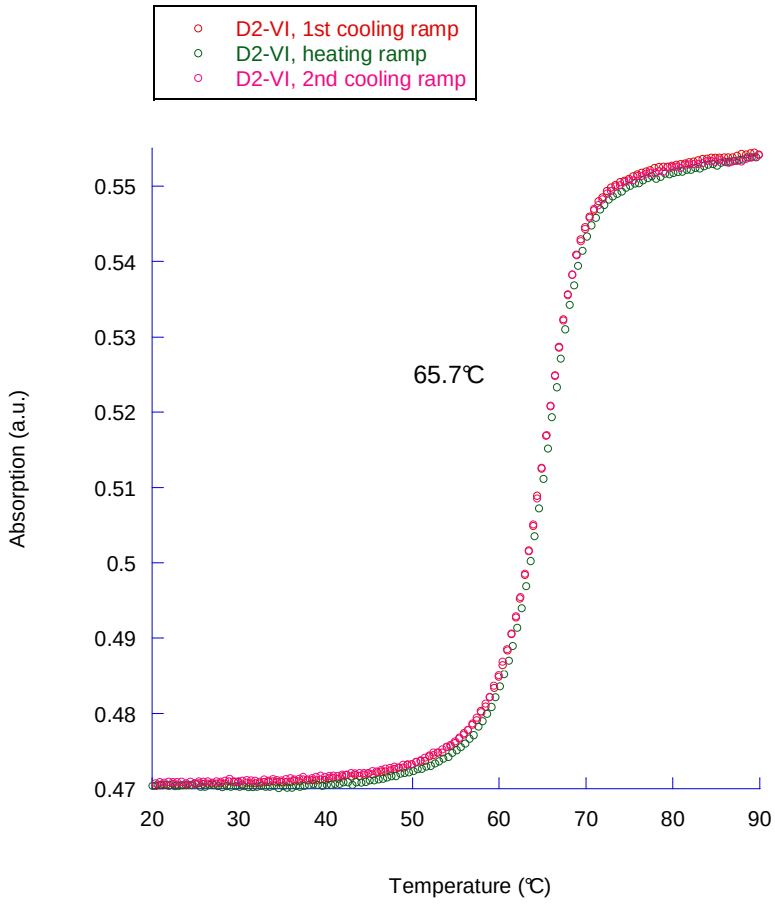

Figure 6.1 UV-Vis melting profile monitored at 260 nm showing two cooling and one heating ramp of hybrid **D2-VI**. Conditions: Singlestrand concentration: 1 µM, 100 mM NaCl, 10 mM phosphate buffer, heating/ cooling rate: 0.5°C/min.

Temperature dependent circular dichroism spectra

The circular dichroism spectra shows the characteristic melting process observed already by the UV-Vis melting profile going from the duplex in the B-form to the separated single strands. The melting temperature is in agreement with the determined one and also the drastic change in CD intensity going from 60°C to 70°C (melting temperature was determined to be 65.7°C) supports the high cooperativity of the melting process.

Looking at the main absorption band of the fluorene derivative at about 315 nm in the region separated from the main absorption band of the natural bases one can observe a negative CD signal which is probably of induced nature. The lack of an exciton coupled

circular dichroism signal (compared to the modification of chapter 5) and the occurrence of an induced signal hints for the two oppositely placed chromophores being independent of each other and that they are not electronically coupled together. Only the chiral environment of the DNA duplex causes the appearance of this induced signal. Furthermore the melting of the duplex between 60°C and 70°C is accompanied by the disappearance of the induced signal caused by the fluorene moieties.

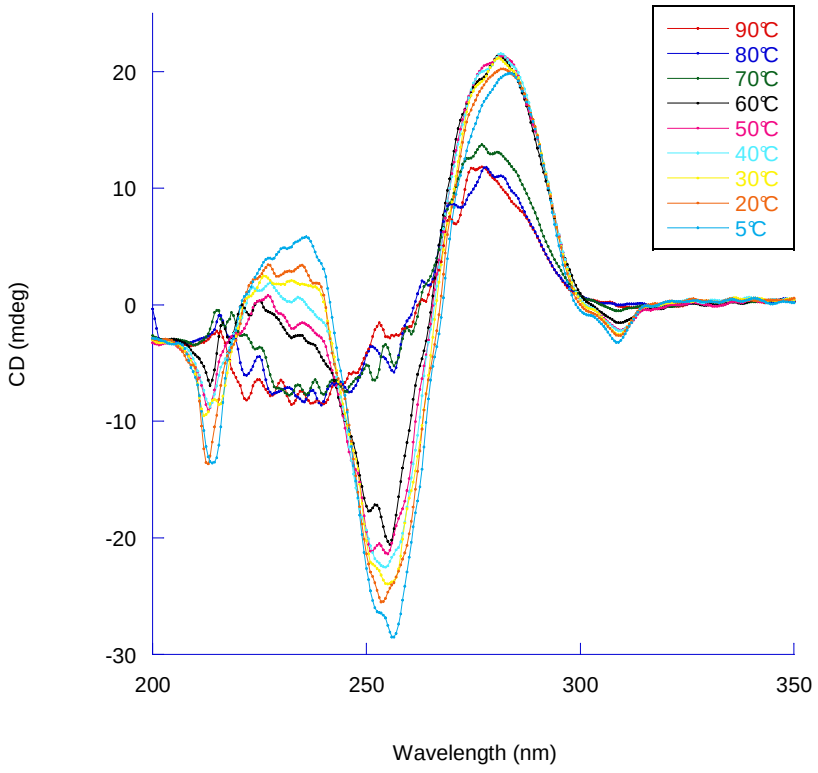

Figure 6.2 Temperature dependent circular dichroism spectrum of the hybrid **D2-VI**. Conditions: Singlestrand concentration: 5 µM, 100 mM NaCl, 10 mM phosphate buffer.

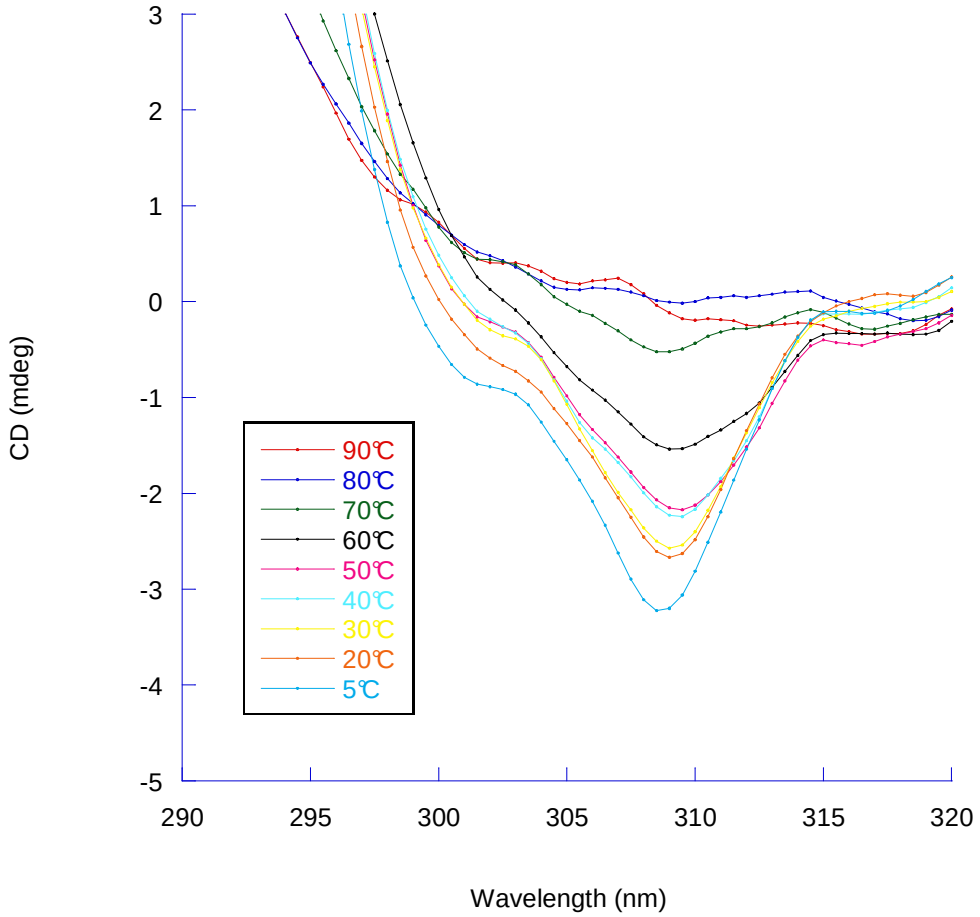

Figure 6.3 Zoom of the temperature dependent circular dichroism spectrum of the hybrid **D2-VI**. Conditions: Singlestrand concentration: 5 µM, 100 mM NaCl, 10 mM phosphate buffer.

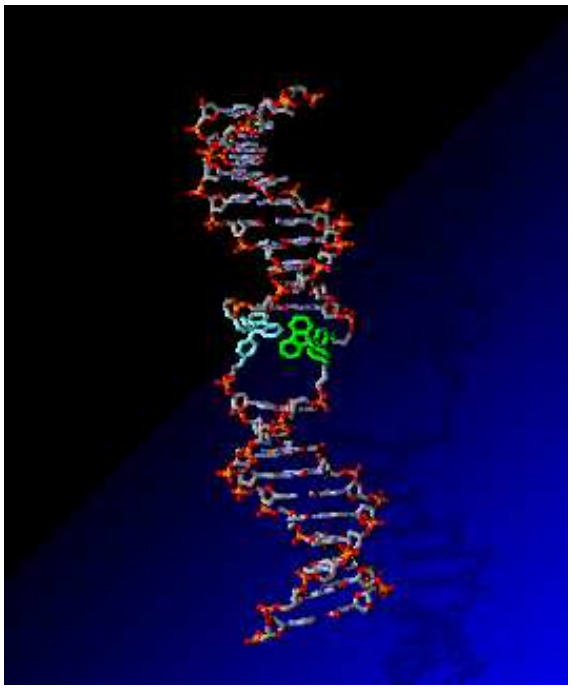

Figure 6.4 Proposed model of the formed duplex **D2-VI** with the incorporated modifications in green and blue

6.4 Conclusion and outlook

The length of the linker used in this study was, based on molecular modelling, the crucial feature which did not allow observing an increased stability and which did not lead to an intermolecular communication as seen by CD spectroscopy by the lack of an exciton coupled signal between the oppositely placed chromophores. Also fluorescence measurements indicate by the occurrence of temperature independent emission wavelength (no excimer) that the two modifications are just simple not in reach of each other manifested in the decreased stability exhibited by the duplex formed. The extension of the linker length could be the key to get the two chromophores to communicate with each other.

6.5 Experimental Section

Synthesis of the non-nucleosidic building block (Referring to Scheme 6.1)

9,9 -Bis(4-hydroxyethoxy-2-ol-phenyl) fluorene **(1)**

1.00 g (2.85 mmol) 9,9-Bis-(4-hydroxyphenyl)-fluorene was dissolved in 20ml of DMF. To this solution 1.95 g (5.86 mmol, 2eq) of Cs_2CO_3 and 0.58ml (8.56 mmol, 3eq) of 2-chloroethanol was added. The solution was heated under reflux at 90°C overnight. After cooling to roomtermperature the DMF was evaporated under reduced pressure and the remaining solid was taken up in 150 ml of water and 100 ml of CH_2Cl_2. The organic phase was washed with brine and dried over $MgSO_4$. The compound was then purified by column chromatography on silica gel (EtOAc:Hexane 3:1) resulting in 600 mg (48 %) of a white solid.

^{1}H-NMR (300 MHz, D_6-DMSO): 3.66 (4H, q, J=5.3), 3.91 (4H, t, J= 5.1), 4.81 (2H, t, J= 5.5), 6.81 (4H, d, J=8.9), 7.00 (4H, d, J= 8.8), 7.30 (2H, t, J= 6.2), 7.38 (4H, t, J=6.8), 7.90 (2H, d, J= 7.0).

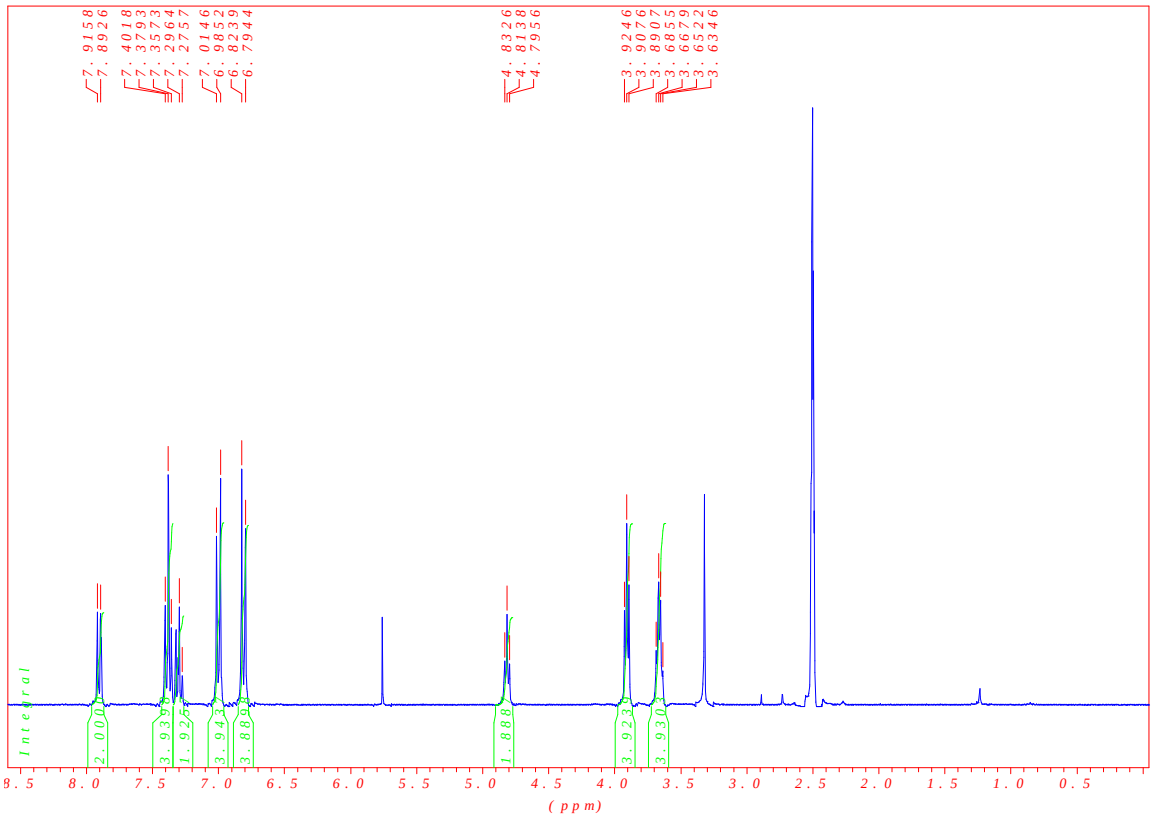

9,9 –(4-hydroxyethoxy-2-ol-phenyl-4-hydroxyethoxy-4,4-dimethoxytrityl) fluorene **(2)**

500 mg (1.14 mmol) of **1** was dissolved in 30 ml of THF and 12 ml of pyridine. 388 mg (1.14 mmol, 1eq) of 4,4-dimethoxytrityl chloride was dissolved in 8ml of THF and added dropwise over two hours to the reaction mixture at room temperature. The solution was then stirred at roomtemperature overnight. The solvents were then evaporated under reduced pressure and the remaining solid was taken up in 200 ml of EtOAc. The solution was twice washed with citric acid (10 %) and once with saturated $NaHCO_3$ and afterwards dried over $MgSO_4$. After removal of the EtOAc the compound was purified via column chromatorgraphy (EtOAc: Hexane 1:1 to EtOAc: Hexane 2:1 with 1 % of triethylamine) yielding 300 mg (36 %) of a white solid.

^{1}H-NMR (300 MHz, D_6-DMSO): 3.22 (2H, t, J=4.5), 3.66 (2H, q, J=5.3), 3.72 (6H, s), 3.91 (2H, t, J=4.9), 4.1 (2H, t, J= 5.1), 4.82 (1H, t, J= 5.6), 6.78-6.90 (8H, m), 6.97-7.07 (4H, m), 7.15-7.34 (9H, m), 7.34-7.44 (6H, m), 7.91 (2H, d, J= 7.4).

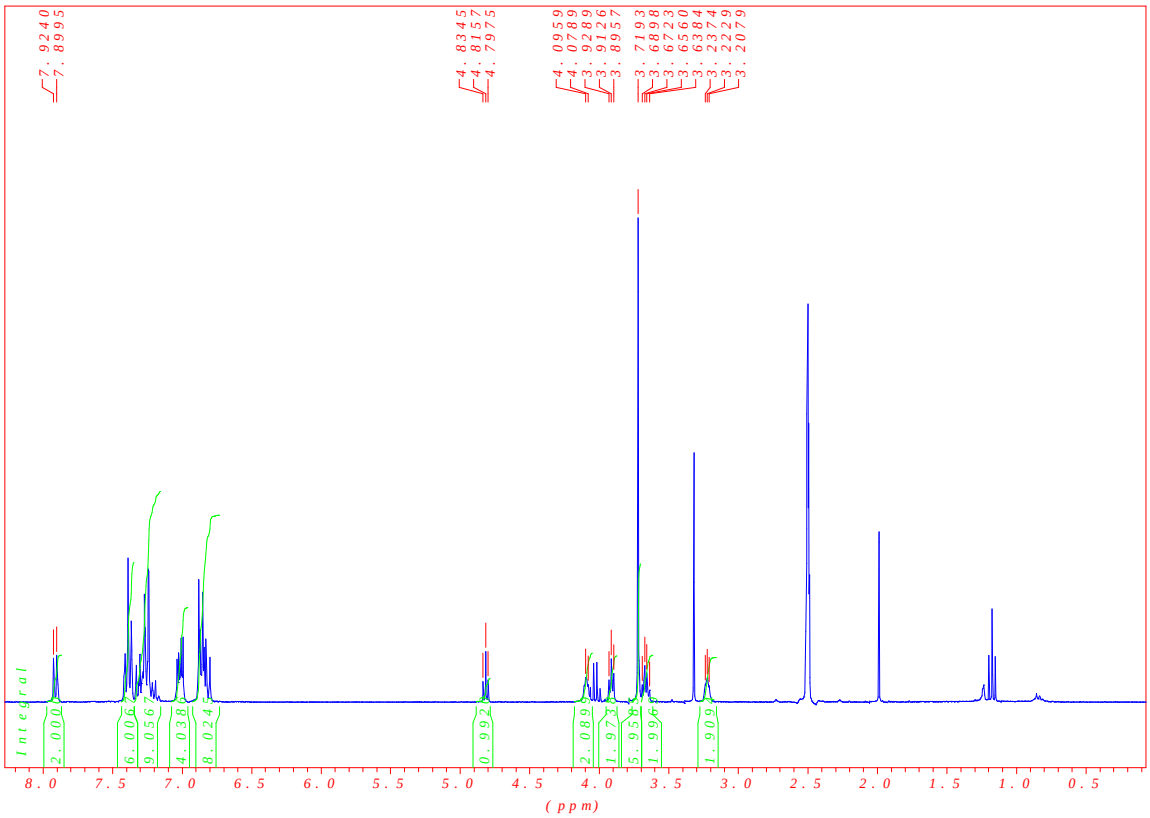

O-2-Cyanoethyl-O`-{9,9–(4-hydroxyethoxy-2-ol-phenyl-4-hydroxyethoxy-4,4-dimethoxytrityl) fluorene -N,N-diisopropyl phosphoramidite (**3**)

200 mg (0.27 mmol) of **2** was dissolved in 10 ml of CH_2Cl_2 and 235 µL of diisopropylethyl amine. 72 mg (0.3 mmol, 1.1eq) of PAMCl was added dropwise at roomtemperature. After 2 hours stirring at roomtemperature the volume of the reaction mixture was reduced and directly applied to column chromatography on silica (CH_2Cl_2 + 1 % triethylamine) yielding 80 mg (79 %) of a white foam.

^{1}H-NMR (300 MHz, D_6-DMSO): 0.93 (4H, t, J=7.2), 1.07-1.16 (12H, m), 2.42 (2H, q, J=7.1), 2.72 (2H, t, J=5.8), 3.22 (2H, t, J=4.4), 3.48-3.61 (2H, m), 3.72 (6H, s), 3.8-3.97 (2H, t, J= 5.1), 4.00-4.15 (4H, m), 6.78-6.90 (8H, m), 6.97-7.07 (4H, m), 7.15-7.34 (9H, m), 7.34-7.44 (6H, m), 7.91 (2H, d, J= 7.4).

^{31}P-NMR (121.5MHz, $CDCl_3$): 147.73

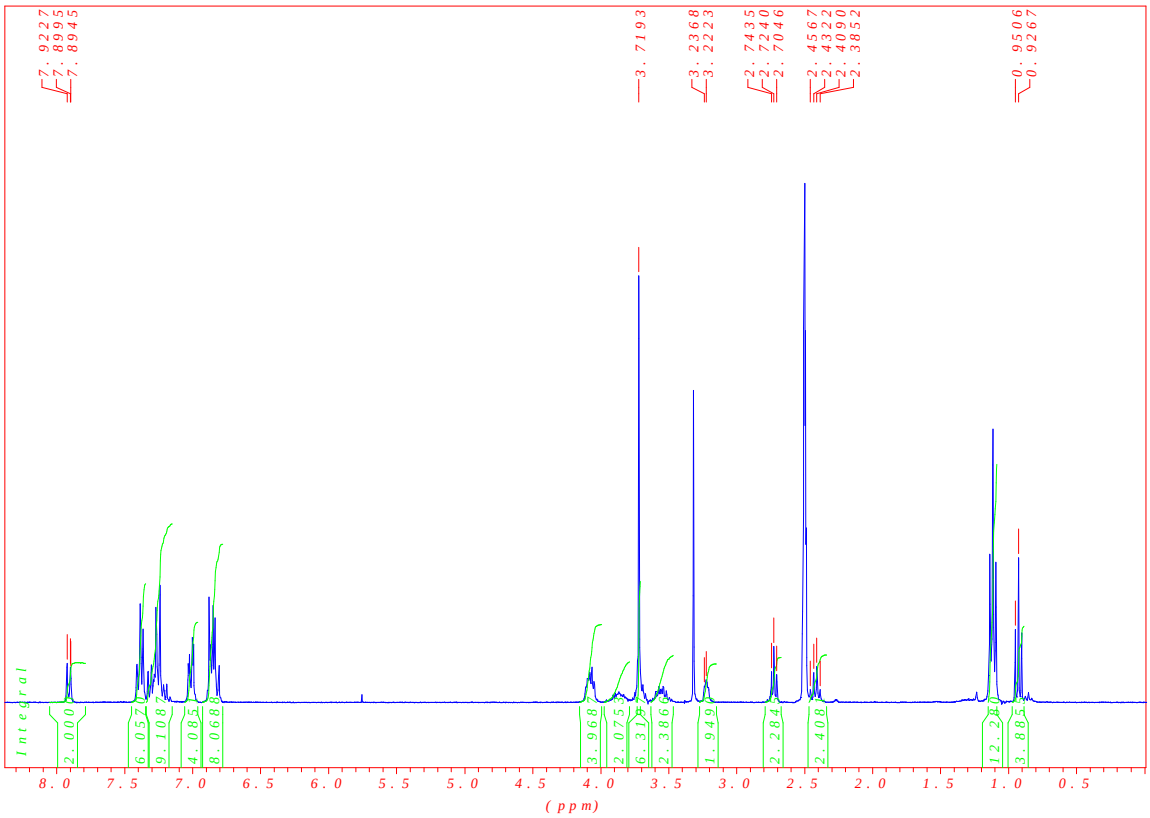
7.9227
7.8995
7.8945
3.7193
3.2368
3.2223
2.7435
2.7240
2.7046
2.4567
2.4322
2.4090
2.3852
0.9506
0.9267
Integral
2.000
6.057
9.108
4.085
8.068
3.968
2.075
6.317
2.386
1.949
2.284
2.408
12.28
3.881
8.0 7.5 7.0 6.5 6.0 5.5 5.0 4.5 4.0 3.5 3.0 2.5 2.0 1.5 1.0 0.5
(ppm)

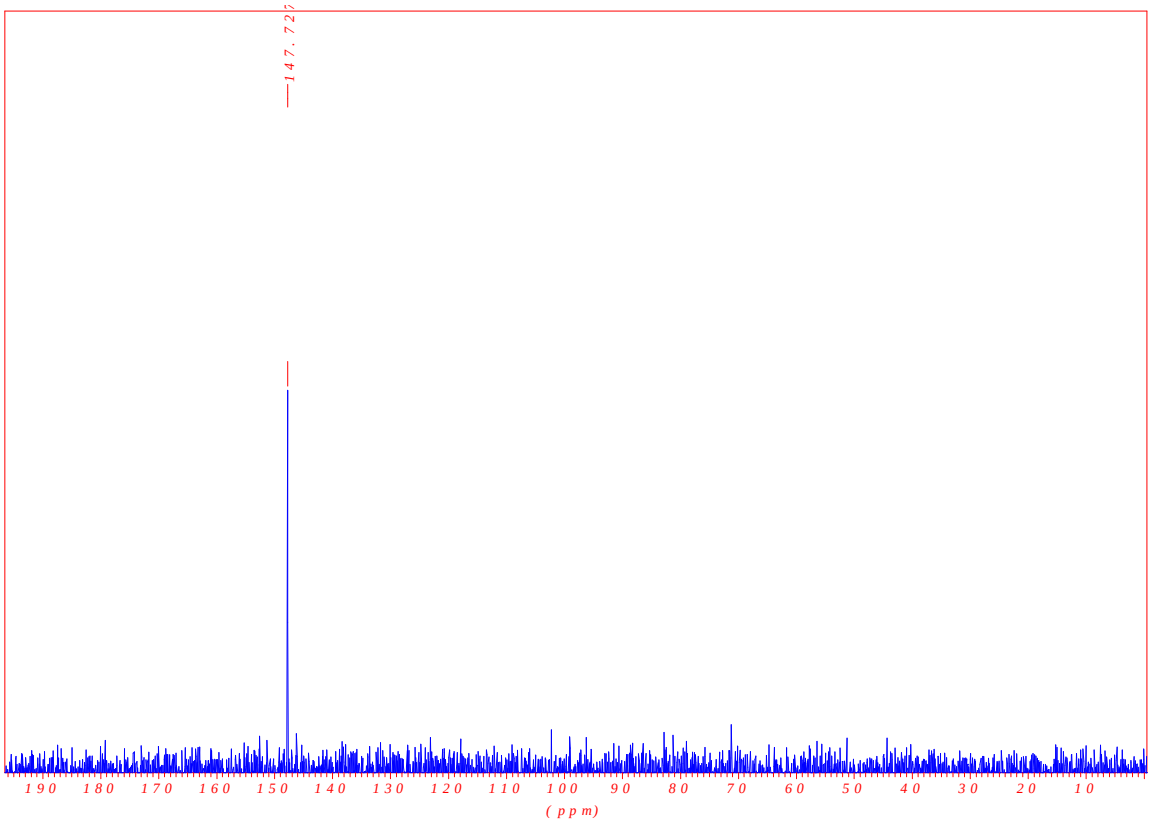

Oligonucleotide synthesis

Nucleoside phosphoramidites were purchased from *SAFC* (Proligo Reagents) with dG (dmf), dC (ac) and dA (bz). Oligonucleotides **ON1-VI** and **ON2-VI** were prepared via automated oligonucleotide synthesis using standard phosphoramidite (Activator: Ethylthiotetrazole 0.3 M in Acetonitrile) on a 394-DNA/RNA synthesizer (*Applied Biosystems*). Oligonucleotides **Ref-1** and **Ref-2** were ordered from *MicroSynth*, Switzerland. For the unnatural building block, which were coupled using 0.1 M solutions in 1,2-dichloroethane, coupling times were increased to 120 seconds instead of 25 seconds used for the natural nucleosides. Cleavage from the solid support and final deprotection was performed manually by treatment with 30 % NH_4OH solution at 55°C overnight. All oligonucleotides were purified by reverse phase HPLC (Instrument: LC-10 AT from *Shimadzu* with a UV detector, column: LiChrospher 100 RP-18, 5 µm, *Merck*); eluent A= $(Et_3NH)OAc$ (0.1 M, pH 7.4); eluent B= 80% MeCN + 20% Eluent A; gradient 5-60% B over 38 min.

For the determination of oligonucleotide stock solution concentrations, small samples were diluted to 10 % and the absorbance at 260 nm was measured on a Nanodrop ND-1000 Spectrophotometer from *Thermo Scientific*. Epsilon values were calculated using 15300, 11700, 7400 and 9000 for A, G, C and T, respectively, and 4600 for the fluorene building block as determined from UV-Vis absorption spectra of the corresponding diol derivatives in THF.

Molecular mass determination of the oligonucleotides was performed with a Sciex QSTAR pulsar (hybrid quadrupole time-of-flight mass spectrometer, *Applied Biosystems*). ESI-MS (negative mode, CH_3CN/H_2O/TEA) data of the compounds **ON1** and **ON2** are presented in Table 6.2.

Oligo #	**Duplex**	**Bruttoformula**	**Calc. aver. mass**	**found**
ON1-VI **ON2-VI**	(3`) ACG TGA GAG CPA CTG GCT CGA (5`) (5`) TGC ACT CTC GPT GAC CGA GCT (3`)	$C_{303}H_{331}N_{71}O_{123}P_{20}$ $C_{302}H_{332}N_{66}O_{125}P_{20}$	7554.8 7505.8	7554.9 7505.2

Table 6.2 Mass spectrometry data (brutto formula, calculated average mass, found mass)

Thermal denaturation experiments (1 µM singlestrand oligonucleotide concentration, 10 mM phosphate buffer pH 7.4, 100 mM NaCl) were carried out on Varian Cary 100 Bio UV-Visible spectrophotometer equipped with a Varian Cary temperature controller and data were collected with Varian WinUV software at various wavelength as indicated in each case. Cooling- heating- cooling cycles in the temperature range of 90°C to 20°C and a heating/ cooling rate of 0.5°C/ min were used and data points every 0.5°C were recorded. Data were analyzed with KaleidaGraph 4 software from *Synergy Software*. Temperature melting values (T_m) were determined as the maximum of the first derivative of the melting curves. If necessary the curves were smoothed with a window of 5 in order to get a reasonable maximum of the first derivative.

Temperature dependent UV-VIS spectra were collected from 90°C to 20°C on a Varian Cary 100 Bio UV-Visible spectrophotometer equipped with a Varian Cary

temperature controller. All experiments were carried out at a 1µM singlestrand oligonucleotide concentration in 10 mM phosphatebuffer (pH 7.4) and 100 mM NaCl.

Temperature dependent fluorescence spectra were recorded from 90°C to 20°C on a Varian Cary Eclipse fluorescence spectrophotometer equipped with a Varian Cary temperature controller (excitation wavelength at 300nm, excitation and emission slitwidth as well as the detector voltage were varied according to the experiment as indicated). All experiments were carried out with a singlestrand concentration of 1 µM. Data were analyzed with KaleidGagraph 4 software from *Synergy Software*.

Circular dichroism spectra were recorded on a *JASCO* J-715 spectrophotometer equipped with a PFD-350S temperature controller. All experiments were carried out with a singlestrand concentration of 5 µM (if not indicated) in 10 mM phosphatebuffer (pH 7.4) and 100 mM NaCl.

Chapter 7: Interactions between structurally different pyrene derivatives

7.1 Abstract

Putting two different pyrene derivatives in opposite position in the context of a DNA duplex results in the formation of stable structures. Comparison of the homo pairs with the hetero pairs shows distinct differences in the maxima of the excimer emission wavelength and hints for a ground state complex.

7.2 Introduction

As there are different pyrene derivatives used in our group the question arose what would happen with two different pyrene derivatives placed opposite each other in the context of the DNA duplex. This chapter tries to get some ideas and answers to this question.

7.3 Results and discussion

The oligonucleotides used in this study each contain one pyrene incorporation and the pyrene derivatives used are two bisalkynpyrene derivatives (1,6 and 1,8) and one carboxamidepyrene derivative (1,8). In table 7.1 the different oligonucleotides as well as the corresponding incorporated pyrene derivatives are shown.

Hybrid #	Oligo #	**Duplex**	**Tm (°C)**

D1-VII	**Ref-1** **Ref-2**	(3`) ACG TGA GAG CTA CTG GCT CGA (5`) (5`) TGC ACT CTC GAT GAC CGA GCT (3`)	70.7
D2-VII	**ON1-VII** **ON2-VII**	(3`) ACG TGA GAG CXA CTG GCT CGA (5`) (5`) TGC ACT CTC GXT GAC CGA GCT (3`)	73.8
D3-VII	**ON3-VII** **ON4-VII**	(3`) ACG TGA GAG CYA CTG GCT CGA (5`) (5`) TGC ACT CTC GYT GAC CGA GCT (3`)	69.5
D4-VII	**ON5-VII** **ON6-VII**	(3`) ACG TGA GAG CSA CTG GCT CGA (5`) (5`) TGC ACT CTC GST GAC CGA GCT (3`)	67.8
D5-VII	**ON1-VII** **ON6-VII**	(3`) ACG TGA GAG CXA CTG GCT CGA (5`) (5`) TGC ACT CTC GST GAC CGA GCT (3`)	69.0
D6-VII	**ON5-VII** **ON2-VII**	(3`) ACG TGA GAG CSA CTG GCT CGA (5`) (5`) TGC ACT CTC GXT GAC CGA GCT (3`)	68.1
D7-VII	**ON3-VII** **ON6-VII**	(3`) ACG TGA GAG CYA CTG GCT CGA (5`) (5`) TGC ACT CTC GST GAC CGA GCT (3`)	67.9
D8-VII	**ON5-VII** **ON4-VII**	(3`) ACG TGA GAG CSA CTG GCT CGA (5`) (5`) TGC ACT CTC GYT GAC CGA GCT (3`)	68.1

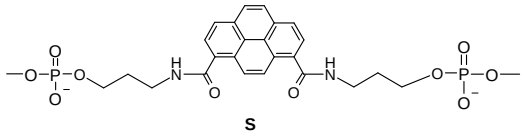

S

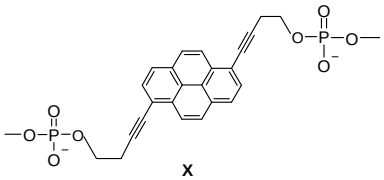

X

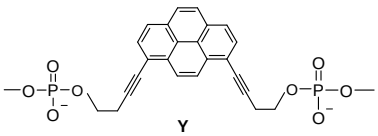

Y

Table 7.1 Oligonucleotide sequences used in this study and hybridization data (Tm, °C) of different oligonucleotides duplexes containing pyrene based building blocks. All measurements were carried out at pH 7.4 in phosphatebuffer and 100 mM NaCl.

Comparing the thermal stability of the different hybrids compared to the all natural reference duplex **D1-VII** one can see that the hybrid **D2-VII** which contains the same pyrene derivative (X) opposite each other leads to a significant stabilization. **D3-VII** shows only a slight destabilizing effect and **D4-VII** shows a destabilizing effect of the pyrene modifications. When looking at the mixed pairs the stabilizing effect is comparable for all four hybrids **D5-VII** to **D8-VII**. The melting profiles for all hybrids showed no hysteresis and a sharp transition was observed for the homo duplexes (Figure 7.1) as well as for the hetero duplexes (Figure 7.2).

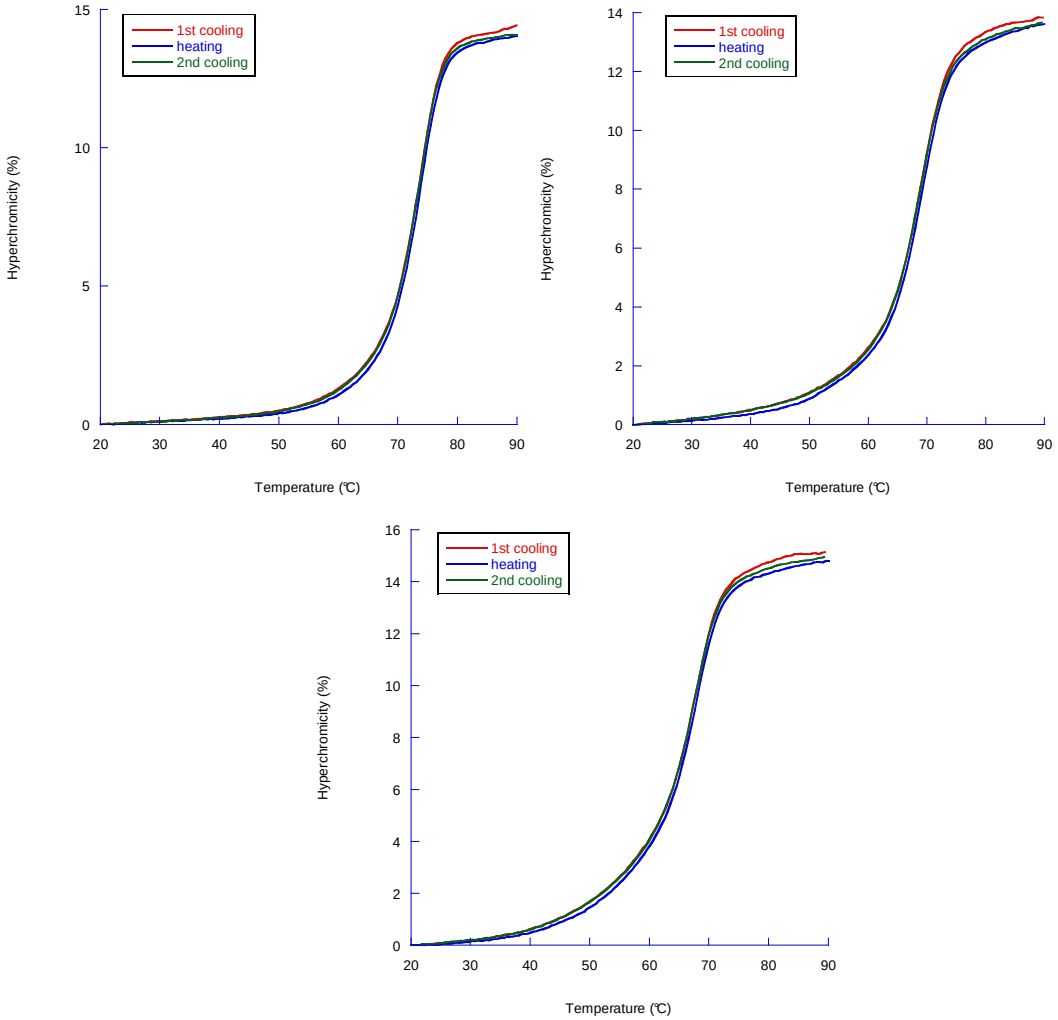

Figure 7.1 Melting profiles of the homo hybrids showing two cooling ramps and one heating ramp. **D2-VII** (top left), **D3-VII** (top right) and **D4-VII** (bottom)

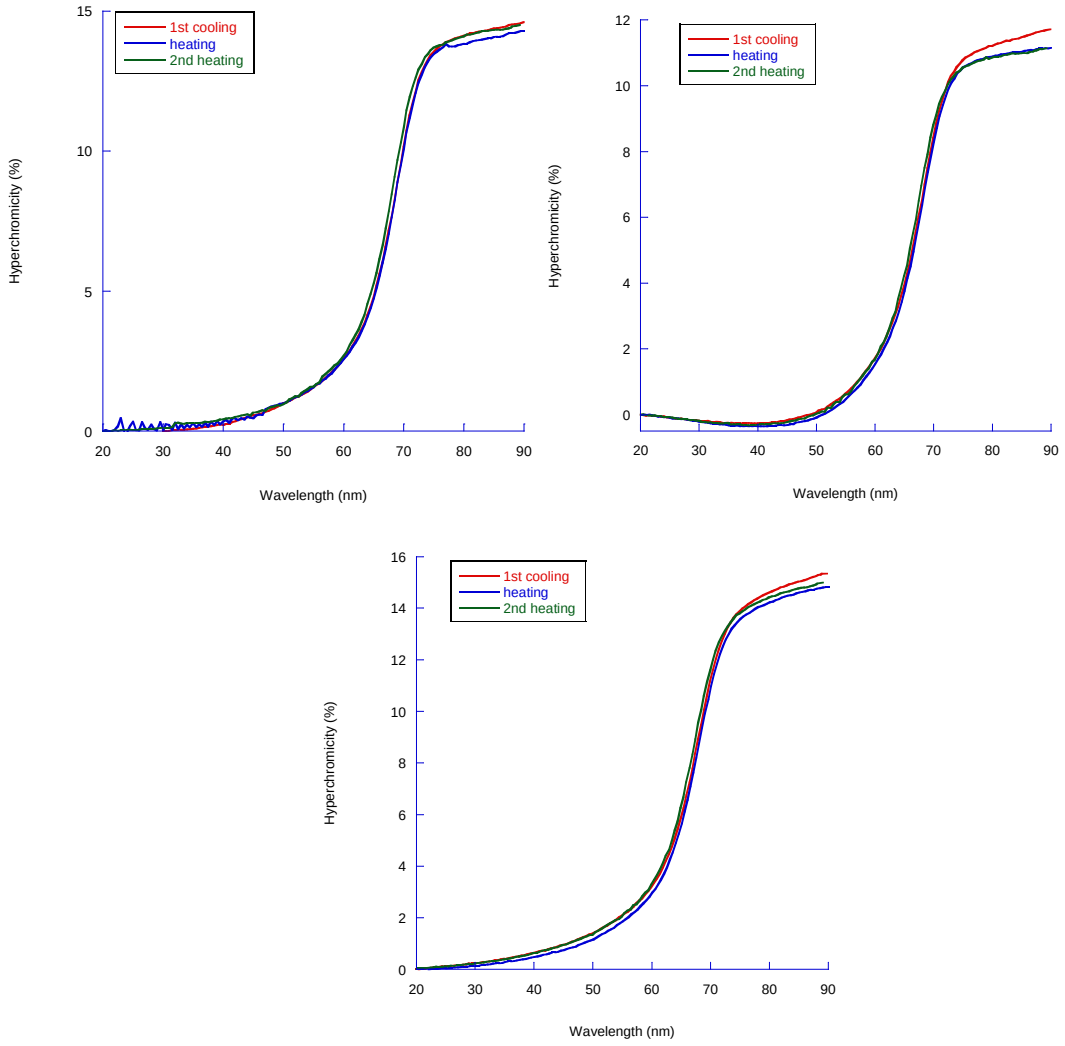

Figure 7.2 Melting profiles of the homo hybrids showing two cooling ramps and one heating ramp. **D5-VII** (top left), **D6-VII** (top right) and **D7-VII** (bottom)

The UV-Vis absorption spectra showed the hyperchromic effect upon heating of the absorption band at around 260 nm corresponding to the nucleobases and the change of the absorption bands of the alkynylpyrenes going from the interstrand stacked mode to the monomeric absorption at elevated temperatures. The hybrid containing the two carboxamide pyrenes shows the broad absorption band which also shows a hyperchromic effect upon heating and an isosbestic point is as well visible for this hybrid.

The spectra of the hetero hybrids show the same behavior of the change in the relative intensites of the absorption bands of the alkynyl pyrene upon heating although of weaker

intensity. Due to the small exctinction coefficient of the carboxamide pyrene its absorption band is dominated by the absorption of the alkynyl pyrene.

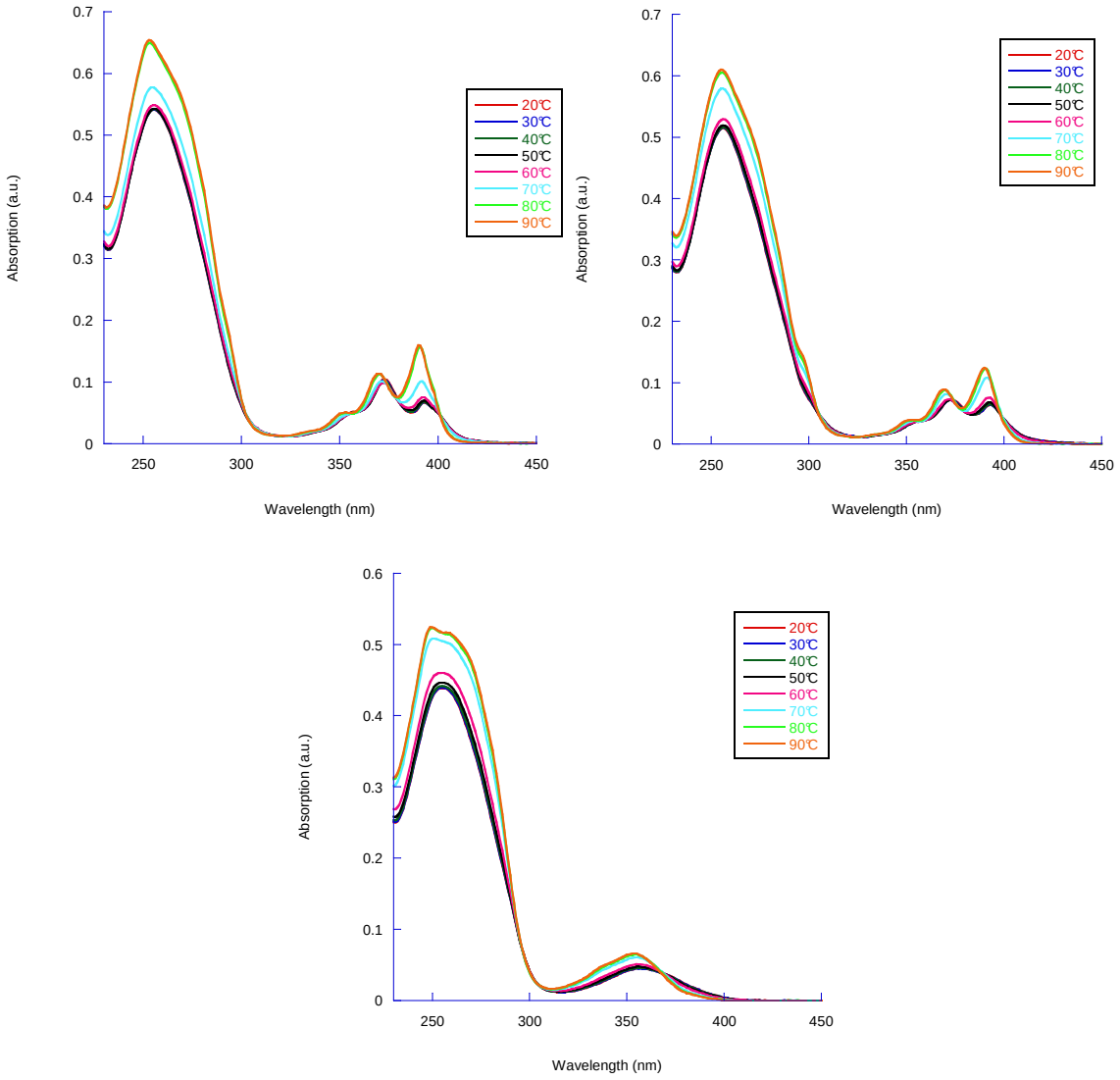

Figure 7.3 Temperature dependent UV-Vis absorption of the homo hybrids **D2-VII** (top left), **D3-VII** (top right) and **D4-VII** (bottom)

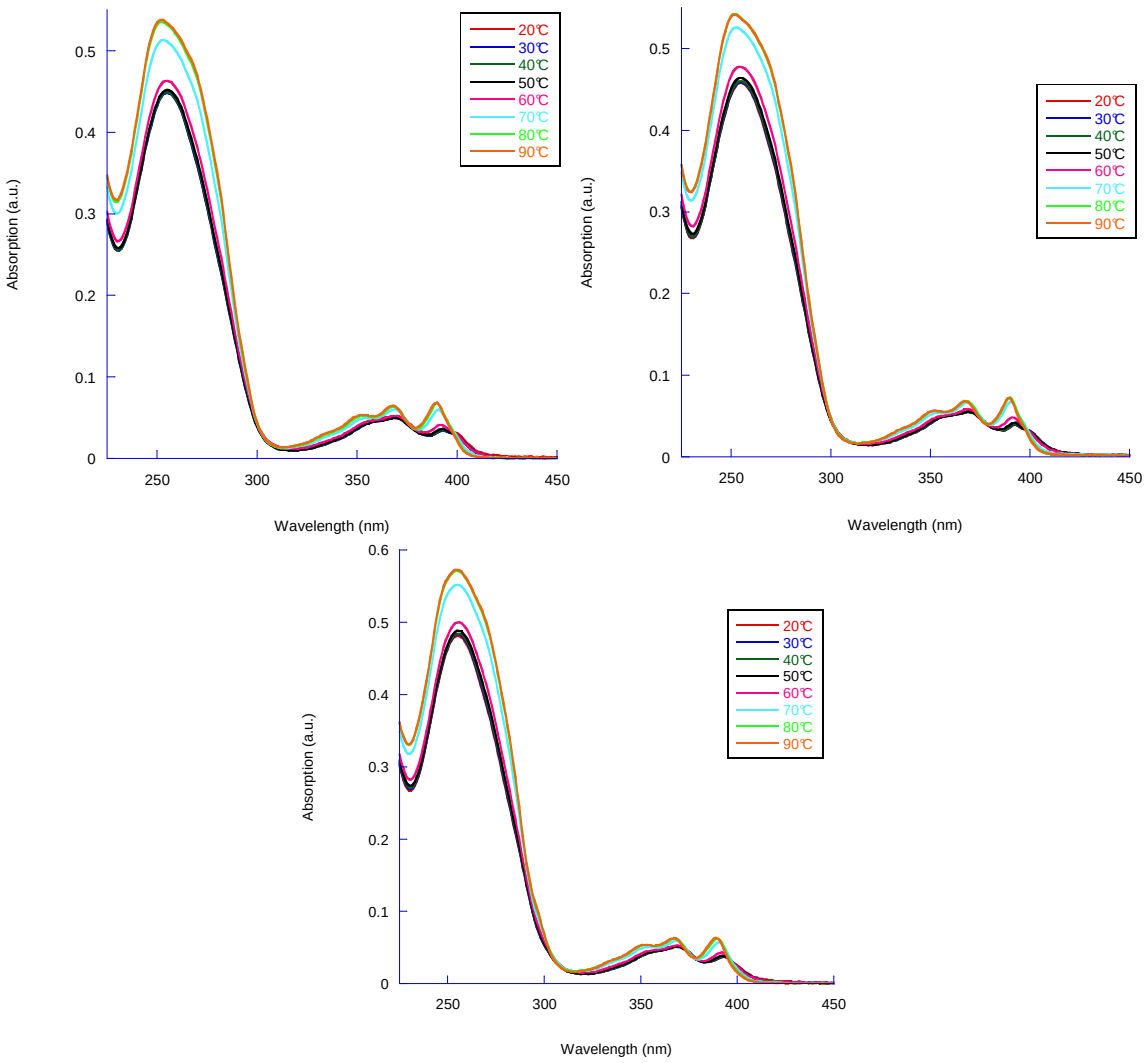

Figure 7.4 Temperature dependent UV-Vis absorption of the hetero hybrids **D5-VII** (top left), **D6-VII** (top right) and **D7-VII** (bottom)

The fluorescence properties of the homo hybrids as already known is characterized by the excimer formation between two carboxamide pyrenes having an emission maximum at 502 nm and the excimer between the 1,6-alkynylpyrene at 528 nm and between the 1,8-alkynylpyrene at 521 nm (Figure 7.5).

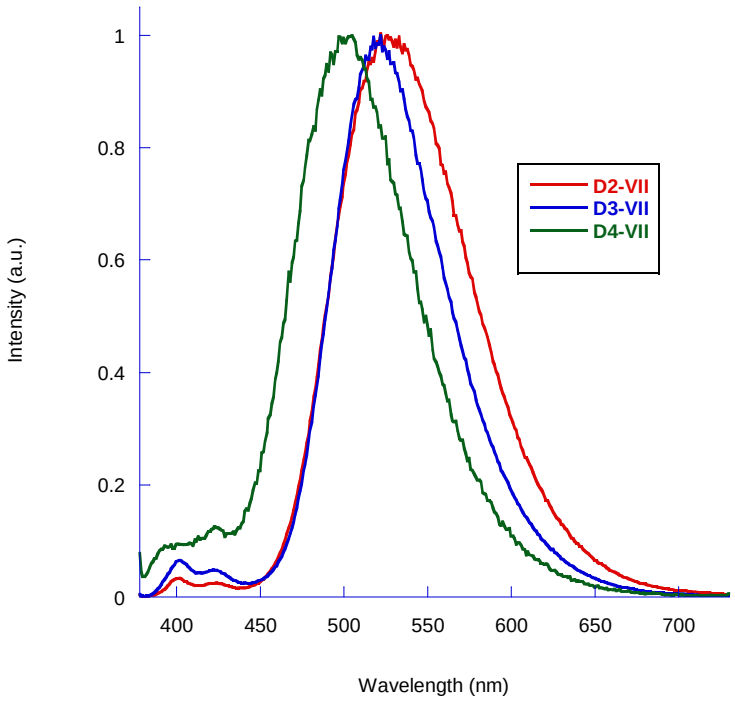

Figure 7.5 Normalized emission spectra of the homo hybrids. Excitation wavelength: 370 nm

The properties of the heterohybrids concerning the emission wavelength of the excimer emission surprisingly resulted in energies not as expected between the emission of the hybrids **D4-VII** and of **D2-VII/D3-VII** but shows an even lower energy of their excimer emission maxima (Figure 7.6 and Table 7.2).

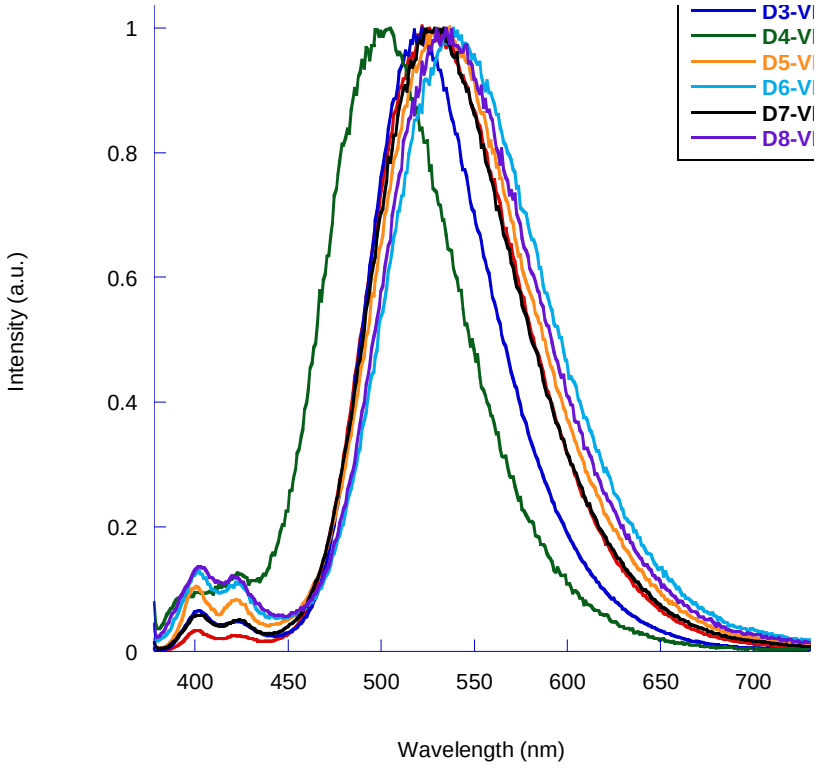

Figure 7.6 Normalized emission spectra of all the hybrids. Excitation wavelength: 370 nm

Hybrid	**D4-VII**	**D3-VII**	**D2-VII**	**D7-VII**	**D5-VII**	**D8-VII**	**D6-VII**
Emission maxima	**502 nm**	**521 nm**	**528 nm**	**529 nm**	**533 nm**	**536 nm**	**540 nm**

Table 7.2 Maxima of emission wavelength of the homo hybrids (yellow) and of the hetero hybrids (green)

In order to get an idea about the origin of this even more red-shifted excimer emission the corresponding excitation spectra were recorded in function of the emission wavelength. Although varying in intensity the excitation spectra are for all emission wavelengths the same when normalized (Figure 7.7 and Figure 7.8).

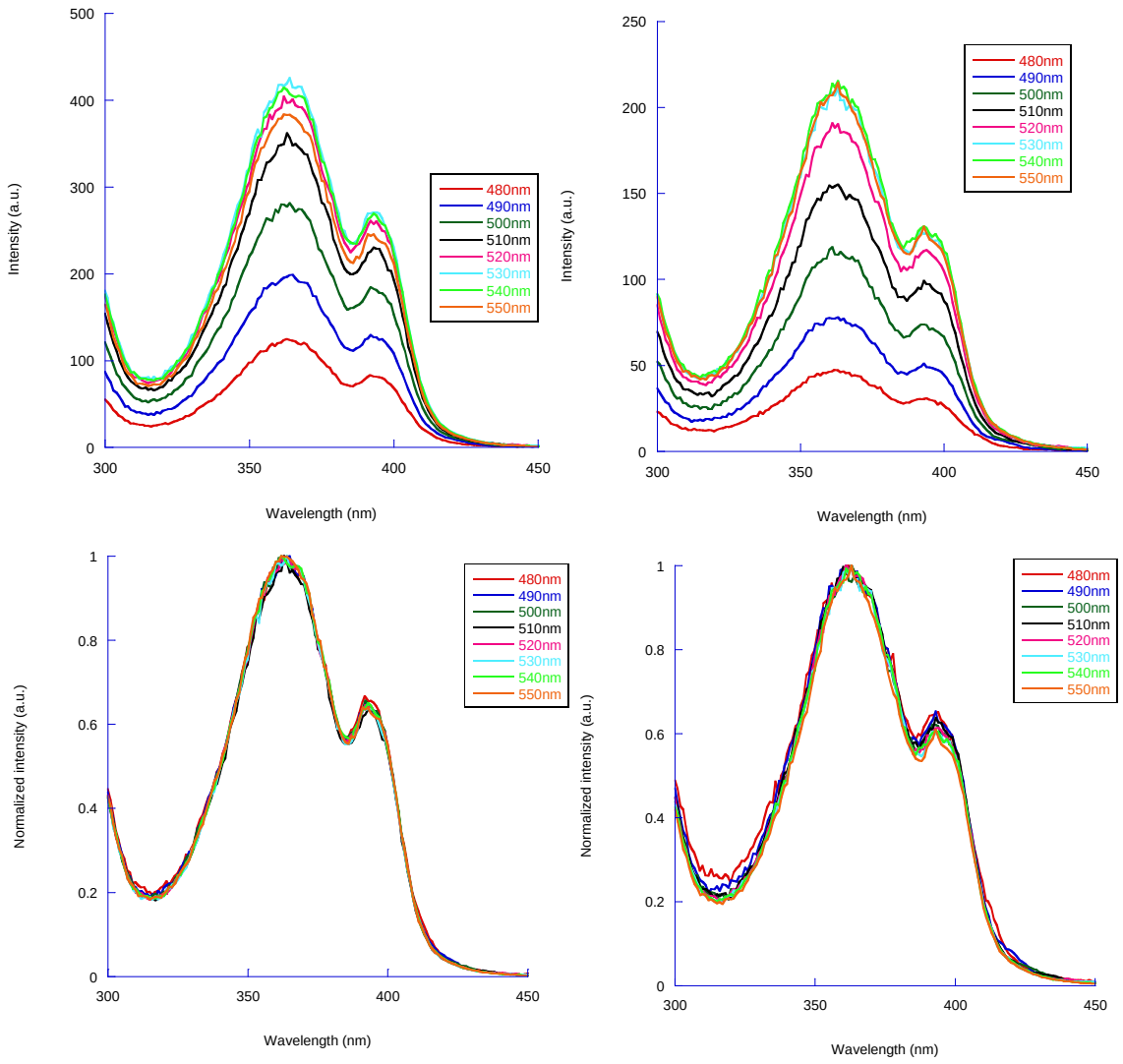

Figure 7.7 Emission wavelength dependent excitation spectra of hybrid **D5-VII** (top left) and **D6-VII** (top right) and normalized excitation spectra of **D5-VII** (bottom left) and **D6-VII** (bottom right).

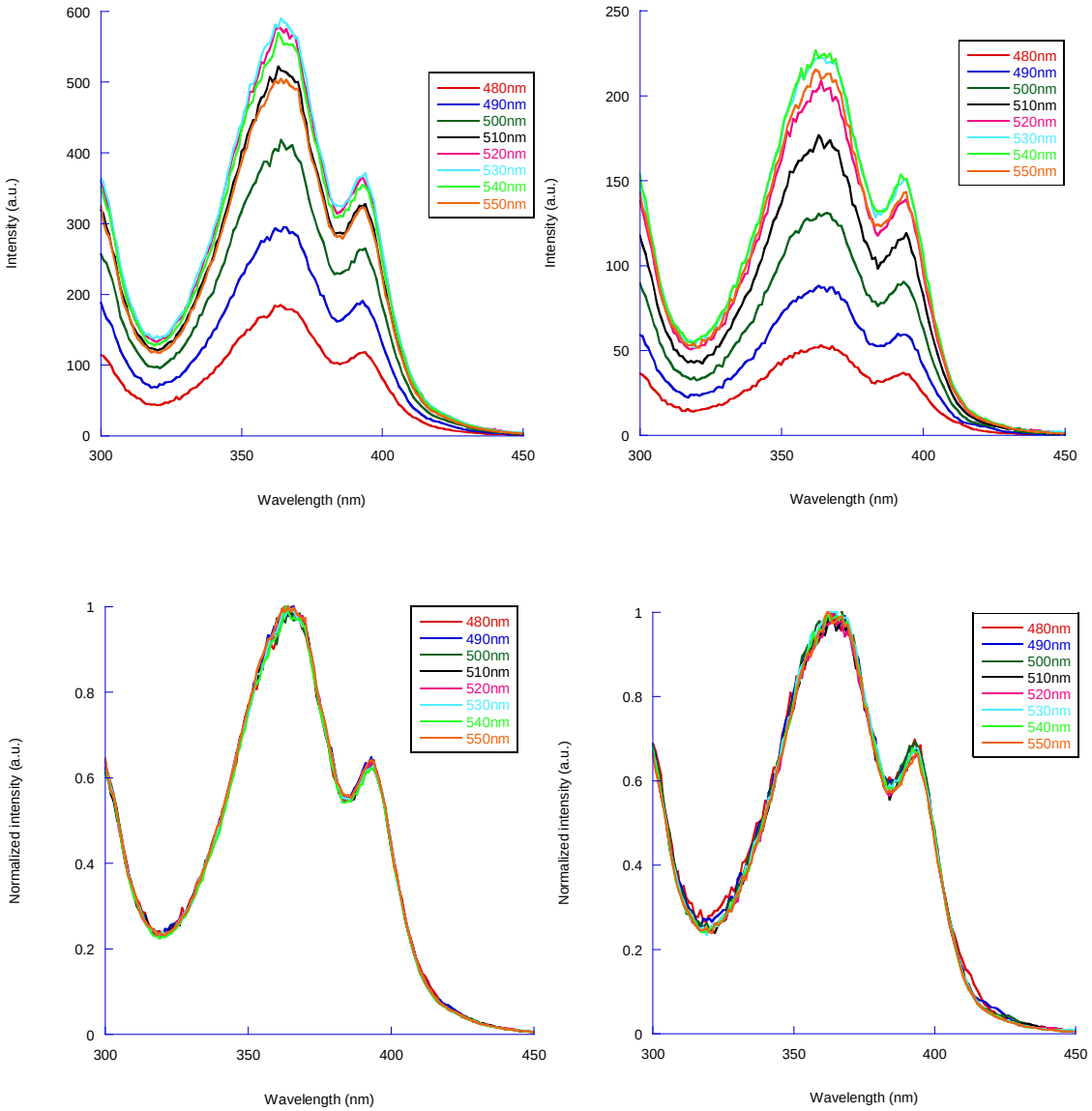

Figure 7.8 Emission wavelength dependent excitation spectra of hybrid **D7-VII** (top left) and **D8-VII** (top right) and normalized excitation spectra of **D7-VII** (bottom left) and **D8-VII** (bottom right).

Circular dichroism experiments performed at 20°C for all the hybrids show that in the case of the homo pairs **D2-VII**, **D3-VII** and **D4-VII** there is exciton coupling observed especially in the case with the alkynyl derivatives whereas the carboxamide derived pyrene only lead to a very weak bisignate CD signal (Figure 7.9 left). In the mixed hybrids there is also exciton coupling observed for all the hybrids. In the case of **D7-VII** this coupled CD signal is of relative high intensity (Figure 7.9 right).

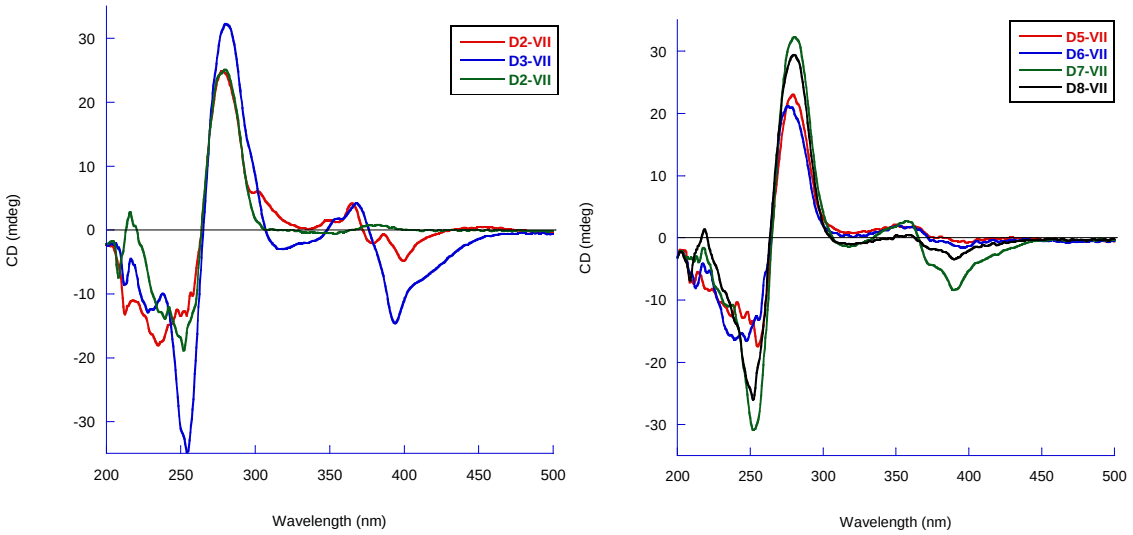

Figure 7.9 CD spectra of the homo hybrids (left) and of the hetero hybrids (right) at 20°C.

7.4 Conclusion and outlook

Putting two different pyrene derivatives opposite each other in the context of a DNA duplex leads to an energy penalty of the overall stability in comparison to the homo hybrids but the overall cooperative melting process is maintained. The absorption spectra of the mixed hybrids are dominated by the alkynyl pyrene derivative which possesses the larger extinction coeffiecient. The fluorescent properties of the mixed hybrids show eximer emission maxima which are not situated between the emission wavelength of the carboxamide pyrene homo hybrid **D4-VII** excimer and the alkynyl pyrene homo hybrids **D2-VII** and **D3-VII** but are even more red-shifted in contrast to the expected exciplex emission. The excitation spectra hint for a ground state complex between the two different pyrene derivatives which are then excitated and emit at lower energy. The exaction coupled CD additionally supports the electronic coupling between the different pyrene derivatives.

The observation of the different emission wavelength depending on the excact nature of the pyrene derivative forming the ground state complex could be further investigated using different derivatives of pyrene or applied and investigated for other aromatic chromophores.

7.5 Experimental section

Oligonucleotides **ON1-VII** to **ON6-VII** were already present in the group and before synthesized and characterized according to [34, 76]

For the determination of oligonucleotide stock solution concentrations, small samples were diluted to 10 % and the absorbance at 260 nm was measured on a Nanodrop ND-1000 Spectrophotometer from *Thermo Scientific*. Epsilon values were calculated using 15300, 11700, 7400 and 9000 for A, G, C and T, respectively, and 8600 for the pyrene carboxamide building block and 20000 for the 1,6 bisalkynyl- and 30000 for the 1,8-bisalkynyl-pyrene building block.

Thermal denaturation experiments (1 µM singlestrand oligonucleotide concentration, 10 mM phosphate buffer pH 7.4, with varying NaCl concentration as indicated in each case) were carried out on Varian Cary 100 Bio UV-Visible spectrophotometer equipped with a Varian Cary temperature controller and data were collected with Varian WinUV software at various wavelengths as indicated in each case. Cooling- heating- cooling cycles in the temperature range of 90°C to 15°C and a heating/ cooling rate of 0.5°C/ min were used and data points every 0.5°C were recorded. Data were analyzed with KaleidaGraph 4 software from *Synergy Software*. Temperature melting values (T_m) were determined as the maximum of the first derivative of the melting curves. If necessary the curves were smoothed with a window of 5 in order to get a reasonable maximum of the first derivative.

Temperature dependent UV-VIS spectra were collected from 90°C to 20°C on a Varian Cary 100 Bio UV-Visible spectrophotometer equipped with a Varian Cary

temperature controller. All experiments were carried out at a 1 µM singlestrand oligonucleotide concentration in 10mM phosphatebuffer (pH 7.4) and 100 mM NaCl.

Fluorescence spectra were recorded at 20°C on a Varian Cary Eclipse fluorescence spectrophotometer equipped with a Varian Cary temperature controller (excitation wavelength at 370 nm, excitation and emission slitwidth as well as the detector voltage were varied according to the experiment). All experiments were carried out with a singlestrand concentration of 1 µM. Data were analyzed with KaleidGagraph 4 software from *Synergy Software*.

Circular dichroism spectra were recorded on a *JASCO* J-715 spectrophotometer equipped with a PFD-350S temperature controller. All experiments were carried out with a singlestrand concentration of 5 µM in 10 mM phosphatebuffer (pH 7.4) and 100 mM NaCl.

References

[1] F. Miescher Hoppe Syeler`s, *Med. Chem. Unters.,* **1871**, 441.

[2] P. A. Levene, W. A. Jacobs, *Berichte der deutschen chemischen Gesellschaft*, **1909**, 42, 2102.

[3] P. A. Levene, E. S. London, *Journal of biological chemistry*, **1929**, 83, 793.

[4] O. T. Avery, C. M. MacLeod, M. McCarty, *Journal of experimental medicine*, **1944**, 79, 137.

[5] E. Chargaff, *Fed. Proc*., **1951**, 10, 654.

[6] M. H. F. Wilkins, W. E. Seeds, A. R. Stockes, H. R. Wilson, *Nature*, **1953**, 172, 759.

[7] J. D. Watson, F. H. Crick, *Nature*, **1953**, 171, 737.

[8] H. G. Khorana, G. M. Teuer, J. G. Moffat, E. H. Pol, *Chem. Ind.* (London), **1956**, 1523.

[9] M. H. Caruthers, M. D. Matteuci, *J. Am. Soc*. **1981**, 103, 3185.

[10] S. L. Beaucage, M. H. Caruthers, *Tet. Lett.,* **1981,** 22, 1859.

[11] N. D. Sinha, J. Biernat, J. McManus, H. Koester, *Nucleic Acids Res.,* **1984**, 11, 4539.

[12] S. Beaucage, R. Iyer, *Nucleic Acids Res*., **1992**, 48, 2223.

[13] F. M. Pohl, T. M. Jovin, *J. Mol. Biol.*, **1972** 67, 375.

[14] A. H. J. Wang, G. J. Quigley, F. J. Kolpak, J. L. Crawford, J. H. Vanboom, G. Vandermarel, A. Rich, *Nature*, **1979**, 282, 680.

[15] T. J. Thamann, R. C. Lord, A. H. J. Wang, A. Rich, *Nucleic Acids Res.*, **1981**, 9, 5443.

[16] A. Haschemeyer, A. Rich, *J. Mol. Biol.*, **1967**, 27, 369.

[17] A. Möller, A. Nordheim, S. A. Kozlowski, D. J. Patel, A. Rich, *Biochemistry*, **1984**, 23, 54.

[18] M. Behe, G. Felsenfeld, *Proc. Natl. Acad. Sci.,* **1981**, 78, 1619.

[19] S. Fujii, A. H. J. Wang, G. Van der Marel, J. H. Van Boom, A. Rich, *Nucleic Acids Res.,* **1982**, 23, 7879.

[20] A. Razin, A. D. Riggs, *Science,* **1980**, 210, 604.

[21] R. D. Sheardy, S. A. Winkle, *Biochemistry,* **1989**, 28, 720.

[22] Z. Y. Dai, G. A. Thomas, E. Evertsz, W. L. Peticolas, *Biochemistry,* **1989**, 28, 6991.

[23] R. D. Sheardy, N. Levine, S. Marotta, D. Suh, J. B. Chaires, *Biochemistry,* **1994**, 33, 1385.

[24] S. C. Ha, K. Löwenhaupt, A. Rich, Y. G. Kim, K. K. Kim, *Nature,* **2005,** 437, 1183.

[25] M. De Rosa, D. De Sanctis, A. L. Rosario, M. Archer, A. Rich, A. Athanasiadis, M. A. Carrondo, *Proc. Natl. Acad. Sci.,* **2010**, 107, 9088.

[26] V. Malinovskii, D. Wenger, R. Häner, *Chem. Soc. Rev.,* **2010**, 39, 410.

[27] H. Kashida, H. Asanuma and M. Komiyama, *Chem. Commun*., **2006**, 2768.

[28] K. Fukui, M. Morimoto, H. Segawa, K. Tanaka and T. Shimidzu, *Bioconjugate Chem.*, **1996**, 7, 349.

[29] S. Smirnov, T. J. Matray, E. T. Kool and C. de los Santos, *Nucleic Acids Res*., **2002**, 30, 5561.

[30] C. Brotschi, G. Mathis and C. J. Leumann, *Chem.–Eur. J*., **2005**, 11, 1911.

[31] S. M. Langenegger and R. Haener, *Tetrahedron Lett.*, **2004**, 45, 9273.

[32] T. S. Kumar, A. S. Madsen, M. E. Ostergaard, J. Wengel and P. J. Hrdlicka, *J.Org. Chem*., **2008**, 73, 7060.

[33] C. B. Nielsen, M. Petersen, E. B. Pedersen, P. E. Hansen and U. B. Christensen, *Bioconjugate Chem*., **2004**, 15, 260.

[34] S. M. Langenegger and R. Haener, *Chem. Commun*., **2004**, 2792.

[35] Z. Johar, A. Zahn, C. J. Leumann and B. Jaun, *Chem.–Eur. J*., **2008**, 14, 1080.

[36] M. N. Dioubankova, A. D. Malakhov, D. A. Stetsenko, M. J. Gait, P. E. Volynsky, R. G. Efremov and V. A. Korshun, *ChemBioChem*, **2003**, 4, 841.

[37] G. T. Hwang, Y. J. Seo and B. H. Kim, *Tetrahedron Lett.*, **2005**, 46, 1475.

[38] P. J. Hrdlicka, B. R. Babu, M. D. Sorensen and J. Wengel, *Chem. Commun*., **2004**, 1478.

[39] C. Gruenewald, T. Kwon, N. Piton, U. Foerster, J. Wachtveitl and J. W. Engels, *Bioorg. Med. Chem.*, **2008**, 16, 19.

[40] M. Nakamura, Y. Ohtoshi and K. Yamana, *Chem. Commun*., **2005**, 5163.

[41] M. Nakamura, Y. Murakami, K. Sasa, H. Hayashi and K. Yamana, *J. Am. Chem. Soc.*, **2008**, 130, 6904.

[42] I. Bouamaied, T. Nguyen, T. Ruhl and E. Stulz, *Org. Biomol. Chem.*, **2008**, 6, 3888.

[43] T. Nguyen, A. Brewer and E. Stulz, *Angew. Chem., Int. Ed*., **2009**, 48, 1974.

[44] E. Mayer-Enthart, C. Wagner, J. Barbaric and H. A. Wagenknecht, *Tetrahedron*, **2007**, 63, 3434.

[45] H. Kashida, M. Tanaka, S. Baba, T. Sakamoto, G. Kawai, H. Asanuma and M. Komiyama, *Chem.–Eur. J*., **2006**, 12, 777.

[46] D. Baumstark and H. A. Wagenknecht, *Chem.–Eur. J*., **2008**, 14, 6640.

[47] V. L. Malinovskii, F. Samain and R. Haener, *Angew. Chem.*, *Int. Ed*., **2007**, 46, 4464.

[48] R. Haener, F. Samain and V. L. Malinovskii, *Chem.–Eur. J*., **2009**, 15, 5701.

[49] W. Wang, W. Wan, H. H. Zhou, S. Q. Niu and A. D. Q. Li, *J. Am. Chem. Soc.*, **2003**, 125, 5248.

[50] Y. Zheng, H. Long, G. C. Schatz and F. D. Lewis, *Chem. Commun*., **2005**, 4795.

[51] R. Iwaura, F. J. M. Hoeben, M. Masuda, A. P. H. J. Schenning, E. W. Meijer and T. Shimizu, *J. Am. Chem. Soc*., **2006**, 128, 13298.

[52] R. Iwaura, M. Ohnishi-Kameyama and T. Iizawa, *Chem.–Eur. J.*, **2009**, 15, 3729.

[53] C. Mao, W. Sun, Z. Shen, N. C. Seeman, *Nature*, **1999**, 397, 144.

[54] A. Okamoto, Y. Ochia and I. Saito, *Chem. Commun*., **2005**, 1128.

[55] R. Tashiro, H. Sugiyama, *J. Am. Chem. Soc*., **2005**, 127, 2094.

[56] K. Fujimoto, S. Aizawa, I. Oota, J. Chiba, M. Inouye, *Chem. Eur. J.*, **2010**, 16, 2401.

[57] A. Zahn, C. J. Leumann, *Bioorg. Med. Chem.*, **2006**, 6174.

[58] A. Zahn, C. J. Leumann, *Chem. Eur. J.*, **2008**, 14, 1087.

[59] S. M. Langenegger, R. Häner, *Tet. Lett.*, **2004**, 9273.

[60] J. W. Chen, Y. Cao, *Acc. Chem. Res.*, **2009**, 42, 1709.

[61] O. Inganas, F. L. Zhang, M. R. Andersson, *Acc. Chem. Res*., **2009**, 42, 1731.

[62] C. Poriel, J. J. Liang, J. Rault-Berthelot, F. Barriere, N. Cocherel, A. M. Z. Slawin, D. Horhant, M. Virboul, G. Alcaraz, N. Audebrand, L. Vignau, N. Huby, G. Wantz, L. Hirsch, *Chem. Eur. J.*, **2007**, 13, 10055.

[63] S. Barik, S. Valiyaveettil, *Macromolecules,* **2008**, 41, 6376.

[64] D. Neher, *Macromol. Rapid Commun.*, **2001**, 22, 1365.

[65] A. C. Grimsdale, K. Müllen, *Adv. Polym. Sci*., **2008**, 212, 1.

[66] A. C. Grimsdale, K. L. Chan, R. E. Martin, P. G. Jokisz, A. B. Holmes, *Chem. Rev.*, **2009**, 109, 897.

[67] R. Abbel, A. P. H. J. Schenning, E. W. Meijer, *J. Polym. Sci. Part A: Polym. Chem.*, **2009**, 47, 4215.

[68] T. Nakano, K. Takewaki, T. Yade, Y. Okamoto, *J. Am. Chem. Soc.*, **2001**, 123, 9182.

[69] G. Hughes, M. R. Bryce, *J. Mater. Chem.*, **2005**, 15, 94.

[70] T. Nakano, T. Yade, *J. Am. Chem. Soc*., **2003**, 125, 15474.

[71] J. C. Sancho-Garcia, *Theor. Chem. Acc*., **2010**, 1.

[72] V. Coropceanu, T. Nakano, N. E. Gruhn, O. Kwon, T. Yade, K. Katasukawa, J. L. Bredas, *J. Phys. Chem. B*, **2006**, 110, 9482.

[73] A. Kaeser, A. P. H. J. Schennning, *Adv. Mater.*, **2010**, 22, 2985.

[74] L. A. Carpino, G. Y. Han, *J. Org. Chem.*, **1972**, 3405.
[75] G. T. Hwang, Y. J. Seo, B. H. Kim, *J. Am. Chem. Soc.*, **2004**, 6528.

[76] H. Bittermann, D. Siegemund, V. L. Malinovskii, R. Häner, *J. Am. Chem. Soc.*, **2008**, 130, 15285.

Acknowledgements

First of all I would like to thank my supervisor Prof. Robert Häner who gave me the opportunity to do my PhD work in his research group and work on all these interesting topics. He was always available for interesting and stimulating discussions. I would also like to thank the current and former members of the Häner and the Leumann group. Furthermore I would like to thank the Ausgabe for their excellent support and help in a lot of aspects. I would also like to thank the MS service for measuring my oligonucleotides and the Hausdienst for providing their help. Last but not least I would like to thank my family and my girlfriend for their moral support through all these years.

List of publications

2011 **D. Wenger**, V. L. Malinovskii, R. Häner
"Modulation of chiroptical properties by DNA-guided assembly of fluorenes"
Chem. Comm, 2011, accepted.

2010 R. Häner, F. Garo, **D. Wenger**, V. L. Malinovskii
"Oligopyrenotides: Abiotic, Polyanionic Oligomers with Nucleic Acid-like Structural Properties"
J. Am. Chem. Soc., 2010, 132, 7466–7471.

2010 V.L. Malinovskii, **D. Wenger**, R. Häner
"Nucleic acid-guided assembly of aromatic chromophores"
Chem. Soc. Rev. 2010, 39, 410-422.

2007 S. M. Langenegger, V. L. Malinovskii, **D. Wenger**, S. Werder, R. Häner
„DNA Containing Non-Nucleosidic Phenanthrene Building Blocks with Asymmetrical Linkers"
Nucleosides, Nucleotides & Nucleic Acids, 2007, 26, 901-903.

Curriculum Vitae

Personal details

Name	Daniel Wenger
Date of birth	30th of june 1982
Hometown	Laengenbuehl (BE)
Maritial status	unmarried, no children
Nationality	Swiss

Education

03/2007 -	Ph.D in the group of Prof. Dr. R. Häner University of Bern, Department for biochemistry and chemistry
01/2007	**Master of Science in Chemistry** University of Bern, Department for biochemistry and chemistry Title of the diplomawork: *„A target assembled tandem oligonucleotide probe assay based on excimer formation for the detection of DNA mismatches“*
10/2002 - 01/2007	**Studies of chemistry** University of Bern, Department for biochemistry and chemistry
08/2001	**Matura** Gymnasium Kirchenfeld, Bern
07/1997 - 08/2001	**Mathematisch-naturwissenschaftliches Gymnasium** Schwerpunkt Physik und Anwendungen der Mathematik

Erklärung

gemäss Art. 28 Abs. 2 RSL 05

Name/Vorname: .....

Matrikelnummer: .....

Studiengang: .....

Bachelor ☐ Master ☐ Dissertation ☐

Titel der Arbeit: .....

.....

.....

LeiterIn der Arbeit: .....

.....

Ich erkläre hiermit, dass ich diese Arbeit selbständig verfasst und keine anderen als die angegebenen Quellen benutzt habe. Alle Stellen, die wörtlich oder sinngemäss aus Quellen entnommen wurden, habe ich als solche gekennzeichnet. Mir ist bekannt, dass andernfalls der Senat gemäss Artikel 36 Absatz 1 Buchstabe o des Gesetztes vom 5. September 1996 über die Universität zum Entzug des auf Grund dieser Arbeit verliehenen Titels berechtigt ist.

.....
Ort/Datum

.....
Unterschrift